Highly oriented conducting polythiophene films for thermoelectric applications

Vishnu Vijayakumar

Université de Strasbourg
Excellence University

UNIVERSITÉ DE STRASBOURG

École doctorale
Physique, chimie-physique
ED 182
Université de Strasbourg

ÉCOLE DOCTORALE Physique et Chime-physique

INSTITUT CHARLES SADRON

UPR 22

THÈSE

présentée par :

Vishnu VIJAYAKUMAR

soutenue le : **07 février 2020**

pour obtenir le grade de : **Docteur de l'université de Strasbourg**

Discipline/ Spécialité : **Physique et Chimie-physique**

Highly oriented conducting polythiophene films for thermoelectric applications

THÈSE dirigée par :

Dr. Brinkmann Martin — Directeur de Recherche, Institut Charles Sadron, Strasbourg

RAPPORTEURS :

Prof. Christian Müller — Professeur, Chalmers University of Technology, Suède

Dr. Alexandre Carella — Chercheur, CEA, Grenoble, France

Examinateurs :

Prof. Sabine Ludwigs — Professeur, Université de Stuttgart, Allemagne

Dr. Nicolas Stein — Maître de conférences, Université de Lorraine, France

“Nothing in life is to be feared, it is only to be understood. Now is the time to understand more, so that we may fear less.” — Marie Curie

Acknowledgements

First of all, It is my genuine pleasure to express my sincere gratitude to my PhD supervisor **Dr. Martin Brinkmann**, who was always there to help me with great patience and interest throughout these years. Over the course of the PhD, we had great scientific and personal discussions. Several ideas in this thesis were the outcomes of these scientific discussions. Joining his lab was the best decision of my life. Thank you so much Martin for giving me this opportunity and without your help, I would not accomplish this milestone.

I would also like to thank my co-supervisor **Dr. Laure Biniek** for her support and the time she devoted to my PhD, where we had a lot of discussions. Her suggestions and discussions helped me to improve my scientific skills. Laure was very helpful and was always there and ready to answer my countless questions.

I would like to thank **Dr. Nicolas Leclerc**, **Dr. Elena Zaborova** and **Pablo Durand** for providing the polymers and doping materials and for all the experimental support given during the revision of the manuscripts.

I would like to thank **Mr. Laurent Herrmann** for helping me with the Seebeck coefficient and electrical conductivity measurements.

I would like to thank **Dr. Mark Shmutz** and **Dr. Christian Blank** for their help and support with the transmission electron microscopic experements.

I thank **Dr. Bernard Lotz** for all his suggestions and advises during my PhD. It was an honor to work with you and I will always keep your words in my heart.

Also thank you **Dr. Thomas Heiser** and **Dr. Jerome Combet** for accepting our invitation to be the Jury members of my mid-thesis presentations.

To my fellow PhD students and group members **Marion Brosset, Huiyan Zeng** and **Viktoriia Untilova**, thanks for the pleasent time and friendship and I wish you all the very best and good luck to yourselves. Moreover I would like to note a special thanks to my friend **Marion** for helping me with all the French administrations and also for organizing and co-ordinating everything on the day of my PhD defence.

I would like to thank the young PhD student **Yuhan Zhong** for all the nice discussion we had during my second year of PhD. I wish you a great PhD ahead with lots of results.

To my previous PhD colleagues **Dr. Amer Hamidi-Sakr** and **Dr. Morgane Diebold** for the great discussions we had during the first years of my PhD. I have learned alot from both of you and thanks for helping me with the initial administration procedures upon my arrival in the lab.

To the rest of the people in **SYCOMMOR team** Philippe, Amparoo, Jean Philippe, Alain**,** Dominique and to the young PhD students Ricardo, Duncan and Quentin, big thanks for all your help and co-operation during these three years.

I would like to express my sincere thanks to **Mme. Odile Lemble**, who was always pleasant, approchable and willing to assist me for all the difficult french administration during these three years. Thank you so much Odile.

To the lunch group memebrs, Geevarghese, Fedir, Anasthasiia, Eualaie, Jean, Othmene, Vaibhav and Justine for all the fun and absurd lunch time discussions.

I wish to thank my primary and high school teachers to create an enthusiasm about science in me.

Also, I would like to thank **Dr. C. Vijayakumar** for his valuable guidance in CSIR-NIIST during my research assistantship work on hybrid thermoelectric materials .

I wish to thank my parents, **Vijayakumar** and **Sucheta**. Big thanks for your support and advice, even when I had this crazy idea to do a PhD abroad. I was always worried about both and missed alot during these three years.

Finally to my sweet wife **Anuja**, thank you so much for all the patience, understanding and the support throughout these 3 years- without you this would not have been possible !

Thanks to God almighty !

Table of contents

Abbreviations used in the text

ACN	Acetonitrile
AFM	Atomic force microscopy
Bi_2Te_3	Bismuth Telluride
Bu_4NPF_6	Tetrabutylammonium hexafluorophosphate
CMS	Charge modulated spectroscopy
CSA	Camphor sulphonic acid
CTS	Charge Transfer State
D	Diffusion coefficient
DD	Direct doping
DBSA	Dodecyl benzene sulphonic acid
DCM	Dichloromethane
DFT	Density functional theory
DSC	Differential scanning calorimetry
D_R	Dichroic ratio
EBSA	Ethyl-benzene sulphonic acid
EDX	Energy dispersive X-ray spectroscopy
Eg	Energy gap
EPR	Electron paramagnetic resonance spectroscopy
FFT	Fast Fourier Transform
F_4TCNQ	2,3,5,6-Tetrafluoro-7,7,8,8-tetracyanoquinodimethane

F_6TCNNQ	2,2-(perfluoronaphthalene-2,6-diylidene)-dimalononitrile
Fe $(TFSI)_3$	Ferric (iii) triflimide
Fe^{+3}-tos_3 .$6H_2O$	Iron(III) p-toluenesulfonate hexahydrate
$FeCl_3$	Ferric Chloride
FTS	Perflurooctyl-trichlorosilane
GIXD	Grazing X-ray diffraction measurement
HH	Head to head
HOMO	Highest occupied molecular orbitals
HOPG	Highly oriented pyrolytic graphite
HT	Head to tail
ICD	Incremental concentration doping
IE	Ionization Energy
IR	Infrared spectroscopy
KBrBz	Potassium 4-bromobenzoate
LUMO	Lowest unoccupied molecular orbitals
M_w	Molecular weight
M_n	Number average molecular weight
NaPSS	Sodium polystyrene sulfonate
N-DMBI	4-(2,3-Dihydro-1,3-dimethyl-1H-benzimidazol-2-yl)-N,N- dimethylbenzenamine
N-DPBI	4-(1,3-Dimethyl-2,3-dihydro-1H-benzoimidazol-2-yl)-N,N- diphenylaniline
OCL	Orientation correlation length
OFET	Organic field effect transistor

OP	Order parameter
PA	Polyacetylene
PDI	Polydispersivity index
P(NDI2OD-T_2)	Poly ([N,N-bis(2-octyldodecyl)-naphthalene-1,4,5,8-bis(dicarboximide)-2,6-diyl]-alt-5,5-(2,2-bithiophene))
P3BT	Poly (3-butylthiophene)
P3HT	Poly (3-hexylthiophene)
PBTTT	Poly(2,5-bis(3-alkylthiophene-2-yl)thieno[3,2-b]thiophene)
$PC_{71}BM$	Phenyl-C_{71}-butyric acid methyl ester
PDMS	Polydimethylsiloxane
PEDOT: PSS	Poly(3,4-ethylenedioxythiophene)polystyrene sulfonate
PF	Power factor
PFO	Poly(9,9'-dioctyl-fluorene)
P_{max}	Maximum power
POM	Polarized optical microscopy
PSCs	Polymer semiconductors
PTFE	Polytetrafluoroethylene
PDOPT	Poly(3-(4-octylphenyl)-2,2'-bithiophene)
$R_{internal}$	Internal resistance
R_{load}	External load
S	Seebeck coefficient
SCE	Standard calomel electrode
SEM	Scanning electron microscopy

STM	Scanning tunneling microscopy
SWCNT	Single walled carbon nanotube
TCB	1,3,5-trichlorobenzene
TCNQ	Tetracyanoquinodimethane
TEM	Transmission electron microscopy
Tos	Tosylate
TT	Tail to tail
VB	Valance band
ZT	Figure of merit
σ	Electrical Conductivity
κ	Thermal Conductivity
μ	Mobility
λ	Wavelength
τ	Characteristic doping time

Thesis Introduction

Thesis introduction

The energy demand of the world is increasing day by day. In particular, the world's electricity demand is steadily increasing from≈13 TW in 2012 to an expected 26 TW in 2050.[1] Currently, we are depending mainly on renewable energy sources such as sunlight, wind and tidal energies. They can be used repeatedly and are naturally replenishing sources of energy. The conversion efficiency of solar energy to useful electricity by solar panels and solar thermal plants is estimated as only 40%. More than 60% of global energy is wasted in the form of heat.[2][3] The conversion of waste heat to electricity may play an important role in our current challenge to develop alternative energy technologies to reduce our dependence on fossil fuels and reduce greenhouse gas emissions. Highly efficient thermoelectric materials can be one solution for converting this huge amount of waste heat to electricity. Inorganic materials such as silicides, Heusler alloys and metallic oxides are widely used for high temperature (>800K) thermoelectric applications. These materials provide excellent thermoelectric performances and are mainly composed of non-toxic elements.[4] Moreover, the situation below 500 K is different. The room temperature and commercially available thermoelectric generators are mainly composed of a special class of inorganic materials called chalcogenides. They are composed of highly toxic elements such as Lead (Pb). The high cost, toxicity and poor processability of these heavy elements limited their applications in various thermoelectric technologies[3].

The ability to convert conjugated polymers from insulating to highly conducting form triggered their use in different electronic applications such as organic field-effect transistors[5][6] (OFET), organic solar cells, organic light-emitting diodes[7] (OLED) and organic thermoelectrics[8]. Pioneering work by Heeger and coworkers on doped polyacetylenes stimulated the field of organic thermoelectrics (use of flexible polymers

as thermoelectric materials).[9] Unlike inorganic materials, these organic materials are characterized by their easy processability. They are composed of abundant elements such as carbon, nitrogen, sulphur and oxygen and they possess lower thermal conductivity (0.37 W m^{-1} K^{-1}) than inorganic materials.[10]. Moreover, they are flexible and they can be processed into large-area devices using suitable methods such as slot-die coating, inkjet printing, brush coating and roll-to-roll coating. Both, flexibility and easy processability of organic conducting polymers results in reduced production costs and lead to the production of cheap organic-based devices, which are now available on the market.

The field of organic thermoelectrics received considerable attention after the publication of the seminal work of Crispin[8] and coworkers on poly (ethylene dioxythiophene) (PEDOT). Crispin et. al[8] have shown that accurate control of the oxidation level combined with the low thermal conductivity of PEDOT can lead to high ZT values of ≈ 0.25 at room temperature. Such performance is good enough for thermoelectric device applications. This discovery triggered much interest, on TE polymers. Doped polythiophenes such as P3HT and PBTTT showed high thermoelectric (TE) performances due to their semi-crystalline or liquid crystalline nature[11][12]. Moreover, studies by Chabinyc[13] and coworkers proposed that the thermoelectric potential (PF) of a doped conducting polymer can be improved by increasing the conductivities of conjugated polymer from the relation $PF \propto \sigma^{1/2}$. Following this work, most of the studies on thermoelectric polymers focused mainly on improving the electrical conductivity of the doped polymers.

A similar approach was followed in the frame of this thesis. Our main focus was to improve the thermoelectric properties of conducting polymers by improving their crystallinity and by introducing long-range order and orientation. We used a method

called high temperature rubbing, which allows to align a large variety of conjugated polymers[14]. Sequential doping of the oriented thin films prepared by this approach produced highly conducting anisotropic films with high degrees of optical, structural and thermoelectric anisotropies. These highly anisotropic conducting polymer thin films are ideal model systems to probe the TE properties both parallel and perpendicular to the chains. They provided experimental evidence of the anisotropic charge transport mechanisms. Moreover, combining polarized UV-Vis-NIR spectroscopy and transmission electron microscopy (TEM) provided a better understanding of the location of the dopant anions in these oriented polythiophene thin films. A clearer picture of dopant induced structural changes in the polymeric unit cells was obtained from electron diffraction measurements.

The first chapter (**Chapter 1**) in my thesis is mainly dealing with the state of the art and basic concepts, which are relevant to my topic of research. The first section of this chapter is mainly dealing with general aspects of conjugated polymers such as their bonding, energy levels, chemical structure, crystal structure and different orientation methods. A short discussion about crystal structure, experimental evidence for the semi-crystalline nature of conventional regioregular P3HT and liquid crystalline PBTTT is included. The second part of the chapter is dealing with the basic principles and concepts of thermoelectricity. This is followed by a brief discussion about different doping methods used for doping conducting polymers. At the end of this chapter, we present the impact of doping on the crystal structure of PBTTT and P3HT. Finally, a summary of representative thermoelectric performances in p-doped polythiophenes PBTTT and P3HT is discussed.

In Chapter 2, we mainly investigate the impact of the side chain length of PBTTT (C_8, C_{12}, C_{14}, C_{18}) on the diffusion coefficients of the dopant anion 2,3,5,6-tetrafluoro-7,7,8,8-

tetracyanoquinodimethane (F_4TCNQ) into the side chain layers of PBTTT. Doping of polymer semiconductors such as PBTTT with acceptor molecules such as (F_4TCNQ) is widely used to tune the charge transport and thermoelectric (TE) properties in thin films. However, the mechanism of dopant insertion in the polymer matrix, the insertion kinetics and the ultimate doping levels were only marginally investigated. Electron diffraction measurements on these doped thin films showed that the Intercalation of F_4TCNQ into the layers of side chains of PBTTT results in an expansion of the lattice along the side chains and the contraction along the π-stacking direction for all polymers. The extent of lattice expansion decreases with increasing side chain length. UV-Vis-NIR spectroscopy demonstrates integer charge transfer for all investigated PBTTTs. The doping kinetics and final doping level depend on both the side chain length and packing. Highly disordered *n*-octyl and crystalline *n*-octyldecyl side chain layers tend to hamper dopant diffusion in the side chain layers contrary to *n*-dodecyl side chains that can host the highest proportion of dopants. Consequently, the best TE properties are observed for C_{12}-PBTTT films. Alignment of the polymers enhances significantly the TE performance by increasing the charge conductivity and the thermopower along the rubbing direction. Aligned films of C_{12}-PBTTT show charge conductivities of 193 S/cm along the rubbing direction and power factors of approx. 100 $\mu W.m^{-2}.K^{-1}$.

Chapter 3 compares the TE properties of P3HT and PBTTT upon doping with a strong oxidizing agent, namely $FeCl_3$. $FeCl_3$ doping of aligned films results in charge conductivities up to 2×10^5 S/cm and metallic-like thermopowers similar to iodine-doped polyacetylene. The films are almost optically transparent and show strongly polarized near infra red polaronic bands (dichroic ratio > 10).

The comparative study of structure-property correlations in P3HT and C_{12}-PBTTT identifies three conditions to obtain conductivities beyond 10^5 S/cm:

i) Achieve high in-plane orientation of conjugated polymers with a high persistence length ii) ensure uniform chain oxidation of the polymer backbones by regular intercalation of dopant molecules in the polymer structure without disrupting the alignment of π-stacked layers and iii) maintain a percolating nano-morphology along the chain direction.

The highly anisotropic conducting polymer films are ideal model systems to investigate the correlations between thermopower S and charge conductivity σ. A scaling law $S \propto \sigma^{-1/4}$ prevails along the chain direction but a different $S \propto -\ln\sigma$ relation is observed perpendicular to the chain direction, which was previously observed by Mateeva[15] et. al for stretch aligned polyaniline. This suggests two different charge transport mechanisms parallel and perpendicular to the polymer chains. The simultaneous increase of charge conductivity and thermopower along the chain direction results in a substantial improvement of thermoelectric power factors up to 2 $mW \cdot m^{-1} \cdot K^{-2}$ in C_{12}-PBTTT

Chapter 4 is a comparative study of the effect of F_6TCNNQ and F_4TCNQ doping on the crystal structure and thermoelectric properties of oriented C_{12}-PBTTT films. F_4TCNQ doping of organic semiconductors such as P3HT and PBTTT has been widely documented in the recent literature. This chapter focuses mainly on doping of C_{12}-PBTTT using a new doping agent, namely F_6TCNNQ. Unlike F_4TCNQ, F_6TCNNQ doping of polythiophenes has been marginally studied. This dopant is chosen because of its deeper LUMO energy level of -5.3 eV, versus -5.1 eV for F_4TCNQ, that can enhance charge transfer between C_{12}-PBTTT and F_6TCNNQ. Oriented C_{12}-PBTTT thin films are prepared by high temperature rubbing and sequentially doped with F_6TCNNQ using a new doping method, called "incremental concentration doping" (ICD). The ICD method implies that a given sample is doped by dipping it successively in dopant solutions of increasing concentration. ICD

of C_{12}-PBTTT using F_6TCNNQ leads to record electrical conductivities of 2430 S/cm and thermoelectric power factors (PF) 530±200 $\mu Wm^{-1}K^{-2}$ along the rubbing direction. Moreover, this method leads to a higher electrical conductivity than the conventional doping method (direct doping). This study demonstrates that a progressive intercalation of dopants in PBTTT crystals using the ICD method helps preserve the high level of order initially present in the aligned C_{12}-PBTTT films.

The diffusion coefficients of both F_6TCNNQ and F_4TCNQ anions have been determined using the doping kinetics followed by UV-Vis NIR spectroscopy. A lower diffusion coefficient is observed for F_6TCNNQ anions, demonstrating the size dependence of diffusion coefficients into the polymer matrix. The longer and bulkier the anion, the lower its diffusion coefficient. Polarized UV-Vis-NIR spectroscopy on these doped thin films showed that F_6TCNNQ^- anions are better oriented in the layers of the alkyl side chains as compared to F_4TCNQ. The estimation of charge carrier mobilities indicates that ICD leads to higher mobilities than DD. The lower degree of ordering of F_4TCNQ^- anions produced lower electrical conductivity than F_6TCNNQ doped C_{12}-PBTTT thin films.

Bibliography

[1] O. Bubnova, X. Crispin, *Energy Environ. Sci.* **2012**, *5*, 9345.

[2] M. G. Kanatzidis, *Chem. Mater.* **2010**, *22*, 648.

[3] M. Campoy-Quiles, *Philos. Trans. R. Soc. A Math. Phys. Eng. Sci.* **2019**, *377*, 20180352.

[4] D. Beretta, N. Neophytou, J. M. Hodges, M. G. Kanatzidis, D. Narducci, M. Martin-Gonzalez, M. Beekman, B. Balke, G. Cerretti, W. Tremel, A. Zevalkink, A. I. Hofmann, C. Müller, B. Dörling, M. Campoy-Quiles, M. Caironi, *Mater. Sci. Eng. R Reports* **2018**, DOI10.1016/j.mser.2018.09.001.

[5] H. Koezuka, A. Tsumura, T. Ando, *Synth. Met.* **1987**, *18*, 699.

[6] H. Sirringhaus, T. Kawase, R. H. Friend, T. Shimoda, M. Inbasekaran, W. Wu, E. P. Woo, *Science (80).* **2000**, *290*, 2123 LP.

[7] J. H. Burroughes, D. D. C. Bradley, A. R. Brown, R. N. Marks, K. Mackay, R. H. Friend, P. L. Burns, A. B. Holmes, *Nature* **1990**, *347*, 539.

[8] O. Bubnova, Z. U. Khan, A. Malti, S. Braun, M. Fahlman, M. Berggren, X. Crispin, *Nat. Mater.* **2011**, *10*, 429.

[9] H. Shirakawa, E. Louis, A. MacDiarmid, C. Chiang, J. Heeger, *J.C.S Chem. Comm* **1977**, *13*, 578.

[10] R. Kroon, D. A. Mengistie, D. Kiefer, J. Hynynen, J. D. Ryan, L. Yu, C. Müller, *Chem. Soc. Rev.* **2016**, *45*, 6147.

[11] M. Brinkmann, J.-C. Wittmann, *Adv. Mater.* **2006**, *18*, 860.

[12] I. McCulloch, M. Heeney, C. Bailey, K. Genevicius, I. MacDonald, M. Shkunov, D.

Sparrowe, S. Tierney, R. Wagner, W. Zhang, M. L. Chabinyc, R. J. Kline, M. D. McGehee, M. F. Toney, *Nat. Mater.* **2006**, *5*, 328.

[13] A. M. Glaudell, J. E. Cochran, S. N. Patel, M. L. Chabinyc, *Adv. Energy Mater.* **2015**, *5*, 1401072.

[14] L. Biniek, S. Pouget, D. Djurado, E. Gonthier, K. Tremel, N. Kayunkid, E. Zaborova, N. Crespo-Monteiro, O. Boyron, N. Leclerc, S. Ludwigs, M. Brinkmann, *Macromolecules* **2014**, *47*, 3871.

[15] N. Mateeva, H. Niculescu, J. Schlenoff, L. R. Testardi, *J. Appl. Phys.* **1998**, *83*, 3111.

[16] Y. Karpov, T. Erdmann, M. Stamm, U. Lappan, O. Guskova, M. Malanin, I. Raguzin, T. Beryozkina, V. Bakulev, F. Günther, S. Gemming, G. Seifert, M. Hambsch, S. Mannsfeld, B. Voit, A. Kiriy, *Macromolecules* **2017**, *50*, 914.

Chapter 1. Fundamental concepts & state of the art

This chapter is dedicated to the fundamental concepts and literature survey, that are relevant to this PhD thesis. The chapter is divided in two sections. The first section mainly focuses on the general aspects of conjugated polymers such as their bonding, energy levels, chemical structure, crystal structure and different orientation methods. A short description of the crystal structure and experimental evidence for the semi-crystalline nature of conventional regioregular P3HT is briefly introduced. Similarly, the crystal structure and experimental evidence for the thin film microstructure of PBTTT is also included. Later, a brief description of different polymer orientation techniques such as rubbing, strain alignment, friction transfer and epitaxy are discussed.

The second part of this chapter is mainly dealing with the thermoelectric properties and doping of polythiophene thin films. A short introduction and discussion of thermoelectric parameters such as electrical conductivity, Seebeck coefficient and power factors are provided. It is followed by a brief summary of different chemical doping methods used for polythiophenes e.g. solution doping, sequential doping, vapor phase doping. The consequence on the resulting thermoelectric properties is discussed. At the end of this chapter, we present the impact of doping on the crystal structure of PBTTT and P3HT. Finally, a summary of representative thermoelectric performances in p-doped polythiophenes PBTTT and P3HT is given.

1. General aspects of conjugated polymers

1.1. Energy level design of conjugated polymers.

Conjugated polymers are organic macromolecules; they are characterized by a conjugated backbone with alternating double and single bonds. They have been the focus of enormous attention in the industrial and academic sector for various optoelectronic applications.[1] The main interest of conjugated polymers stems from the π electron cloud. π electrons in the double bonds can be delocalized over several monomeric units in the polymer chains. Because of this electron delocalization from one monomer to another monomer, they have the ability to conduct electrical charges mainly along the conjugated backbone.

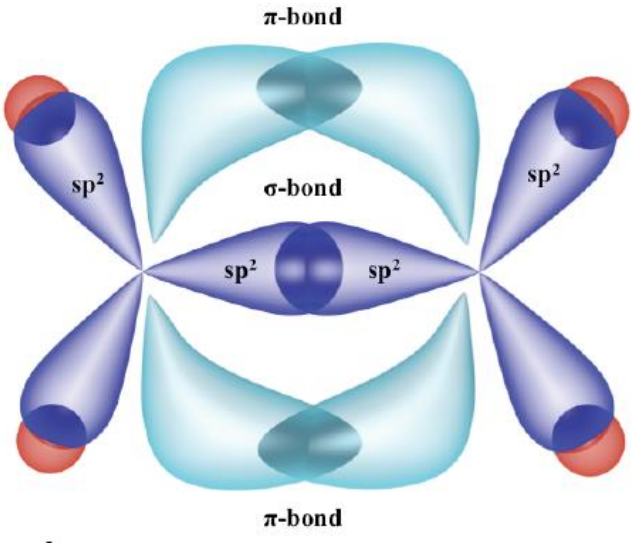

Figure 1.1. *Schematic illustration of bonding and hybridization in ethylene molecule. Reproduced from (2)*

Let us consider the simplest case of the ethylene molecule. The ground state electronic configuration of the carbon atom is $1S^2\ 2S^2 2P^2$. In the case of ethylene, the carbon atom is in sp^2 hybridization and hence one electron in the 2S orbital can be promoted to the vacant P orbital. Now the excited state configuration of the carbon atom become $1S^2\ 2S^1 2P^3$. The electrons in the 2S, $2P_x$ and $2P_y$ orbital undergo sp^2 hybridization, which gives rise to three hybridized orbitals. Two of these three orbitals overlap with 2 hydrogen

atoms, which results in two carbon-hydrogen sigma bonds and the third orbital can be used to form a sigma bond with the next $-CH_2$ units, resulting in a C-C sigma bond in ethylene. The unused $2P_Z$ orbitals undergo sidewise overlapping which produces the π bond in the ethylene molecule (see figure 1.1). The sidewise overlap of the $2P_Z$ orbitals results in a restricted rotation along the bond axis and gives rise to a planarized and stiff polymeric backbone.[2] The electrons present in the overlapped P_z orbitals do not belong to one single bond but are delocalized over several atoms. The length scale of delocalization of these π electrons is the conjugation length.

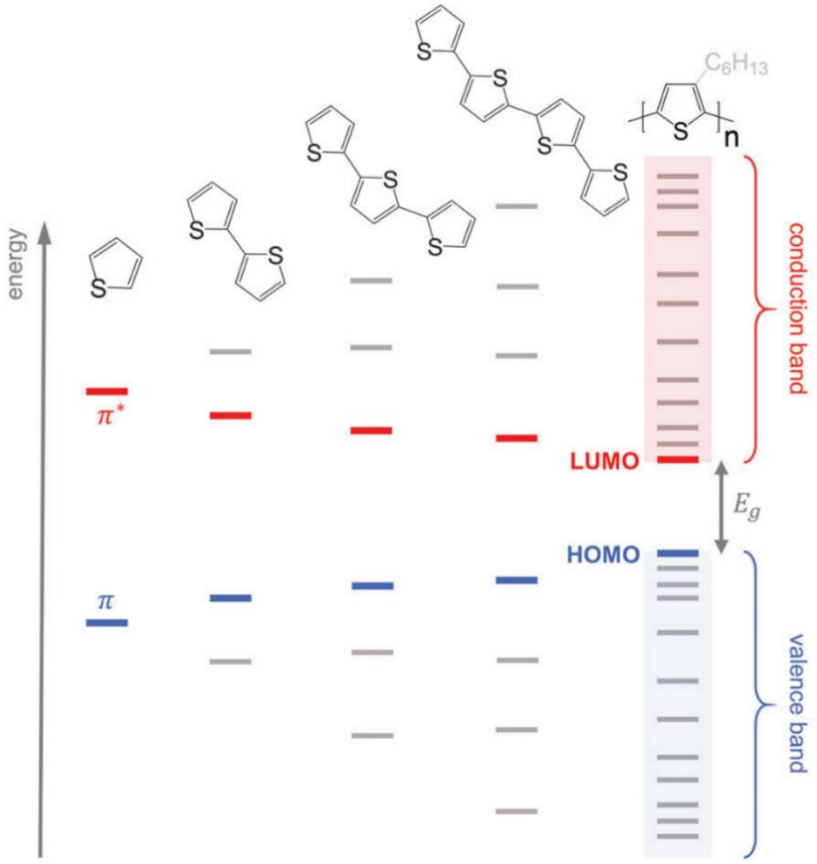

Figure 1.2. *Evolution of HOMO and LUMO levels and the bandgap (E_g) with an increasing number of thiophene repeating units and the resulting valence and conduction bands in polythiophene. Reproduced from (3)*

The presence of alternating double and single bonds in conjugated polymers is responsible for the semiconducting properties of conjugated polymers. The smallest identical repeating unit of a polymer is called a monomer.

During polymerization reactions, the chemical coupling of the monomers leads to orbital interactions and hence it results in an energy level splitting of the π (bonding) and π* (antibonding) orbitals. The π (bonding) orbitals are known as the highest occupied molecular orbitals (HOMO) and π* orbitals are known as the lowest unoccupied molecular orbitals (LUMO).[3] The valence band is arising from the π orbitals while the π* orbitals form the conduction band (see figure 1.2). The energy gap between the HOMO and LUMO is the bandgap (E_g). The bandgap of a polymer depends on its chemical structure and on the extent of conjugation. The longer the conjugation length, the smaller the bandgap. The sigma bond between the monomer preserves the structure of the molecule. The electrons in the π orbitals are free to undergo electronic and optical excitation and the charges can be delocalized along the polymer chains.

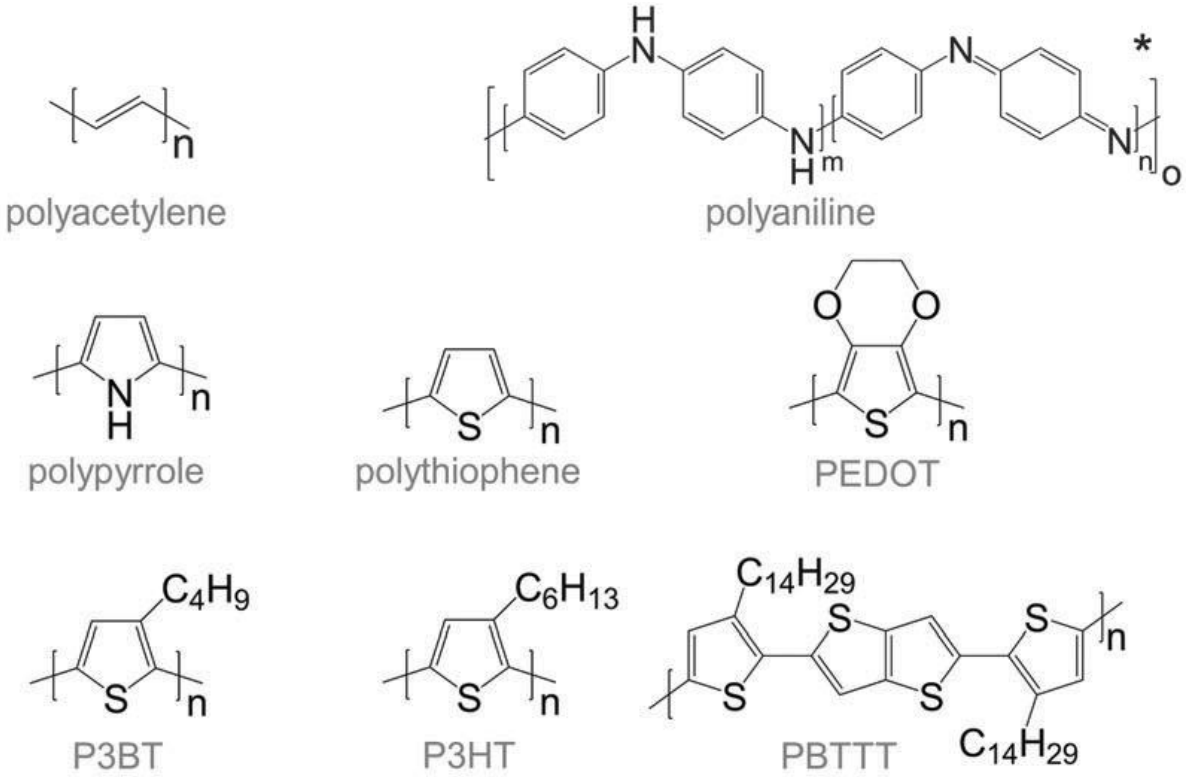

Figure 1.3. *Chemical structures of most commonly used conjugated polymers. Reproduced from (3)*

The conjugated polymers are semiconductors or insulators in their intrinsic form and they can be converted to a conductor via doping. In 1977, Heeger and coworkers

reported high conductivity in iodine-doped polyacetylene.[4][5] Although doped polyacetylene has limited commercial applications, its discovery led to major developments in the field of organic electronics. Soon after the discovery of doped polyacetylene, extensive research work was carried out on other conducting polymers such as polythiophenes, polyanilines and polypyrroles (see figure 1.3) for different industrial and scientific applications.

1.2. P3HT: The working horse among organic semiconductors

Soluble semi-conducting polymers attracted wide attention from the scientific community because of their excellent semiconducting properties and easy solution processability. This made them excellent candidates for flexible electronic devices prepared by roll-to-roll manufacture at low cost. Among semi-conducting polymers, regio-regular poly (3-hexylthiophene) (P3HT) is one of the most popular polymers as it combines unique crystalline and optoelectronic properties. The first synthesis of unsubstituted polythiophene was reported by Lin and coworkers in 1980.[6] This discovery was followed by highly conducting Iodine doped thin films of these unsubstituted thiophenes by Yamamoto et al.[7]

Alkyl side chains were introduced on the polymeric backbone to help solubilize the polymer in common organic solvents.[7][8] Introduction of alkyl side chains on polythiophene gives rise to three main regio isomers that differ in the position of the coupling between two successive monomers. The term “regio regularity” indicates the control of the configuration of the hexyl side chains. Depending on the position of the hexyl side chain, different regioisomers can be found in P3HT. The HH (head to head) regioisomer is produced by the coupling of two monomeric units through 2,2 position. The 2,5 coupling leads to the HT (head to tail) isomer and 5,5 coupling leads to the TT (tail to tail) isomer. The different monomers are represented in figure 1.4. Yamamoto

and coworkers were the first to predict the existence of regioisomers in P3HT. The isomer with HT-HT coupling is called regioregular (rr) isomer.

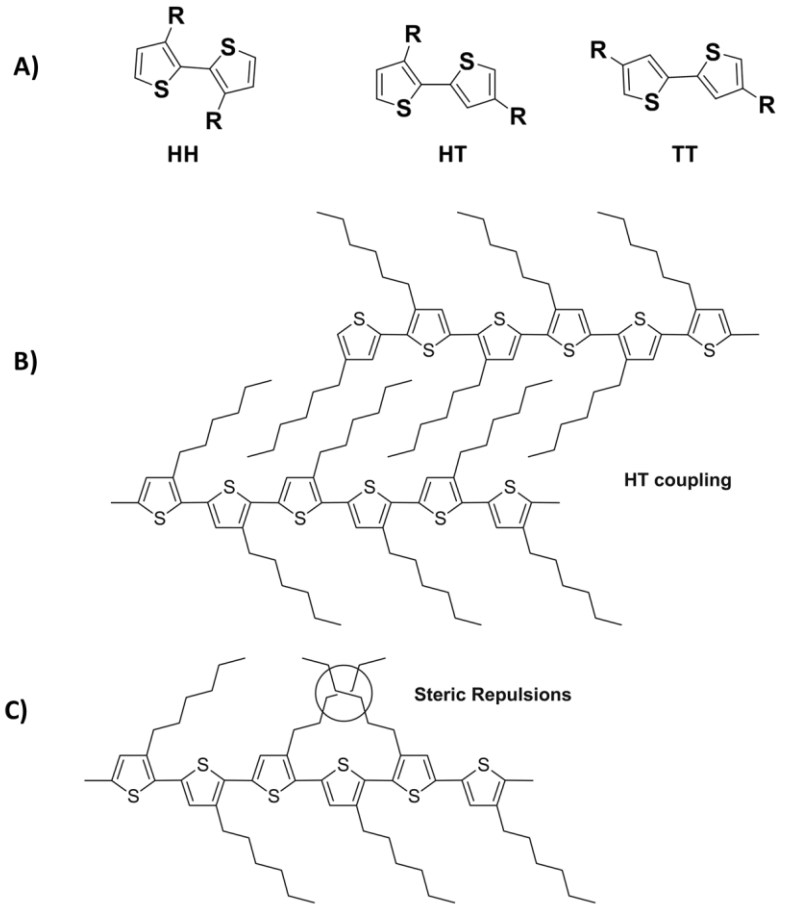

Figure 1.4. *A) Structures of possible coupling in 3-alkylthiophene dimers. B) Solid-state packing of HT coupled P3HT. C) Steric repulsion in P3HT as a result of the irregular coupling of monomers. Reproduced from (8)*

The HH and TT isomers are regioirregular isomers. In a fully regioregular P3HT chain, all the monomeric units are coupled in head to tail manner.[8] In regioirregular P3HT (HH and TT coupling), the steric repulsions between the adjacent alkyl side chains in the monomeric units can produce twists in the polymeric backbone. Such twisting reduces the conjugation length and packing efficiency and finally leads to poor optical and electrical properties. The rr-configuration produces thin films of P3HT with very high crystallinity. The high crystallinity is a key parameter for various optoelectronic and charge transport applications.

rr-P3HT has a very high HOMO level (-5.1 eV) and possesses a bandgap of 2 eV. Highly crystalline P3HT was one of the first polymers to show high mobilities of 0.1 $cm^2/V.s$ in field-effect transistors[9]. The main advantage of P3HT is that it can be crystallized very easily from the solution to produce well-oriented crystals of large size. However, the grain boundaries are detrimental for charge transport and mobility. Depending on the processing method, different morphologies were obtained in P3HT. Crossland and coworkers were able to obtain a high FET mobility of 0.1 $cm^2/V.s$ in films with spherulitic P3HT.[10] The high FET mobility was obtained due to the reduction in the grain boundaries as a result of precise control of the nucleation and growth of anisotropic spherulitic structures in P3HT. Most interesting optical and charge transport properties in P3HT derived from its high crystallinity.

Single crystals were also obtained from P3HT. Similar to inorganic semiconductors, P3HT is also characterized by a crystal lattice (monoclinic form I) with well-defined unit cell parameters[11]. Unlike inorganic crystals, single crystals of P3HT show high anisotropy in optical and electrical properties. For example, charge transport along the chain direction (c axis) is higher than that along the π stacking (b axis) direction (see figure 1.5 A). The poorest charge transport is along the alky side chain direction (a-axis). P3HT slowly emerged as a benchmark semiconductor polymer due to its easy synthesis procedure, solution processability and highly crystalline microstructure. More detailed investigations of the microstructure and transistor performance of P3HT provided important guidelines for the design of new polymer semi-conductors with enhanced device performance.[9][12,13] [14–17]

2. Semi-crystalline P3HT- lamellar morphology

Many conjugated polymers are semi-crystalline in nature, which means that they consist of ordered polymer chains in the crystalline regions while the chain ends and chain folds

are mainly present in the amorphous parts of the polymer. So-called tie chains connect adjacent crystals through the amorphous regions of the polymer. Chain folding is an inherent nature of semi-crystalline polymers. The lamellar morphology of the polymer is mainly produced due to the crystallization mechanism. During crystallization, some of the chains tend to align in a specific manner and create ordered regions in the form of lamellar crystals or fibrils. The chain ends and chains folds cannot be accommodated in the crystals and are rejected to the amorphous phase of the semi-crystalline polymer. Hence, the lamellar structure implies a regular alternation of crystalline regions with ordered chains and amorphous regions with chain folds, chain ends, and chemical defects. The chain folding of poly(alkylthiophenes) was first revealed in the initial work of Mena – Osteritz, and coworkers. They were able to observe chain folding in regioregular poly(alkylthiophenes) prepared by epitaxial orientation on highly oriented pyrolytic graphite (HOPG) using scanning tunnelling microscopy (STM).[12,13] STM studies evidenced the existence of chain folds in regioregular polythiophenes and also evidenced the interdigitation of the alkyl side chains (see figure 1. 6 A and B).

Further evidence for the semi-crystalline structure in P3ATs was obtained by Brinkmann et al. using transmission electron microscopy (see figure 1.5 B). [14–17]. Transmission electron microscopic studies by Brinkmann and Rannou on epitaxially oriented P3HTs determined the molecular weight (M_n) for which the chain folding occurs. They proposed that chain folding occurs for $M_n \geq 7.3$ kDa. The presence of chain folding at higher molecular weight leads to a saturation of the lamellar periodicity. Typically, a lamellar period of 28 nm is observed when $M_n \geq 18.8$ kDa. Lower molecular weight fractions form a crystalline phase without chain folds i.e. extended chain crystals. As the molecular weight increases, the number of chain folds inside the amorphous zones increases and the polymer becomes semi-crystalline. Moreover, another interesting observation is the increase in lattice parameter ($\mathbf{a_{P3HT}}$) with the increase in molecular weight of the

polymer[18]. As the number of chain folds increases in the amorphous zones, chains re-enter the crystalline part of the lamellae and exert a stress on the crystalline lattice i.e. increases the separation along the alkyl side chains.[17,19,20]

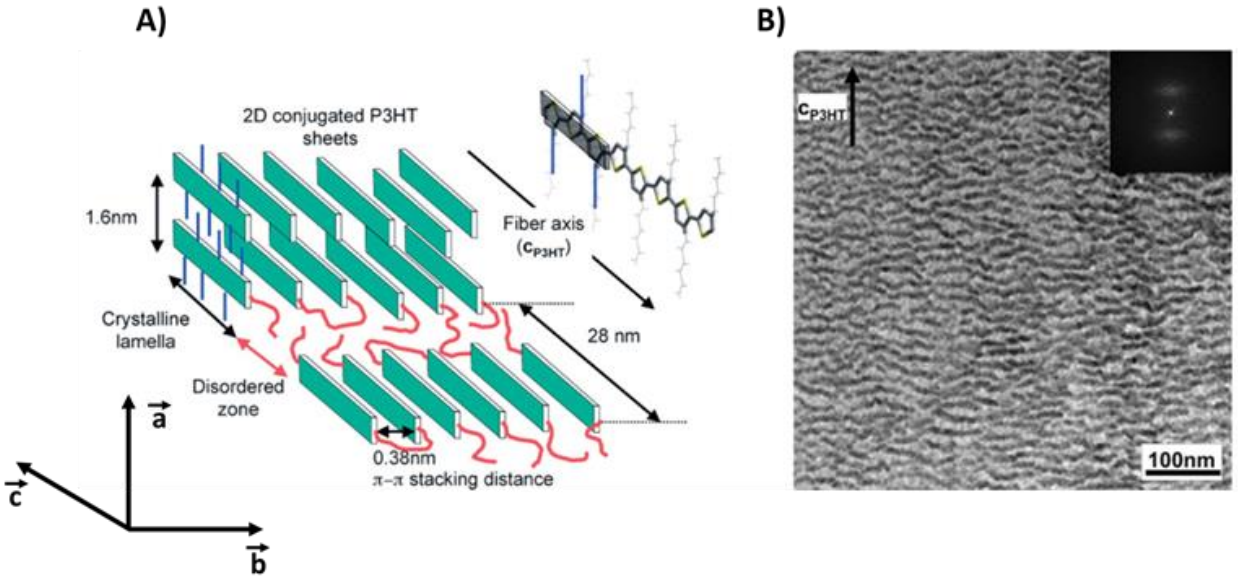

Figure 1.5. *A) Schematic representation of the semi-crystalline morphology observed in an oriented P3HT film. B) Corresponding bright-field transmission electron microscopy image showing alternating crystalline and amorphous regions. A lamellar periodicity of 28 nm was obtained from the fast Fourier transform (FFT), which is shown in the inset. Reproduced from (14)*

Apart from the molecular weight and regio regularity, the crystallinity and morphology of P3HT thin films can also be affected by processing conditions. The crystallization kinetics is an important factor that determines the crystallinity of a thin film. It has been observed that the polymer thin films deposited from higher boiling point solvents had higher crystallinity than the films deposited from low boiling solvents. For example, solution-processed thin films cast from chlorobenzene showed higher crystallinity than the films prepared from chloroform. This indicates that slower solvent evaporation is beneficial for higher crystallinity in solution-processed thin films.[21–23] Film deposition conditions can also affect the crystallinity of thin films. It has been reported that fast

spin coating gives rise to less crystalline films than a slow drop-casting. The crystallinity and morphology of the thin films can be tuned by changing the molecular weight, processing conditions, solvent.

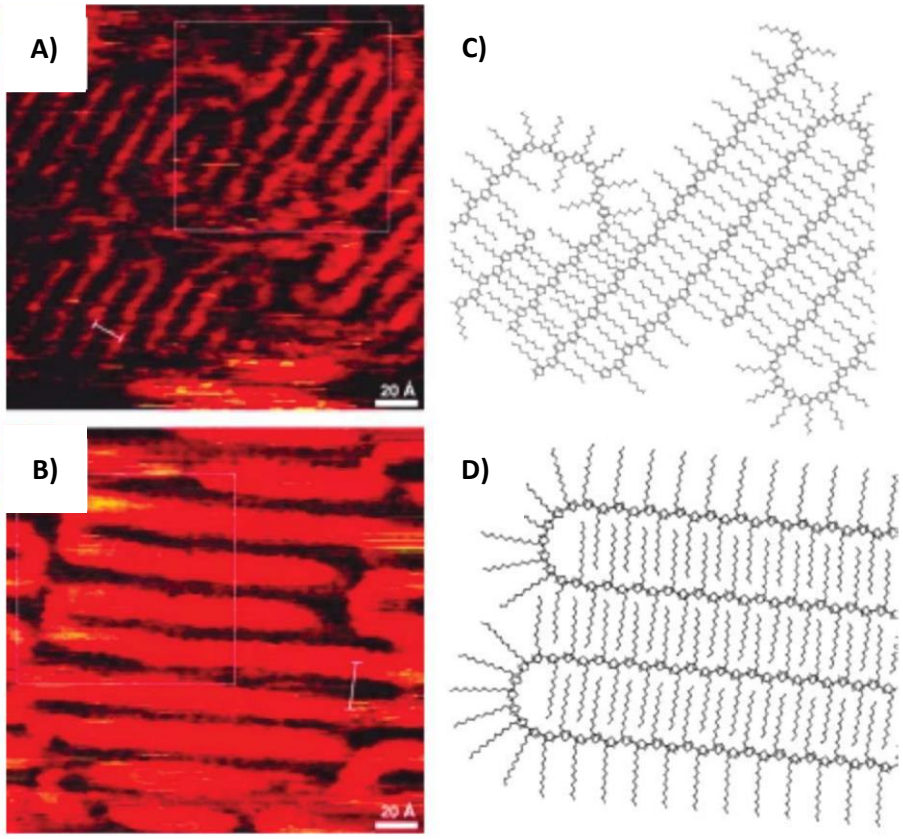

Figure 1.6. *A&B) STM images showing chain folding in regioregular poly(alkyl thiophenes) epitaxially oriented on HOPG. The 2D crystalline packing C) and D) are obtained after modelling using semi-empirical calculations. Reproduced from (12&13)*

Since our main focus of the thesis is to study the orientation and the anisotropic thermoelectric properties, the subsequent discussion is limited to the relevant crystal structures and orientation techniques of polymers.

2.1. Crystal structure of P3HT

As discussed earlier, regioregular poly (3-hexylthiophene) (rr-P3HT) is one of the most studied semi-crystalline polymers. Since it has high levels of crystallinity, the crystal structure of P3HT was an interest for crystallographers. Several studies helped to

elucidate the crystal structure of P3HT. In 1992, Prosa and coworkers reported a structural model for P3HT, which consists of well-defined "lamellae" made of π-stacked polymer backbones uniformly spaced by the layers of hexyl side chains.[24] Two polymorphs were identified: form II has interdigitated side – chains contrary to form I, that is dominant in thin films used in devices.

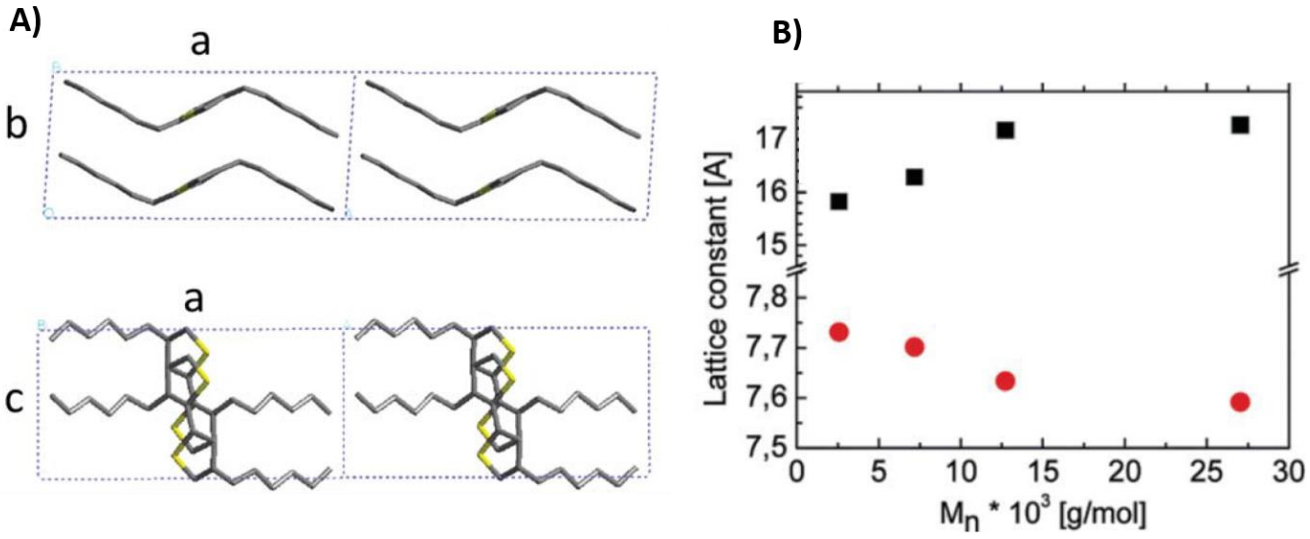

Figure 1.7. *A) Representation of the crystal structure of P3HT form I proposed by Kayunkid and coworkers. Fig B) represents the evolution of lattice parameters as a function of molecular weight. Reproduced from (11&18)*

An important structural refinement of form I P3HT was performed by Tashiro et. al[25] in 1997. The structural model was refined from X-ray data obtained on stretch-aligned P3HT films. Molecular modelling, polarized FTIR and Raman spectroscopy were combined to propose various models. One of the models implies an orthogonal unit cell with lattice parameters a= 16.63 Å, b= 7.75 Å, and c = 7.77 Å. Tashiro et. al proposed various structures that contain a different number of polymer chains in the unit cell. However, they were not able to discriminate between different possible models based on the results of X-ray diffraction.

Later in 2010, Brinkmann and coworkers proposed a new structural model for P3HT (form I) based on electron diffraction measurements on epitaxially oriented P3HT films

from trichlorobenzene.[11] According to this model, P3HT crystallizes in a monoclinic unit cell (see figure 1.5 A) with lattice parameters a= 16.6 Å, b= 7.8 Å, and c = 7.8 Å, γ = 86.5 °, a is the direction along the alkyl side chains ($\mathbf{a_{P3HT}}$), b is the direction along the π-π stacking ($\mathbf{b_{P3HT}}$) and c is the direction along the polymeric backbone ($\mathbf{c_{P3HT}}$). From the electron diffraction studies and crystallographic calculations, Kayunkid[11] et. al predicted that the unit cell of P3HT contains 4 thiophene monomers. One chain is shifted with respect to the second chain along the c axis (see figure 1.7 A). The shift along the backbone is produced as a result of crystallization of the hexyl side chains into an orthogonal sublattice.[11] Moreover, they were able to assign a new space group $P2_1/c$ for the proposed structure. In the scope of this thesis, we used the P3HT crystal structure proposed by Kayunkid[11] and coworkers.

3. Liquid – crystalline polymers with enhanced structural order

Structure-property studies on P3HT provided important guidelines for the design of new polymer semiconductors with enhanced efficiency. The hexyl thiophene monomer lacks a centre of symmetry and this limits the various polymerization techniques to produce highly regioregular polymers, which is necessary to obtain highly crystalline films.[26,27]Also, the delocalized π-electron system of P3HT is susceptible to various oxidation reactions. Thirdly the high side-chain density of P3HT prevents the interdigitation and reduces the long-range order in the polymer. Because of these limitations, new polythiophenes, mainly thienothiophene-based polymers were designed.

In 2006, McCulloch and coworkers reported very high mobilities of 0.2 to 0.6 $cm^2/V.s$ for a new class of liquid crystalline polymers Poly(2,5-bis(3-alkylthiophene-2-yl)thieno[3,2-b]thiophene) (C_n-PBTTT).[28] It is a copolymer of thieno[3,2-b]thiophene and 4,4-dialkyl 2,2-bithiophene monomer units (see figure 1.8).In comparison to P3HT, the density of

the alkyl side chains is large in P3HT with respect to PBTTT since the thienothiophene bears no side chains. In addition, the electron delocalization from the thienothiophene ring to the backbone of the polymer is less energetically favourable because of the high resonance stability of the thienothiophene unit. This reduced electron delocalization and the limited inductive effect of the alkyl side chain (+I effect) reduces the electron delocalization and lowers the HOMO of PBTTT.[28,29]

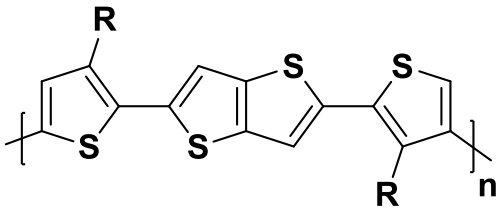

Figure 1.8. *Chemical structure of Poly(2,5-bis(3-alkylthiophene-2-yl)thieno[3,2-b]thiophene)*

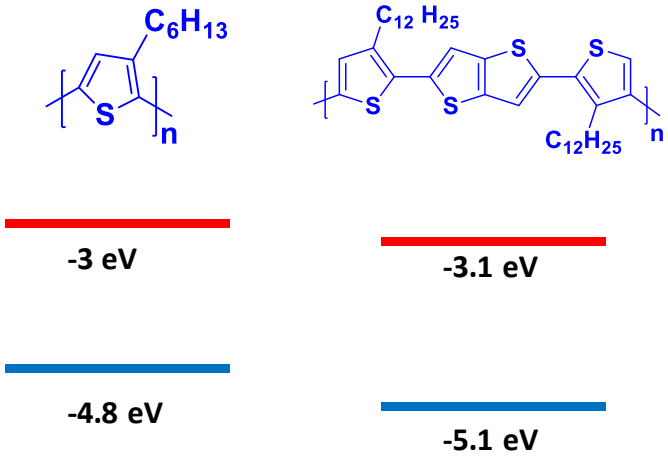

Figure 1.9. *Chemical structure and HOMO – LUMO energy levels of P3HT and Poly(2,5-bis(3-alkylthiophene-2-yl)thieno[3,2-b]thiophene)*

The increase in ionization energy (IE) with respect to P3HT is consistent with a redshift of 20 nm in the absorption maxima of PBTTT (see figure 1.9). It has been found that the polymer backbone of PBTTT is more rigid than P3HT and it can go through a liquid crystal phase transition around 140 °C. PBTTT can form ordered domains with planarized backbones over a distance of 100 nm.[28] in 2007, Hamadani and coworkers reported

impressive hole mobilities of 1 cm^2/V.s in undoped Poly (2, 5-bis(3-tetradecylthiophene-2-yl)thieno[3,2-b]thiophene) (C_{14}-PBTTT). Moreover in 2008, Kumada and coworkers reported mobilities of 1 cm^2/V.s in Poly(2,5-bis(3-hexadecyldecylthiophene-2-yl)thieno[3,2-b]thiophene) (C_{14}-PBTTT).[30] Such high mobilities observed in PBTTT indicate that a high degree of structural order in conjugated polymers is essential for the application of polymers in organic electronics

3.1. Crystal structure of PBTTT

The thin film microstructure of PBTTT was investigated quite intensively because of its excellent performance in thin-film transistors. Simple models of crystalline structure of PBTTT were proposed by McCulloch and coworkers in 2006.[28] Synchrotron X-ray scattering studies on annealed C_{12}-PBTTT gave evidence for the lamellar structure of this family of polymers.

X-ray scattering studies provided evidence for a highly ordered lamellar structure (see figure 1.10) characterized by numerous h00 reflections (out-of-plane) which are representative of the interlayer separation along the alkyl chains of PBTTT **(a_{PBTTT})**. The obtained d_{100} spacing for the first order interchain separation along the alkyl chain is equal to 19.6 Å in C_{12}-PBTTT. The intensity of the d_{100} reflection was enhanced by annealing at a higher temperature. However, there was no clear evidence for the interdigitation and tilting of side chains. It can be either interdigitated or closely packed without interdigitation and tilted with respect to the plane of the backbones. The (0k0) peaks in the in-plane scan is a fingerprint of the π-stacking (3.72 Å). Moreover, the (00l) reflections are representative of the periodic order along the chain direction (c=13.5 Å). These results proved the existence of highly ordered crystalline domains in the C_{12}-PBTTT polymer. C_{12}-PBTTT films showed mobilities of 0.2 to 0.6 cm^2/V.s and mobilities of 0.7 cm^2/V.s were obtained for the corresponding C_{14}-PBTTT. These mobilities are about one

order of magnitude larger than that of P3HT because of the enhanced structural order. Structural order in the polymer is significantly enhanced by annealing the liquid crystalline phase.

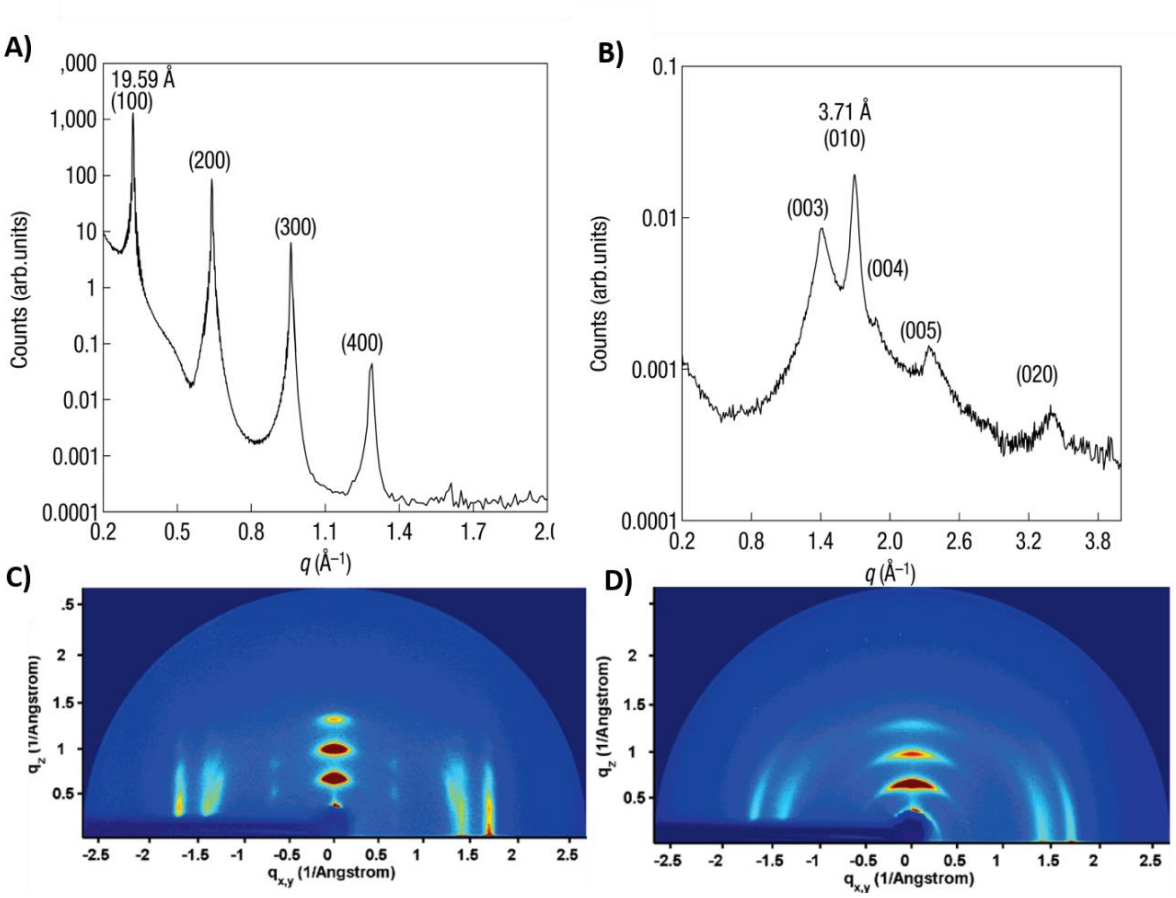

Figure 1.10. *A&B) out of plane and in-plane scattering from C_{12}-PBTTT. Figure (C&D) grazing incident X-ray scattering from C_{12}-PBTTT.C) as spun C_{12}-PBTTT D) annealed (180 °C) C_{12}-PBTTT on OTS/SiO_2 substrate. Reproduced from (28&31)*

Chabinyc and coworkers proposed a more detailed investigation of the crystal structure of PBTTT in 2007. They investigated the substrate effect on crystal structure and charge mobilities of PBTTT.[31] It has been previously demonstrated that for P3HT, the crystalline domains in the thin films can nucleate from the film/substrate interface. These results proved the importance of the interfacial interactions on the thin film microstructure.[32] Chabinyc and coworkers observed high mobilities of (0.2 to 0.5 $cm^2/V.s$) on silicon

dioxide dielectrics, which were treated with alkyl trichlorosilane. However, poor mobilities (0.005 $cm^2/V.\ s$) were observed on bare silicon dioxide.

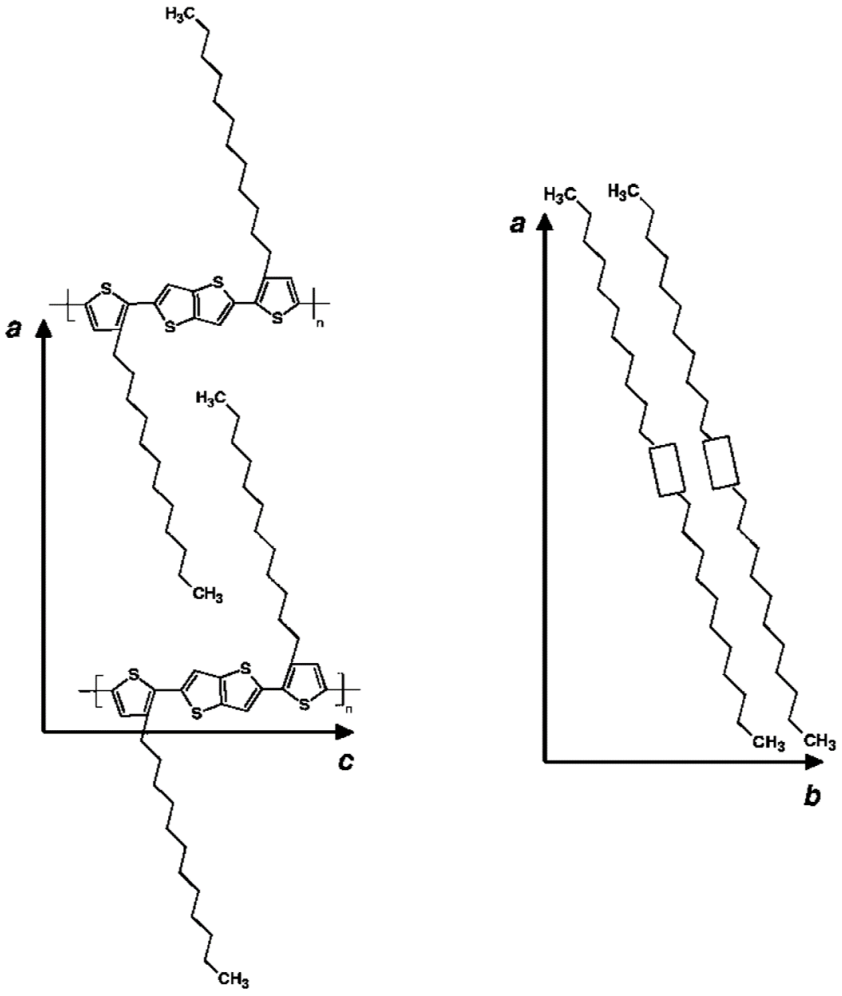

Figure 1.11. *Simple packing model of C_{12}-PBTTT based on X-ray scattering data. The lamellar stacking due to the alkyl side chains can be seen along the **a**-axis, π- stacking occurs along **b**-axis, and **c** is the chain direction. Alkyl side chains are interdigitated. Reproduced from (31)*

X-ray scattering studies of C_{12}-PBTTT and C_{14}-PBTTT polymers on trichlorosilane-coated silicon dioxide produced similar X-ray scattering patterns as observed by McCulloch and coworkers in 2006.[28] For both polymers, the lamellar stacking was observed along the (q_z) direction while the peaks along the (q_{xy}) direction contain the 003 and 010 peaks: crystals were oriented edge-on the substrate. The interplanar spacing (d_{003}) and (d_{010}) were nearly the same for both C_{12}-PBTTT and C_{14}-PBTTT, but a larger d_{100} spacing was

observed for C_{14}-PBTTT than for C_{12}-PBTTT. Based on X-ray scattering studies, a simple packing model was proposed for PBTTT. This model suggests interdigitation of alkyl side chains (see figure 1.11).

A)

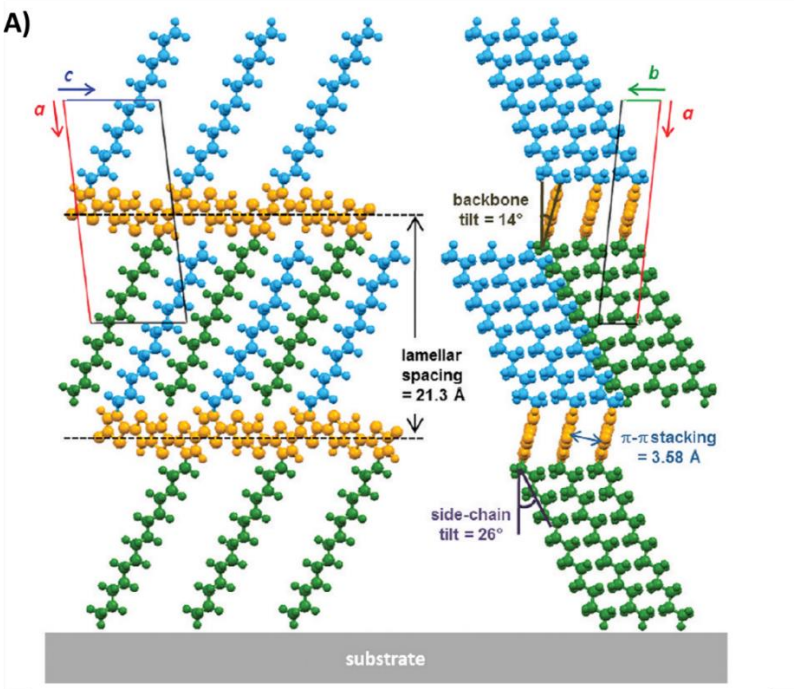

B)

	PBTTT-C_{12}	PBTTT-C_{14}	PBTTT-C_{16}
lattice parameters			
a (Å)	19.6	21.5	23.5
b (Å)	5.4	5.4	5.4
c (Å)	13.5	13.5	13.5
α (°)	137	137	137
β (°)	85	86	87
γ (°)	86	89	92
lamellar spacing (Å)	19.1	21.3	23.5
π-stacking distance (Å)	3.54	3.58	3.62
backbone tilt angle (°)	16	14	10
side-chain tilt angle (°)	25	26	27

Figure 1.12. *A) Simulated model representing the packing in C_{14}-PBTTT viewed along the b and c- axes. The polymer backbone is shown in orange. The alkyl side-chains are shown in blue and green. B) Structural parameters as a function of side-chain length in the simulated PBTTT unit cells. Reproduced from (33)*

Brédas and coworkers did a detailed investigation of the structure of PBTTT in 2012. The structural model of C_n-PBTTT (n=C_{12}, C_{14}, C_{16}, C_{18}) was obtained by a combination of experimental X-ray diffraction studies and computational modelling.[33] They proposed

a triclinic unit cell for C_{14}-PBTTT with lattice parameters a= 21.5Å, b=5.4 Å, c=13.5 Å, α=137°, β=86°=ϒ=89°. These parameters were consistent with the previous results from McCulloch on C_{12}-PBTTT. In addition to this, they demonstrated that the PBTTT backbone is planar and tilted by 14 ° to the substrate normal. The π- stacking distance was calculated as 3.58 Å. This short π - stacking distance leads to strong π overlaps. Alkyl side chains are highly interdigitated and form a lamellar structure with a d spacing of 21.3 Å. The side chains are tilted 26° to the conjugated backbone direction (see figure 1.12).

The alkyl side chain length is an important parameter, which can affect the structure and optoelectronic properties of a conjugated polymer.[34,35] Molecular models of the structure of C_{12}-PBTTT and C_{14}-PBTTT were proposed based on grazing incidence X-ray diffraction and molecular simulations. It has been observed that the size and shape of the simulated unit cell were slightly modified by increasing the length of the alkyl side chain from dodecyl (C_{12}) to hexyl decyl (C_{16}). The proposed packing determined by simulation was in a good agreement with the experimental data. The addition of two more methylene groups to C_{12}-PBTTT resulted in an increase of the lamellar spacing by 2 Å. Also, the angles β (the angle between c and a) and ϒ (angle between a and b) increase by 1° and 3° respectively. In the refined models, the alkyl side chains are interdigitated and form a very dense sublattice. The π- stacking distance remained constant in the range between 3.5 Å - 3.6 Å.[33] The band structure measurement of these polymers confirmed that the bandgap is independent of the side-chain length. The measured bandgap is equal to 2.2 eV for all polymers, which indicates that they must have similar electronic properties.

4. Controlling orientation of conjugated polymers

Polymer orientation is an interesting technique because the resulting oriented films show improved optical and electronic properties over non-oriented polymers. During

polymer orientation, randomly oriented polymer chains can be aligned or crystallized in a specific manner leading to improved anisotropic physical properties. Different polymer orientation techniques were developed for industrial and scientific applications. Depending on the method of orientation, different structures and morphologies can be produced, which affect the charge transport and optical properties.[10,14,36,37] Orientation techniques can be classified mainly in three families. The first family involves the use of shearing forces (Rubbing, Friction transfer) on the surface of the polymers. These forces can align the polymer chains in the direction of the applied forces. The second family of orientation methods involves the use of orienting substrates on top of which the polymers can nucleate and crystalize.

The third class of orientation methods rests on flow-orientation. The flow of a solution of polymers can lead to alignment of fibrillar nanocrystals of semiconducting polymers.[38] However, the efficiency of orientation depends on molecular weight and usually poor alignment is achieved for large M_w polymers.

4.1. Orientation by mechanical rubbing

Rubbing is an established method used for aligning polyimides layers and for the fabrication of liquid crystal displays.[39,40] This method was also used for aligning small molecules such as α-sexithiophenes.[41,42] The rubbing process involves the use of shearing forces on the surface of polymer films to align them in the direction of shearing. Usually, the procedure (see figure 1.13) involves the use of a rotating cylinder covered with a microfiber tissue, which can be translated over the conjugated polymer on a substrate maintained at a suitable temperature (see figure 1.13). In 2002, Heil and coworkers reported an enhancement of mobility in regioregular P3HT which was aligned by mechanical rubbing at room temperature.[43]They were able to prepare highly

oriented P3HT films with a dichroic ratio of 5.1 with 800 % enhancement of mobility with respect to non-oriented samples.

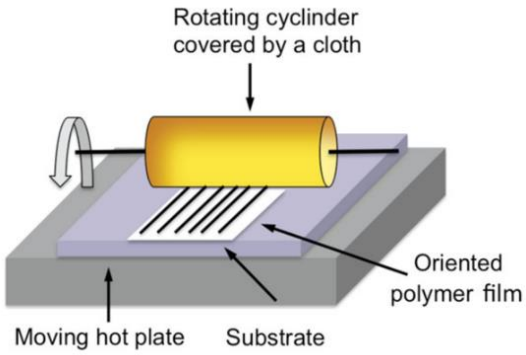

Figure 1.13. *Schematic illustration of the rubbing method. Reproduced from (36)*

From a structural point of view, more work on the orientation of P3HT was done by Brinkmann et. al in 2011.[43] Upon rubbing, the polymer chains were aligned in the direction of rubbing and crystals change the contact plane from edge-on to face-on with an increasing number of rubbing cycles (see figure 1.14). Polymer orientation was also studied as a function of molecular weight. A higher degree of chain orientation was observed for low molecular weight P3HT (≤ 7.9 kDa), while very poor orientation was observed for higher molecular weights (>50 kDa). The poor alignment of higher molecular weight fractions was observed due to the high degree of chain entanglement, which hindered the chain orientation. In addition to this, hole mobilities were also measured along the parallel and perpendicular directions to the rubbing for low M_w samples. It has been observed that the mobility was enhanced along the direction parallel to the rubbing and an anisotropy ($\mu_{//}/\mu_{\perp}$) of 20 was obtained. In most of the studies using rubbing, alignment was performed exclusively at room temperature.[39,40]

This rubbing technique was improved later in the Brinkmann group by introducing temperature as an additional parameter. Biniek[44] et. al applied high temperature rubbing to C_{12}-PBTTT in 2012 (see figure 1.15). A high degree of in-plane alignment was

observed in C_{12}-PBTTT by rubbing the polymer at a temperature in the range 75 °C ≤ T_R ≤125 °C.[44] It has been demonstrated that temperature is an important parameter for polymer orientation. The applied temperature helps to melt the alkyl side chains which imparts some plasticity to the film that can be easily aligned.

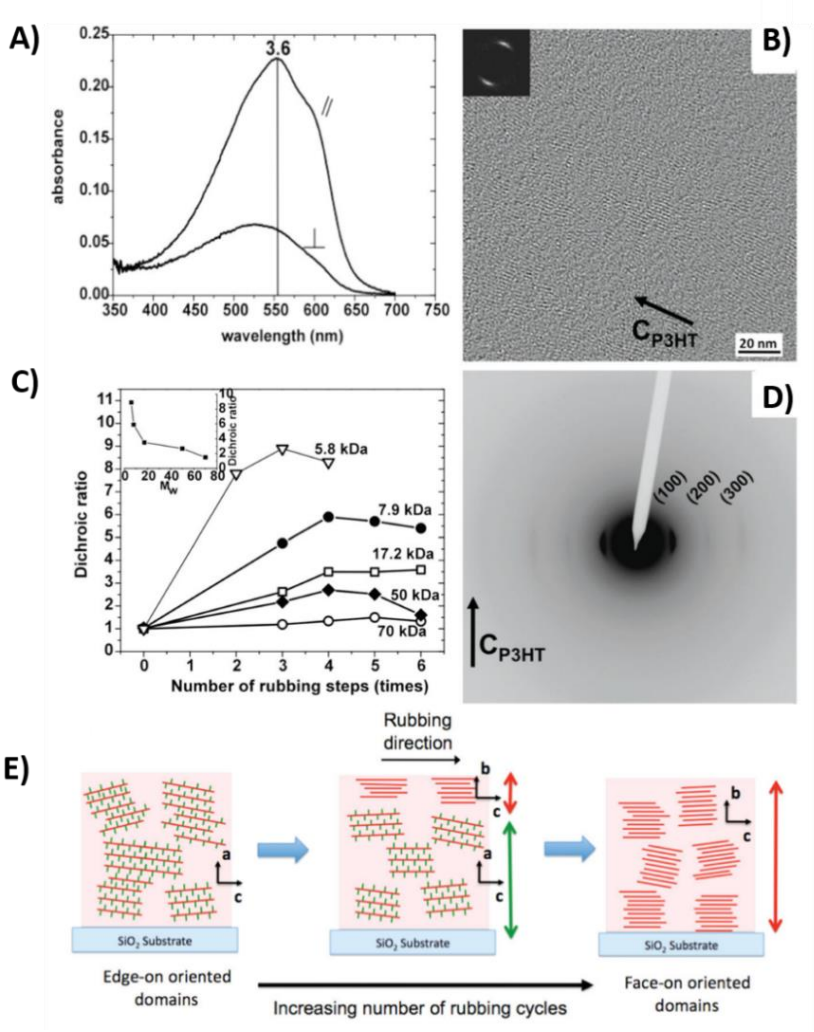

Figure 1.14. *A) UV-Vis polarized optical absorbance spectra of an oriented P3HT thin film (17.2 kDa). Parallel and perpendicular absorbance are shown in the figure. B) & D) High-resolution TEM image and electron diffraction pattern of as-rubbed P3HT thin films (17.2 kDa). C) Evolution of the dichroic ratio for rubbed P3HT films of different molecular weights. E) Schematic illustration of edge on to face-on transformation during rubbing. All films were aligned at room temperature. Reproduced from (49)*

Highly oriented films of C_{12}-PBTTT were obtained upon rubbing at 125 °C (see figure 1.15). Films show a high degree of anisotropy in optical and charge transport properties.

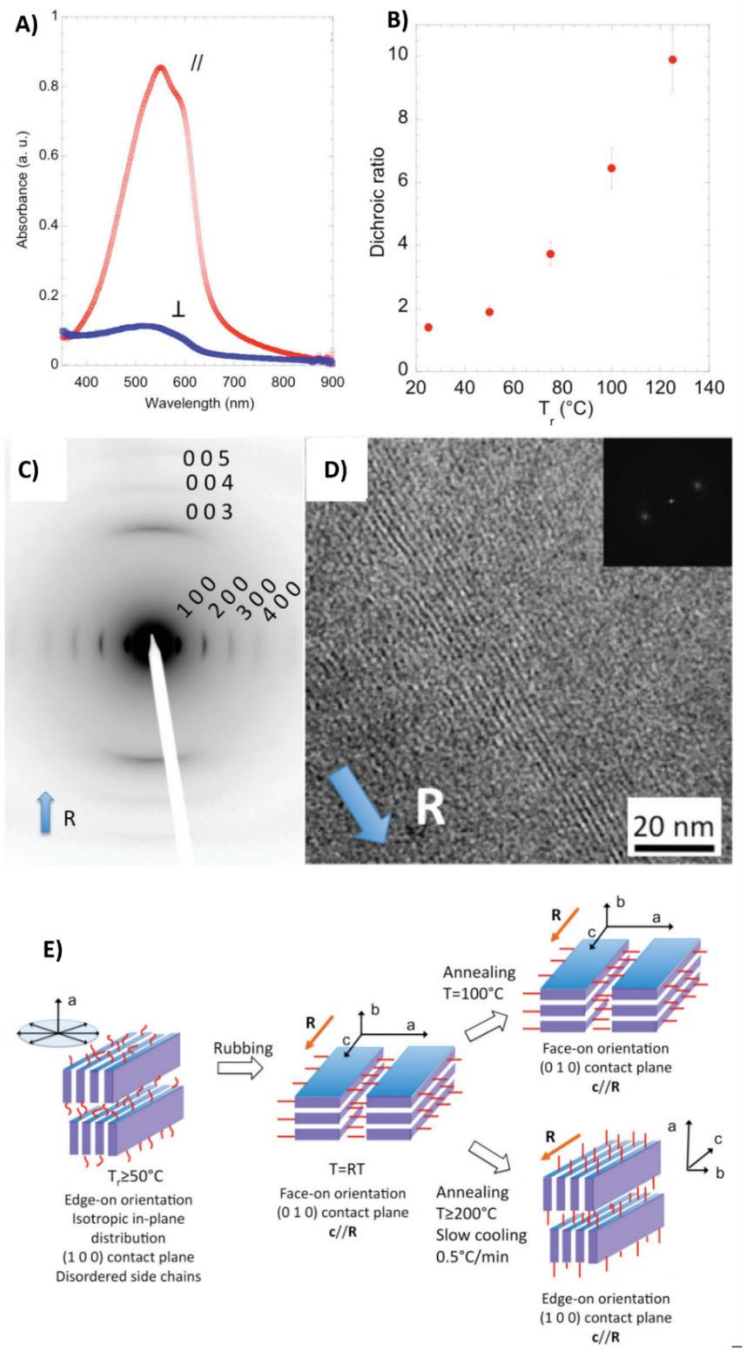

Figure 1.15. *A) UV-Vis polarized optical absorbance spectra of an oriented PBTTT thin-film rubbed at 125 °C (Parallel and perpendicular absorbance are shown in the figure). B) Evolution of the dichroic ratio as a function of the rubbing temperature (T_R). C) and D) are the electron diffraction and high-resolution electron microscopy images of oriented PBTTT rubbed at 125 °C. E) Schematic illustration of edge-on to face-on transformation during rubbing. Reproduced from (44)*

The oriented films were birefringent in an optical microscope and electron diffraction patterns reveal a high degree of order along the chain direction. Because of this, the

mobilities were enhanced along the rubbing direction. High-resolution TEM revealed the nanomorphology of the oriented PBTTT films. Similar to P3HT, the presence of sulphur in the oriented backbone generates a specific contrast relative to the alkyl side chain in the high-resolution images of PBTTT (see figure 1.15D). [16,19,36,45]

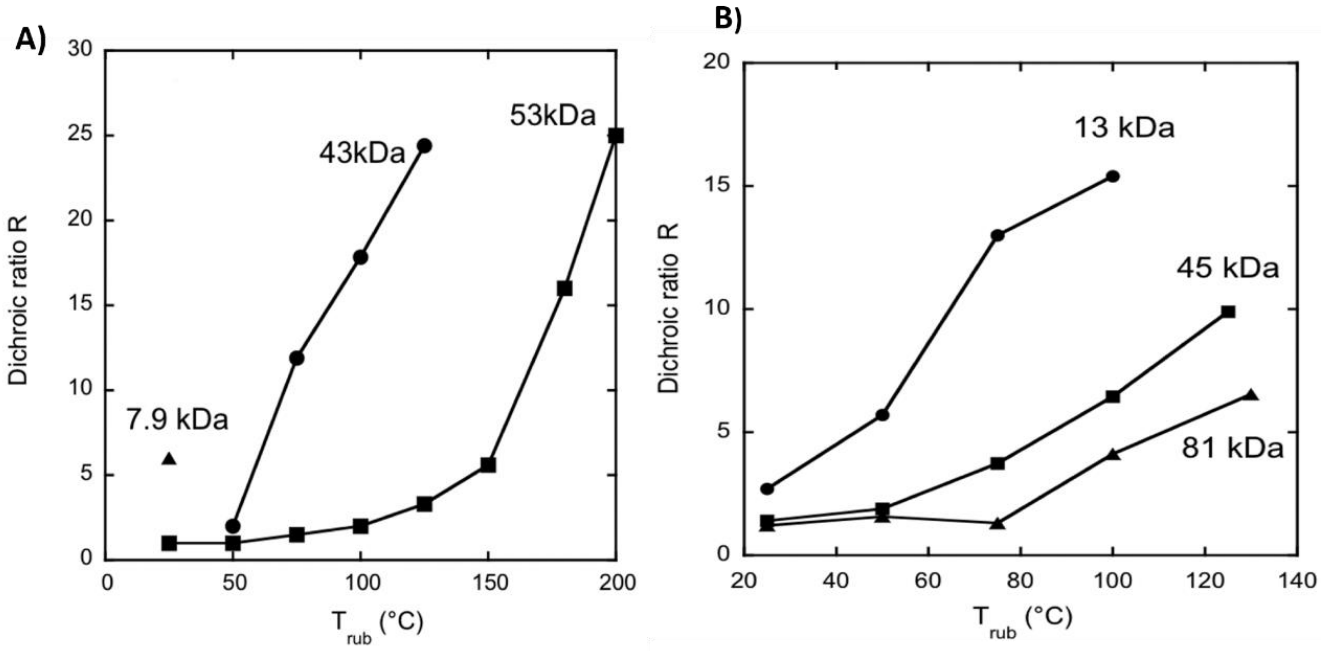

Figure 1.16. *Temperature dependence of the dichroic ratio in A) P3HT and B) PBTTT for samples with different molecular weights (M_w). Reproduced from (36)*

The molecular weight of a conjugated polymer is also an important parameter that influences the degree of orientation. Hence, the correlation between molecular weight and degree of alignment is an important point to discuss in this chapter. In 2014, Brinkmann and coworkers studied the effect of molecular weight on the orientation of P3HT and PBTTT batches with different molecular weights. It was observed that the lower molecular weight P3HT (13 KDa) was aligned at room temperature while the higher molecular weight (43 kDa) showed an onset of alignments at 50 °C (see figure 1.16). The P3HT batch with a molecular weight of 53 kDa was poorly oriented at low temperature and showed a high degree of alignment at higher rubbing temperature.[36] The same trend was also observed in the case of PBTTT.

High temperature rubbing was used by Hamidi-Sakr et al. to fabricate highly oriented and crystalline films of P3HT. They were able to obtain the semi-crystalline morphology in oriented films with a very high dichroic ratio > 25.[15] Mobility measurements were also carried out as a function of rubbing temperature on organic field-effect transistors (OFET). The mobilities along the rubbing direction were larger than those measured perpendicular to the rubbing. The measured mobilities did not improve with increasing T_R because of the existence of amorphous interlamellar zones that slow down the hole migration between crystalline domains along the rubbing direction.

Later in 2017, Hamidi-Sakr et al. showed that doping of oriented P3HT with suitable electron acceptors such as 2,3,5,6-Tetrafluoro-7,7,8,8-tetracyanoquinodimethane (F_4TCNQ) produces oriented thin films with highly anisotropic electrical conductivity. In addition, they observed that the measured conductivity was enhanced along the rubbing direction. Anisotropy in the 8-10 range was observed for the conductivity and a maximum conductivity of 22 S/cm for F_4TCNQ doped P3HT along the parallel direction.[46] High temperature rubbing was shown to be an effective method for preparing highly oriented and crystalline polymer films with enhanced conductivity along the rubbing direction.

In the frame of my thesis, I used high-temperature rubbing to align different polythiophenes for thermoelectric applications, as discussed in chapter 2, 3 and 4.

4.2. Orientation by friction transfer

Smith and Wittmann pioneered this method of polymer orientation for oriented PTFE (Polytetrafluoroethylene) layers.[47,48] Friction transfer is a versatile method and it can be widely applied to align a large palette of polymers including P3HT, poly(9,9'-dioctyl-fluorene) (PFO) etc.

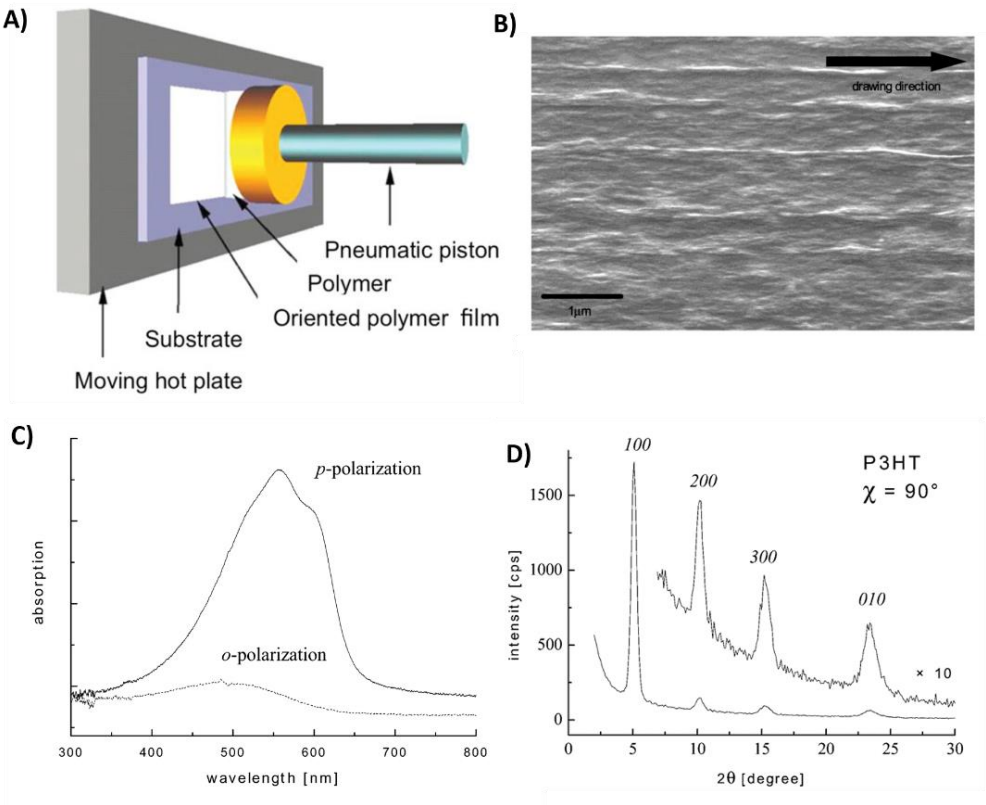

Figure 1.17. *A) Schematic representation of the friction transfer deposition method. B) SEM image of an aligned P3HT film-oriented by friction transfer. C) and D) represent corresponding polarized Uv-Vis spectra along the parallel and perpendicular direction and the section profile from Grazing incidence X-ray diffraction respectively. Reproduced from (49&50)*

The polymer to be aligned is first compressed in the form of a cylindrical pellet under high pressure. This pellet is translated over a hot substrate at a constant speed and a thin oriented polymer film is deposited on the hot substrate (see figure 1.17).[49] Nagamatsu and coworkers applied this technique for the fabrication of oriented films of P3HT and poly(3-dodecylthiophene).[50] The oriented P3HT displayed an order parameter close to unity. The distribution of in-plane orientation of P3HT chain axis is of around 10 ° as evidenced by Grazing X-ray diffraction measurements. X-ray diffraction measurements indicate that the π stacking (b axis) is perpendicular to the substrate plane and the polymer crystals adopt a face-on orientation after alignment. Poly(3-dodecyl thiophene) films oriented by friction transfer also showed high degree of

orientation along the drawing direction. Mobility measurements were carried out parallel and perpendicular to the direction of rubbing in OFET devices. The measured mobilities were highly anisotropic and anisotropy factors of $\mu_{//}/\mu_{\perp}$ =8 were observed in these films.The main disadvantage of this method is that the substrate must be heated to very high temperature and the thickness of the deposited film is difficult to control. Moreover, large amounts of polymers are necessary to prepare the pellets.

4.3. Orientation by strain alignment

Strain alignment is an alternating technique used for aligning semiconducting polymers. In this method, the active polymer is deposited on a stretchable substrate such as Polydimethylsiloxane (PDMS). After deposition, the substrate can be stretched in a specific direction and hence the crystals and polymeric chains (backbones) can be aligned in the direction of stretching.

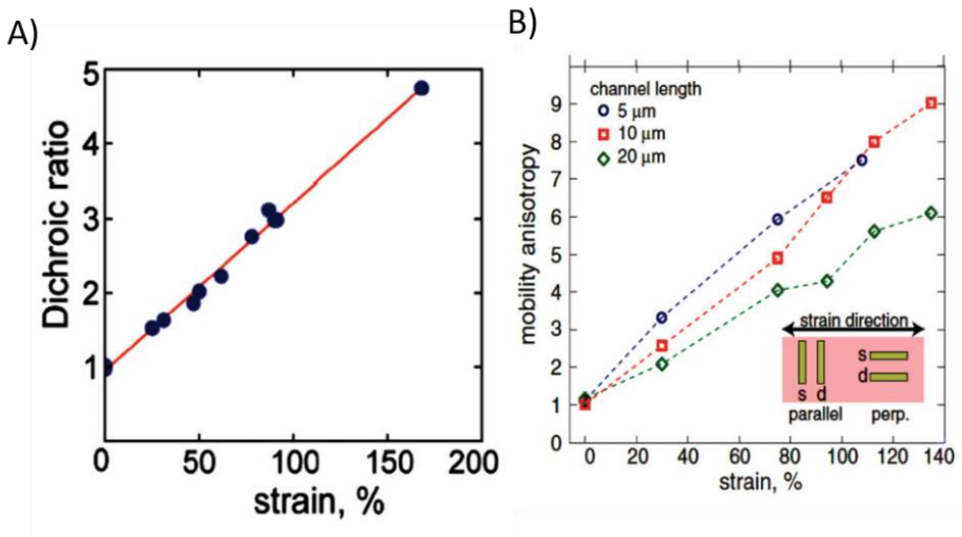

Figure 1.18. *A) Evolution of the dichroic ratio as a function of applied stress. B) Anisotropy of hole mobilities in strain aligned P3HT films in OFETs. Reproduced from (52)*

Dyreklev et. al used the strain alignment method to obtain polarized electroluminescence out of a thin film of poly(3-(4-octylphenyl)-2,2'-bithiophene) (PTOPT) with a dichroic ratio of 2.4.[49,51] DeLongchamp and coworkers[52] applied strain

alignment on regioregular P3HT. The substrate layer was PDMS. High levels of orientation were observed in strained P3HT in which polymer backbones were aligned in the direction of stretching with a dichroic ratio of 4.8. The high degree of polymeric backbone alignment along the stretching direction resulted also in anisotropy of charge mobilities. The mobilities measured along the stretching direction were higher than those along the direction perpendicular to the rubbing (see figure 1.18). An anisotropy ($\mu_{//}/\mu_{\perp}$) ≈ 9 was reported.

4.4. Orientation by using an orienting substrate (Epitaxy)

Epitaxy is defined as the natural or artificial growth of a crystal (guest) over a crystalline substrate (host) that determines their mutual orientations.[53] If the host and guest have a different chemical nature, then it is known as heteroepitaxy. If they have the same chemical nature, then it is known as homo epitaxy. Lattice matching is an important criterion for epitaxial growth. Epitaxy of semi-crystalline polymers on aromatic crystals produced thin films of high orientation with a regular orientation of crystalline domains.[49]

The epitaxy of semi-crystalline polymers can be achieved on a large variety of substrates such as NaCl, KCl and aromatic crystals.[49,54,55] 10 to 15% of lattice mismatch is the upper limit for successful epitaxial growth. In the beginning, epitaxy was widely used for only inorganic materials but, the epitaxial orientation of polymers on organic or polymeric materials was widely exploited later in the 1980s following the pioneering work of Lotz and Wittmann[53,56].

A systematic investigation of polymer epitaxy was performed by Lotz and Wittmann in the 1980s. [53,56] They studied epitaxial growth of polymers such as polyethylene, *n*-paraffins and aliphatic polyesters on aromatic crystals such as benzoic acid. Later Brinkmann and Wittmann attempted epitaxial orientation of P3HT. P3HT was oriented

on the surface of aromatic crystals of 1,3,5-trichlorobenzene (TCB). TCB plays a two-fold role in the epitaxial crystallization of P3HT. Firstly, TCB plays the role of a solvent when molten and once it crystallizes, TCB acts as a substrate for the oriented crystallization. 1- dimensional epitaxy explains the alignment of P3HT on TCB. It has been found that $C_{P3HT} \approx 2C_{TCB}$. After the orientation, the TCB layer was removed by vacuum evaporation that creates large areas of highly oriented P3HT crystals on a glass substrate.

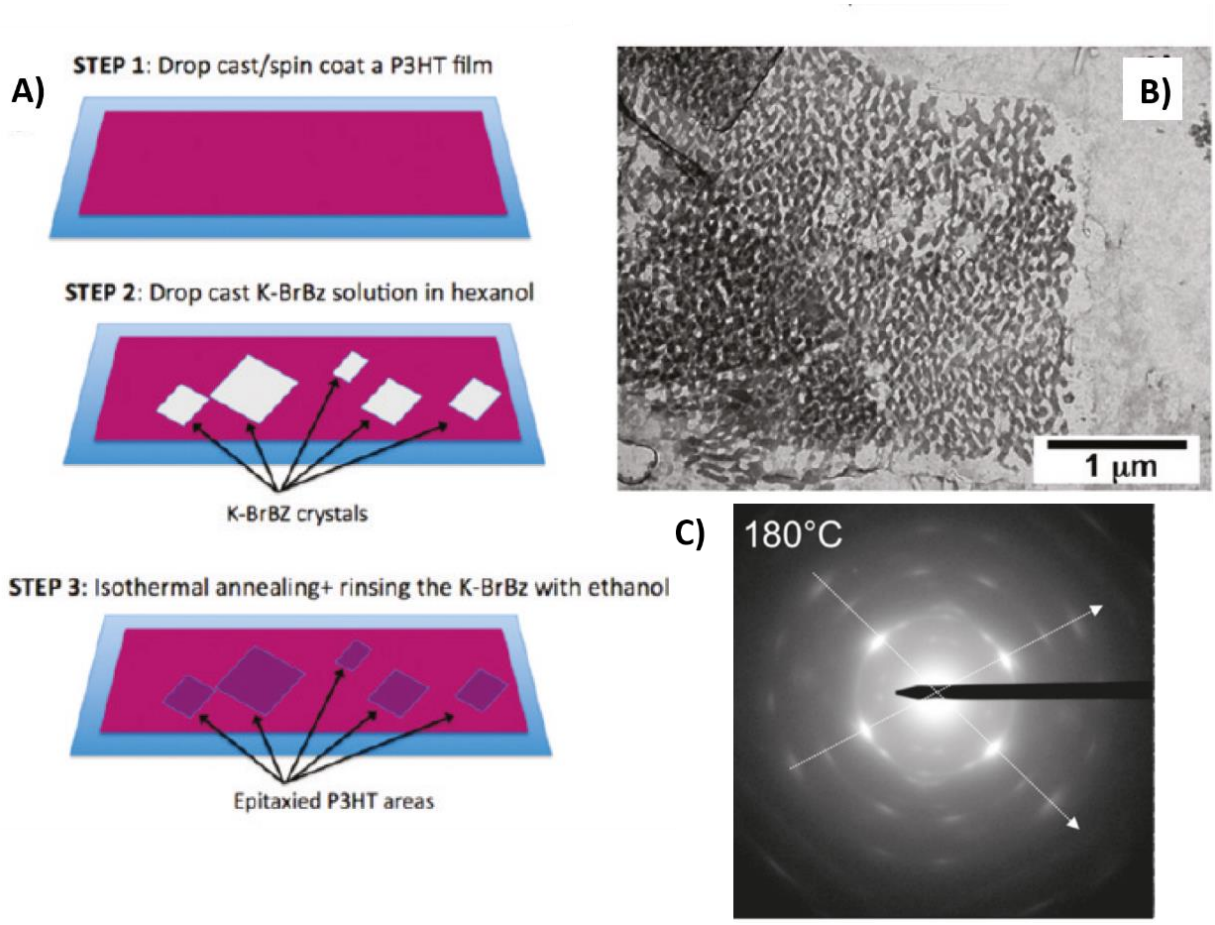

Figure 1.19. *A) Schematic representation of epitaxial growth of P3HT on potassium 4-bromobenzoate. B) TEM bright-field image showing an oriented and nanostructured P3HT film after removal of the KBrBz. C) Electron diffraction pattern of crystallized P3HT thin films at 180 °C on KBrBz. Reproduced from (55)*

Aromatic molecules like anthracene and *p*-terphenyl crystals are widely used as a substrate for epitaxial growth of polyethylene. In 2009, Brinkmann et al. reported a new epitaxial orientation of P3HT on aromatic potassium 4-bromobenzoate (KBrBz). [55] The

procedure consists of three steps. The first step involves the preparation of large surface of KBrBz crystal. In the second step, the polymer is deposited on the top of the KBrBz crystals (see figure 1.19). Finally, isothermal annealing is applied to promote the epitaxial orientation of P3HT. The orienting substrate is removed by rinsing with ethanol. Finally, highly oriented films of P3HT were obtained after epitaxy, as demonstrated from the electron diffraction patterns (figure 1.19)

5. Anisotropy of charge transport

Conducting polymers such as PBTTT and P3HT are characterized by well-defined unit cells. As described above, the charge transport in these unit cells is highly anisotropic. For instance, charge transport along the chain direction (c axis) is higher than that along the π stacking direction (b axis). The poorest charge transport is along the alky side chain direction (a axis).

At a larger length scale, the polymers show a semi- crystalline morphology where crystalline and amorphous regions alternate. The crystalline region is composed of highly extended and ordered chains but the amorphous zones contain chain ends, chain folds and tie chains which connect successive crystalline regions. Taking this microstructure into account, Lan[57] and coworkers predicted the charge transport behavior of regioregular P3HT films by using theoretical calculations (see figure 1.20).[57] They proposed that within the ordered regions of P3HT, the hole mobility along the intrachain route (along the polymer backbone) is significantly larger (1 $cm^2 V^{-1} s^{-1}$) than the mobility along the π stacking direction (10^{-2} $cm^2 V^{-1} s^{-1}$). The chain ends and chain folds present in the amorphous zone reduce charge transport. The tie chains (bridging chain) help channel charges from one crystalline region to another. However, the presence of multiple crossing points between the chain ends in the amorphous zones further slows down charge mobility.

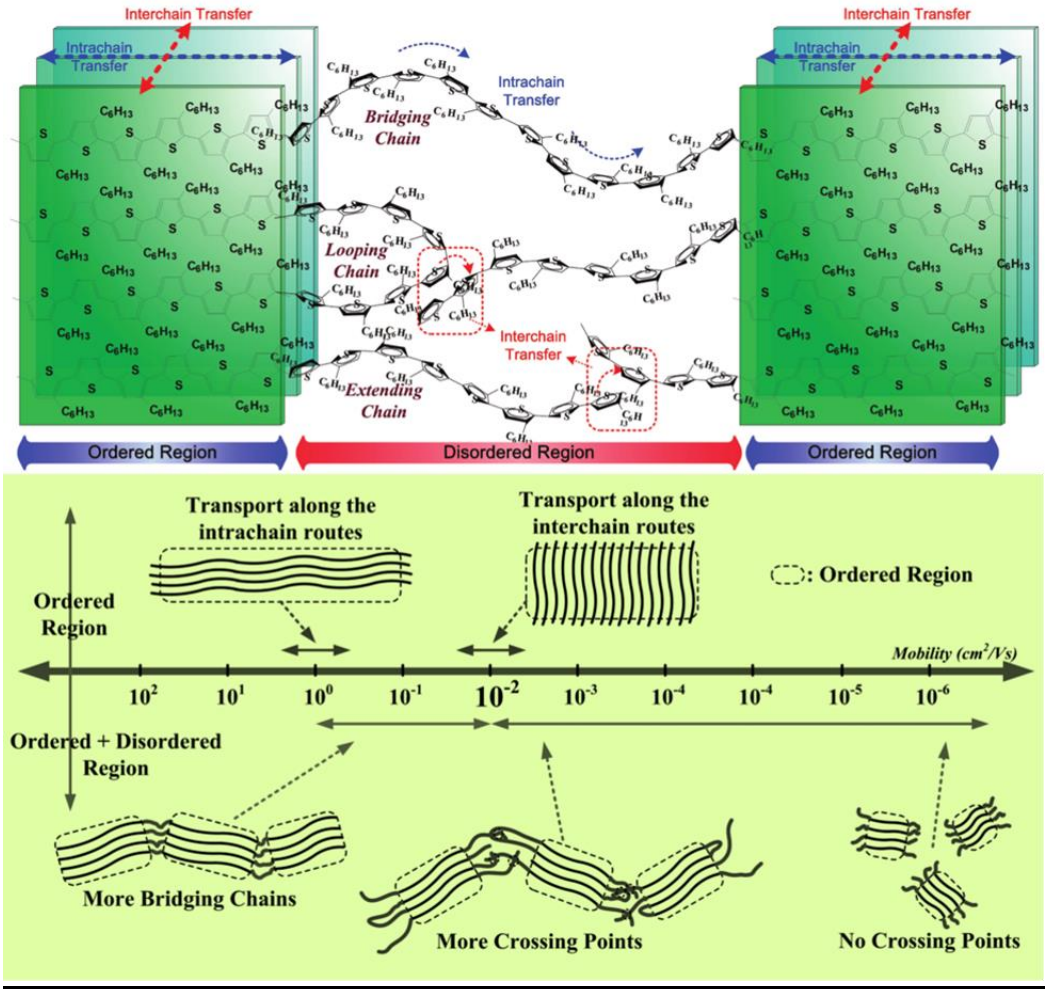

Figure 1.20. *Schematic representation (top) of the semi-crystalline morphology of P3HT. The green colour represents the crystalline regions. The intra and intermolecular charge transport in the crystalline region are represented. The amorphous zones and the corresponding mobilities are shown in the bottom. Reproduced from (57)*

Detailed investigations were carried out to determine the charge transport anisotropies in P3HT. For instance, Jimison[58] and coworkers showed that in directionally crystallized P3HT films (face- on oriented crystals), the charge transport is highly anisotropic with high mobilities measured along the chain direction in the crystalline regions (grains) because of the difference in charge transport along the chain direction ($\mathbf{c_{P3HT}}$) and along the direction of alkyl side chains ($\mathbf{a_{P3HT}}$). The mobilities along the chain were at least one order of magnitude higher than along the perpendicular direction. O'Connor[52] et. al were able to obtain enhanced mobilities along the chain direction in strain aligned P3HT

films with an anisotropy of 9. A similar situation was also seen by Hartmann[19] and coworkers in highly anisotropic thin films of P3HT prepared by rubbing at room temperature. The reported anisotropy in mobility was $\mu_{//}/\mu_{\perp} \approx 22$ for the best in-plane oriented samples of low molecular weight P3HT (6.4 kDa). But only an anisotropy of 2 was obtained for the high molecular weight P3HT due to highly interconnected crystalline domains, which prevent the alignment of crystalline domains upon rubbing at room temperature.[19]

Anisotropic charge transport of PBTTT was also investigated[59]. Biniek[44] et. al applied high temperature rubbing to liquid crystalline C_{12}-PBTTT and a detailed investigation was done on the anisotropy of mobilities. Highest mobilities of 4×10^{-3} cm^2 V^{-1} s^{-1} were observed parallel to rubbing at a temperature of 100 °C, at which the films show high in-plane alignment. Xue et. al applied strain alignment on liquid crystalline PBTTT and observed that the polymer chains were oriented in the direction of the applied strain and the resulting mobility 1.67 cm^2 V^{-1} s^{-1} was the highest reported in the case of oriented PBTTT. Similar results on mobility anisotropy were previously observed by Lee et. al in zone cast films of uniaxially oriented PBTTT[60].

All these results on the polymer orientation prove that obtaining a high degree of in-plane alignment is mandatory to reach higher charge mobilities in conjugated polymer thin films. Based on these results, we have decided to apply high-temperature rubbing to a series of polythiophenes including P3HT and PBTTT with different alkyl side chains for thermoelectric applications. The present project aims at developing new polymeric thermoelectric materials in oriented and highly crystalline films. Our strategy is to control the level of crystallization and the alignment of the conducting polymer before transforming the semi-conducting films into their doped conducting form by sequential doping. Both crystallinity and orientation of conducting polymers were recognized as key points to obtain more efficient thermoelectric films. In our approach, we will

decouple the doping of the polymer from the crystallization and take advantage of the very high level of order in undoped semiconductor polymers that can be obtained by high-temperature rubbing. Once oriented and crystallized, the semiconducting films will be doped by different methods. The thermoelectric properties of the semi-crystalline doped polymers can be controlled by precise tuning of the crystallinity and by changing the doping conditions.

6. Thermoelectricity

Thermoelectricity refers to the direct conversion of heat to electricity and vice versa. Highly efficient thermoelectric materials are important for power generation applications because they have the ability to convert waste heat to electricity. At present, inorganic materials are the best performing TE materials. The thermoelectric material's efficiency at a given temperature T depends on its conductivity (σ), on its Seebeck coefficient (S) and thermal conductivity (κ) via the figure-of-merit $ZT=\sigma S^2/\kappa$. The numerator σS^2 corresponds to the power factor (PF) of the thermoelectric material. To determine the usefulness of a material in a thermoelectric generator or a thermoelectric cooler, the power factor is calculated by its Seebeck coefficient (S) and its electrical conductivity (σ) under a given temperature difference. Materials with a high power factor are able to 'generate' more energy. Bismuth Telluride (Bi_2Te_3), Alloys of Bismuth- Antimony -Telluride and Bismuth chalcogenides are three important classes of inorganic TE materials with a ZT ≈1 at room temperature. The expensive raw materials and reduced abundance of the components lead the scientific community to propose to replace inorganic TE materials by organic conducting polymers. Recently, remarkable TE performances were reported in poly(3,4-ethylenedioxythiophene) polystyrene sulfonate (PEDOT:PSS) by Crispin and coworkers.[61] A ZT value of 0.25 was obtained at room temperature for this conducting polymer. This initial result obtained for a conducting polymer such as PEDOT:PSS motivated the scientific community to

investigate the TE performance of other conducting polymers, for instance, polythiophenes.

6.1. Basic principles of thermoelectricity

In the early 1800s, Thomas Seebeck observed that when the junctions of two dissimilar materials are kept at two different temperatures (T and T+ΔT), a voltage difference is produced between them (ΔV).[62] This Voltage difference is proportional to the applied temperature gradient(ΔT).

$$S = \frac{\Delta V}{\Delta T} \quad (1)$$

The ratio of the voltage gradient to the applied temperature gradient is called the Seebeck coefficient (S), which is an intrinsic property of a material. The Seebeck coefficient is usually small for metals (μV/K) and large (up to several mV/K) for insulators. The sign of the Seebeck coefficient indicates the type of charge carriers. S>0 for holes (p-type semiconductors) and S<0 for electrons (n-type semiconductors). The physicist A.F loffe introduced the concept of figure of merit. The thermoelectric performance of a material is determined by the figure of merit ZT. The dimensionless ZT represents the measure of thermoelectric efficiency.[63]

$$zT = \frac{\sigma . S^2}{\kappa} T \quad (2)$$

where σ is the charge conductivity, S is the Seebeck coefficient, T is the absolute temperature and κ is the thermal conductivity. The thermal conductivity (κ) of a conducting polymer is the sum of the electronic and lattice contribution i.e $\kappa=\kappa_e+\kappa_L$, where κ_e is the contribution from the charge carriers and κ_L accounts for the contribution from the lattice vibrations.

The inorganic Bi_2Te_3 shows ZT ≈1 at room temperature while the organic materials were characterized by very low ZT values usually below 0.1.[64] Due to the difficulties of thermal conductivity measurements in polymer films, the power factor (PF) is used to compare the TE performance of different polymers.[3]

$$PF = S^2\sigma \quad (3)$$

The thermoelectric parameters such as S, σ and κ are mutually dependent and this affects the optimization of TE performances. The optimization of one of these factors adversely affect the other ones and hence the optimization is impossible without compromising the other parameters.

$$\sigma = nq\mu \quad (4)$$

The electrical conductivity (σ) depends on the mobility (μ) and the number of charge carriers (n) (see equation 4). n is determined by the amount of dopants and the number of free charge carriers. μ is determined by solid-state order (crystallinity, orientation). Numerous studies demonstrate that the electrical conductivity and the mobility of charge carriers depend critically on the initial crystalline structure of the polymer.[36,46] The electrical conductivity increases upon doping but the Seebeck coefficient decreases. The electrical conductivity can vary from 10^{-7} S/cm for undoped to 10^5 S/cm for heavily doped polymers.[65] The Seebeck coefficient varies from 10^3 μV/K for undoped conjugated polymers to 10 μV/K for heavily doped semiconductors and S <10 μV/K for conductors.

A thermoelectric device is made of an array of individual TE legs connected in series (see figure 1.21) which is the smallest repeating unit of a thermoelectric device.[3][66] The two legs of a thermoelectric element must be made of dissimilar materials with different Seebeck coefficients to make sure that the resulting thermovoltage does not cancel, i.e.

S_2-$S_1 \neq 0$. Generally, thermoelectric devices of inorganic materials are made by a combination of n-type and p-type materials. Each leg contributes to the total open-circuit voltage of the TE device (V_{oc}).

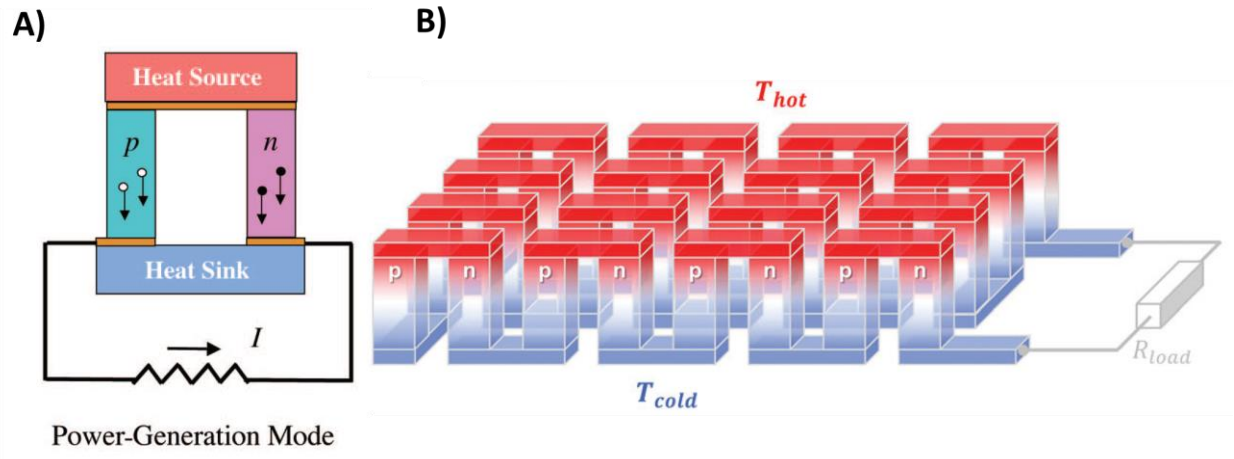

Figure 1.21. *A) Diagram of a thermocouple made of n-type and p-type materials. Power generation or refrigeration modes are possible depending on the configuration. I is the current. B) A conventional thermoelectric module that comprises an array of elements, which are connected electrically in series but thermally in parallel. Reproduced from (3&66)*

$$V_{OC} = N(S_2 - S_1)\Delta T \quad (5)$$

Where N is the number of legs and V_{oc} is the open-circuit voltage and ΔT is the temperature gradient. The maximum power (P_{max}) output is obtained when the external load (R_{load}) is equal to the internal resistance ($R_{internal}$), i.e. $R_{load} = R_{internal}$, which is related to the V_{oc}:

$$P_{max} = \frac{V_{OC}^2}{4R_{int}} \quad (6)$$

6.2. Thermoelectricity in conducting polymers

The ability to tune the conductivity of a polyacetylene film from insulating to metallic level was achieved by the joint work of Alan J. Heeger, Alan G. MacDiarmid and Hideki

Shirakawa.[67,68] Remarkable electrical conductivities of 10^5 S/cm and power factors of 1350 $\mu Wm^{-1}K^{-2}$ were obtained for Iodine doped polyacetylenes.[69,70] However, high instability of the iodine dopant in air and difficult processing of the oriented polyacetylene films prevented their use for thermoelectric applications. As a result, researchers turned their attention to air-stable and high-performance polymers for thermoelectric applications. In 2010, air-stable thin films of polyelectrolytes were developed by Mai et al. with high Seebeck coefficients, S ≈ 195 μV/K and very low thermal conductivity (κ). However, the PF was only of 0.84 $\mu Wm^{-1}K^{-2}$ due to their poor conductivity of 0.22 S cm^{-1}.

An important contribution to the field of organic thermoelectrics was achieved by Bubnova et al. in 2011. Crispin and coworkers managed to achieve a PF ≈ 324 $\mu Wm^{-1}K^{-2}$ on poly (3,4-ethylenedioxythiophene):tosylate (PEDOT:TOS) with a high ZT ≈ 0.25 at room temperature.[61] They showed that the thermoelectric properties of organic semiconductors can be enhanced by suitable processing and precise tuning of doping levels. Organic materials were envisioned to replace in part inorganic materials currently used for thermoelectric applications. As compared to inorganic materials, the main advantage of polymer semiconductors is due to their facile processability and low thermal conductivity. The work of Crispin et al. triggered a large interest for research on organic thermoelectric materials. The dominant strategy to improve TE properties was accordingly based on improving the electrical conductivity of doped polymers

New polymers, new dopants and new doping strategies were introduced to boost the TE performances of conducting polymers. An important milestone in the field of organic TE was achieved by Yim[71] and coworkers in 2008. They studied the influence of the HOMO energy levels of various p-type polymers on doping strength. The high electrical conductivity of 10^{-1} S/cm was obtained for P3HT with respect to other polymers due to

a favourable energetical offset between the HOMO (-4.8 eV) of P3HT and LUMO of F_4TCNQ.[71] Solution doping of P3HT mainly triggered by the work of Yim et al in 2008.[71] Thermoelectric properties of other polythiophenes such as PBTTTs were also exploited by Glaudell et al. in 2015. The studies evidenced that the deeper HOMO (-5.1 eV) level of PBTTT is also favourable for doping with conventional F_4TCNQ and results in electrical conductivities of $\approx$ 3 S/cm and $\alpha \approx 60$ µV/K.[72]

P3HT and PBTTT were two suitable model systems for chemical doping due to their high structural order.[14] Both the semi-crystalline structure of P3HT and the liquid crystalline nature of PBTTT are characterized by high degrees of structural order, which can lead to high mobilities and conductivities in thin films.

7. Doping of conjugated polymers

a) Electronic Process involved upon P-type doping

Doping can be defined as the addition of impurities into an extremely pure semiconductor in order to enhance its electrical performance. In the case of an inorganic semiconductor, the highest occupied energy levels form a conduction band (CB) while the lowest occupied energy levels form the valence band (VB). The energy gap between the two bands is known as the bandgap (E_g). The electronic conductivity is possible only if an electron from the VB reaches the CB. This happens only if the two bands are close enough.

Unlike inorganic semiconductors, doping of an organic semiconductor is a complex mechanism in which a "charge transfer agent is used to generate, by oxidation or reduction, positive or negative charges in an intrinsically conducting polymer". [3] The doping of conducting polymers can be achieved by two methods.1) Redox doping, which involves the transfer of an electron between the conducting polymer and the dopant species to form a charge-transfer complex. 2) Acid-Base doping, which involves the

transfer of a cation or an anion to the polymer backbone (see figure 1.22). A common example for the acid doping is camphor sulphonic acid (CSA) and dodecyl benzene sulphonic acid (DBSA) doping of polyaniline. The protonation of the emeraldine form of polyaniline gives rise to highly conducting polyanilines with an electrical conductivity of ≈ 100 S/cm.[73] Acid doping is also applicable to polythiophenes such as PBTTT and P3HT. Ethyl-benzene sulphonic acid (EBSA) and perflurooctyl-trichlorosilane (FTS) doping has been widely experienced with PBTTT.[74]

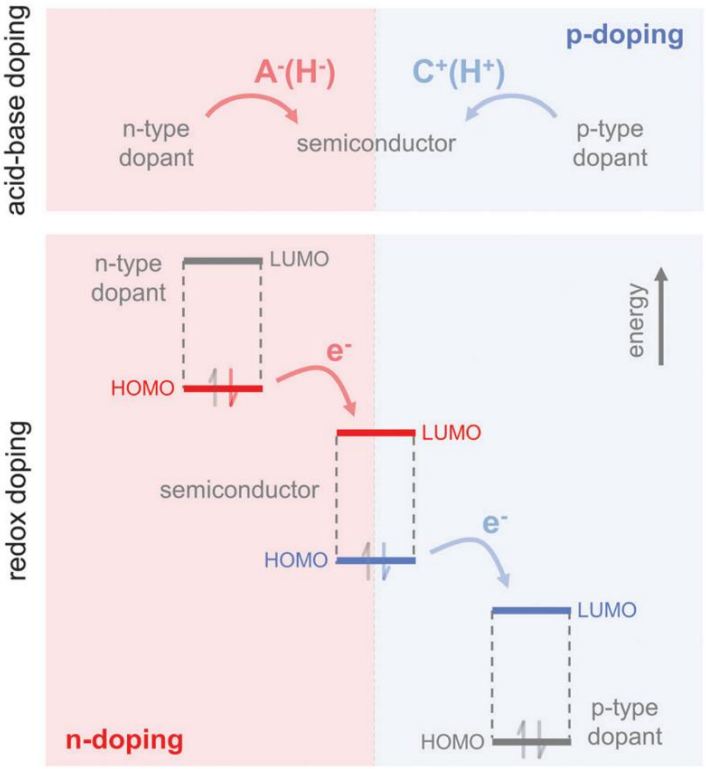

Figure 1.22. *The basic principle of acid-base doping (Top) and redox doping (bottom) that involves the transfer of an electron from the LUMO or from the HOMO. Reproduced from (3)*

The doping mechanism which involves the transfer of a hydride ion (H^-) to the organic semiconductor corresponds to n-type or base doping. 4-(2,3-Dihydro-1,3-dimethyl-1H-benzimidazol-2-yl)-N,N-dimethylbenzenamine (N-DMBI) and (4-(1,3-Dimethyl-2,3-dihydro-1H-benzoimidazol-2-yl)-N,N-diphenylaniline) N-DPBI are two common n-type

doping agents. They can dope poly{[N,N-bis(2-octyldodecyl)-naphthalene-1,4,5,8-bis(dicarboximide)-2,6-diyl]-alt-5,5-(2,2-bithiophene)} P(NDI_2OD-T_2).

In the case of P-type doping, an added dopant molecule can remove one electron from the highest occupied molecular orbital (HOMO) of the polymer which creates a hole in the VB and reduces the bandgap. This hole can be delocalized to the neighbouring polymeric chains and this migration of holes is at the origin of electrical conductivity. By adjusting the dopant concentration, the conductivity of a polymer can be tuned from 10^{-7} S/cm (for the undoped polymer) to 10^5 S/cm for highly doped polymers.[65]

Hereafter I will mainly focus on P-type doping of conjugated polymers such as P3HT and PBTTT due to its relevance for my thesis.

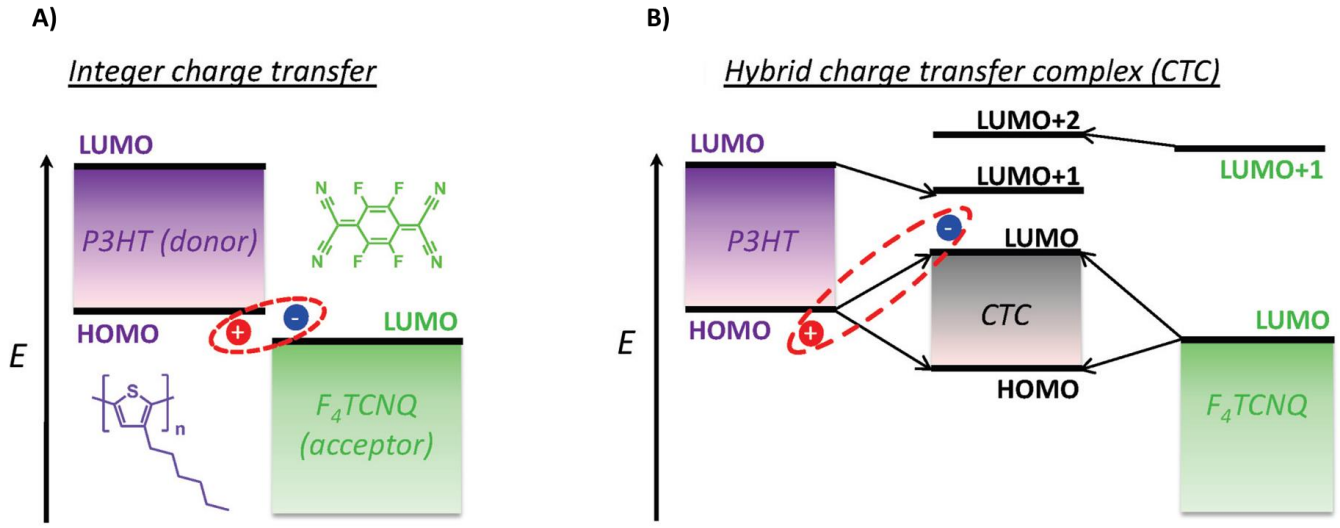

Figure 1.23. *Different models for explaining electron transport from P3HT to the dopant F_4TCNQ Reproduced from (75)*

P3HT is a widely exploited polymer for solar cells and OFET applications because of its high mobility performance and solution processability. Due to the same reasons, P3HT is a well-studied system for thermoelectric applications. Doping the semi-crystalline structure of P3HT with highly stable and strong molecular dopants can produce highly conducting thin films. In the following, we will focus on the model system P3HT/F_4TCNQ.

Different models were proposed in order to explain the electron transfer between P3HT and F_4TCNQ. Mainly, two contradictory models were proposed so far (see figure 1.23). The first one implies integer charge transfer i.e. one electron from the polymer is transferred to the dopant molecule, which creates a hole in the HOMO of the polymer.[75] These holes in the polymer can either be trapped by the anion or move within the lattice of the polymer in the form of "free" charge carriers. Another model was proposed by Aziz et al.[76] They suggested that there is only a partial charge transfer between the polymer and the dopant and the electron transfer is taking place through the formation of a "supramolecular" Charge Transfer State (CTS). Both the HOMO and LUMO of the CTS are derived from the HOMO and LUMO of the neutral P3HT and F_4TCNQ respectively. This model was questioned by the work of Pingel et al.[75] who followed the charge transfer in P3HT and F_4TCNQ from a very low concentration (ppm) of dopant to very high concentration with the help of optical spectroscopy, Kelvin probe measurements and conductivity. They demonstrated that there is always a one-electron transfer between P3HT and F_4TCNQ. Similarly, integer charge transfer was clearly demonstrated by Hamidi-Sakr [46] and coworkers in doped P3HT thin films using polarized UV-Vis-NIR spectroscopy.

Similar to P3HT, PBTTT is another important candidate for thermoelectric applications due to its high degree of structural order and high charge in mobility OFETs.[26,29,77,78]

Evidence of charge transfer between PBTTT and F_4TCNQ was obtained by the detailed investigation of Cochran[79] et al. in 2014. They concluded that due to a favourable energy offset between the HOMO of the PBTTT and the LUMO of the dopant, F_4TCNQ can be used as an effective dopant for C_{14}-PBTTT.[79] Later, in 2015, Glaudell[72] and coworkers reported promising TE performances in F_4TCNQ doped PBTTT. These initial results on doping and TE performances of polythiophenes such as PBTTT and P3HT led to extensive research on TE properties of conducting polymers. Due to the growing

demand of TE applications, different doping agents, doping methods and new processing schemes were introduced for improving TE properties of polythiophenes (see figure 1.24). The dopant F_4TCNQ was progressively replaced by much stronger oxidizing agents such as Ferric Chloride ($FeCl_3$) and 2,2-(perfluoronaphthalene-2,6-diylidene)-dimalononitrile (F_6TCNNQ).

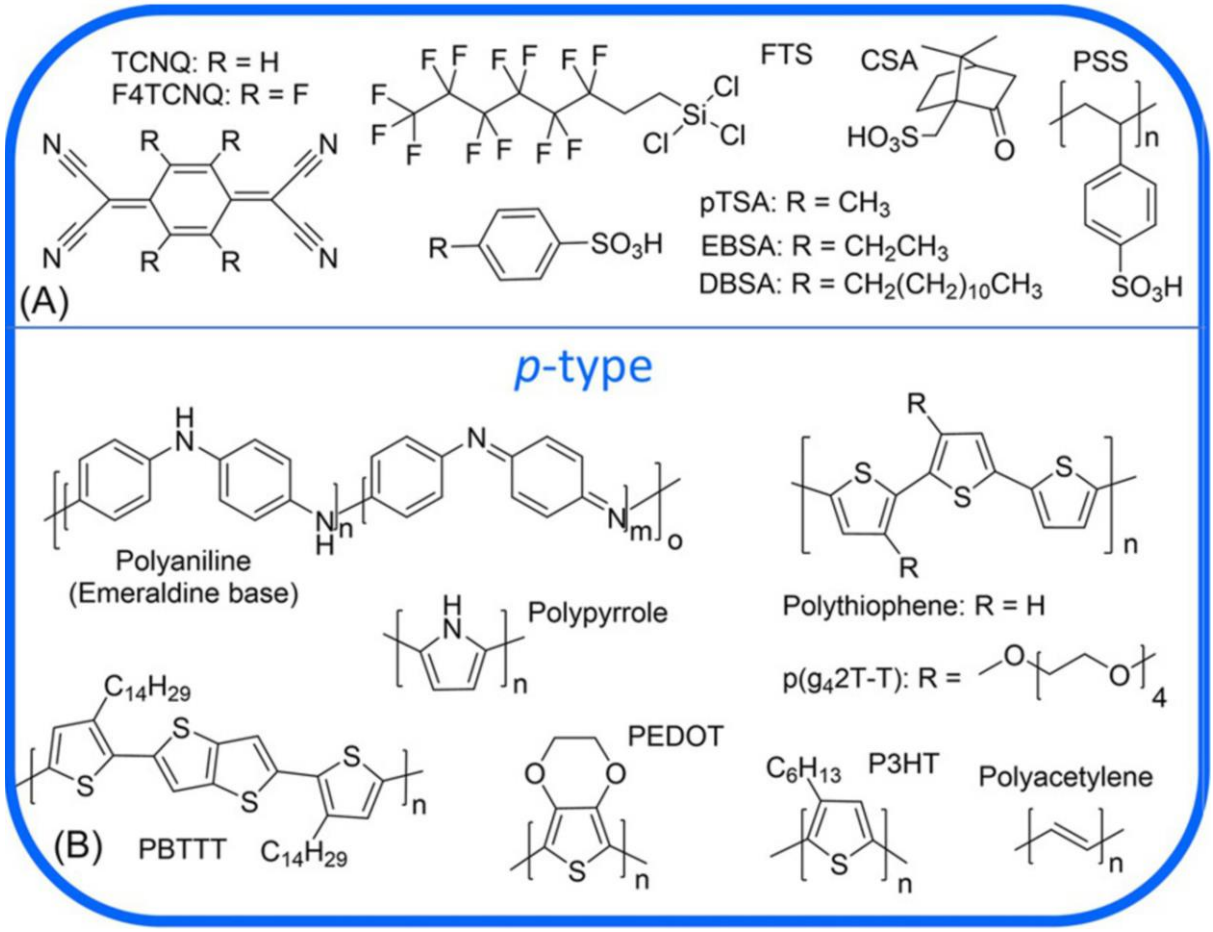

Figure 1.24. *A) Common P-type dopants and B) Polymers used for thermoelectric applications. Reproduced from (5)*

More efforts to enhance the thermoelectric properties were done by Karpov[80] and coworkers in 2016. They have introduced a new dopant F_6TCNNQ which had a slightly lower LUMO energy level than for conventional F_4TCNQ. Molecular doping of P3HT with this strong electron-deficient molecular acceptor produced a high electrical conductivity of ≈ 7 S/cm, greater than conventional P3HT:F_4TCNQ systems.[80] It was concluded that

a polymer: dopant system with more positive energy offset between the HOMO of the polymer and LUMO of the dopant can produce better charge transfer compared to a polymer dopant pair with similar energy levels.

$FeCl_3$ is a strong Lewis acid, which is capable of accepting an electron pair from a Lewis base to form an acid-base adduct. $FeCl_3$ has been used extensively to dope polyacetylene [81] leading to high electrical conductivities of 100 S/cm. Sakai et al. investigated the mechanism of $FeCl_3$ doping on polyacetylene using Mössbauer spectroscopy. Mössbauer spectroscopy reveals the existence of two chemical species of iron atoms, namely $FeCl_2$ and $FeCl_4^-$. Based on this experimental observation, Sakai and coworkers proposed a mechanism of electron transfer between $FeCl_3$ and polyacetylene.

$$FeCl_3 + e^- \longrightarrow FeCl_2 + Cl^- \quad (1)$$

$$FeCl_3 + Cl^- \longrightarrow FeCl_4^- \quad (2)$$

In the proposed mechanism, there are two kinds of $FeCl_3$ dopants which have their individual roles in polyacetylenes: one acts as an electron acceptor from polyacetylene and the other stabilizes the Cl^- ion produced as a result of the reduction of $FeCl_3$.

In the framework of my thesis, I will be mainly investigating the impact of F_4TCNQ, F_6TCNNQ and $FeCl_3$ doping on the crystal structure and TE properties of oriented PBTTT and P3HT thin films prepared by high temperature rubbing. New dopants and new polymers were synthesized by utilizing the wide toolbox of organic chemistry which is represented above (see figure 1.24). A more detailed investigation of doping of polythiophenes such as PBTTT and P3HT is described in section 7.1 of chapter 1 and in the following chapters 2,3 and 4.

b) Charge carriers in conducting polymers

Polarons in a conducting polymer can be generated by several methods such as chemical doping or by electrochemical methods. As discussed in the previous charge transfer

models, the doping of polythiophenes such as PBTTT and P3HT can generate highly conducting radical cations, called polarons. Brédas and coworkers made a detailed investigation of the energetics of polarons and bipolarons upon suitable doping.[82]

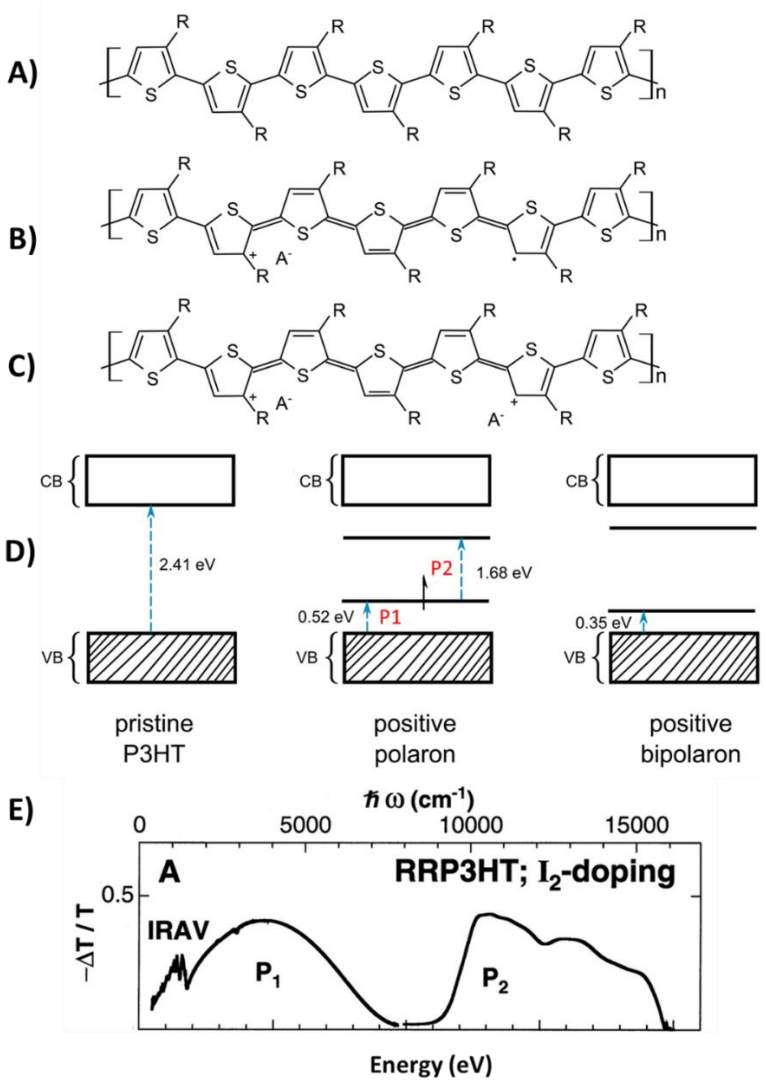

Figure 1.25. *Chemical structure of P3HT A) and the corresponding polaronic B) and bipolaronic C) structures. D) Energy levels of P3HT corresponding to the structural change. E) Doping induced absorption bands of RR P3HT doped with Iodine. Reproduced from (83&84).*

Experimental evidence for the formation of polaron and bipolaron in polymers such as P3HT was obtained by Christina[83] and coworkers using electron paramagnetic resonance spectroscopy (EPR) and Infrared spectroscopy (IR). The presence of a charge on a polymer chain modifies the bond lengths in the thiophene chain and produces a

new state called polaron. It is associated with a new energy level below the bottom of the CB and a level above the VB (see figure 1.25). This reduces the energy gap. These new energy levels produced within the bandgap lead to additional Mid and NIR transitions (labelled as P1 and P2 transitions) in the absorption spectra of doped P3HT (see figure 25D). Vardeny and coworkers also observed these two polaronic transitions in Iodine doped P3HT (see figure 1.25 E).[84] This polaronic distortion in the polymer chains extends over several monomers depending on the structure of the polymer. Further removal of an electron from this polaronic state generates a dication named bipolaron (see figure 1.25 C).

Delocalization of polarons is responsible for the electrical conductivity. In the case of amorphous materials, the polarons are highly localized, leading to very low charge carrier mobilities and conductivities even at high doping levels. For example, amorphous regiorandom P3HT displays poor conductivities of $\approx$ 0.01 S/cm upon vapor phase doping with F_4TCNQ while the regioregular P3HT(RR $\geq$ 84%) showed enhanced conductivities up to 5 S/cm. [85] In the case of semi-crystalline polymers, extended intrachain order helps to delocalize these polarons to a larger number of monomers while the amorphous parts containing the chain ends and folds tend to localize polarons. More generally, polaronic transport in conducting polymers can be i) intrachain via delocalization along the polymer backbone. ii) via hopping between the polymer segments.

7.1. Factors influencing doping and thermoelectric properties of polythiophenes

The ability to dope polythiophenes with strong acceptors such as F_4TCNQ stimulated the exploitation of thermoelectric properties of the PBTTT and P3HT family. One has to optimize several parameters in order to maximize TE performance for a dopant: polymer pair and hence it is a complex process. The easiest way to improve the TE performance of a conducting polymer is by improving its electrical conductivity, whereby one can

improve the PF. The doping and electrical conductivities of conjugated polymers such as polythiophenes can be affected by parameters such as regio-regularity, solid-state order, initial crystallinity of polymer films, IE of polymers, size and EA of the dopants, different doping methods, alkyl side chain length of the polymers and polymer orientation methods. The next section discusses these parameters in detail.

a) Regioregularity, solid-state order and crystallinity: The influence of regioregularity of P3HT on electrical conductivity was studied by Hynynen and coworkers on vapor doped F_4TCNQ: P3HT thin films. The study showed that doping of highly regio-regular P3HT leads to electrical conductivities of ≈ 5.3 S/cm while the amorphous P3HT domains are poorly conducting. Moreover, the electrical conductivity of the regio-regular P3HT was further improved to 12.7 S/cm by increasing the *solid-state* order of P3HT thin films by processing from p-xylene. The enhanced electrical conductivity in regio-regular and p-xylene treated P3HT was attributed to the increased charge carrier mobility.[85][86] Detailed investigations on the crystallinity and electrical conductivity were reported by Scholes et al. in 2017[87]. The properties of molecularly doped films of conjugated polymers were explored as a function of polymer crystallinity.[87] The electrical conductivity of sequentially doped P3HT-F_4TCNQ was higher in films of P3HT with higher crystallinity. The higher electrical conductivities were attributed to the enhanced polaronic delocalization in the crystalline samples, which was evidenced by the UV-Vis-NIR spectroscopy. [87]

b) Thermal conductivity

As discussed in the previous section (6.1), the ZT value of a conducting polymer is also depends on the thermal conductivity. This thermal conductivity is the sum of the electronic (κ_e) and lattice (κ_L) contributions. Few studies reported that the thermal conductivity of conducting polymers are in the range of 0.1 to 0.7 $Wm^{-1}K^{-1}$, similar to

amorphous solids.[88,89] Such low values indicate that the contribution from the electronic thermal conductivity is not significant. The electronic contribution of thermal conductivity (κ_e) is estimated ≈ 0.002 $Wm^{-1}K^{-1}$ based on the electron gas model and using the Wiedermann-Franz law, $\kappa_e = LT\sigma$, where L is the Lorentz factor, which is equal to $2.4\times10^{-8}J^2$ K^{-2} C^{-2} , σ is equal to 300 S/Cm for a conducting polymer and T is the temperature.[90] Thermal conductivity measurements on doped polyaniline further supported this low contribution from κ_e.[87] Hence the main contribution to the thermal conductivity is coming from the lattice vibrations (κ_L). This can be affected by doping, as it changes the number of charge carriers and the volume of the unit cell.

Conducting polymers can either be amorphous, semi-crystalline or liquid crystalline. No systematic studies have been reported so far to investigate the relationship between morphology, crystallinity and the thermal conductivity. Moreover, the room temperature thermal conductivity measurement demands high stability of doped semiconductor.

The thermal conductivity can also be anisotropic. The anisotropy in thermal conductivity is coming from the orientation of polymer chains. Some research work reported an anisotropy of 4 ($\kappa_{//}/\kappa_{\perp}$) in oriented polyimide thin films[91] and 10 in polyethylene.[92] Some of our preliminary results on thermal conductivity measurements in oriented P3HT further support this observation. Engineering of κ is an alternative approach to tune the TE properties but the existing strategies were not reported in this introduction.

c) Size and electron affinity of dopant and IE of polymer

Size and electron affinity of dopants can have a direct impact on the polaronic delocalization and electrical conductivity. It has been already proved that the electron transfer between polythiophenes and dopant molecule is possible only if they have an energetically favourable offset between the HOMO of the polymer and LUMO of the

dopant.[71][79] Marder[93] and coworkers studied a series of dopants with different sizes and electron affinities combined with a number of polymers of different ionization energies. They investigated how these parameters influence the electrical conductivity and TE properties.[93] They have observed that, at lower dopant loading, the molybdenum based dopant Mo (tfd_3) with high electron affinity and large size gave 800 times greater electrical conductivity than $FeCl_3$ doping on the same polymer. *The observed high electrical conductivity was due to high E_A of the dopant and also to the shielding of the Coulombic interaction between the polaron and anion by the large-sized molybdenum dopant.* Unfortunately, the doping efficiency of the molybdenum complex was saturated at low doping level but $FeCl_3$ managed to effectively dope the polymers to reach higher doping level. Another example is the enhanced electrical conductivity observed by Karpov[80] and coworkers in F_6TCNNQ doped P3HT due to a deeper LUMO of the dopant than F_4TCNQ.

Electron transfer between the polymer and the dopant is possible only if they have an energetically favourable offset. For instance, the importance of IE energy of the semiconducting polymers on doping was proposed by Kiefer and coworkers in 2019.[94]They proposed that sometimes the dopants can accept two electrons instead of a single electron from the polymer backbone. This can be possible only when the IE energy of the neutral polymer is not only less than that of the EA of the dopant, but also less or similar to the E_A of the dopant anion. In this case, the dopant can remove one electron to form a di-anion and the dopant anion is also able to remove one electron to become the di-anion. Hence the use of stronger doping agents with the ability to extract two electrons from the polymers of higher IE can produce highly conducting materials.

d) Polymer orientation techniques such as high temperature rubbing[46], epitaxy[55] and tensile stretching[95] are some common methods used to produce highly oriented and crystalline polymers. Several studies showed that the electrical conductivities of

oriented polymers are highly anisotropic and high electrical conductivities and mobilities were measured mainly along the direction of the applied force. [46] For instance, Hamidi-Sakr and coworkers observed an enhanced electrical conductivity of ≈ 22 S/cm along the rubbing direction in oriented P3HT thin films. The film was aligned using high temperature rubbing.[46]. Hynynen and coworkers employed tensile drawing on P3HT to create free-standing films with a high degree of uniaxial alignment. Sequential doping of these aligned films with a molybdenum tris(dithiolene) complex leads to 5-fold enhancement of the power factors up to 16 $\mu Wm^{-1}K^{-2}$ and electrical conductivity of ≈ 13 S/cm along the drawing direction.[95]

e) Doping methods and resulting thermoelectric properties of polythiophenes

Three important doping procedures are mainly used for doping of polythiophenes. They are i) Solution doping ii) Sequential doping from solution and iii) Vapor phase doping.

i) Solution doping of polythiophenes

Solution doping refers to a doping method where both the polymer and the dopant are mixed together in a common organic solvent. The resulting solution is then used to cast thin films. (See figure 1.26 A). Original work by Aziz [76] et al. and Yim et al. reported that rather low conductivities in the range ≈ 0.1-1.0 S cm^{-1} are obtained in P3HT doped with F_4TCNQ in chloroform.[71][72,96–98] Duong [97] et al. demonstrated that in solution mixed doping of P3HT- F_4TCNQ, there exists two doping regimes, the weak and strong doping regimes.[97] At low doping regime (molar concentration of dopant ≤ 0.012), the dopant remains heavily solvated, does not donate the electron to the polymer and stays preferentially in the amorphous regions of P3HT(see figure 1.27 A). Within the strong doping regime (≥ 0.03 to 0.17), most of the F_4TCNQ undergoes spontaneous charge transfer with the polymer and forms $P3HT^+$/ F_4TCNQ^-. This leads to high electrical conductivities in the strong doping regime. Duong[97] and coworkers hypothesized that

the observed conductivity at this strong doping regime might be due to the intercalation of dopant into the crystalline regions of the polymer (see figure 1.27B).

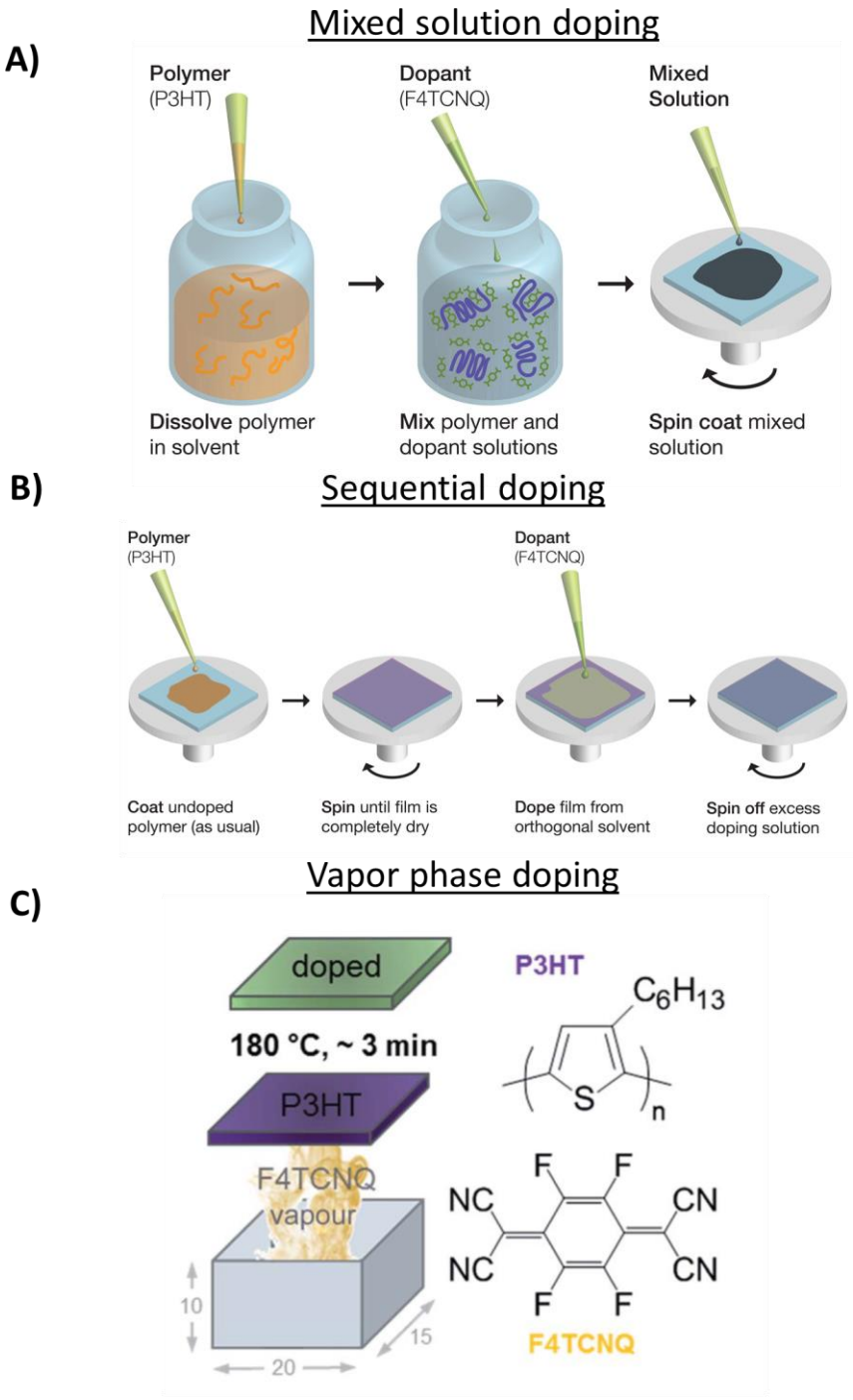

Figure 1.26. *Different doping methods used for polythiophenes. A) Mixed solution doping of P3HT. The dopant and polymer are mixed in a common solvent before casting thin films. B) Sequential doping method. The polymer is spin-coated on a suitable substrate and then the dopant dissolved in an orthogonal solvent is spin-coated on*

the polymer surface. C) Vapor phase doping of P3HT using F_4TCNQ in which the precasted P3HT thin film is exposed to the vapors of F_4TCNQ. Reproduced from (85&96)

Solution doping of PBTTT with F_4TCNQ was first reported by Cochran and coworkers in 2014.[79] The main difficulties during the solution doping were the formation of aggregates, charge transfer salts and precipitation at room temperature. This mixed solution was maintained at 110 °C to 120 °C in order to avoid gelation prior to film casting, which leads to poor doping efficiencies and conductivities. Similarly to P3HT, Glaudell[72] and coworkers showed that solution doping of PBTTT always results in poor conductivities.

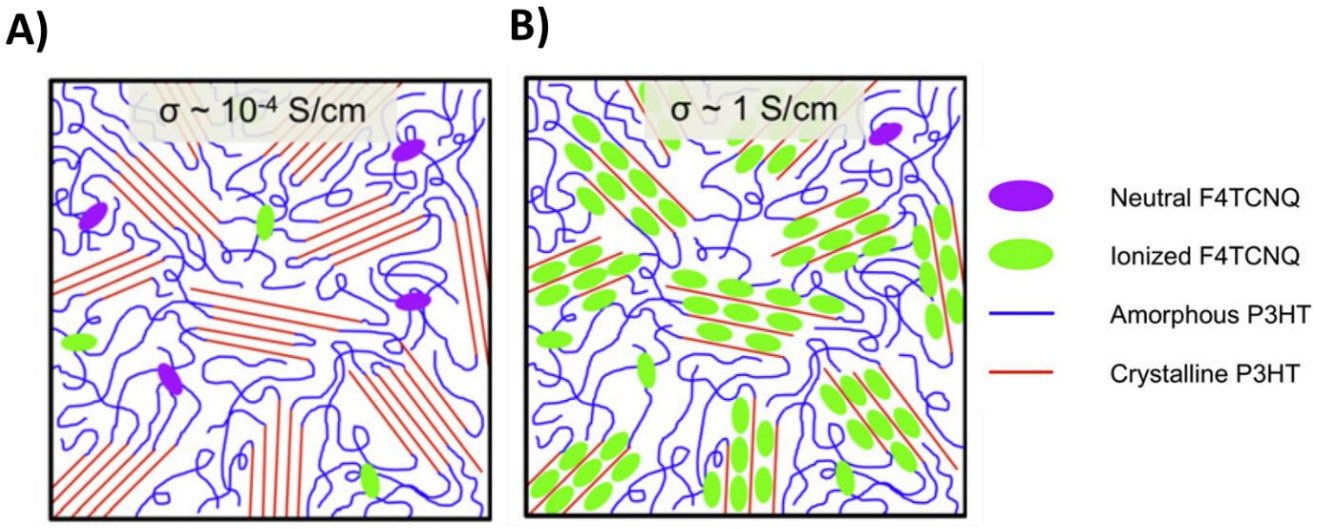

Figure 1.27. *Illustration of doping dependence of electrical conductivity based on the location of dopant anion. A) At lower doping concentration, the ionized F_4TCNQ prefers to reside in the amorphous regions of P3HT. This results in poor conductivity. B) At higher doping concentration, the ionized F_4TCNQ prefers to reside in the crystalline regions of P3HT. This improves electrical conductivity. Reproduced from (97)*

To conclude on solution doping, the main disadvantage is the aggregate formation due to the spontaneous charge transfer between the polymer and dopant in solution. As a consequence, the cast thin films show poorly ordered domains which prevent effective charge transport between ordered P3HT crystals and limits ultimately the conductivity.[96]

ii) Sequential doping of polythiophenes

In order to avoid the aggregation mechanism and poor conductivities in solution doping, a new doping procedure was introduced by Scholes[99] et. al in 2015 which is known as sequential doping. The polymer is first dissolved in a suitable solvent and spin-coated. In the next step, the polymer film is doped by a solution of dopant in an orthogonal solvent (see figure 1.26 B). High electrical conductivity of ≈ 5.5 S/cm was obtained in sequentially doped F_4TCNQ - P3HT.[99] *During sequential doping, the introduction of F_4TCNQ into P3HT preserves the initial structure and orientation of the pristine polymer crystallites and produces a film with lower surface roughness than the mixed solution doping.* Later in 2016, the sequential doping procedure was studied in detail by Jacobs et al.[96] They demonstrated that sequential doping in P3HT- F_4TCNQ occurs rapidly (<1 sec) and that the doping level of the film can be precisely controlled by varying the concentration of the doping solution. Atomic Force Microscopy (AFM) confirmed that sequential doping produces more uniform films as compared to mixed-solution doping. Sequentially doped films contain a large number of tie chains that improve the electrical conductivity in these films.

The sequential doping protocol was successfully applied to other polymer/dopant systems such as P3HT: F4OCTCNQ, P3HT:Mo(tfd)$_3$, P3HT:DDQ and PBTTT:F_4TCNQ and demonstrated the wide applicability of this method [96].

The sequential doping method was also applied to oriented thin films. [46] Highly oriented and crystalline polymer films of P3HT were prepared by high-temperature rubbing and subsequently doped using followed by sequential doping from Acetonitrile (ACN)-F_4TCNQ.

The results on sequentially doped P3HT demonstrate that, in order to reach enhanced electrical conductivities and mobilities, it is important to preserve the initial thin film

morphology and crystal structure of the polymer. Moreover, it is important to intercalate the dopant into the polymer matrix without modifying too much its initial crystal structure.

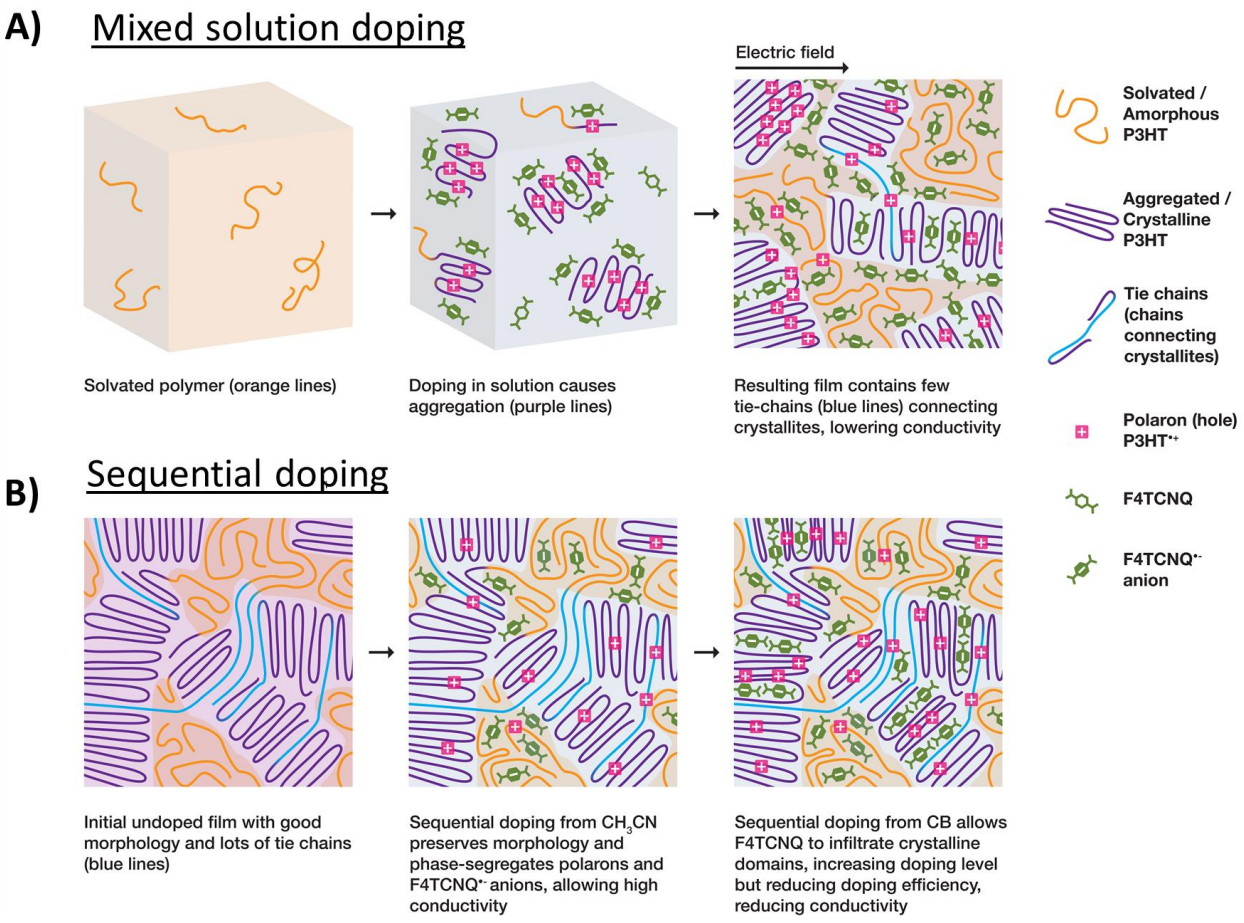

Figure 1.28. *Morphological changes in mixed solution and sequential doping. In the mixed solution doping A) Initially, solvated P3HT tend to aggregate in solution upon addition of F_4TCNQ. These aggregates form disconnected domains with few tie chains. This prevents the delocalization of polarons. In the sequential doping B) the initial morphology of P3HT is maintained after sequential doping with Acetonitrile- F_4TCNQ and the F_4TCNQ^- anions reside in the amorphous regions of P3HT. Incorporation of dopants into crystalline parts occurs by sequential doping from chlorobenzene - F_4TCNQ mixture. Reproduced from (96)*

iii) Vapor phase doping.

An alternative doping method similar to sequential doping makes use of vapor phase deposition of the dopant on the polymer film. A precast polymer film is exposed to the vapors of the dopant for a certain exposure time which helps to control the amount of

dopant incorporated in the film. [85] The advantage of this approach is to avoid any contact of the polymer with an orthogonal solvent. Some of the first examples of such doping were reported by Chabinyc[59] and coworkers for PBTTT and F_4TCNQ. They compared the effect of solution and vapor phase doping with F_nTCNQ (n=2 and 4) on the thin-film microstructure and resulting electrical conductivities of PBTTT. It was observed that the vapor phase doping results in 2 to 3 orders of magnitude higher conductivities than solution doping. Soft X-ray scattering studies on the vapor doped sample indicated that the higher conductivity was due to higher orientation correlation length (OCL - length scale of aligned backbones). Due to higher OCL, vapor doped F_4TCNQ-P3HT films showed very high electrical conductivity of ≈ 670 S/cm and a Seebeck coefficient of 42±6 µV/K. This leads to a PF of ≈ 120 $\mu Wm^{-1}K^{-2}$ for PBTTT: F_4TCNQ, one among the highest PF ever reported for P-type semiconducting polymers.

Various groups have shown that this doping method can be applied to numerous polymers and dopants with similar beneficial effects over solution doping. [85][100] For instance, Hynynen and coworkers showed that the vapor phase doping of P3HT using F_4TCNQ lead to high electrical conductivity of ≈12.7 S/cm. [85] Chabinyc and coworkers further demonstrated that the vapor phase infiltration of F_4TCNQ into the P3HT thin films does not strongly change the initial film morphology and lead to higher electrical conductivities than the solution doped P3HT films. [100] The reported results also indicate that the way the dopant molecules are introduced into the polymer film impacts very strongly the resulting properties of the doped layers. This is why we will investigate in details different doping protocols for oriented PBTTTs (see chapter 2,3 and 4).

7.2. Dopant induced structural changes in polythiophenes

Doping of P3HT and PBTTT with molecules such as F_4TCNQ opens important questions on the exact location of dopants in the polymer matrix. Indeed, those polymers are

either semi-crystalline or liquid-crystalline in structure, which must impact the doping mechanism. In the case of P3HT, one must determine if the dopant prefers to reside in the crystalline domains or in the amorphous zones that contain tie chains, chain ends and chain folds. Several groups have tried to address these issues.

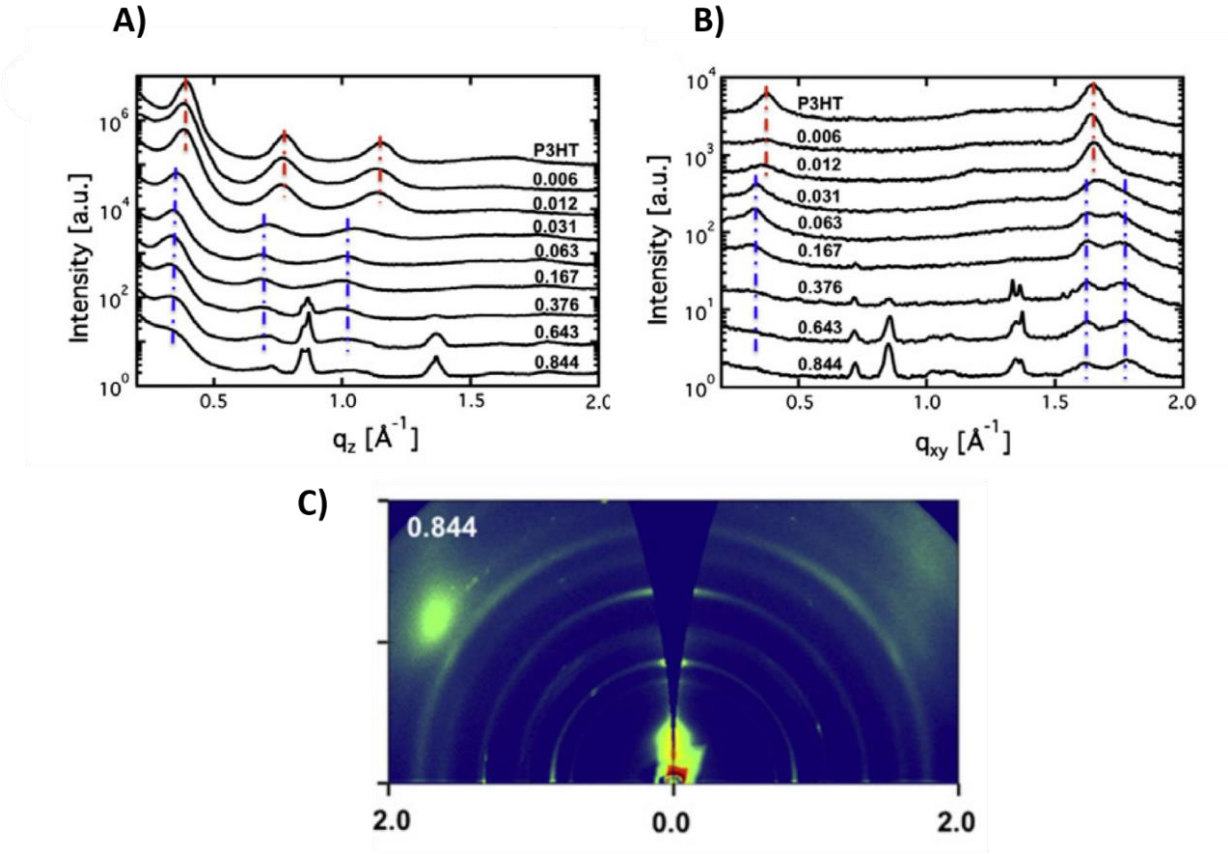

Figure 1.29. *A) Out of plane and B) In-plane scattering profiles of F_4TCNQ doped P3HT thin films extracted from GIXD e. C) 2D GIXD pattern of F_4TCNQ doped P3HT thin film. Reproduced from (97)*

An initial indication on the location of F_4TCNQ^- anion in solution doped P3HT was proposed by Salleo and coworkers[97]. They have proposed that the F_4TCNQ^- anion prefer to reside in the amorphous regions at low dopant concentration and move to the crystalline regions upon higher dopant loading which leads to high conductivities. This is reflected by the changes in the lattice parameters of P3HT thin film. The d_{100} and d_{020} spacing are changed to 18.5 Å and 3.59 Å respectively as evidenced by GIXD (see figure 1.29 A to C).

Following this, Moulé[96] and coworkers reported that the location of the dopant anion is governed by the solvent in which the dopant is dissolved. They reported that sequential doping of P3HT with F_4TCNQ in acetonitrile results in localization of the F_4TCNQ^- anion in the amorphous regions. Moreover, doping from chlorobenzene allows the infiltration of the dopant into the crystalline part (see figure 1.28 B).

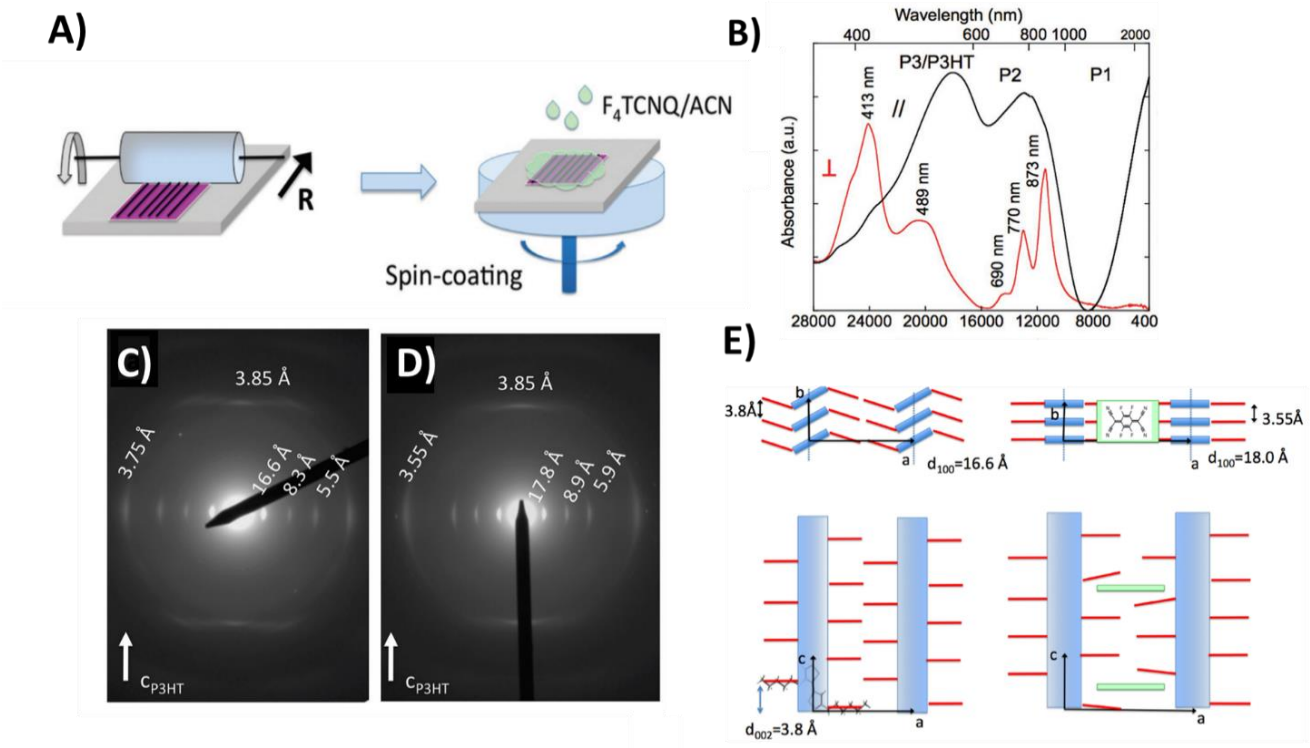

Figure 1.30. *A) Method of preparation of oriented conducting polymer films by a combination of high-temperature rubbing and doping from a solution of F_4TCNQ in acetonitrile. B) Polarized UV-Vis-NIR spectroscopy of oriented P3HT thin films doped by F_4TCNQ in acetonitrile. The polaronic bands (P1, P2 and P3) are polarized along the rubbing direction while the F_4TCNQ^- anions are polarized perpendicular to the direction of rubbing. C) and D) Electron diffraction pattern of as-rubbed and doped P3HT thin films upon sequential doping with F_4TCNQ in acetonitrile. E) Illustrates the corresponding structural changes in the P3HT unit cell as a result of the intercalation of F_4TCNQ into the alkyl side chain layers. Reproduced from (46).*

A more convincing picture of the dopant localization in the crystalline regions was obtained later in the study by Hamidi-Sakr[46] and coworkers on oriented P3HT. A combination of electron diffraction and polarized UV-Vis-NIR spectroscopy were applied to follow the doping mechanism in oriented P3HT films. Electron diffraction

measurements showed that the crystal lattice of P3HT was expanded in the direction of the alkyl side chain layers (d_{100}) and compressed along the direction of π stacking (d_{020}). Polarized UV –Vis-NIR spectroscopy showed that the dopant F_4TCNQ^- lies in a plane perpendicular to the oriented P3HT backbone. The dopant anions are therefore located in the layers of alkyl side chains within the crystalline regions (see figure 1.30 E). This model was widely accepted and later other groups observed the same structural changes in doped P3HT unit cell irrespective of the doping method.[85][99]

Doping PBTTT with F_4TCNQ results in quite similar effects on the crystal structure as for P3HT, namely, an expansion of the lattice along the alkyl side chains and a contraction of the lattice along the π-stacking. An initial investigation of the dopant induced structural changes in solution doped PBTTT was done by Cochran et al. in 2014. [79] Based on GIXD measurements, they proposed that the dopant can be intercalated between conjugated backbones within the π stacks of the polymer. A clear structural model was not proposed due to relatively low intensity of diffraction peaks.

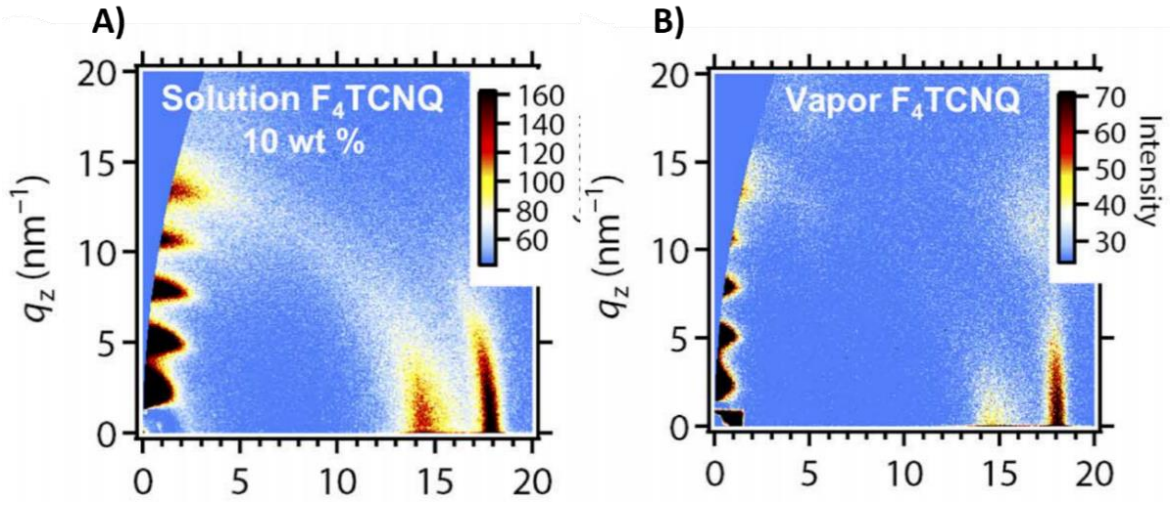

Figure 1.31. *A) and B) GIXD images of the solution and vapor doped F_4TCNQ/C_{14}-PBTTT thin films respectively. Same structural changes in PBTTT irrespective of doping methods. Reproduced from (59).*

Watanabe and coworkers [101] proposed that F_4TCNQ^- anion mainly *reside inside the alkyl side chain layers in the crystalline regions of PBTTT.* In vapor doped C_{14}-PBTTT thin films,

the presence of the anions in the amorphous part was not evidenced experimentally.[97][46] Later, more details on dopant induced structural changes and the orientation of the F_4TCNQ^- anion in PBTTT matrix was evidenced by the work of Hamidi-Sakr et. al[46,102] and by the work of Chabinyc and coworkers (see figure 1.33 A and D).[59] Similar to P3HT, they have observed an expansion of the PBTTT crystal lattice along the alkyl chain direction (d_{100}) and a slight compression along the π stacking direction Moreover, the F_4TCNQ^- anions orient perpendicular to the PBTTT backbone similarly to P3HT.

It is worth to mention that the real reason for the observed decrease in the π-π stacking is still controversial. Hamidi-Sakr et.al[46] proposed that it might be due to the re-organisation of the crystal structure due to the incorporation of the dopant molecules into the side chain layers. However, Liu and coworkers suggested another mechanism based on DFT calculation.[103] They proposed that the polaron delocalization between the adjacent polymer chains and the resulting attractive forces between them is responsible for the reduced π-π stacking distance in doped polythiophenes. The incorporation of the dopants into the side chain region contributes only 0.1 Å to the observed reduction in π stacking. The main contribution is coming from the attractive forces between the charged polymer chains.

It is important to mention that structural characterization methods such as electron diffraction and grazing incidence X-ray diffraction are only able to reveal the structural changes, that occur in the crystalline part of the polymers upon doping. Hence, the presence of dopant anions in the amorphous phase of the polymer is not accessible via TEM. However, our polarized spectroscopic measurements on PBTTT and P3HT doped from F_6TCNNQ and F_4TCNQ (see chapter 2 and 4) do not show any reduction in the absorption of the amorphous part (⊥ direction) upon doping. Some of the recent publication revealed the presence of the dopants in the amorphous part of the polymer.

Hynynen and coworkers proposed the intercalation of Mo (tfd-$COCF_3$)$_3$ dopant into the amorphous part of aligned P3HT. Wide-angle X-ray scattering (WAXS) does not show any evidence of incorporation of this dopant in the crystallites. [94] Yee and coworkers recently demonstrated the dopant induced ordering in amorphous regions of regiorandom P3HT using dopant such as F_4TCNQ and $FeCl_3$. This can be considerd as an evidence for the presence of dopant in the amorphous part.[104]

In conclusion, doping P3HT and PBTTT with F_4TCNQ results in the intercalation of dopant molecules in the crystal lattice of the polymers and more precisely inside the layers of alkyl side chains. The presence of the dopant anions in the amorphous part of the polymer is still a question of debate but seems to depend strongly on the type of dopant.

7.3. TE properties of a few representative using P3HT and PBTTT

Table 1.1 is a non-exhaustive collection of recent results on doped polythiophene thin films (P3HT and PBTTT) including hybrid materials with inorganic nanoparticles, graphene or carbon nanotubes. Mixing of Polymers with suitable fillers like carbon nanotubes, Tellurium nanoparticles, Bismuth Telluride[105] nanoparticles and graphene[106] was also tempted to improve thermoelectric properties of thin films. For instance, Müller and coworkers obtained high conductivities of 10^3 S/cm and a PF of 25 $\mu Wm^{-1}K^{-2}$ in composite films of P3HT and single walled carbon nanotube (SWCNT).[107] The strong π –π interactions between the carbon nanotubes or graphene and P3HT ensures uniform mixing.[106,108–112]

$FeCl_3$ and different iron-based salts were used for higher thermoelectric output because of the strong oxidizing nature of the dopant for P3HT. Ferric salts of triflimide anions (Fe $(TFSI)_3$)[113] and Iron(III) p-toluenesulfonate hexahydrate (Fe^{+3}-tos_3 .$6H_2O$)[114] were also used for P3HT doping.

Table 1.1 Representative thermoelectric performances in p-doped polythiophenes PBTTT and P3HT

Semicon-ductor	Dopant	Doping method	Filler and binder	σ (S cm^{-1})	α (μVK^{-1})	$\propto^2 \sigma$ (μWmK^{-2})	Reference
P3HT	Fe_3-$tos_3.6H_2O$	Sequential Solution		55.4	64	30	Hwang et. al[114]
P3HT			CNT	345 ± 88	97±11	325±101	Hong et. al[112]
P3HT (rr)	$Fe(TFSi_3)$	Sequential (Solution)		96.1	42.2	17.10	Qu et. al[113]
P3HT	$FeCl_3$	Sequential Solution	SWCNT	2760 ± 170	31.1±2.1	267±38	Hong et. al[115]
P3HT			SWCNT	501 ± 32	37.5±1.1	71.8±5.2	Lee et. al[108]
P3HT	$FeCl_3$			254	37.2	35	Hong et. al[116]
P3HT	I_2 Vapor			4.7×10^{-1}	386	7	Zhu et. al[117]
P3HT			MWCNT	1.3×10^{-3}	131		Du et. al[109]
P3HT			Te nano wires		285		Yang et. al[110]
P3HT			Graphene	1.2	35.56	0.16	Du et. al[106]
P3HT	FeTf			87.5	44	20	Müller et. al[107]
P3HT			MWCNT	0.11	11.3	0.0012	Du et. al[111]
P3HT	$FeCl_3$		SWCNT	10^3	48	95	Müller et. al[107]
P3HT	F_4TCNQ	Solution		0.63			Glaudell et. al[72]
P3HT	F_4TCNQ	Solution		0.1			Yim et. al[71]
P3HT	F_4TCNQ	Solution		0.1			Kiefer et. al[98]
P3HT	F_4TCNQ	Solution		1			Aziz et. al[76]
P3HT	F_4TCNQ	Solution		1.8			Duong et. al[97]
P3HT	F_4TCNQ	solution		8			Jacobs et. al[96]
P3HT	F_6TCNNQ	solution		7			Karpov et. al[80]
PBTTT	F_4TCNQ	Solution		2			Cochran et. al[79]

PBTTT	F_4TCNQ	Solution		3.5±0.05	60±9	1.3±5.2	Chabinyc et. al[59]
P3HT	F_4TCNQ	Sequential (Solution)		5.5			Scholes et. al[99]
P3HT	F_4TCNQ	Sequential (Solution)		3			Jacobs et. al[96]
P3HT oriented	F_4TCNQ	Sequential (Solution)		22			Hamidi-Sakr et. al[46]
PBTTT oriented	F_4TCNQ	Sequential (Solution)		187±7	73±12	101	This work[102]
P3HT oriented	$FeCl_3$	Sequential (Solution)		570±100	5.4±0.5	21±6	This work [65]
P3HT oriented	Mo(tfd-$COCF_3)_3$	Sequential (Solution)		13		16	Hynynen et. al[95]
PBTTT oriented	$FeCl_3$	Sequential (Solution)		2×10^5	9.4±0.5	1944±626	This work [65]
PBTTT oriented	F_6TCNNQ	Sequential (Solution		2430±500	47±7	530±200	This work
P3HT	F_4TCNQ	Sequential (Vapor)		5.3			Kang et. al[101]
P3HT	FTS	Sequential (Vapor)		27±0.1	60±9	10±3	Glaudell et. al[72]
P3HT	FTS	Sequential (Vapor)		50±20			Podzorov et. al[118]
PBTTT	FTS	Sequential (Vapor)		604±0.7	19±3	22±7	Glaudell et. al[72]
PBTTT	FTS	Sequential (Vapor)		1100			Podzorov et. al[118]
PBTTT	F_4TCNQ	Sequential (Vapor)		220±0.02	39±5	32±9	Chabinyc et. al[59]
PBTTT	F_2TCNQ	Sequential (Vapor)		36±3	140±20	70±20	Chabinyc et. al[59]

It is worth to mention that most of the iron-based dopants and a combination of them with carbon nanotubes showed satisfactory thermoelectric performances. The solution doping of P3HT and PBTTT using TCNQ derivatives such as F_4TCNQ and F_6TCNNQ produced highly stable and conducting polythiophene thin films.[71][72]|[76][97]|[98][96] [58[99]

8. Conclusion

This literature survey indicates that enhancing TE properties of conjugated polymers is possible by improving the electrical conductivity of the polymer. This can be

achieved by polymer orientations technique or by selecting different doping methods and processing of polymers.

An extensive literature survey on doping methods and resulting TE properties provided some important guidelines to enhance thermoelectric performances in polymer-based systems.

1. Casting a neat semi-crystalline film that forms locally π stacked domains with a long-range conjugated backbone can provide excellent microstructure for efficient charge transport[59].
2. The molecular dopant must be introduced into the polymer microstructure[86,94,98,101] (Vapor or Sequential doping) without disturbing the local order while maintaining or enhancing the long-range order of conjugated backbones. Preserving the orientation, crystallinity and improving the length scale of backbone order are two key methods to enhance thermoelectric properties.

Highly crystalline thin films prepared by high temperature rubbing show enhanced electrical conductivity along the rubbing direction.[34,46,77] Preliminary studies on sequential doping of oriented P3HT films gave important informations on the delocalization of polarons and the location of dopant anions in these systems. Based on these preliminary results, in the framework of my thesis, I will be working on orientation of PBTTT thin films. Once the polymers are aligned by rubbing, different doping methods and different doping agents will be used and correlations between structure and TE properties will be established**.**

Bibliography

[1] H. Peng, X. Sun, W. Weng, X. Fang, in (Eds.: H. Peng, X. Sun, W. Weng, X.B.T.-P.M. for E. and E.A. Fang), Academic Press, **2017**, pp. 9–61.

[2] O. Bubnova, *Thermoelectric Properties of Conducting Polymers.*

[3] R. Kroon, D. A. Mengistie, D. Kiefer, J. Hynynen, J. D. Ryan, L. Yu, C. Müller, *Chem. Soc. Rev.* **2016**, *45*, 6147.

[4] H. Shirakawa, E. Louis, A. MacDiarmid, C. Chiang, J. Heeger, *J.C.S Chem. Comm* **1977**, *13*, 578.

[5] D. Beretta, N. Neophytou, J. M. Hodges, M. G. Kanatzidis, D. Narducci, M. Martin-Gonzalez, M. Beekman, B. Balke, G. Cerretti, W. Tremel, A. Zevalkink, A. I. Hofmann, C. Müller, B. Dörling, M. Campoy-Quiles, M. Caironi, *Mater. Sci. Eng. R Reports* **2018**.

[6] J. W.-P. Lin, L. P. Dudek, *J. Polym. Sci. Polym. Chem. Ed.* **1980**, *18*, 2869.

[7] T. Yamamoto, K. Sanechika, A. Yamamoto, *J. Polym. Sci. Polym. Lett. Ed.* **1980**, *18*, 9.

[8] K. Tremel, S. Ludwigs, *P3HT Revisited – From Molecular Scale to Solar Cell Devices*, Springer Berlin Heidelberg, Berlin, Heidelberg, **2014**.

[9] H. Sirringhaus, P. J. Brown, R. H. Friend, M. M. Nielsen, K. Bechgaard, B. M. W. Langeveld-Voss, A. J. H. Spiering, R. A. J. Janssen, E. W. Meijer, P. Herwig, D. M. de Leeuw, *Nature* **1999**, *401*, 685.

[10] E. J. W. Crossland, K. Tremel, F. Fischer, K. Rahimi, G. Reiter, U. Steiner, S. Ludwigs, *Adv. Mater.* **2012**, *24*, 839.

[11] N. Kayunkid, S. Uttiya, M. Brinkmann, *Macromolecules* **2010**, *43*, 4961.

[12] E. Mena-osteritz, A. Meyer, B. M. W. Langeveld-voss, R. A. J. Janssen, E. W. Meijer, P. Bäuerle, **2000**, 2679.

[13] E. Mena-Osteritz, *Adv. Mater.* **2002**, *14*, 609.

[14] M. Brinkmann, J.-C. Wittmann, *Adv. Mater.* **2006**, *18*, 860.

[15] A. Hamidi-Sakr, L. Biniek, S. Fall, M. Brinkmann, *Adv. Funct. Mater.* **2016**, *26*, 408.

[16] M. Brinkmann, *J. Polym. Sci. Part B Polym. Phys.* **2011**, *49*, 1218.

[17] M. Brinkmann, P. Rannou, *Adv. Funct. Mater.* **2007**, *17*, 101.

[18] A. Zen, M. Saphiannikova, D. Neher, J. Grenzer, S. Grigorian, U. Pietsch, U. Asawapirom, S. Janietz, U. Scherf, I. Lieberwirth, G. Wegner, *Macromolecules* **2006**, *39*, 2162.

[19] L. Hartmann, K. Tremel, S. Uttiya, E. Crossland, S. Ludwigs, N. Kayunkid, C. Vergnat, M. Brinkmann, *Adv. Funct. Mater.* **2011**, *21*, 4047.

[20] M. Brinkmann, P. Rannou, *Macromolecules* **2009**, *42*, 1125.

[21] J.-F. Chang, J. Clark, N. Zhao, H. Sirringhaus, D. W. Breiby, J. W. Andreasen, M. M. Nielsen, M. Giles, M. Heeney, I. McCulloch, *Phys. Rev. B* **2006**, *74*, 115318.

[22] J.-M. Verilhac, G. LeBlevennec, D. Djurado, F. Rieutord, M. Chouiki, J.-P. Travers, A. Pron, *Synth. Met.* **2006**, *156*, 815.

[23] J. Clark, C. Silva, R. H. Friend, F. C. Spano, *Phys. Rev. Lett.* **2007**, *98*, 206406.

[24] T. J. Prosa, M. J. Winokur, J. Moulton, P. Smith, A. J. Heeger, *Macromolecules* **1992**, *25*, 4364.

[25] K. Tashiro, M. Kobayashi, T. Kawai, K. Yoshino, *Polymer (Guildf).* **1997**, *38*, 2867.

[26] I. McCulloch, M. Heeney, M. L. Chabinyc, D. DeLongchamp, R. J. Kline, M. Cölle,

W. Duffy, D. Fischer, D. Gundlach, B. Hamadani, R. Hamilton, L. Richter, A. Salleo, M. Shkunov, D. Sparrowe, S. Tierney, W. Zhang, *Adv. Mater.* **2009**, *21*, 1091.

[27] R. S. Loewe, P. C. Ewbank, J. Liu, L. Zhai, R. D. Mccullough, **2001**, *34*, 4324.

[28] I. McCulloch, M. Heeney, C. Bailey, K. Genevicius, I. MacDonald, M. Shkunov, D. Sparrowe, S. Tierney, R. Wagner, W. Zhang, M. L. Chabinyc, R. J. Kline, M. D. McGehee, M. F. Toney, *Nat. Mater.* **2006**, *5*, 328.

[29] I. Mcculloch, M. Heeney, M. L. Chabinyc, D. Delongchamp, R. J. Kline, M. Cölle, W. Duffy, D. Fischer, D. Gundlach, B. Hamadani, R. Hamilton, L. Richter, A. Salleo, M. Shkunov, D. Sparrowe, S. Tierney, W. Zhang, *Adv. Mater.* **2009**, *21*, 1091.

[30] T. Umeda, D. Kumaki, S. Tokito, *J. Appl. Phys.* **2009**, *105*, 24516.

[31] M. L. Chabinyc, M. F. Toney, R. J. Kline, I. McCulloch, M. Heeney, *J. Am. Chem. Soc.* **2007**, *129*, 3226.

[32] R. Joseph Kline, M. D. McGehee, M. F. Toney, *Nat. Mater.* **2006**, *5*, 222.

[33] E. Cho, C. Risko, D. Kim, R. Gysel, N. Cates Miller, D. W. Breiby, M. D. McGehee, M. F. Toney, R. J. Kline, J.-L. Bredas, *J. Am. Chem. Soc.* **2012**, *134*, 6177.

[34] R. J. Kline, D. M. DeLongchamp, D. A. Fischer, E. K. Lin, L. J. Richter, M. L. Chabinyc, M. F. Toney, M. Heeney, I. McCulloch, *Macromolecules* **2007**, *40*, 7960.

[35] J. M. Szarko, J. Guo, Y. Liang, B. Lee, B. S. Rolczynski, J. Strzalka, T. Xu, S. Loser, T. J. Marks, L. Yu, L. X. Chen, *Adv. Mater.* **2010**, *22*, 5468.

[36] L. Biniek, S. Pouget, D. Djurado, E. Gonthier, K. Tremel, N. Kayunkid, E. Zaborova, N. Crespo-Monteiro, O. Boyron, N. Leclerc, S. Ludwigs, M. Brinkmann, *Macromolecules* **2014**, *47*, 3871.

[37] A. Hamidi-Sakr, D. Schiefer, S. Covindarassou, L. Biniek, M. Sommer, M.

Brinkmann, *Macromolecules* **2016**, *49*, 3452.

[38] D. M. DeLongchamp, R. J. Kline, Y. Jung, D. S. Germack, E. K. Lin, A. J. Moad, L. J. Richter, M. F. Toney, M. Heeney, I. McCulloch, *ACS Nano* **2009**, *3*, 780.

[39] N. A. J. M. van Aerle, M. Barmentlo, R. W. J. Hollering, *J. Appl. Phys.* **1993**, *74*, 3111.

[40] M. F. Toney, T. P. Russell, J. A. Logan, H. Kikuchi, J. M. Sands, S. K. Kumar, *Nature* **1995**, *374*, 709.

[41] G. Horowitz, B. Bachet, A. Yassar, P. Lang, F. Demanze, J.-L. Fave, F. Garnier, *Chem. Mater.* **1995**, *7*, 1337.

[42] T. Matsushima, H. Murata, *Appl. Phys. Lett.* **2011**, *98*, 253307.

[43] H. Heil, T. Finnberg, N. von Malm, R. Schmechel, H. von Seggern, *J. Appl. Phys.* **2003**, *93*, 1636.

[44] L. Biniek, N. Leclerc, T. Heiser, R. Bechara, M. Brinkmann, *Macromolecules* **2013**, *46*, 4014.

[45] S. T. Salammal, E. Mikayelyan, S. Grigorian, U. Pietsch, N. Koenen, U. Scherf, N. Kayunkid, M. Brinkmann, *Macromolecules* **2012**, *45*, 5575.

[46] A. Hamidi-sakr, L. Biniek, J.-L. Bantignies, D. Maurin, L. Herrmann, N. Leclerc, P. Lévêque, V. Vijayakumar, N. Zimmermann, M. Brinkmann, *Adv. Funct. Mater.* **2017**, *27*, 1700173.

[47] F. Motamedi, K. J. Ihn, D. Fenwick, J.-C. Wittmann, P. Smith, *J. Polym. Sci. Part B Polym. Phys.* **1994**, *32*, 453.

[48] J. C. Wittmann, P. Smith, *Nature* **1991**, *352*, 414.

[49] M. Brinkmann, L. Hartmann, L. Biniek, K. Tremel, N. Kayunkid, *Macromol. Rapid Commun.* **2014**, *35*, 9.

[50] S. Nagamatsu, W. Takashima, K. Kaneto, Y. Yoshida, N. Tanigaki, K. Yase, K. Omote, *Macromolecules* **2003**, *36*, 5252.

[51] P. Dyreklev, M. Berggren, O. Inganäs, M. R. Andersson, O. Wennerström, T. Hjertberg, *Adv. Mater.* **1995**, *7*, 43.

[52] B. O'Connor, R. J. Kline, B. R. Conrad, L. J. Richter, D. Gundlach, M. F. Toney, D. M. DeLongchamp, *Adv. Funct. Mater.* **2011**, *21*, 3697.

[53] J. C. Wittmann, B. Lotz, *Prog. Polym. Sci.* **1990**, *15*, 909.

[54] J. A. Koutsky, A. G. Walton, E. Baer, *J. Polym. Sci. Part A-2 Polym. Phys.* **1966**, *4*, 611.

[55] M. Brinkmann, C. Contal, N. Kayunkid, T. Djuric, R. Resel, *Macromolecules* **2010**, *43*, 7604.

[56] J. C. Wittmann, A. M. Hodge, B. Lotz, *J. Polym. Sci. Polym. Phys. Ed.* **1983**, *21*, 2495.

[57] Y.-K. Lan, C.-I. Huang, *J. Phys. Chem. B* **2009**, *113*, 14555.

[58] L. H. Jimison, M. F. Toney, I. McCulloch, M. Heeney, A. Salleo, *Adv. Mater.* **2009**, *21*, 1568.

[59] S. N. Patel, A. M. Glaudell, K. A. Peterson, E. M. Thomas, K. A. O'Hara, E. E. Lim, M. L. Chabinyc, K. O'Hara, E. E. Lim, M. L. Chabinyc, B. Oschmann, J. Lawrence, M. W. Schulze, J. M. Ren, A. Anastasaki, Y. Luo, M. D. Nothling, C. W. Pester, K. T. Delaney, L. A. Connal, A. J. McGrath, P. G. Clark, C. M. Bates, C. J. Hawker, *Sci. Adv.* **2017**, *3*, e1700434.

[60] M. J. Lee, D. Gupta, N. Zhao, M. Heeney, I. McCulloch, H. Sirringhaus, *Adv. Funct. Mater.* **2011**, *21*, 932.

[61] O. Bubnova, Z. U. Khan, A. Malti, S. Braun, M. Fahlman, M. Berggren, X. Crispin, *Nat. Mater.* **2011**, *10*, 429.

[62] T. J. Seebeck, *Der, Abhandlungen der Deut Schen Akad. Berlin, Wissenshafften zu* **1823**, *265*, 1822.

[63] A. F. Ioffe, L. S. Stil'bans, E. K. Iordanishvili, T. S. Stavitskaya, A. Gelbtuch, G. Vineyard, *Phys. Today* **1959**, *12*, 42.

[64] K. C. See, J. P. Feser, C. E. Chen, A. Majumdar, J. J. Urban, R. A. Segalman, *Nano Lett.* **2010**, *10*, 4664.

[65] V. Vijayakumar, Y. Zhong, V. Untilova, M. Bahri, L. Herrmann, L. Biniek, N. Leclerc, M. Brinkmann, *Adv. Energy Mater.* **2019**, *9*, 1900266.

[66] T. M. Tritt, M. A. Subramanian, *MRS Bull.* **2006**, *31*, 188.

[67] H. S. A. J. Heeger, A. G. MacDiarmid, *Macromolecules* **2002**, *35*, 1137.

[68] A. J. Heeger, *Rev. Mod. Phys.* **2001**, *73*, 681.

[69] J. Tsukamoto, A. Takahashi, *Synth. Met.* **1990**, *29*, 125.

[70] Y. Nogami, H. Kaneko, T. Ishiguro, A. Takahashi, J. Tsukamoto, N. Hosoito, *Solid State Commun.* **1990**, *76*, 583.

[71] K.-H. Yim, G. L. Whiting, C. E. Murphy, J. J. M. Halls, J. H. Burroughes, R. H. Friend, J.-S. Kim, *Adv. Mater.* **2008**, *20*, 3319.

[72] A. M. Glaudell, J. E. Cochran, S. N. Patel, M. L. Chabinyc, *Adv. Energy Mater.* **2015**, *5*, 1401072.

[73] Y. Cao, P. Smith, A. J. Heeger, *Synth. Met.* **1992**, *48*, 91.

[74] S. N. Patel, A. M. Glaudell, D. Kiefer, M. L. Chabinyc, *ACS Macro Lett.* **2016**, *5*, 268.

[75] P. Pingel, D. Neher, *Phys. Rev. B - Condens. Matter Mater. Phys.* **2013**, *87*, 1.

[76] E. F. Aziz, A. Vollmer, S. Eisebitt, W. Eberhardt, P. Pingel, D. Neher, N. Koch, *Adv. Mater.* **2007**, *19*, 3257.

[77] M. L. Chabinyc, M. F. Toney, R. J. Kline, I. McCulloch, M. Heeney, *J. Am. Chem. Soc.* **2007**, *129*, 3226.

[78] I. McCulloch, M. Heeney, C. Bailey, K. Genevicius, I. MacDonald, M. Shkunov, D. Sparrowe, S. Tierney, R. Wagner, W. Zhang, M. L. Chabinyc, R. J. Kline, M. D. McGehee, M. F. Toney, *Nat. Mater.* **2006**, *5*, 328.

[79] J. E. Cochran, M. J. N. Junk, A. M. Glaudell, P. L. Miller, J. S. Cowart, M. F. Toney, C. J. Hawker, B. F. Chmelka, M. L. Chabinyc, *Macromolecules* **2014**, *47*, 6836.

[80] Y. Karpov, T. Erdmann, M. Stamm, U. Lappan, O. Guskova, M. Malanin, I. Raguzin, T. Beryozkina, V. Bakulev, F. Günther, S. Gemming, G. Seifert, M. Hambsch, S. Mannsfeld, B. Voit, A. Kiriy, *Macromolecules* **2017**, *50*, 914.

[81] H. Sakai, Y. Maeda, T. aki Kobayashi, H. Shirakawa, *Bull. Chem. Soc. Jpn.* **1983**, *56*, 1616.

[82] J. L. Bredas, G. B. Street, *Acc. Chem. Res.* **1985**, *18*, 309.

[83] C. Enengl, S. Enengl, S. Pluczyk, M. Havlicek, M. Lapkowski, H. Neugebauer, E. Ehrenfreund, *ChemPhysChem* **2016**, *17*, 3836.

[84] R. Österbacka, C. P. An, X. M. Jiang, Z. V Vardeny, *Science (80-.).* **2000**, *287*, 839 LP.

[85] J. Hynynen, D. Kiefer, L. Yu, R. Kroon, R. Munir, A. Amassian, M. Kemerink, C. Müller, *Macromolecules* **2017**, *50*, 8140.

[86] J. Hynynen, D. Kiefer, C. Müller, *RSC Adv.* **2018**, *8*, 1593.

[87] D. T. Scholes, P. Y. Yee, J. R. Lindemuth, H. Kang, J. Onorato, R. Ghosh, C. K. Luscombe, F. C. Spano, S. H. Tolbert, B. J. Schwartz, *Adv. Funct. Mater.* **2017**, *27*, 0.

[88] D. Moses, A. Denenstein, *Phys. Rev. B* **1984**, *30*, 2090.

[89] H. Yan, N. Sada, N. Toshima, *J. Therm. Anal. Calorim.* **2002**, *69*, 881.

[90] O. Bubnova, X. Crispin, *Energy Environ. Sci.* **2012**, *5*, 9345.

[91] Y. S. Ju, K. Kurabayashi, K. E. Goodson, *Thin Solid Films* **1999**, *339*, 160.

[92] A. G. Gibson, D. Greig, M. Sahota, I. M. Ward, C. L. Choy, *J. Polym. Sci. Polym. Lett. Ed.* **1977**, *15*, 183.

[93] Z. M. Liang, Y. D. Zhang, M. Souri, X. Y. Luo, A. M. Boehm, R. P. Li, Y. Zhang, T. R. Wang, D. Y. Kim, J. G. Mei, S. R. Marder, K. R. Graham, *J. Mater. Chem. A* **2018**, *6*, 16495.

[94] D. Kiefer, R. Kroon, A. I. Hofmann, H. Sun, X. Liu, A. Giovannitti, D. Stegerer, A. Cano, J. Hynynen, L. Yu, Y. Zhang, D. Nai, T. F. Harrelson, M. Sommer, A. J. Moulé, M. Kemerink, S. R. Marder, I. McCulloch, M. Fahlman, S. Fabiano, C. Müller, *Nat. Mater.* **2019**, *18*, 149.

[95] J. Hynynen, E. Jarsvall, R. Kroon, Y. D. Zhang, S. Barlow, S. R. Marder, M. Kemerink, A. Lund, C. Muller, *ACS Macro Lett.* **2019**, *8*, 70.

[96] I. E. Jacobs, E. W. Aasen, J. L. Oliveira, T. N. Fonseca, J. D. Roehling, J. Li, G. Zhang, M. P. Augustine, M. Mascal, A. J. Moulé, *J. Mater. Chem. C* **2016**, *4*, 3454.

[97] D. T. Duong, C. Wang, E. Antono, M. F. Toney, A. Salleo, *Org. Electron. physics, Mater. Appl.* **2013**, *14*, 1330.

[98] D. Kiefer, L. Yu, E. Fransson, A. Gómez, D. Primetzhofer, A. Amassian, M. Campoy-Quiles, C. Müller, *Adv. Sci.* **2017**, *4*, 1600203.

[99] D. T. Scholes, S. A. Hawks, P. Y. Yee, H. Wu, J. R. Lindemuth, S. H. Tolbert, B. J. Schwartz, *J. Phys. Chem. Lett.* **2015**, *6*, 4786.

[100] E. Lim, K. A. Peterson, G. M. Su, M. L. Chabinyc, *Chem. Mater.* **2018**, *30*, 998.

[101] K. Kang, S. Watanabe, K. Broch, A. Sepe, A. Brown, I. Nasrallah, M. Nikolka, Z. Fei, M. Heeney, D. Matsumoto, K. Marumoto, H. Tanaka, S. I. Kuroda, H. Sirringhaus, *Nat. Mater.* **2016**, *15*, 896.

[102] V. Vijayakumar, E. Zaborova, L. Biniek, H. Zeng, L. Herrmann, A. Carvalho, O. Boyron, N. Leclerc, M. Brinkmann, *ACS Appl. Mater. Interfaces* **2019**, *11*, 4942.

[103] Z. X. Song, M. N. Banis, L. Zhang, B. Q. Wang, L. J. Yang, D. Banham, Y. Zhao, J. N. Liang, M. Zheng, R. Y. Li, S. Y. Ye, X. L. Sun, *Nano Energy* **2018**, *53*, 716.

[104] P. Y. Yee, D. T. Scholes, B. J. Schwartz, S. H. Tolbert, *J. Phys. Chem. Lett.* **2019**, acs. jpclett.9b02070.

[105] M. He, J. Ge, Z. Lin, X. Feng, X. Wang, H. Lu, Y. Yang, F. Qiu, *Energy Environ. Sci.* **2012**, *5*, 8351.

[106] Y. Du, K. F. Cai, S. Z. Shen, P. S. Casey, *Synth. Met.* **2012**, *162*, 2102.

[107] C. Bounioux, P. Díaz-Chao, M. Campoy-Quiles, M. S. Martín-González, A. R. Goñi, R. Yerushalmi-Rozen, C. Müller, *Energy Environ. Sci.* **2013**, *6*, 918.

[108] W. Lee, C. T. Hong, O. H. Kwon, Y. Yoo, Y. H. Kang, J. Y. Lee, S. Y. Cho, K.-S. Jang, *ACS Appl. Mater. Interfaces* **2015**, *7*, 6550.

[109] Y. Du, S. Z. Shen, W. D. Yang, S. Chen, Z. Qin, K. F. Cai, P. S. Casey, *J. Electron. Mater.* **2012**, *41*, 1436.

[110] Y. Yang, Z.-H. Lin, T. Hou, F. Zhang, Z. L. Wang, *Nano Res.* **2012**, *5*, 888.

[111] Y. Du, S. Z. Shen, W. D. Yang, K. F. Cai, P. S. Casey, *Synth. Met.* **2012**, *162*, 375.

[112] C. T. Hong, Y. H. Kang, J. Ryu, S. Y. Cho, K.-S. Jang, *J. Mater. Chem. A* **2015**, *3*, 21428.

[113] S. Qu, Q. Yao, W. Shi, L. Wang, L. Chen, *J. Electron. Mater.* **2016**, *45*, 1389.

[114] S. Hwang, W. J. Potscavage, R. Nakamichi, C. Adachi, *Org. Electron.* **2016**, *31*, 31.

[115] C. T. Hong, W. Lee, Y. H. Kang, Y. Yoo, J. Ryu, S. Y. Cho, K.-S. Jang, *J. Mater. Chem. A* **2015**, *3*, 12314.

[116] C. T. Hong, Y. Yoo, Y. H. Kang, J. Ryu, S. Y. Cho, K.-S. Jang, *RSC Adv.* **2015**, *5*, 11385.

[117] H. Zhu, C. Liu, H. Song, J. Xu, F. Kong, J. Wang, *Electron. Mater. Lett.* **2014**, *10*, 427.

[118] C. Y. Kao, B. Lee, L. S. Wielunski, M. Heeney, I. McCulloch, E. Garfunkel, L. C. Feldman, V. Podzorov, *Adv. Funct. Mater.* **2009**, *19*, 1906.

Chapter 2. Impact of alkyl side chain length on doping kinetics, crystal structure & thermoelectric properties of oriented PBTTT

Doping of polymer semiconductors such as PBTTT with acceptor molecules such as F_4TCNQ is widely used to tune the charge transport and thermoelectric (TE) properties in thin films. However, the mechanism of dopant insertion in the polymer matrix, the insertion kinetics and the ultimate doping levels have been investigated only marginally. This chapter addresses the impact of alkyl side chain length on the doping mechanism of a series of PBTTTs with linear side chains ranging from *n*-octyl to *n*-octyldecyl.

The study focuses on thin films oriented by high temperature rubbing and sequentially doped in F_4TCNQ solution. Structure-property correlations are established as a function of side chain length by a combination of transmission electron microscopy, polarized UV-Vis-NIR spectroscopy, charge transport and thermopower measurements. Intercalation of F_4TCNQ into the layers of the alkyl side chains results in the expansion of the lattice along the side chains and the contraction along the π-stacking direction for all polymers. The extent of lattice expansion decreases with increasing side chain length. UV-Vis-NIR spectroscopy demonstrates integer charge transfer for all investigated PBTTTs. The doping kinetics and final doping level depend on both the side chain length and packing. Highly disordered *n*-octyl and crystalline *n*-octyldecyl side chain layers tend to hamper dopant diffusion in the side chain layers contrary to *n*-dodecyl side chains that can host the highest proportion of dopants. Consequently, the best TE properties are observed for C_{12}-PBTTT films. Alignment of the polymers enhances significantly the TE performance by increasing the charge conductivity and the thermopower along the

rubbing direction. Aligned films of C_{12}-PBTTT show charge conductivities of 193 S/cm along the rubbing direction and power factors of approximately 100 µW $m^{-2}K^{-1}$ versus a few µW·$m^{-2}K^{-1}$ for non-oriented films.

1. Introduction

Doping of semi-conducting polymers is a simple yet powerful way to control their charge transport properties by tuning the charge carrier densities. Depending on the doping level, different applications can be envisioned in plastic electronics. Low dopant concentrations can be used in blends of semi-conducting and insulating polymers to enhance on/off ratio and charge mobilities in organic field-effect transistors (OFET).[1,2] Doped interface layers can ease charge injection at metallic electrodes.[3] More recently, Crispin and coworkers demonstrated remarkable thermoelectric properties of conducting polymers such as poly(3,4-ethylenedioxythiophene) – tosylate (PEDOT-Tos) by fine-tuning the doping level in the thin films.[4] Another challenging system, of high interest to the scientific community, is regioregular poly(3-hexylthiophene) (P3HT) doped with 2,3,5,6-tetrafluoro-7,7,8,8-tetracyanoquinodimethane (F_4TCNQ). As shown in chapter 1, doping impacts strongly the resulting charge conductivity in thin films. Blending P3HT with F_4TCNQ in solution results in poor charge conductivities.[5–9] Conversely, sequential doping of crystalline P3HT films by spin-coating or by dipping into a solution of F_4TCNQ in an orthogonal solvent results in improved conductivities approaching 10 S/cm.[4–10] As a consequence, the charge conductivity in sequentially doped P3HT can be up to ten times higher than that of doped materials prepared from blends in solution.

Different mechanisms of doping have been considered: formation of a charge-transfer complex with partial charge transfer in quaterthiophene *versus* integer charge transfer in P3HT/F_4TCNQ.[11,12] The crystallinity/morphology of the pristine polymer films prior to doping is also a key parameter that controls the final conductivities. In F_4TCNQ vapor-phase doped films, conductivities of 12.7 S/cm are common for highly crystalline P3HT[13] *versus* 220 S/cm for annealed PBTTT films.[14] Given the high charge transport anisotropy

of P3HT, alignment of the polymer films prior to doping is one additional and very effective method to enhance charge conductivity in doped thin films.[15,16] F_4TCNQ-doping of thin films oriented by high temperature rubbing yields highly oriented conducting polymer films with enhanced conductivities and thermopowers along the rubbing direction.[17] Transmission electron microscopy and polarized UV-Vis-NIR spectroscopy analysis of highly oriented thin films of F_4TCNQ-doped P3HT demonstrated that the F_4TCNQ^- anions are located in the layers of alkyl side chains within crystalline P3HT domains with the molecular long axis of F_4TCNQ^- oriented perpendicular to the polymer backbone.[17] This result raises new questions about the doping mechanism in the majority of semiconducting polymers bearing solubilizing alkyl side chains. In particular, to what extent do the packing (interdigitated or not) and the length of alkyl side chains impact the doping kinetics and ultimate doping level. This is of high importance for the design of new TE materials as the choice of alkyl side chains may help achieve well-defined doping levels and thus to tune the TE properties of doped polymer semiconductors.

The present chapter focuses on a series of poly(2,5-bis(3-alkylthiophen-2-yl)thieno[3,2-*b*]thiophene) (PBTTT) polymers that differ by the length of their linear alkyl side chains, from *n*-octyl to *n*-octyldecyl (C_8, C_{12}, C_{14}, C_{18}) (see figure 2.1). PBTTT is a semi-conducting polymer that exhibits high charge carrier mobilities (up to 1 $cm^2 \cdot V \cdot s$). It has a layered structure composed of highly π-stacked backbones separated by layers of alkyl side chains.[18,19] PBTTT can readily be oriented by both blade coating or high temperature rubbing.[20–23] PBTTT with dodecyl side chains (C_{12}-PBTTT) showed a very high dichroic ratio of more than 10 and high anisotropy in charge mobilities in thin films rubbed at 125°C.[21] Since doping in F_4TCNQ/Acetonitrile (ACN) solution preserves the alignment of the oriented PBTTT films, the combination of rubbing and solution doping is an effective

method to prepare highly oriented conducting polymer films. This strategy is extended here to a family of PBTTTs with different alkyl side chains from *n*-octyl (C_8) to *n*-octyldecyl (C_{18}).

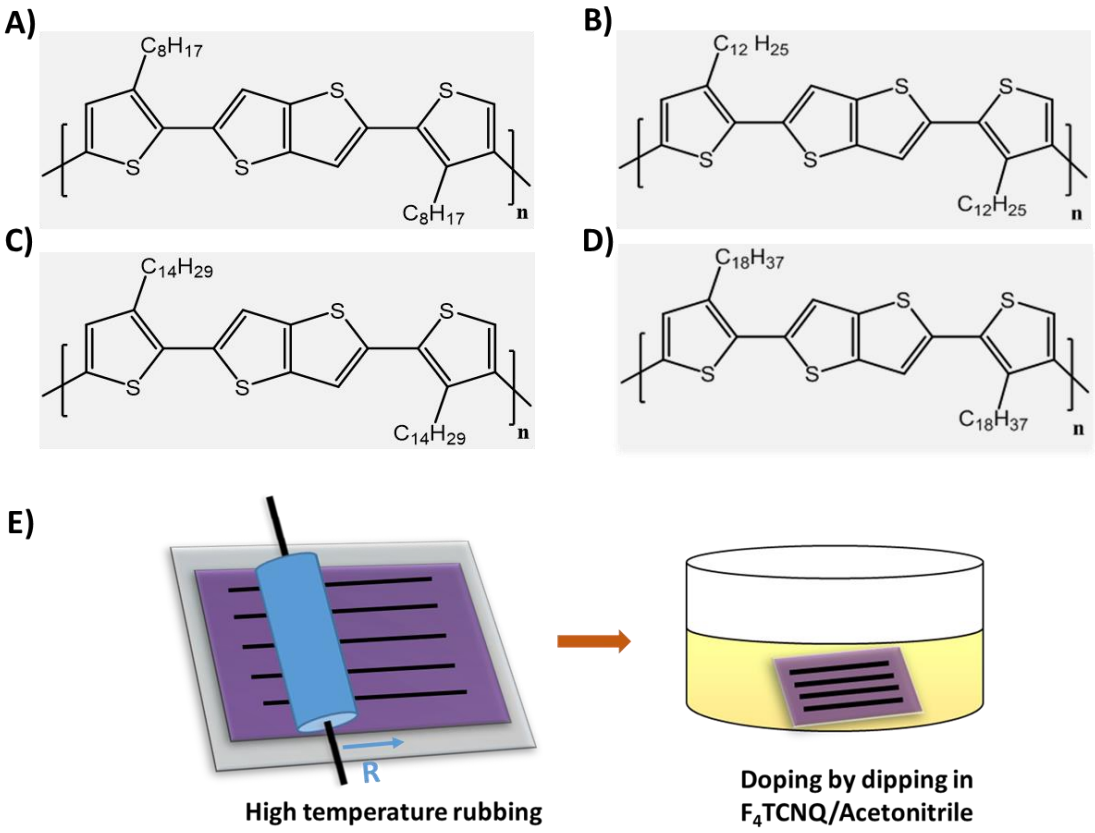

Figure 2.1. *Chemical structures of A) C_8-PBTTT B) C_{12}-PBTTT C) C_{14}-PBTTT and D) C_{18}-PBTTT. E) Schematic illustration of high temperature rubbing and doping of PBTTT thin films by dipping in the dopant F_4TCNQ solution in acetonitrile.*

To that aim, the doping protocol is identical for all polymers i.e. using acetonitrile as a solvent and fixing the F_4TCNQ concentration to 1 mg/ml. Acetonitrile has been chosen as it is an orthogonal solvent for all PBTTTs. As anticipated, all investigated PBTTTs exhibit high orientation prior to and after doping with F_4TCNQ. The kinetics of F_4TCNQ doping in solution is measured for four PBTTTs, namely C_8-PBTTT, C_{12}-PBTTT, C_{14}-PBTTT and C_{18}-PBTTT. The structure of the films with maximum doping level is investigated by low dose electron diffraction and polarized UV-Vis spectroscopy. Finally, the anisotropic

charge transport and Seebeck coefficients are measured in the rubbed thin films. Structure-property correlations are drawn as a function of doping time and alkyl side chain length.

2. Results and discussion

2.1. Fabrication of highly oriented and conducting PBTTT thin films

As demonstrated in our previous work[17], combining high temperature rubbing and doping of the oriented films from a solution of F_4TCNQ in an orthogonal solvent such as acetonitrile affords highly oriented films of conducting polymers. The structure and charge transport properties of which are readily controlled by adjusting the dopant concentration fixed to 1mg/ml in this study[17]. Hereafter, we show that the doping level can also be controlled via the doping time i.e. the contact time between the oriented polymer films and the solution of dopant.

Figure 2.2 illustrates the high birefringence in the doped films and the change in polarized UV-Vis absorption for two PBTTTs with C_{12} and C_{18} side chains. The polarized optical microscopy (POM) images show that the birefringence and thus orientation of the films are preserved after doping. Polarized UV-Vis-NIR spectroscopy was performed with the light polarization either parallel or perpendicular to the rubbing direction. It evidences the presence of highly polarized signals from the polaron (P1 and P2 bands), the neutral polymer (N) and from the F_4TCNQ^- anion.

The neutral and polaronic absorption bands are polarized along the rubbing direction (figure 2.2.A and C) contrary to the characteristic bands of the F_4TCNQ^- anions. For POL⊥R (black curves in figures 2.2 C and F), a weak contribution from amorphous PBTTT (a) is apparent as a shoulder around 500 nm. [21] All PBTTTs show a dominant absorption of the F_4TCNQ^- anion polarized perpendicular to the backbone of PBTTT indicating that

the long axis of the F_4TCNQ^- anion is oriented essentially perpendicular to the polymer backbone. [17] For all investigated side chain lengths (C_8 to C_{18}), the dopant molecules are hosted within the layers of alkyl side chains. The small remaining absorption of F_4TCNQ^- anions for POL//R is either due to the mis-oriented domains of PBTTT or to a possible small tilt of the long axis of F_4TCNQ^- anions away from the normal to the polymer backbone.

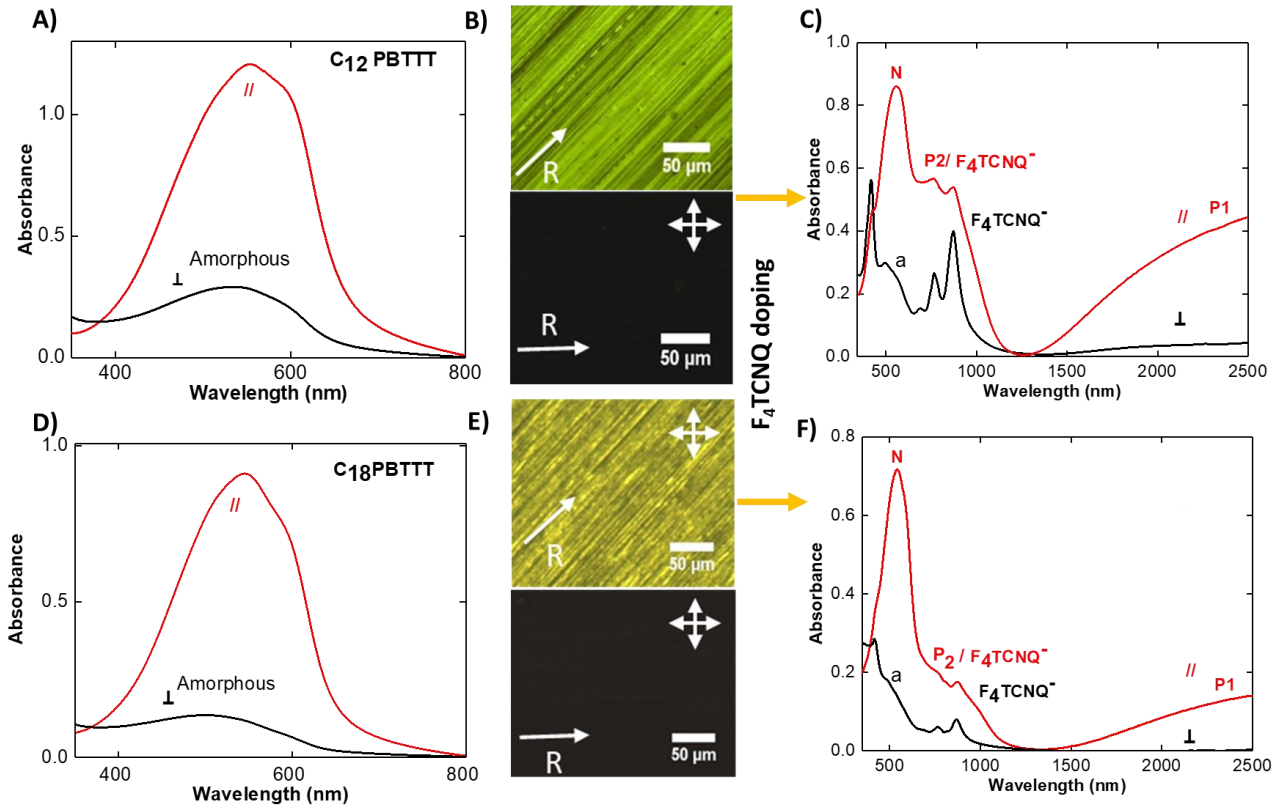

Figure 2.2. *Example of alignment induced by high temperature rubbing (T_R=125°C) for C_{12}-PBTTT and C_{18}-PBTTT thin films and evolution upon doping in solution with F_4TCNQ/ACN (1mg/ml). A) and D) Polarized UV-Vis spectra prior to doping. B) and E) POM images under crossed polarizers showing a high birefringence of the rubbed films when the films are oriented with the rubbing direction (R) at 45° to the polarizer and full extinction when R is parallel to the polarizer. The rubbing direction is given by the arrow R. C) and F) Polarized UV-Vis-NIR spectra of the doped PBTTT films at saturation, in red when the light polarization is parallel to the rubbing direction (POL//R), in black when the light polarization is perpendicular to the rubbing direction (POL⊥R). The main spectral features are highlighted. P1 and P2 correspond to polaronic bands of doped PBTTT. The F_4TCNQ^- bands are highlighted as well as the neutral polymer N and the amorphous non-oriented fraction of the polymer 'a'.*

Having set the basis of the orientation and doping procedures and outcome, we will successively consider in the following, the kinetics of doping, the integer charge transfer and doping level reached at saturation, the structural changes induced by doping and finally the evolution of TE properties versus side chain length.

2.2. Doping kinetics using polarized UV-Vis-NIR spectroscopy

Sequential doping of polymer semi-conductors is a complex mechanism based on the diffusion of dopants in the semi-crystalline polymer matrix coupled to a redox reaction between polymer and dopant. So far, little attention has been paid to the doping kinetics of semiconducting polymers such as PBTTT. It was mostly assumed that the doping is fast and almost instantaneous. Hereafter, UV-Vis-NIR spectroscopy is used to follow the kinetics of doping versus doping time.

Oriented films of various PBTTTs are doped sequentially by increasing the time of contact between the film and the dopant solution in acetonitrile (1mg/ml). The evolution of the UV-Vis spectrum in both parallel (POL//R) and perpendicular (POL⊥R) polarizations vs rubbing direction are shown in figures 2.3 and 2.4 for four PBTTTs with different side chains, respectively.

For POL//R, the main absorption peaks after doping correspond to the polaronic P1 and P2 bands with a fraction of undoped polymer (N). For POL⊥R, the spectrum is quickly dominated by the F_4TCNQ^- anion peaks (413 nm, 770 nm and 875 nm) beside a contribution from amorphous PBTTT that varies little with doping time. For all polymers, the absorption bands of the polaron (P1 and P2) and of the F_4TCNQ^- anion increase with doping time and saturate for long doping times (>10 min). The saturation indicates that a maximum doping concentration is reached for all polymers. For a very short doping time of 5 s, the polaronic bands and anion bands are already intense for C_{12}-PBTTT whereas for C_{18}-PBTTT no doping is observed. In the same time interval, the absorption

peak of the neutral polymer decreases substantially for C_8-PBTTT, C_{12}-PBTTT and C_{14}-PBTTT whereas a smaller decrease of absorbance is evidenced in the case of C_{18}-PBTTT.

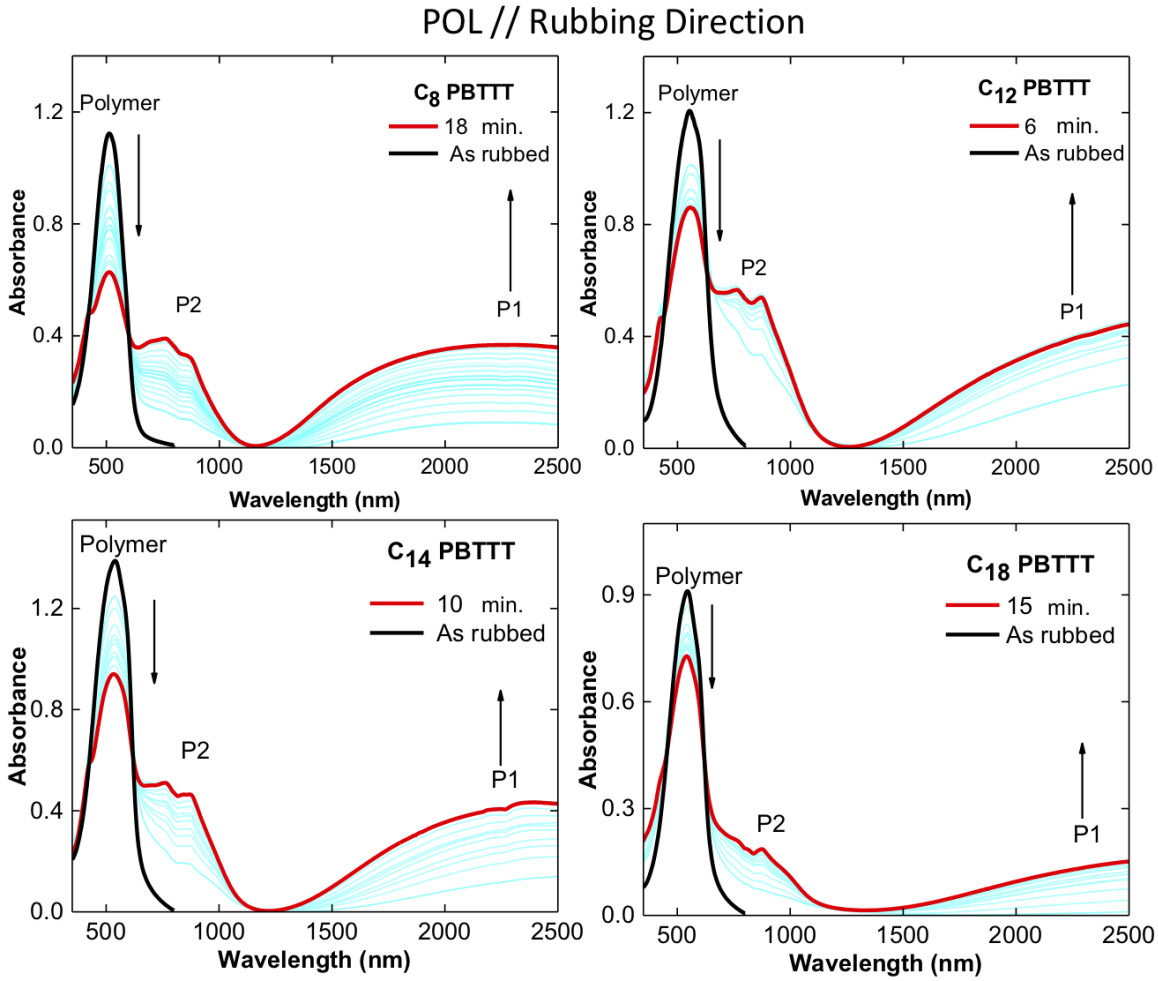

Figure 2.3. *Kinetics of PBTTT doping with F_4TCNQ in acetonitrile (1mg/ml) for POL//R as a function of side chain length. Polaronic bands are labelled P1 and P2. Note that the P2 band overlaps with a small contribution from the F_4TCNQ^- anion. The spectra for the saturation of doping are highlighted in red. The absorption spectra of the undoped films are shown in black.*

The peak maximum of the polaronic band P1 is around 2200 nm (0.56 eV) in PBTTT C_8 but beyond 2500 nm (0.50 eV) for the other three investigated PBTTTs. Recent work by Ghosh et. al on polarons in P3HT indicate that the P1 peak position is determined, at least in part, by the distance between the polythiophene backbone and the F_4TCNQ^- anion located in the layers of alkyl side chains.[24,25] When the polaron and the anion are

placed at infinite distance, the P1 band is most red-shifted. Upon increasing Coulombic interactions, the P1 band progressively shifts to higher energy. Our observation of an apparent larger P1 energy for C_8-PBTTT is therefore consistent with a shorter polaron-anion distance in C_8-PBTTT as compared to the other PBTTTs with longer side chains.

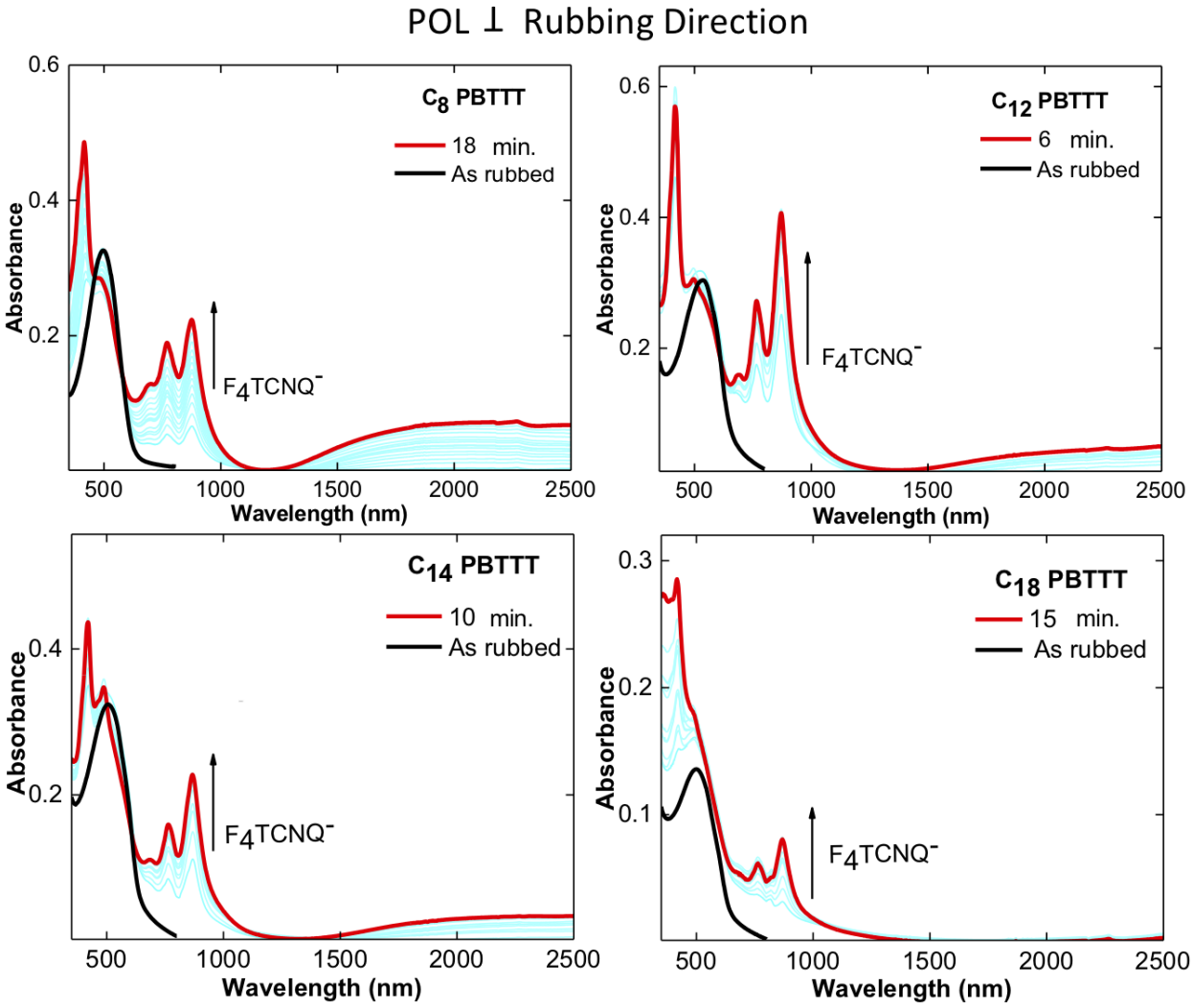

Figure 2.4. *Kinetics of PBTTT doping with F_4TCNQ in acetonitrile (1mg/ml) for POL⊥R as a function of side chain length. Polaronic bands are labelled P1 and P2. The spectra after saturation of doping are highlighted in red. The absorption spectra of the undoped films are shown in black.*

A more quantitative analysis of the doping kinetics is obtained by plotting the intensity of the F_4TCNQ^- anion band at 875 nm as a function of time (see figure 2.5). The absence

of UV-Vis signature of neutral F_4TCNQ in the films[26] indicates that each neutral F_4TCNQ diffused into the polymer film is ionized almost instantaneously upon redox reaction in the polymer film. Accordingly, the kinetics of the absorbance of F_4TCNQ^- anions should reflect the diffusion of the ionized dopant in the polymer matrix. For all polymers, the absorbance of the anion intensity scales like $\sqrt{t}$ for short doping times and it tends to saturate at long doping times(see figure 2.5 A). Each polymer is characterized by a typical doping time τ. However, this time constant τ increases with film thickness. This is related to the dependence between the characteristic doping time and the film thickness l. In a diffusion-limited regime: $l = \sqrt{D\tau}$. The finite film thickness is responsible for the saturation of the doping kinetics.

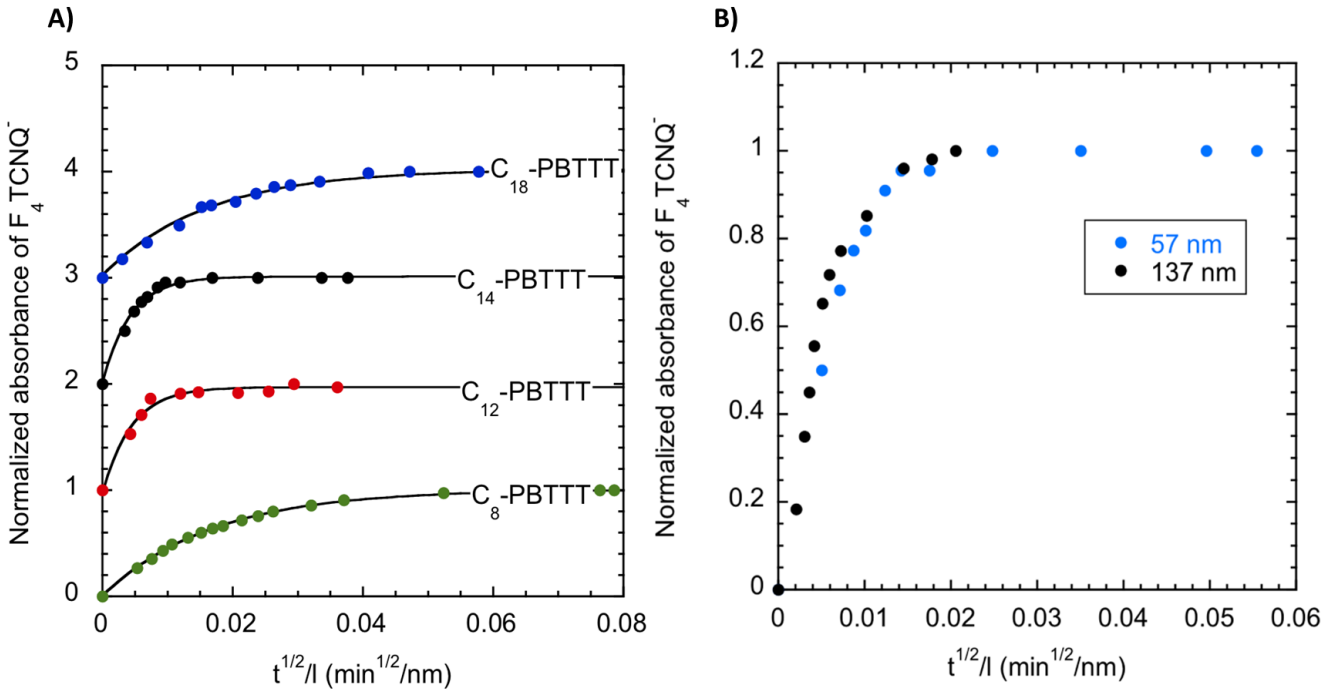

Figure 2.5. *A) Doping kinetics of PBTTTs with F_4TCNQ in acetonitrile (1mg/ml) for various lengths of alkyl side chains as indicated by the time dependence of the F_4TCNQ^- anion absorption peak (0-0 vibronic band in the range 870-883 nm). The representation against $t^{1/2}/l$ is independent of the nominal film thickness l and allows to extract the diffusion coefficient D for each polymer. For clarity, the kinetics curves are shifted along the ordinate axis. (see Table 2.1). The continuous lines are the result of the fitting following the phenomenological equation is given in the text. B) Doping kinetics of two oriented C_{14}-PBTTT films with different thicknesses showing that the curves*

fall on a common master curve when plotted against $t^{1/2}/l$ showing that both films are characterized by a common diffusion coefficient of F_4TCNQ^- in C_{14}-PBTTT.

Accordingly, plotting the normalized F_4TCNQ^- absorption against $t^{1/2}/l$ helps extract the diffusion coefficients of F_4TCNQ^- in the polymer matrix, D, for each PBTTT (In particular, it is possible to verify that two films with different thickness fall on a single master curve (see figure 2.5 B).[27] The time-dependence of the band intensity of the absorption peak at 875 nm, $A_{875}(t)$, was accordingly adjusted using the phenomenological equation:

$$A_{875}(t) = A_0\left(1 - \exp\left(-\frac{\sqrt{D}}{l}(t)^{\frac{1}{2}}\right)\right) \qquad (1)$$

Where A_0 is the final absorbance reached at saturation, l is the film thickness and D is the diffusion coefficient of F_4TCNQ^- in the polymer.

Table 2.1. *Estimated diffusion coefficients of F_4TCNQ^- anions from doping kinetics in oriented thin films of PBTTT with various linear alkyl side chains*

Polymer	C_8-PBTTT	C_{12}-PBTTT	C_{14}-PBTTT	C_{18}-PBTTT
Characteristic doping time τ (s)	50±5	5±1	8+1	59±5
Diffusion constant of dopant 10^{-12} $cm^2 \cdot s^{-1}$	0.58±0.3	9.0±4.5	8.8±3.2	0.61±0.25

As seen in figure 2.5 B, the kinetics of doping of all polymers are very well described by equation (1). The extracted diffusion coefficients are collected in table 1. C_{12}-PBTTT and C_{14}-PBTTT show the highest diffusion coefficients of approx. $9 \cdot 10^{-12}$ cm^2/s which is close to that reported by Maliakal for the diffusion of iodine into P3HT films.[28] In strong contrast, both C_8-PBTTT and C_{18}-PBTTT show significantly smaller diffusion coefficients of approximately $0.6 \cdot 10^{-12}$ cm^2/s.

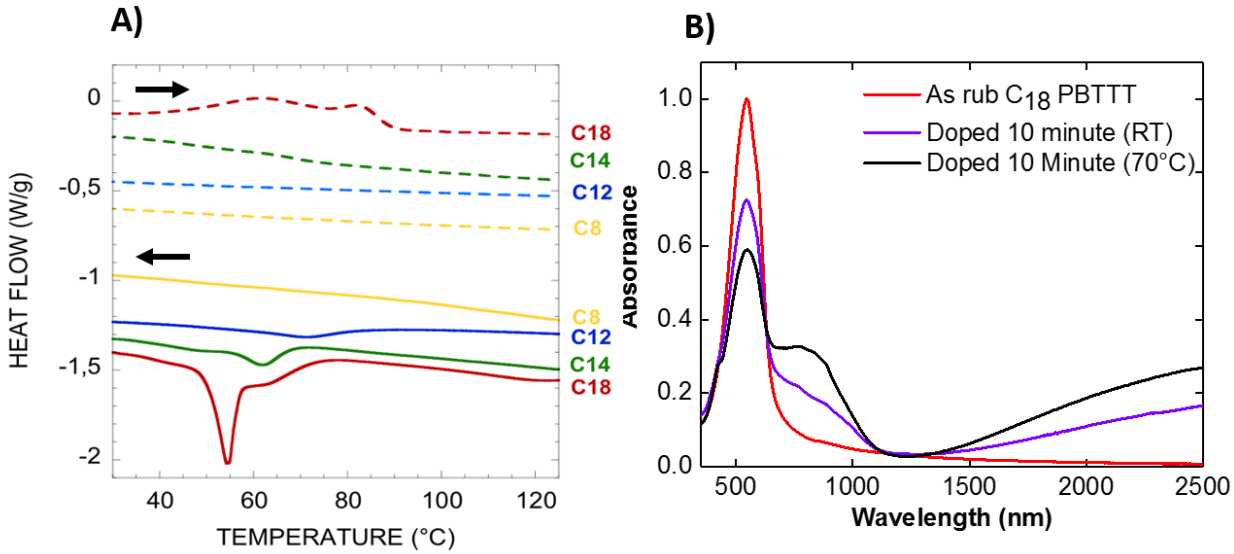

Figure 2.6. *Differential Scanning Calorimetry on PBTTTs powder. Heating and cooling DSC curves showing the side chain melting/crystallization for C_8-PBTTT, C_{12}-PBTTT, C_{14}-PBTTT and C_{18}-PBTTT. B) Comparison of the UV-Vis-NIR spectra of F_4TCNQ-doped C_{18}-PBTTT films at room temperature and 70°C i.e. above the melting of C_{18} side chains. Note the higher intensity of polaronic bands and the decreased absorbance of the neutral polymer when doped at 70°C.*

Table 2.2. *Melting (T_m) and crystallization (T_c) temperatures and their corresponding enthalpy ΔHm and ΔHc, attributed to side chains of four PBTTTs. The temperatures have been measured at the peak maximum, the enthalpy has been measured from the area of the entire peak.*

	T_c (°C)	T_m (°C)	Δ H_c sc (J/g)	Δ H_m sc (J/g)
PBTTT-C_8	-	-	-	-
PBTTT-C_{12}	71.3		4.3	
PBTTT-C_{14}	62.2	62.7	14.9	
PBTTT-C_{18}	54.3	82.2, 62.5	33.9	47.5

The difference in diffusion coefficients of F_4TCNQ^- into the different PBTTTs underlines the essential role of side chain length and packing on the diffusion mechanism of F_4TCNQ in the side chain layers. This assumption is further supported by differential scanning calorimetry (DSC) results that show well-defined side chain crystallization/melting peaks for C_{18}-PBTTT, whereas no such peaks are seen for C_8-PBTTT and only broad and weak peaks for C_{12}-PBTTT and C_{14}-PBTTT (see figure 2.6 and table 2.2). The important

melting/crystallization peaks for C_{18}-PBTTT are consistent with those observed for the corresponding poly(3-alkylthiophene).[29] Accordingly, only C_{18}-PBTTT shows evidence for a well-defined crystalline packing of side chains, contrary to the other PBTTTs. Thus, if C_{18} side chains are effectively packed to form a tight polymethylene sublattice, the inclusion of dopant molecules will be more difficult leading to lower doping levels and slower diffusion kinetics.

The detrimental effect of crystalline side chains on dopant intercalation is further investigated using hot solution doping. For this experiment, an oriented PBTTT thin film is doped by dipping in a hot solution of F_4TCNQ/Acetonitrile mixture at a temperature of 70 °C. This temperature is slightly above the melting temperature of C_{18} side chains. The polarized UV-Vis-NIR spectroscopy showed a higher oxidation level and a higher intensity of P1 and P2 bands in samples doped at 70 °C (see figure 2.6 B). This further supports our previous argument that highly crystalline side chains can have a detrimental effect on dopant diffusion.

The intermediate cases of C_{12} and C_{14} side chains seem most adapted to host the dopant molecules as the layers of side chains are only imperfectly packed. In the crystal structure of C_{14}-PBTTT proposed by Cho et. al the area per alkyl side chain (stem) is 24 $Å^2$ versus 18 $Å^2$ for a polyethylene crystal.[30–32] This implies that there is substantial space for hosting dopant molecules in the imperfectly packed layers of C_{12} and C_{14} side chains. The reason why the doping kinetics is also slow for C_{18}-PBTTT is not yet clear. However, one may suppose that the side chain layers of C_8-PBTTT are too disordered so that the F_4TCNQ molecules cannot be well intercalated between alkyl side chains. This would also be consistent with the UV-Vis-NIR results showing that the F_4TCNQ^- anions are not well oriented in the layers of side chains (anion peaks Visible for both // and $\perp$ polarization). Overall, the results on doping kinetics give strong evidence on the important role of side

chain packing and length on the ultimate doping levels and doping kinetics. This is further supported by the dependence of doping level on alkyl side chain length as seen hereafter.

2.3. Estimation of doping level and integer charge transfer.

The oriented character of the doped PBTTT films helps to establish the saturation level of doping since the contributions of polarons and F_4TCNQ^- are dominant for light polarization parallel and perpendicular to the rubbing direction, respectively. Therefore, the concentration of F_4TCNQ^- can be more readily quantified as compared to non-oriented films for which multi-peak fitting is necessary to disentangle polaronic and F_4TCNQ^- contributions.[7] Regarding F_4TCNQ^-, the extinction coefficient ε of the 0-0 absorption at 880 nm is known (ε= 50000 mol^{-1} L cm^{-1}).[33] We also know the lattice parameters of the doped phases for all PBTTTs at saturation. Hence, it is possible to extract the ratio of concentrations of both F_4TCNQ^- anion and thiophene cycles in the doped films at saturation.

The doping level i.e. the number of F_4TCNQ^- anion per thiophene cycle was calculated at the saturation of the doping in solution from the UV-Vis-NIR absorption spectra for POL $\perp$ R. To that aim, we have first determined the absorbance of the anion and used the extinction coefficient of F_4TCNQ^- reported in the literature for the 0-0 component (ε= 50000 L mol^{-1} cm^{-1}) to obtain the corresponding concentration inside the thin films following the equation $C_{F4TCNQ-}$=Abs(0-0)/ εt where t is the film thickness determined from the absorbance of the undoped film. The absorbance of the 0-0 component of F_4TCNQ^- overlaps partially with the P2 polaronic band as well as the tail of the absorption of the amorphous undoped fraction of the polymer. Rather than performing an arbitrary multipeak fitting using several Gaussians to account for the underlying absorbance of P2 and amorphous fraction[7], we decided to use a linear baseline between 615 nm and

1060 nm to extract the absorbance of the F_4TCNQ^- anion at 875−880 nm. The volume concentration of thiophene in the films ($C_{thiophene}$) was determined from the volume of the unit cell of the doped phases (we assume orthorhombic unit cells with two chains per unit cell). The cell parameters of the doped phases of the PBTTTs are determined from the values of d_{003}, d_{100}, and d_{020} of the diffraction patterns at saturation.

Table 2.3. *Estimated values of the number of F_4TCNQ- anions per thiophene cycles for various PBTTT side chains.*

Polymer	C_8 PBTTT	C_{12} PBTTT	C_{14} PBTTT	C_{18} PBTTT
F_4TCNQ^- anion per thiophene cycle * (%)	7.6±2	14±3	6.9±2	3.3±1

The obtained values are reported in table 2.3. C_{12}-PBTTT shows the highest doping concentration of 14±3 % of F_4TCNQ^- anion per thiophene cycle whereas the lowest doping level is observed for C_{18}-PBTTT (3.3%). Both C_{14}-PBTTT and C_8-PBTTT show intermediate doping levels around 7 %.

The amount of generated anion depends on the possibility of charge transfer between the PBTTT backbone and the neutral F_4TCNQ molecules that have diffused inside the side chain layers. Charge transfer between PBTTT and F_4TCNQ depends on the energetic difference between the donor's HOMO and the acceptor's LUMO.

Cyclic-voltammetric measurements[34] indicate that all four PBTTTs have very close HOMO levels (see figure 2.7 and table 2.4) and therefore, the slight differences in HOMO positions cannot account on their own for the observed differences in doping levels for the PBTTTs. We observe a decrease in doping level from the C_{12} to C_{18}-PBTTT suggesting that the length of side chain layers is one important parameter influencing the final

doping level. However, C_8-PBTTT shows a doping level quite similar to C_{14}-PBTTT which suggests that another parameter must influence the final doping level.

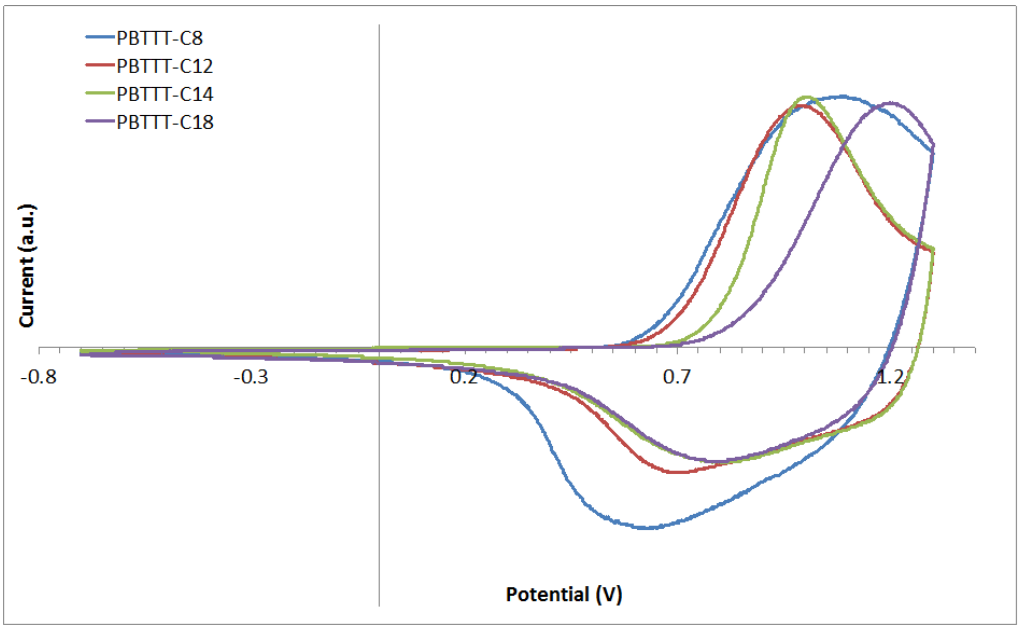

Figure 2.7. *Cyclic voltammograms, in the anodic region, of PBTTT thin-films in ACN containing 0.1 M tetra-n-butylammonium hexafluorophosphate at 20 °C; scan rate 100 mVs^{-1}. All peaks were calibrated against ferrocene (Fc^+/Fc) at E½ = 0.41 V vs SCE.*

Table 2.4. *Oxidation potentials Eox and HOMO energy levels of PBTTT polymers.*

	E_{ox} (V)	**HOMO level (eV)**
C_8-PBTTT	0.65	-5.05
C_{12}-PBTTT	0.70	-5.10
C_{14}-PBTTT	0.80	-5.20
C_{18}-PBTTT	0.85	-5.25

As shown previously for the doping kinetics, the diffusion coefficient D of F_4TCNQ^- in the layers of side chains depends also on the crystallinity/packing of the side chains. As demonstrated by DSC, the layers of alkyl side chains are particularly well and tightly packed for C_{18}-PBTTT, which explains the slow and difficult diffusion of F_4TCNQ for this

polymer, hence the low doping level. In strong contrast, the absence of crystallization/melting observed for C_8-PBTTT indicates that the disordered packing of C_8 side chains is also detrimental for the diffusion and intercalation of dopant molecules. Finally, it is also worth mentioning the potential role of the solvent used for the doping. Fujimoto et al. demonstrated that doping levels are also determined by the choice of solvents e.g. acetonitrile versus fluorinated solvents.[35] Different solvents can show different miscibilities with the polymers. In the case of acetonitrile, the miscibility in the polymer should decrease from C_8 to C_{18}-PBTTT. However, C_8-PBTTT should have the highest miscibility with acetonitrile and does not show the largest doping level. In addition, the diffusion kinetics is slow in C_8-PBTTT. Hence, the differences seen in doping level and kinetics with side chain length cannot be explained based on different extents of acetonitrile diffusion in the four PBTTTs.

It is further important to determine if the doping mechanism is typical of integer charge transfer as observed for F_4TCNQ-doped P3HT.[12] The orientation of the PBTTT films helps analyze quite precisely and independently the time dependence of polaronic and F_4TCNQ^- bands (see figures 2.3 and 2.4). Accordingly, it is relatively simple to identify correlations between the absorbances of the PBTTT polaron and the F_4TCNQ anion as expected in case of integer charge transfer between PBTTT and F_4TCNQ. Figure 2.8 illustrates the correlation between the polaron and anion absorbances for all four investigated PBTTTs. All four polymers show a linear correlation between the intensities of both components, supporting integer charge transfer for all the PBTTTs. Thus, the mechanism of doping implying integer charge transfer between F_4TCNQ and PBTTT is independent of the alkyl side chain length. The observed linear trends also suggest that only polaronic species and no bipolarons are generated in the range of investigated doping concentration.

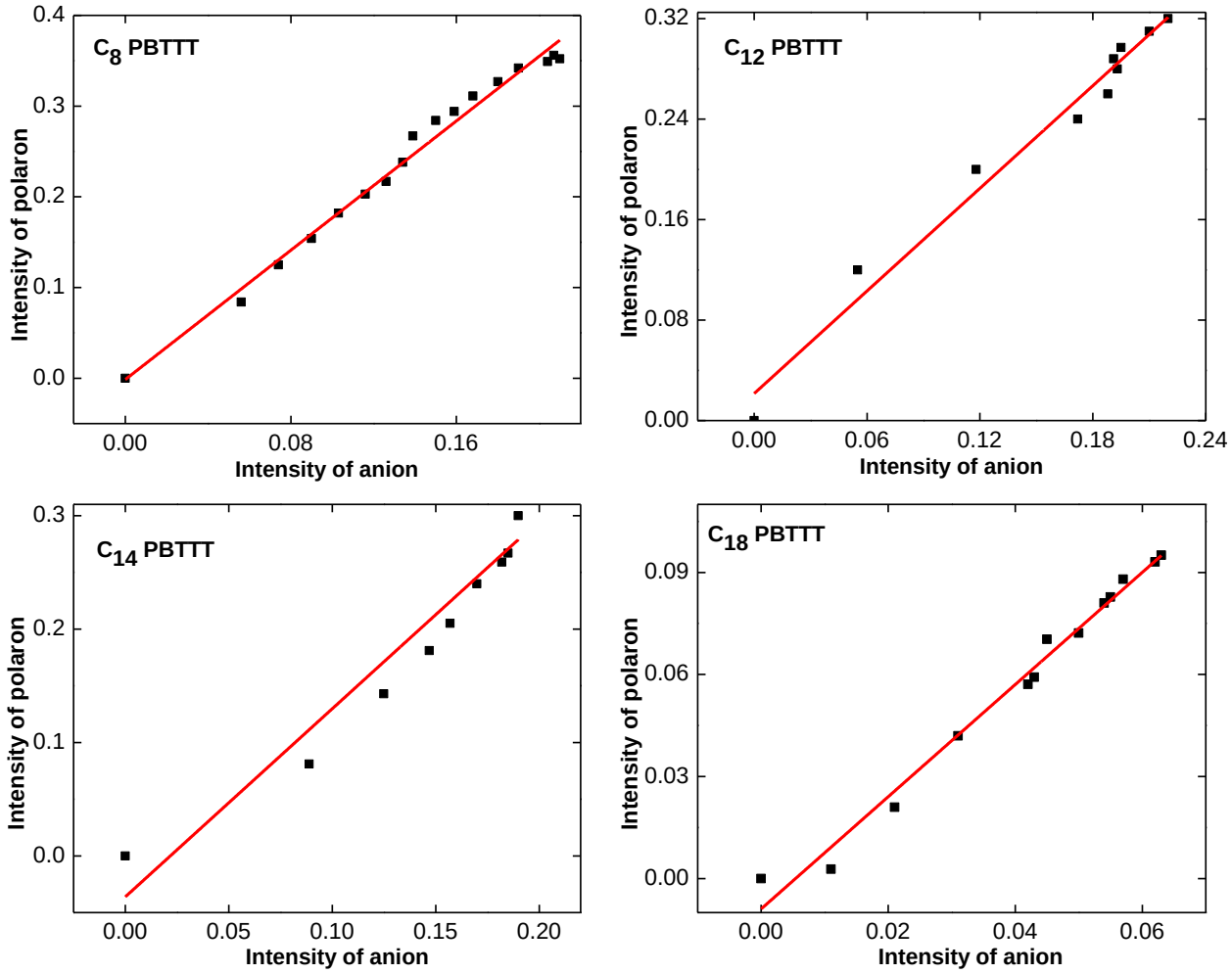

Figure 2.8. *Correlation between the absorbance of the polaron peak P_1 at 2000 nm and the intensity of the F_4TCNQ^- anion peak at 875 nm as observed for different PBTTTs doped in solution of F_4TCNQ/ACN (1mg/ml) at various time intervals.*

2.4. Impact of alkyl side chain length on the structure and final doping concentration.

Low dose electron diffraction (ED) was used to investigate the structural changes upon doping for the oriented PBTTT thin films. Figure 2.9 collects diffraction patterns before and after doping (saturation regime) for four PBTTTs with increasing side chain length. All electron diffraction patterns are characterized by a set of equatorial (h00) (h=1,2,3,4) and a meridional 003 reflection indicating that they are mostly made of face-on domains.[20] A minority of edge-on domains is also present as indicated by the weak equatorial 020 reflection.

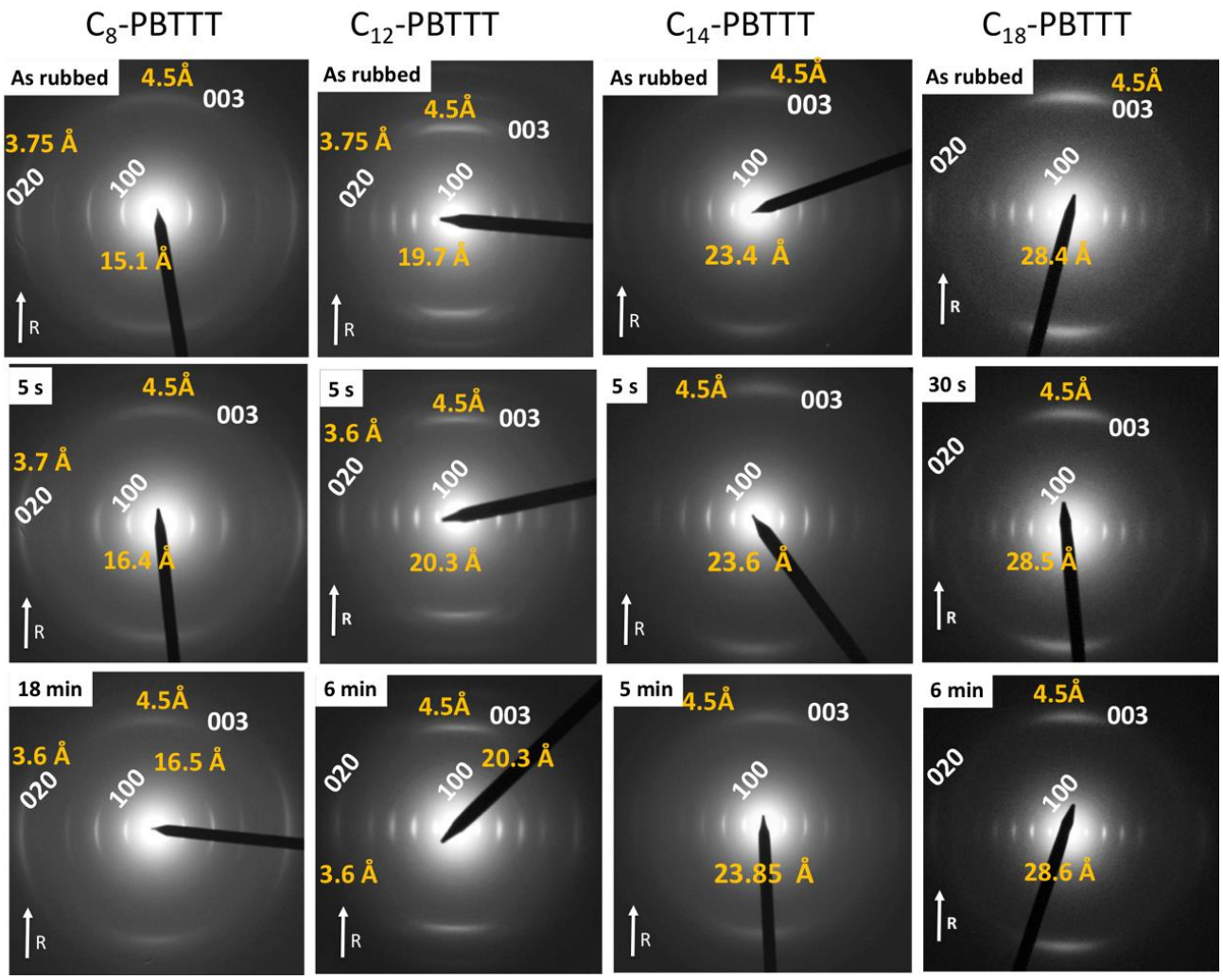

Figure 2.9. *Evolution of the electron diffraction patterns of oriented thin films of various PBTTTs in as-rubbed films (T_R=125°C) and after doping with F_4TCNQ at different doping times. The reticular distances for the interlayer spacing d_{100} and for the π-stacking period 020 are given in orange. The arrow R indicates the chain direction induced upon rubbing*.

For all polymers, ED confirms the previous UV-Vis-NIR and POM observations: doping in F_4TCNQ-acetonitrile preserves the alignment and the original orientation of PBTTT crystals observed in the rubbed films. In particular, the intensity of the meridional (003) reflection along the PBTTT backbone direction is preserved upon doping for all four polymers without important in-plane broadening. This is consistent with previous observations on P3HT oriented films.[17]

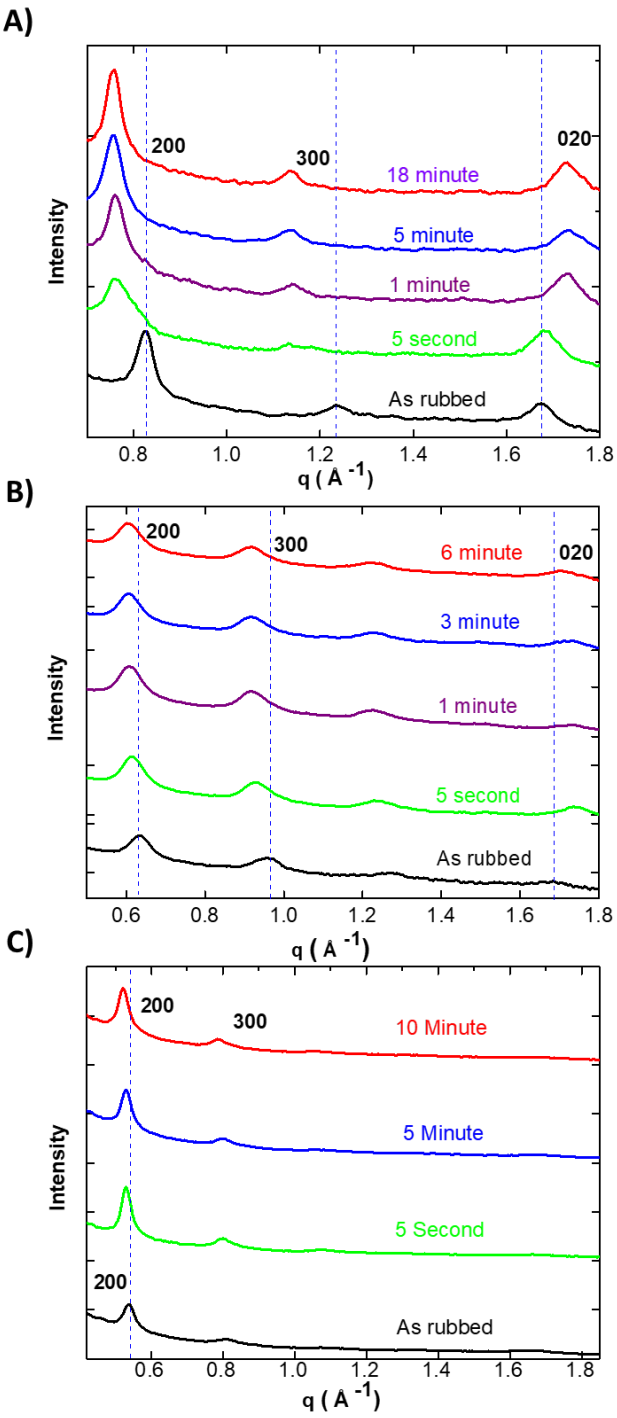

Figure 2.10. *Equatorial section profiles of the ED patterns for thin films oriented by rubbing of PBTTTs with different side chains upon doping at different time intervals in a solution of F_4TCNQ in acetonitrile for: A) C_8-PBTTT, B) C_{12}-PBTTT and C) C_{14}-PBTTT*

Importantly, the relative intensity of 100 and 020 reflection associated to *face-on* vs *edge-on* oriented domains is not modified upon doping indicating no reorientation of

crystal contact plane. Second, as observed in our previous study for P3HT, the inter-layer spacing d_{100} shows a sizable variation upon increasing doping time for C_8-PBTTT, C_{12}-PBTTT and C_{14}-PBTTT.

The equatorial section profiles of the ED patterns help visualize the kinetics of the structural change (see figure 2.10) while the dependence of the interlayer spacing d_{100} and of the π-stacking distance d_{020} with doping time are shown in figure 2.11.

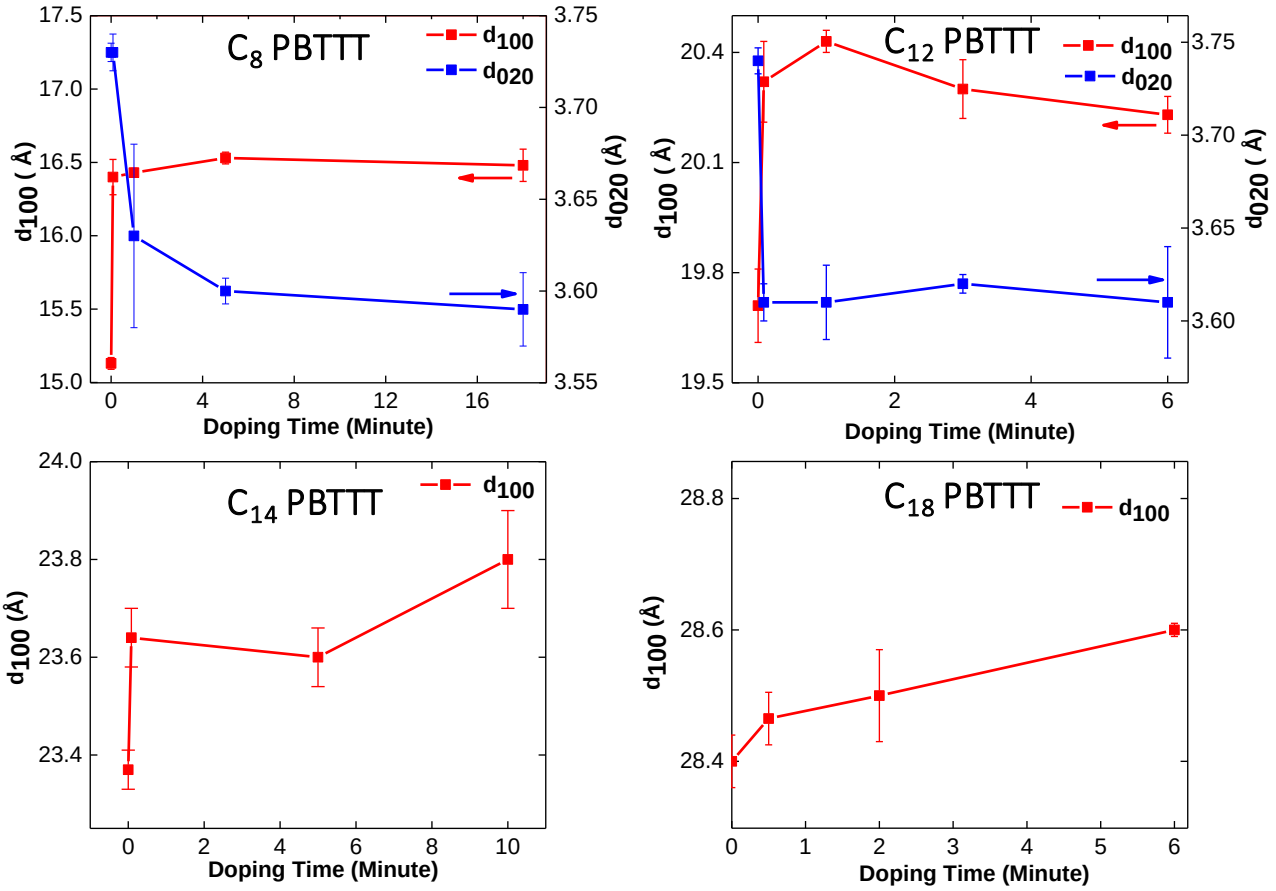

Figure 2.11. *Kinetics of the structural changes associated to the interlayer spacing d_{100} and to the π-stacking d_{020} observed upon doping of the PBTTT thin films in a solution of F_4TCNQ in acetonitrile for different side chain lengths.*

For C_{12}-PBTTT and C_{14}-PBTTT, the changes in unit cell parameters occur within a few seconds and saturation of the unit cell parameters is observed after 1 min of doping, in

agreement with the kinetics of doping evidenced by UV-Vis spectroscopy. For C_{18}-PBTTT, the evolution of the unit cell parameters is slower and similar to that observed in UV-Vis-NIR spectroscopy. More generally, for all PBTTTs the kinetics of the structural changes observed by TEM agree with the doping kinetics evidenced by UV-Vis spectroscopy. More precisely, for C_8-PBTTT, a clear expansion of the interlayer spacing is observed from 15.1 Å to 16.4 Å and a contraction of π-stacking from 3.75 Å to 3.60 Å. Importantly, for t≥1min, there is no coexistence of doped and undoped phase: only one 100 reflection corresponding to the doped phase is observed. This is similar to previous observations for F_4TCNQ-doped P3HT and indicates that the remaining absorbance of neutral C_8-PBTTT seen in the UV-Vis spectrum must correspond to non-doped chain segments enclosed inside the crystals of the doped phase and not to chains within undoped PBTTT crystals.[16] In this regard, the doping of PBTTT with F_4TCNQ is clearly different from the co-crystallization of PBTTT and PCBM that shows the coexistence of the pure PBTTT and the co-crystal phases.[32]

For C_{12}-PBTTT, expansion of the interlayer spacing is from 19.6 Å to 20.4 Å whereas the π-stacking periodicity decreases from 3.75Å to 3.60 Å. The situation is different for C_{18}-PBTTT, that shows a marginal interlayer spacing variation from 28.4 Å to 28.6 Å (see figure 2.11 D). **In other words, the shorter the alkyl side chains, the larger the variation of the unit cell parameters upon doping.**

As seen in figure 2.12, it is possible to correlate the variation in interlayer spacing at doping saturation Δd_{100} with the original interlayer spacing of the pristine undoped PBTTT. Basically, we observe that the polymers with small interlayer spacing show the largest variation in the unit cell parameter after doping. Taking the two extreme cases, Δd_{100} = 1.5 Å for C_8-PBTTT, whereas Δd_{100} = 0.2 Å for C_{18}-PBTTT. The length of alkyl side chains does affect the final structural modification after doping. Most interestingly,

P3HT also follows the trend of PBTTTs evidenced herein, even though it has shorter and non-interdigitated C_6 side chains. This trend might be general and valid for other semiconducting polymers

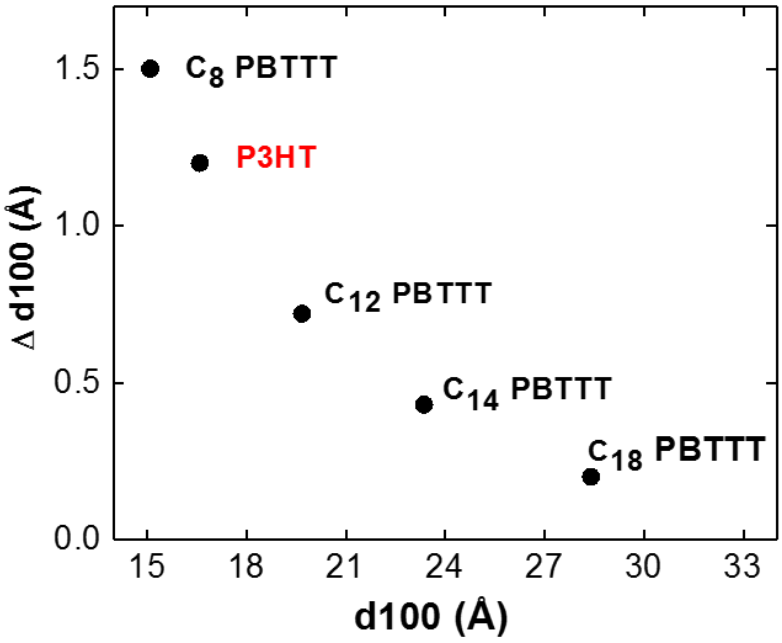

Figure 2.12. *Dependence of the interlayer spacing variation Δd_{100} as a function of the original interlayer spacing d_{100} for F_4TCNQ doped PBTTTs (C_8-PBTTT to C_{18}-PBTTT). The data for F_4TCNQ-doped P3HT is taken from ref. 17*

2.5. Anisotropy of thermoelectric properties

Doping oriented thin films of P3HT with F_4TCNQ induces a substantial increase in power factors because both charge conductivity and thermopower are enhanced in the alignment direction.[17] In order to evaluate the benefits of alignment on the TE efficiency of doped PBTTTs, we have measured the evolution in charge conductivity and Seebeck coefficients of films subjected to different doping times in a solution of F_4TCNQ/ACN. Figure 2.13 illustrates the values of charge conductivity ($\sigma_{//}$ and $\sigma_{\perp}$), Seebeck coefficients ($S_{//}$ and $S_{\perp}$) and the resulting power factors $PF=\sigma S^2$ for C_{12} -PBTTT that shows the best TE performances. The corresponding results (S,σ and PF) for the other PBTTTs are shown in figure 2.15 and 2.16.

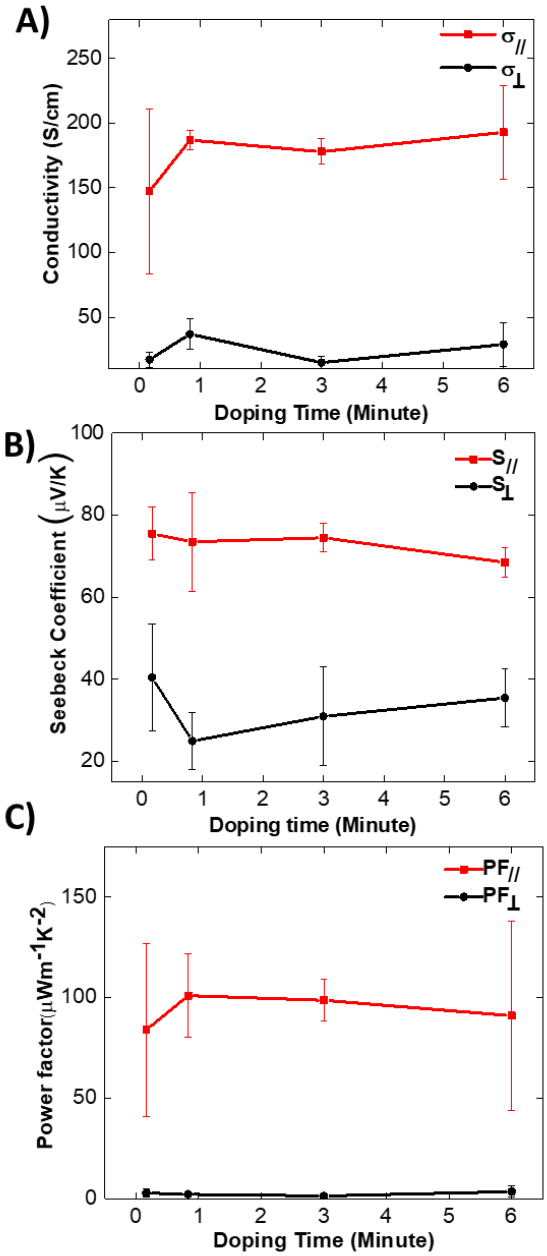

Figure 2.13. *Evolution of the charge conductivity, Seebeck coefficient and power factor as a function of increasing doping concentration of F_4TCNQ for oriented thin films of C_{12}-PBTTT. All values are measured along the directions parallel (//) and perpendicular (⊥) to the rubbing.*

The highest conductivities measured for the four polymers, follow the sequence: C_{12}-PBTTT > C_{14} -PBTTT > C_8-PBTTT > C_{18}-PBTTT. The best value of $\sigma_{//}$ is 193 S/cm for C_{12}-PBTTT. This value is much larger than for non-oriented C_{12}-PBTTT and comparable to that

for non-oriented vapor-phase doped PBTTT.[14,36,37] For C_{12}-PBTTT, the conductivity values tend to saturate very rapidly since the doping kinetics is very fast. The fact that C_{12}-PBTTT reaches the highest conductivity is also consistent with the fact that this polymer shows the highest doping level as determined from the absorbance of the F_4TCNQ^- anion (see table 2.3). The lowest conductivities are observed for C_{18}-PBTTT with the longest side chains ($\sigma_{//}$ of a few S/cm), which is consistent with the fact that it has the smallest doping level at saturation (3.3%). The polymers C_{14}-PBTTT and C_8-PBTTT show intermediate doping levels around 7% and their conductivity $\sigma_{//}$ lies in the 15- 40 S/cm range.

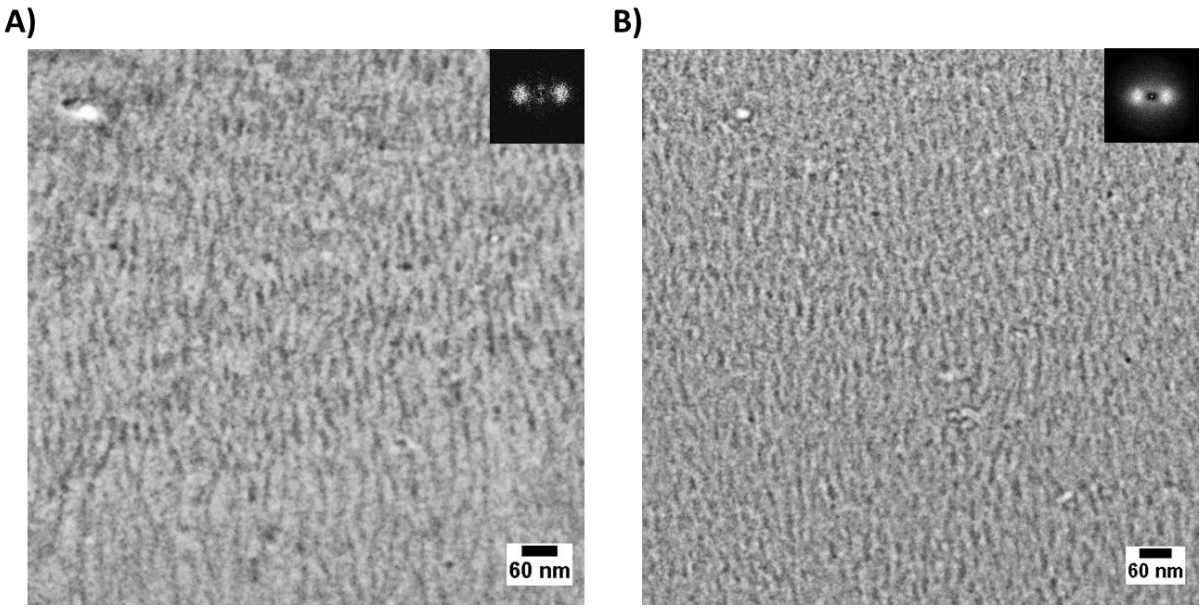

Figure 2.14. *Comparison of the TEM bright field images of C_8-PBTTT films oriented by high temperature rubbing prior to doping (A) and after doping (B) with F_4TCNQ/ACN (0.5 mg/ml). The insets correspond to the Fast Fourier Transforms (FFTs) and indicate a lamellar periodicity of 22±2 nm in both cases.*

The relatively low conductivity of C_8-PBTTT may have different origins. First, this polymer shows the most blue-shifted polaronic bands, suggesting stronger polaron localization due to stronger Coulombic interactions between the polaron and the F_4TCNQ^- anions.[24,25] Second, C_8-PBTTT has a relatively low molecular weight. It is known that

molecular weight significantly impacts structure and morphology thus the charge mobility in polymer semiconductors.[38] As a matter of fact, C_8-PBTTT is the only investigated polymer that shows clearly a semi-crystalline lamellar morphology with a 22 nm periodicity much alike P3HT (see figure 2.14).[17]

Analyzing the ratio $\sigma_{//}/\sigma_{\perp}$ for the four polymers helps identify the impact of side chain length on the charge transport anisotropy (see figure 2.16 B). In the direction perpendicular to the rubbing, the highest values of $\sigma_{\perp}$ are close to 35 S/cm for C_{12}-PBTTT which results in anisotropies $\sigma_{//}/\sigma_{\perp}$ in the range 5-6. For C_8-PBTTT, the anisotropy is close to 2. It is much larger for C_{18}-PBTTT (typically 16-18). The trend in the charge transport anisotropy $\sigma_{//}/\sigma_{\perp}$ versus length of side chain is clear (see figure 2.16 B): the longer the side chains, the larger the anisotropy $\sigma_{//}/\sigma_{\perp}$. This is consistent with the fact that the rubbed films consist mainly of aligned face-on oriented crystals (see ED patterns in figure 2.9). In other words, charge transport measured perpendicular to the rubbing should be dominated by transport along the insulating alkyl side chains, which should be lowest for C_{18}-PBTTT The Seebeck coefficients of all samples exhibit an important anisotropy in oriented thin films. The thermopower parallel to the rubbing $S_{//}$ is always larger than perpendicular to the rubbing $S_{\perp}$. Anisotropy of Seebeck coefficient in oriented conducting polymers has been reported previously for doped polyacetylene (PA) and polyaniline.[39–41] In Iodine-doped PA, the anisotropy $S_{//}/S_{\perp}$ was of the order of two whereas the anisotropy of conductivity $\sigma_{//}/\sigma_{\perp}$ was in the range 50-100. Kaiser as well as Pukaci et. al proposed that the anisotropy of Seebeck coefficient is related to the heterogenous nature of the films where both metallic and semi-conducting domains coexist. This interpretation would also apply in the present case since the UV-Vis spectra of all doped films show the coexistence of doped (metal-like) and undoped (semi-conducting) domains in the thin films (see figure 2.3 and 2.4). It can be anticipated that

such a co-existence of doped and undoped phases could be beneficial in oriented films to observe simultaneously a high charge conductivity and a high Seebeck coefficient. In chapter 3, we develop in more details the heterogenous system model to account for the observed differences in Seebeck coefficients.

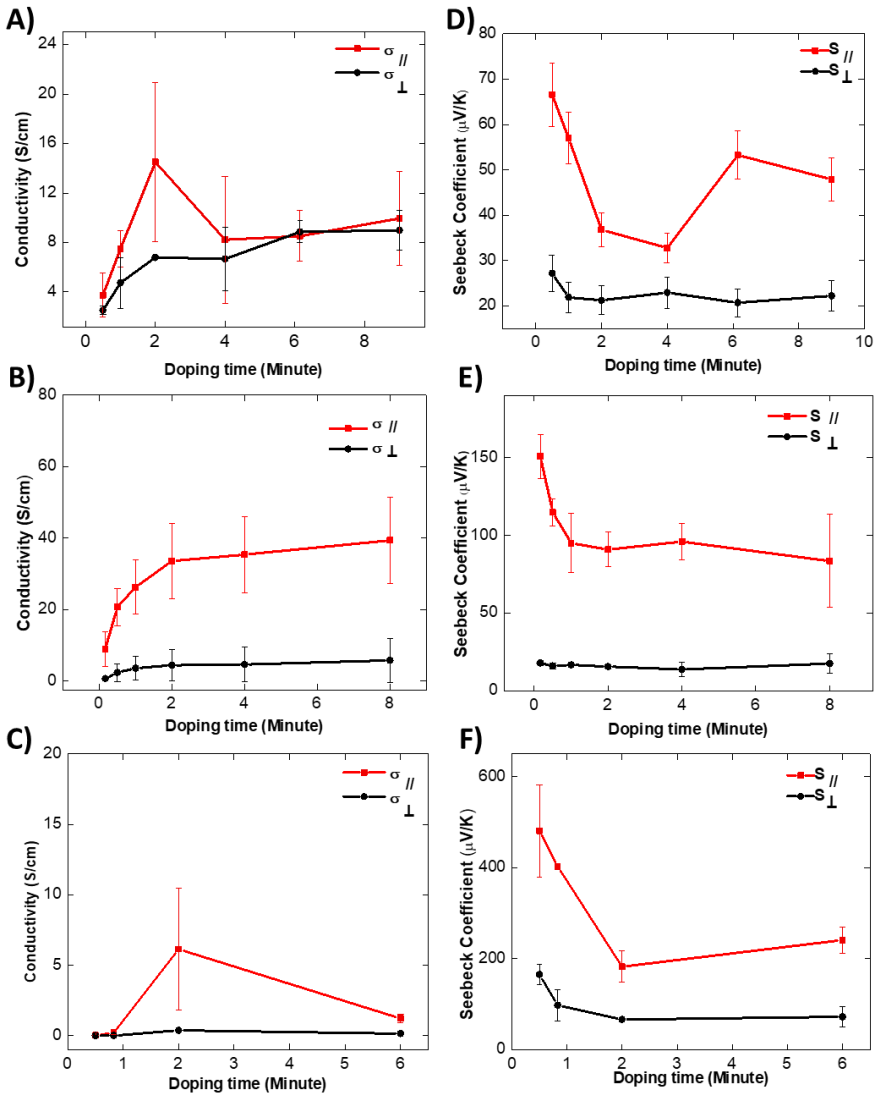

Figure 2.15. *(A-C) Evolution of the charge conductivity versus doping time for C_8-PBTTT, C_{14}-PBTTT and C_{18}-PBTTT respectively. (D-F) Evolution of the Seebeck coefficient versus doping time for C_8-PBTTT, C_{14}-PBTTT and C_{18}-PBTTT respectively. All values are measured along the directions parallel (//) and perpendicular (⊥) to the rubbing.*

For C_{12}-PBTTT, $S_{\perp}$ is close to the value of the non-oriented films (35 µV/K) whereas $S_{//}$ is two to three times larger and can reach values of 77 µV/K for conductivities of 193 S/cm

(doping time = 1 min.). The C_8-PBTTT has the lowest anisotropy (1.4-2.6) whereas C_{18} has the highest one (3-4.1). The anisotropy in Seebeck coefficient parallels that of the charge conductivity. However, as already noted for rubbed films of P3HT doped with F_4TCNQ, the anisotropy of S is always lower than that of the charge conductivity σ.[17] The dependence of $S_{//}$ with doping time parallels the kinetics of doping evidenced by UV-Vis spectroscopy *versus* side chain length. Both C_8-PBTTT and C_{18}-PBTTT have the slowest doping kinetics. Hence the Seebeck coefficients observed at low doping times are particularly high, especially for C_{18}-PBTTT with $S_{//}$> 400 µV/K for t= 5 s. Conversely, for C_{12}-PBTTT and its fast doping kinetics, the variation of S with doping time is limited.

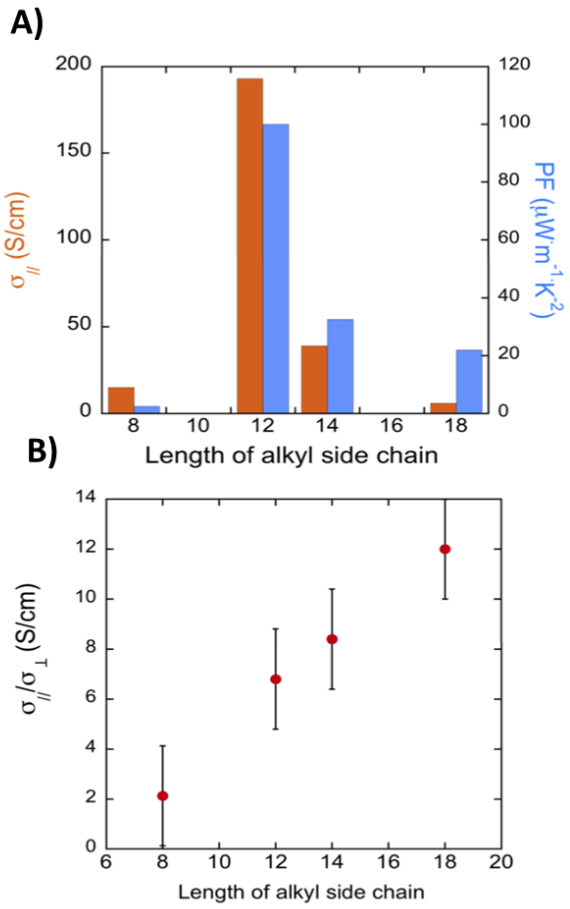

Figure 2.16. *Evolution of the maximum conductivity ($\sigma_{//}$) and power factor (PF) along the rubbing direction (a) and of the average charge conductivity anisotropy $\sigma_{//}/\sigma_{\perp}$ (b) versus side chain length in F_4TCNQ-doped PBTTT films oriented by high temperature rubbing.*

The simultaneous increase of charge conductivity $\sigma_{//}$ and thermopower $S_{//}$ along the rubbing direction results in a substantial increase of power factors $PF=S^2\sigma$ along the rubbing direction. As seen in figure 2.13 C, the values of PF are substantially enhanced along the rubbing direction and the anisotropies can be very high. They reach 66 for C_{12}-PBTTT and 320 for C_{18}-PBTTT. The maximum PF for the C_8-PBTTT, C_{14}-PBTTT and the C_{18}-PBTTT are 2.4 $\mu W \cdot m^{-1} \cdot K^{-2}$, 32.6 $\mu W \cdot m^{-1} \cdot K^{-2}$ and 20.6 $\mu W \cdot m^{-1} \cdot K^{-2}$, respectively. However, C_{12}-PBTTT surpasses the three other polymers, with power factors of the order of 100 $\mu W \cdot m^{-2} \cdot K^{-1}$ that are comparable to those observed for vapor-phase doped PBTTT.[36,37]

For C_{12}-PBTTT and C_{18}-PBTTT, the PF shows an optimum versus doping time and tends to decrease slightly at long doping times, when the doping level increases beyond a critical concentration. This trend is well known in many systems such as PEDOT-Tos.[4]

3. Conclusion

The influence of alkyl side chain length on the F_4TCNQ-doping mechanism of a series of PBTTTs was investigated from various points of view including structural variation, UV-Vis-NIR spectroscopic and thermoelectric properties. UV-Vis-NIR spectroscopy and DSC evidence the key role of side chain length and packing on the doping mechanism and helped determine the dopant diffusion coefficients and doping levels at saturation. Both, disordered C_8 and crystalline C_{18} side chain layers hamper efficient dopant diffusion in the polymer films whereas loosely packed side chain layers of C_{12} and C_{14}-PBTTT allow for fast dopant diffusion. The observed charge conductivity of the oriented PBTTT films correlates well with the doping level at saturation: an optimum in TE properties is observed for C_{12}-PBTTT films. For all PBTTTs, alignment enhances substantially the TE performances by increasing simultaneously the charge conductivity and the thermopower along the chain direction. Aligned films of C_{12}-PBTTT show charge conductivities of 193 S/cm along the rubbing direction and power factors of

approximately 100 $\mu W \cdot m^{-2} \cdot K^{-1}$. More generally, this study underlines the importance to perform a controlled crystallization and orientation of the polymer semiconductors prior to doping from solution in order to enhance their TE properties. On-going studies indicate that the same trends observed for solution-doped PBTTTs are also valid when doping from the vapor phase.

Bibliography

[1] J. Panidi, A. F. Paterson, D. Khim, Z. Fei, Y. Han, L. Tsetseris, G. Vourlias, P. A. Patsalas, M. Heeney, T. D. Anthopoulos, *Adv. Sci.* **2018**, *5*, 1700290.

[2] G. Lu, J. Blakesley, S. Himmelberger, P. Pingel, J. Frisch, I. Lieberwirth, I. Salzmann, M. Oehzelt, R. Di Pietro, A. Salleo, N. Koch, D. Neher, *Nat. Commun.* **2013**, *4*, 1588.

[3] S. Braun, W. R. Salaneck, M. Fahlman, *Adv. Mater.* **2009**, *21*, 1450.

[4] O. Bubnova, Z. U. Khan, A. Malti, S. Braun, M. Fahlman, M. Berggren, X. Crispin, *Nat. Mater.* **2011**, *10*, 429.

[5] I. E. Jacobs, E. W. Aasen, J. L. Oliveira, T. N. Fonseca, J. D. Roehling, J. Li, G. Zhang, M. P. Augustine, M. Mascal, A. J. Moulé, *J. Mater. Chem. C* **2016**, *4*, 3454.

[6] D. T. Duong, C. Wang, E. Antono, M. F. Toney, A. Salleo, *Org. Electron. physics, Mater. Appl.* **2013**, *14*, 1330.

[7] C. Wang, D. T. Duong, K. Vandewal, J. Rivnay, A. Salleo, *Phys. Rev. B* **2015**, *91*, 85205.

[8] J. Hynynen, D. Kiefer, L. Yu, R. Kroon, R. Munir, A. Amassian, M. Kemerink, C. Müller, *Macromolecules* **2017**, *50*, 8140.

[9] D. T. Scholes, S. A. Hawks, P. Y. Yee, H. Wu, J. R. Lindemuth, S. H. Tolbert, B. J. Schwartz, *J. Phys. Chem. Lett.* **2015**, *6*, 4786.

[10] D. T. Scholes, P. Y. Yee, J. R. Lindemuth, H. Kang, J. Onorato, R. Ghosh, C. K. Luscombe, F. C. Spano, S. H. Tolbert, B. J. Schwartz, *Adv. Funct. Mater.* **2017**, *27*, 1702654.

[11] H. Méndez, G. Heimel, S. Winkler, J. Frisch, A. Opitz, K. Sauer, B. Wegner, M. Oehzelt, C. Röthel, S. Duhm, D. Többens, N. Koch, I. Salzmann, *Nat. Commun.* **2015**, *6*, 8560.

[12] P. Pingel, D. Neher, *Phys. Rev. B* **2013**, *87*, 115209.

[13] J. Hynynen, D. Kiefer, C. Muller, *Rsc Adv.* **2018**, *8*, 1593.

[14] S. N. Patel, A. M. Glaudell, K. A. Peterson, E. M. Thomas, K. A. O'Hara, E. Lim, M. L. Chabinyc, *Sci. Adv.* **2017**, *3*, e1700434.

[15] L. Hartmann, K. Tremel, S. Uttiya, E. Crossland, S. Ludwigs, N. Kayunkid, C. Vergnat, M. Brinkmann, *Adv. Funct. Mater.* **2011**, *21*, 4047.

[16] A. Hamidi-Sakr, L. Biniek, S. Fall, M. Brinkmann, *Adv. Funct. Mater.* **2016**, *26*, 408.

[17] A. Hamidi-sakr, L. Biniek, J.-L. Bantignies, D. Maurin, L. Herrmann, N. Leclerc, P. Lévêque, V. Vijayakumar, N. Zimmermann, M. Brinkmann, *Adv. Funct. Mater.* **2017**, *27*, 1700173.

[18] I. McCulloch, M. Heeney, C. Bailey, K. Genevicius, I. MacDonald, M. Shkunov, D. Sparrowe, S. Tierney, R. Wagner, W. Zhang, M. L. Chabinyc, R. J. Kline, M. D. McGehee, M. F. Toney, *Nat. Mater.* **2006**, *5*, 328.

[19] E. Cho, C. Risko, D. Kim, R. Gysel, N. Cates Miller, D. W. Breiby, M. D. McGehee, M. F. Toney, R. J. Kline, J.-L. Bredas, *J. Am. Chem. Soc.* **2012**, *134*, 6177.

[20] D. M. DeLongchamp, R. J. Kline, Y. Jung, D. S. Germack, E. K. Lin, A. J. Moad, L. J. Richter, M. F. Toney, M. Heeney, I. McCulloch, *ACS Nano* **2009**, *3*, 780.

[21] L. Biniek, N. Leclerc, T. Heiser, R. Bechara, M. Brinkmann, *Macromolecules* **2013**, *46*, 4014.

[22] L. Biniek, S. Pouget, D. Djurado, E. Gonthier, K. Tremel, N. Kayunkid, E. Zaborova, N. Crespo-Monteiro, O. Boyron, N. Leclerc, S. Ludwigs, M. Brinkmann, *Macromolecules* **2014**, *47*, 3871.

[23] M. Brinkmann, L. Hartmann, L. Biniek, K. Tremel, N. Kayunkid, *Macromol. Rapid Commun.* **2014**, *35*, 9.

[24] R. Ghosh, A. R. Chew, J. Onorato, V. Pakhnyuk, C. K. Luscombe, A. Salleo, F. C. Spano, *J. Phys. Chem. C* **2018**, *122*, 18048.

[25] R. Ghosh, C. K. Luscombe, M. Hambsch, S. C. B. Mannsfeld, A. Salleo, F. C. Spano, *Chem. Mater.* **2019**, *31*, 7033.

[26] Regarding the presence of the 408 nm peak in the UV-Vis spectra of the doped films, the reader is invited to consider reference 17 showing that it is a characteristic feature of the anion F_4TCNQ^- and not of neutral F_4TCNQ

[27] H. Mehrer in Diffusion in Solids. Fundamentals, Methods, Materials, Diffusion-limited Processes, Springer Series in Solid-State Sciences, Springer Verlag, 2007, 41-45.

[28] A. J. Maliakal, *ACS Appl. Mater. Interfaces* **2013**, *5*, 8300.

[29] D. M. DeLongchamp, R. J. Kline, Y. Jung, E. K. Lin, D. A. Fischer, D. J. Gundlach, S. K. Cotts, A. J. Moad, L. J. Richter, M. F. Toney, M. Heeney, I. McCulloch, *Macromolecules* **2008**, *41*, 5709.

[30] N. Kayunkid, S. Uttiya, M. Brinkmann, *Macromolecules* **2010**, *43*, 4961.

[31] D. L. Dorset, O. U. Press, *Crystallography of the Polymethylene Chain: An Inquiry Into the Structure of Waxes*, OUP Oxford, **2005**.

[32] N. C. Miller, E. Cho, M. J. N. Junk, R. Gysel, C. Risko, D. Kim, S. Sweetnam, C. E.

Miller, L. J. Richter, R. J. Kline, M. Heeney, I. McCulloch, A. Amassian, D. Acevedo-Feliz, C. Knox, M. R. Hansen, D. Dudenko, B. F. Chmelka, M. F. Toney, J.-L. Brédas, M. D. McGehee, *Adv. Mater.* **2012**, *24*, 6071.

[33] D. A. Dixon, J. C. Calabrese, J. S. Miller, *J. Phys. Chem.* **1989**, *93*, 2284.

[34] A. P. Kulkarni, C. J. Tonzola, A. Babel, S. A. Jenekhe, *Chem. Mater.* **2004**, *16*, 4556.

[35] R. Fujimoto, Y. Yamashita, S. Kumagai, J. Tsurumi, A. Hinderhofer, K. Broch, F. Schreiber, S. Watanabe, J. Takeya, *J. Mater. Chem. C* **2017**, *5*, 12023.

[36] S. N. Patel, A. M. Glaudell, D. Kiefer, M. L. Chabinyc, *ACS Macro Lett.* **2016**, *5*, 268.

[37] K. Kang, S. Watanabe, K. Broch, A. Sepe, A. Brown, I. Nasrallah, M. Nikolka, Z. Fei, M. Heeney, D. Matsumoto, K. Marumoto, H. Tanaka, S. Kuroda, H. Sirringhaus, *Nat. Mater.* **2016**, *15*, 896.

[38] R. J. Kline, M. D. McGehee, E. N. Kadnikova, J. Liu, J. M. J. Fréchet, M. F. Toney, *Macromolecules* **2005**, *38*, 3312.

[39] W. Pukacki, J. Plocharski, S. Roth, *Synth. Met.* **1994**, *62*, 253.

[40] A. B. Kaiser, *Phys. Rev. B* **1989**, *40*, 2806.

[41] Q. Wei, M. Mukaida, K. Kirihara, T. Ishida, *ACS Macro Lett.* **2014**, *3*, 948.

Chapter 3. Bringing conducting polymers to high order: towards conductivities beyond 10^5 S/cm and thermoelectric power factors of 2 $mW{\cdot}m^{-1}{\cdot}K^{-2}$

This chapter presents an effective design strategy of polymer thermoelectric materials based on structural control in doped polymer semiconductors. The strategy is illustrated for two archetypical polythiophenes e.g. poly(2,5-bis(3-dodecyl-2-thienyl)thieno[3,2-*b*]thiophene) (C_{12}-PBTTT) and regioregular poly(3-hexylthiophene) (P3HT). $FeCl_3$ doping of aligned films results in charge conductivities up to $2{\cdot}10^5$ S/cm and metallic-like thermopowers similar to iodine-doped polyacetylene. The films are almost optically transparent and show strongly polarized near-infra-red polaronic bands (dichroic ratio > 10). The comparative study of structure-property correlations in P3HT and C_{12}-PBTTT identifies three conditions to obtain conductivities beyond 10^5 S/cm:

I. Achieve high in-plane orientation of conjugated polymers with high persistence length
II. Ensure uniform chain oxidation of the polymer backbones by regular intercalation of dopant molecules in the polymer structure without disrupting the alignment of π-stacked layers.
III. Maintain a percolating nano-morphology along the chain direction.
IV. The highly anisotropic conducting polymer films are ideal model systems to investigate the correlations between thermopower S and charge conductivity σ. A scaling law $S\alpha\sigma^{-1/4}$ prevails along the chain direction but a different $S\propto\ln\sigma$ relation is observed perpendicular to the chains, suggesting different charge transport mechanisms. The simultaneous increase of charge conductivity and

thermopower along the chain direction results in a substantial improvement of thermoelectric power factors up to 2 mW·m^{-1}·K^{-2} in C_{12}-PBTTT.

1. Introduction

Conducting polymers were at the forefront of research in plastic electronics several decades ago and opened the new and vast research field of plastic electronics. A. Heeger, A. G. McDiarmid and H. Shirakawa were among the pioneers in this domain and their success on conducting polymers were recognized by the award of a Nobel Prize in 2000.[1] Among all conducting polymers, iodine-doped polyacetylene (PA) demonstrated some of the highest conductivities - up to 10^5 S/cm at room temperature for stretch-aligned films as well as very high thermoelectric power factors of 1.3 $mW{\cdot}m^{-1}{\cdot}K^{-2}$.[2–4][5] However, PA could only be processed in the form of free-standing films several tens of microns in thickness that are difficult to use for TE device fabrication. To alleviate this lack of processing of pure conjugated polymers, alkyl side chains were introduced to design new semi-conducting polymers that are soluble in organic solvents, and thus easily processable via spin-coating, inkjet printing and other solution-based coating methods.[6,7] With the further control of regioregularity, highly ordered polymer semiconductors (PSCs) with charge mobilities beyond 1 $cm^2/V{\cdot}s$ ideally suited for OFETs were designed. [7] In the subsequent decades, research efforts focused on to the way to fine-tune the electronic properties of the semi-conducting polymers used in the fabrication of organic light-emitting diodes, field-effect transistors and organic solar cells.[8] Chemical engineering helped identify the required structures of conjugated polymers necessary to tune their bandgap and/or their absorption spectra to match the solar spectrum.[9]

Recently, new interest in conducting polymers was triggered by the pioneering work of Crispin et al. on thermoelectric (TE) applications based on the conducting polymer poly(ethylenedioxythiophene) (PEDOT) doped with tosylate (Tos).[10,11] Conducting polymers such as PEDOT-Tos have a layered structure of positively charged

poly(ethylenedioxythiophene) chains alternating with layers of tosylate anions.[11] PEDOT-Tos shows remarkable thermoelectric properties due to the combination of high charge conductivity, reasonable thermopowers and low thermal conductivity. [10,11]Despite promising TE properties, the crystallization of PEDOT-Tos in thin films is difficult to control. So far, no simple method is available to either orient in-plane the PEDOT chains or to select the preferential contact plane of crystals on a given substrate. For a large part the synthetic method is to blame: it requires the use of *in-situ* polymerization techniques with low control over the polymerization process and finally the structure of the polymer thin films. The only improvements in charge transport were obtained via control of secondary crystallization e.g. by using co-solvents such as ethylene glycol that helps extract the non-conducting polystyrene sulfonate from the bulk of the PEDOT-PSS films.[12,13]

In strong contrast, advanced control of crystallization, crystal orientation and alignment have all been demonstrated for polymer semiconductors (PSCs) such as regio-regular poly(3-hexylthiophene) (P3HT) or poly(2,5-bis(3-dodecyl-2-thienyl)thieno[3,2-*b*]thiophene) (C_{12}-PBTTT) (see figure 3.1A).[14,15] Numerous methods including self-seeded growth, blade-coating, epitaxy or high temperature rubbing help control precisely the crystal dimensions and their orientation in thin films, resulting in diverse morphologies: single crystals, spherulites, aligned crystalline lamellae.[14–20]

It is therefore natural to take profit of the high structural control gained on polymer semiconductors such as P3HT or PBTTT to further improve their charge transport and thermoelectric properties after doping. Doping of thin films of P3HT or PBTTT with fluoroalkylsilanes (FTS) or F_4TCNQ has led to high conductivities typically of the order of a few hundred to one thousand S/cm.[21–23] Vapor-phase doping of P3HT and PBTTT with F_4TCNQ leads to conductivities of 12.7 S/cm and 200 S/cm, respectively.[22,23] Controlled

doping of well-crystallized and oriented conjugated polymer can further lead to anisotropic conducting polymer films.[24] Sequential doping of rubbed P3HT films with F_4TCNQ afforded aligned conducting polymers with conductivities of the order of 22 S/cm whereas vapor phase doping of highly crystalline P3HT afforded 12.7 S/cm conductivities.[22,24]

In the second chapter of this thesis, the impact of the alkyl side chains on the efficiency of doping, its kinetics and the ultimate TE properties, was investigated for the family of PBTTT with alkyl side chains from C_8 to C_{18}.[25] However, the obtained TE properties remain below the best conductivities reported for doped polyacetylene (PA) or even PEDOT-Tos.[11]

The main aim of this chapter is to enhance the electrical conductivity and thermoelectric performance of polythiophenes by taking advantage of their high degree of chain orientation and crystallinity that can be maintained upon doping with strong inorganic Lewis acid-based doping agents such as $FeCl_3$. We will mainly investigate the following issues:

i) Is it possible to reach the conductivities of doped PA close to 10^5 S/cm for oriented films of P3HT or PBTTT (see figure 3.1 A) after doping?

ii) What limits the ultimate conductivities?

To answer these questions, we have investigated the possibility to reach high doping levels in films of P3HT and PBTTT oriented by high temperature rubbing.[14,24,26,27] The choice of the two polymers is guided by their structural differences in terms of nano-morphology in rubbed thin films: P3HT has a periodic semi-crystalline lamellar morphology whereas C_{12}-PBTTT shows a liquid-crystalline-like structure. [14,15] The choice

of $FeCl_3$ is motivated by the fact that it is a stronger oxidant than F_4TCNQ.[28] Accordingly, this chapter is divided into three sections dealing with:

1) The structural and spectroscopic features induced by $FeCl_3$-doping on aligned P3HT and C_{12}-PBTTT films.

2) The dependence of charge transport and thermopower on [$FeCl_3$] concentration.

3) The analysis of the S-σ correlations in the oriented films of P3HT and C_{12}-PBTTT.

2. Results and discussion

2.1. Fabrication of highly oriented and conducting thin films

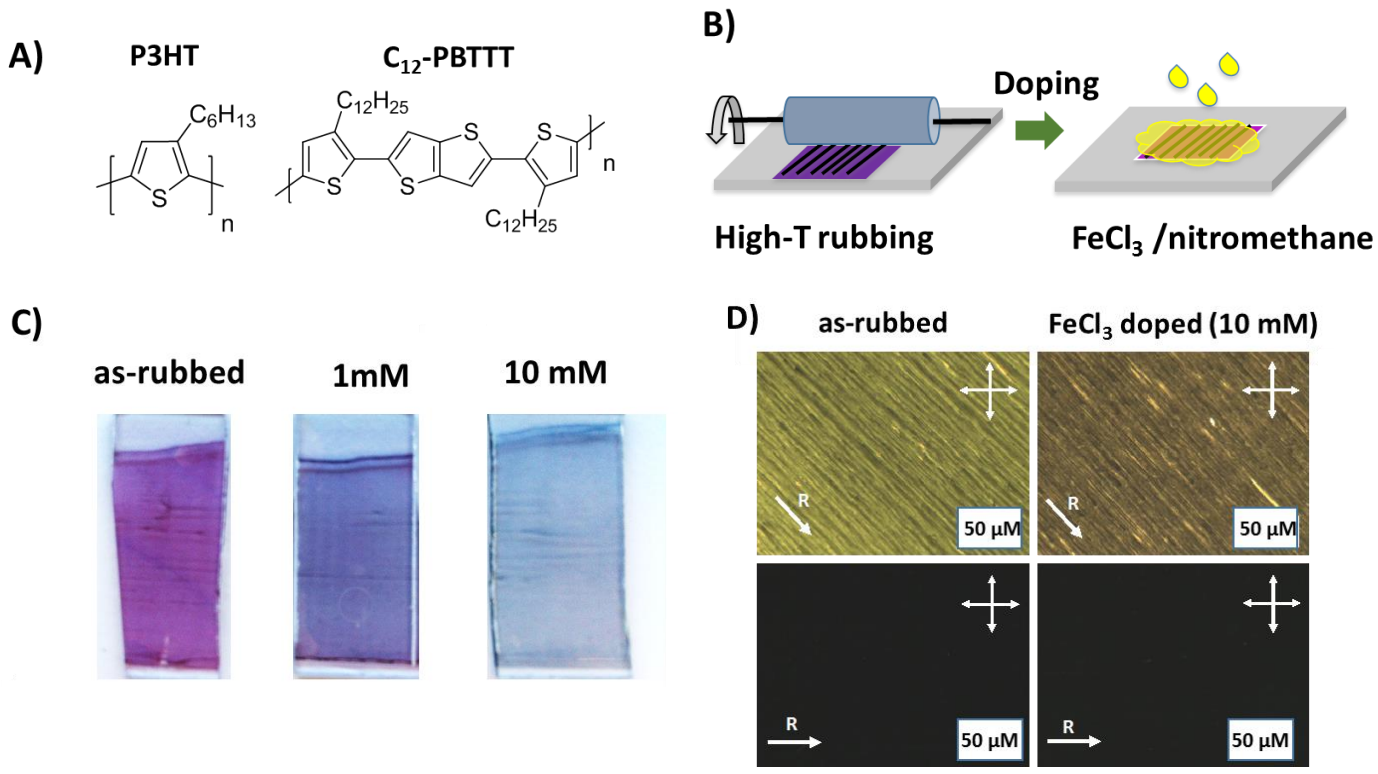

Figure 3.1. *A) Chemical structure of P3HT and C_{12}-PBTTT. B) Schematic illustration of the two-step process to prepare oriented conducting thin films combining high temperature rubbing and subsequent doping in a solution of $FeCl_3$ in nitromethane. C) Illustration of the color change in rubbed C_{12}-PBTTT films (left) upon doping with 1 mM and 10 mM $FeCl_3$/nitromethane solutions. D) Polarized optical microscope images under crossed polarizers showing the high birefringence in the as-rubbed and doped C_{12}-PBTTT films.*

As demonstrated previously for P3HT and F_4TCNQ[24], the combination of an orientation method such as mechanical rubbing and sequential doping in an orthogonal solvent (see figure 3.1) yields highly oriented and crystalline conducting polymer films. The same strategy was applied to P3HT and C_{12}-PBTTT doped with $FeCl_3$. A drastic change of the film's color from purple to light blue (see figure 3.1 C) is observed after doping the polymer films with 10mM $FeCl_3$ in nitromethane. polarized optical microscopy (POM) shows that doping does not suppress the orientation of the films, even for high $FeCl_3$ concentrations (10mM) (see figure 3.1 D).

2.2. Structure and nanomorphology of doped thin films by Transmission electron microscopy

Electron diffraction and high-resolution techniques were used to investigate the dopant induced structural changes in the unit cell of PBTTT and P3HT. Figure 3.2 (A to D) compares the electron diffraction patterns of the pristine and $FeCl_3$-doped P3HT and PBTTT oriented films. The preserved orientation in the doped films is also demonstrated by transmission electron microscopy (TEM). The electron diffraction (ED) patterns of pristine oriented films indicate that the chain direction is parallel to the rubbing direction R and that crystalline domains are oriented mainly face-on the substrate in C_{12}-PBTTT whereas face-on and edge-on crystals coexist in oriented P3HT films. Both the in-plane orientation and crystal contact plane are maintained after doping for P3HT and C_{12}-PBTTT for the whole range of [$FeCl_3$]. However, on closer inspection, the ED patterns after doping for [$FeCl_3$] = 10 mM reveals a loss of crystallinity characterized by a partial loss of higher-order equatorial h00 reflections, a broadening of the remaining h00 and a reduction in the intensity of the meridional 002 reflection.

As seen in figure 3.2.C&D and doping modifies the unit cell parameters of C_{12}-PBTTT and P3HT but to different extents (see also figure 3.3 A and B). For both polymers, the unit cell expands along the alkyl side chain direction (d_{100}) and the π-stacking periodicity

d(020) is reduced, demonstrating that dopant molecules penetrate inside the layers of alkyl side chains of the crystalline phase and that the change in lattice parameters correlate with the amount of incorporated dopants. For both polymers, the interlayer spacing d_{100} increases with [$FeCl_3$] and saturates for [$FeCl_3$] approaching 10 mM. A maximum of doping has been reached. d_{100} increases from 19.7 Å (pristine) to 23.6 Å (10 mM) in C_{12}-PBTTT and from 16.4 Å (pristine) to 18.1 Å (10 mM) for P3HT. In the case of C_{12}-PBTTT, the increase in lattice spacing is much larger than for F_4TCNQ. Δ d_{100} is equal to 4 Å for $FeCl_3$ doped C_{12}-PBTTT and ≈0.9 Å for F_4TCNQ.

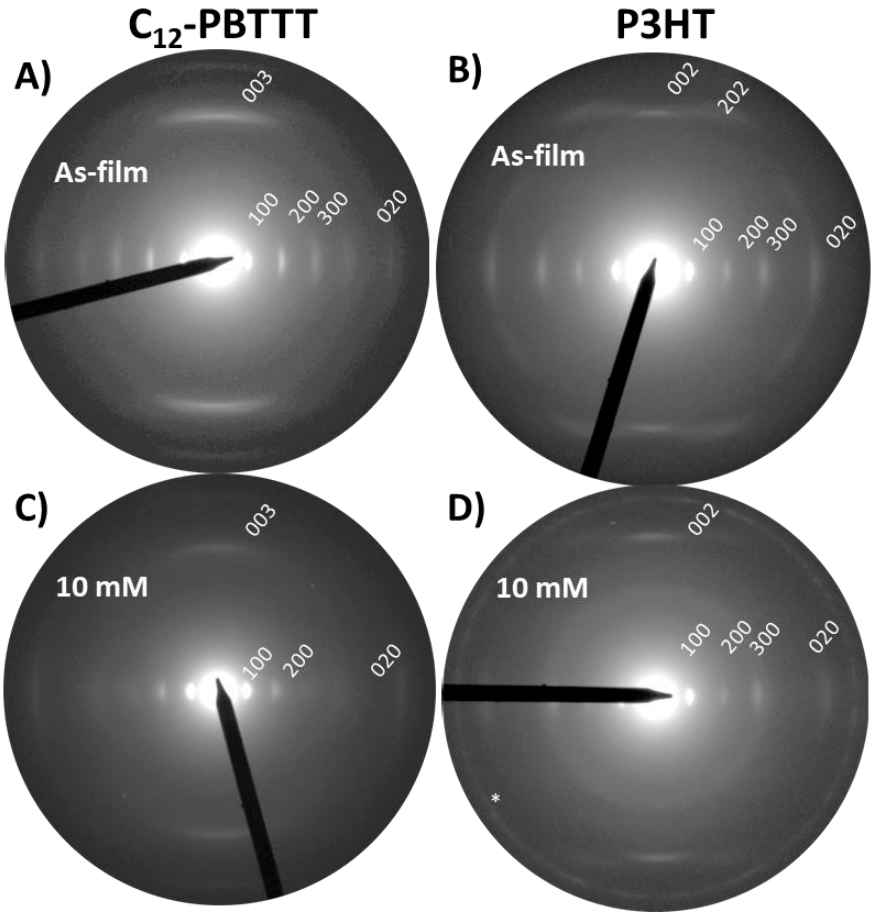

Figure 3.2. *Structure evolution in doped P3HT and C_{12}-PBTTT upon doping with $FeCl_3$ as obtained by low dose TEM. Electron diffraction patterns of C_{12}-PBTTT before A) and after C) doping with 10 mM $FeCl_3$. Electron diffraction patterns of P3HT before B) and after D) doping with 10 mM $FeCl_3$. The asterisk marks a Scherrer ring from excess $FeCl_3$ on the surface of the doped P3HT film.*

For both polymers, doping results in a small decrease of the π-stacking periodicity similar to that observed with F_4TCNQ doping. [24,25] The main difference between C_{12}-PBTTT and P3HT resides in the evolution of the side chain spacing. In C_{12}-PBTTT, the maximum change in d_{100} is equivalent to 3 CH_2-CH_2 bonds i.e. 3.9 Å whereas in P3HT it is only 1.7 Å. In both cases, the increase of d_{100} is smaller than the 7.4 Å van der Waals diameter of $FeCl_4^-$. Even more telling is the variation in unit cell volume ΔV in both cases. Assuming orthorhombic unit cells with two chains per unit cell for both P3HT (a=16.5 Å, b=7.8 Å and c=7.77 Å) and C_{12}-PBTTT (a=19.7 Å, b=7.4 Å, c=13.5 Å), ΔV=20-30 Å^3 for P3HT versus ΔV=230-250 Å^3 for C_{12}-PBTTT. Intercalation of small molecules such as phenyl-C_{71}-butyric acid methyl ester ($PC_{71}BM$) into the structure of PBTTT has been extensively analyzed and modelled.[29–31]

It has been shown that $PC_{71}BM$ molecules intercalate in the structure of PBTTT and form bimolecular crystals of $PC_{71}BM$ and C_{14}-PBTTT. The bimolecular crystal phase is characterized by an expanded unit cell parameter along the alkyl side chain direction. Since the van der Waals diameter of $FeCl_4^-$ (7.4 Å) is below that of $PC_{71}BM$, it is tempting to propose a similar scenario for $FeCl_3$-doped C_{12}-PBTTT. Comparing the value of ΔV with the molecular volumes of $FeCl_2$ (42 Å^3) and $FeCl_4^-$ (69 Å^3) suggests that up to four dopant molecules i.e. 2 $FeCl_2$ and 2 $FeCl_4^-$ can be hosted in the unit cell of C_{12}-PBTTT (see Figure 3.3.D). This would imply a stoichiometry of one $FeCl_4^-$ plus one $FeCl_2$ per four thiophene rings in a unit cell at saturation (corresponding thus to an atomic ratio S/Fe=2). Such a stoichiometry is further consistent with that observed in the heavily doped phase of PEDOT:Tos.[32,33] To confirm this stoichiometry, we further analyzed our samples using EDX – STEM.

Figure 3.4 (A to F) shows the elemental analysis in terms of EDX spectra and 2D maps for 5 mM $FeCl_3$-doped C_{12}-PBTTT and P3HT. First, one can see that there is a uniform

distribution of both S and Fe atoms in the doped layers, indicating that doping is uniform in the samples. Second, the EDX spectra help determine the atomic ratio of S and Fe elements. For C_{12}-PBTTT, one obtains a value close of 1.9±0.2 whereas for P3HT it is approximately 2.5±0.2. The S/Fe ratio for C_{12}-PBTTT is in full agreement with the value deduced from the unit cell parameter variation assuming it is related to the uptake of 2 $FeCl_4^-$ and 2 $FeCl_2$.

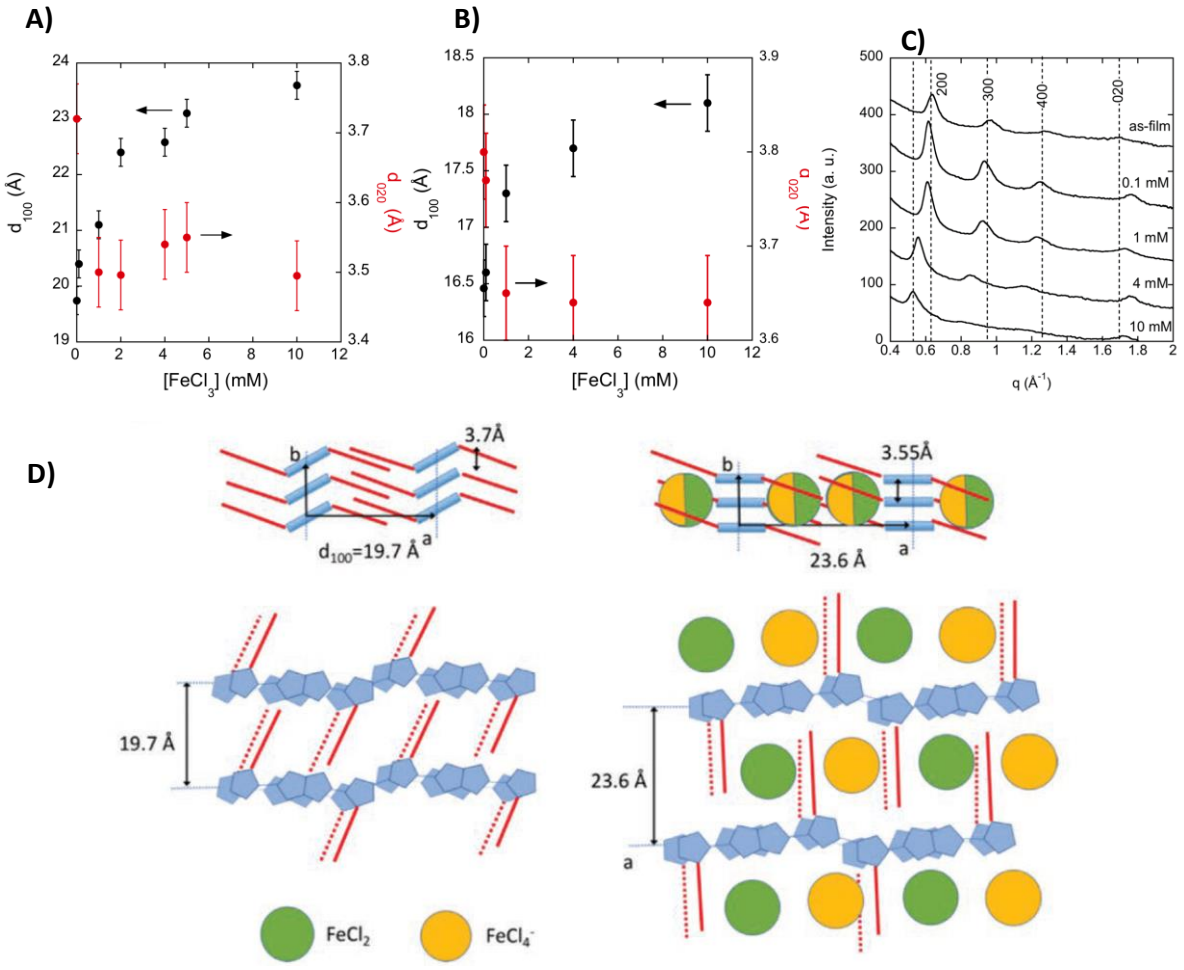

Figure 3.3. *A) Interlayer spacing d_{100} and π-stacking distance versus $FeCl_3$ concentration in nitromethane for A) C_{12}-PBTTT films and B) P3HT films. C) Equatorial section profiles of the ED patterns of oriented C_{12}-PBTTT films upon doping with $FeCl_3$ in nitromethane at different concentrations. The profiles have been shifted along the ordinate axis for clarity. D) Illustration of the structural change induced by $FeCl_3$ doping for C_{12}-PBTTT ([$FeCl_3$] =10 mM) that results in the formation of a bimolecular crystal.*

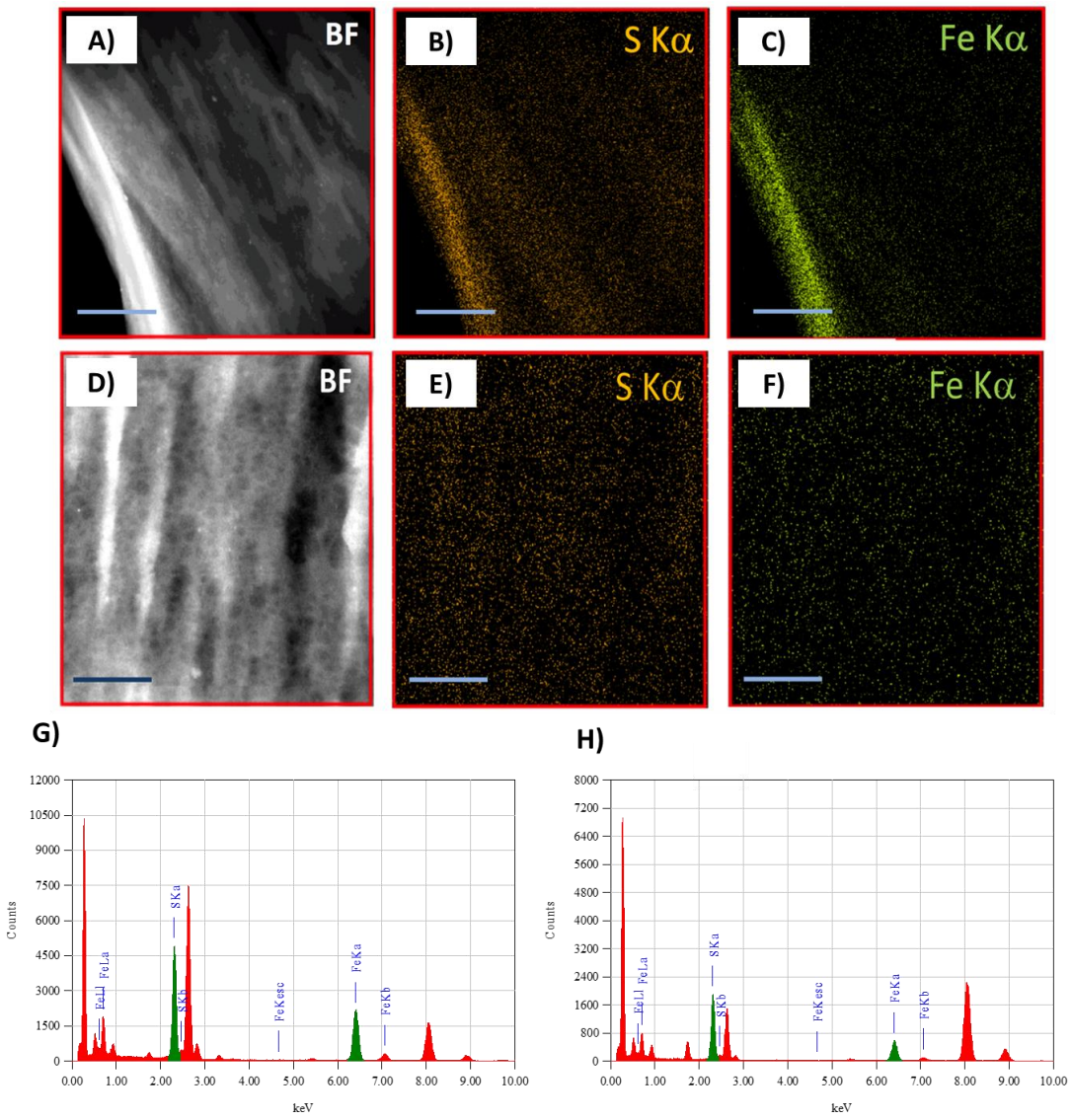

Figure 3.4. *A) Bright field STEM image of an oriented C_{12}-PBTTT film doped with 5mM $FeCl_3$/nitromethane. Corresponding* energy dispersive X-Ray (EDX) spectroscopy (EDX) *2D maps for S Kα B) and for Fe Kα C). D) Bright field STEM image of an oriented P3HT film doped with 5mM $FeCl_3$/nitromethane. Corresponding energy dispersive X-Ray (EDX) spectroscopy (EDX) 2D maps for S Kα E) and for Fe Kα F). G) and H) represent the EDX spectra of C12-PBTTT and P3HT film doped with 5mM $FeCl_3$/nitromethane respectively.*

For P3HT, the situation is different as the unit cell expansion is moderate and does not reflect the uptake of dopants. The absence of important unit cell variation in P3HT suggests that the alkyl side chain layers of P3HT can accommodate more readily the intercalation of $FeCl_4^-$ and $FeCl_2$ molecules possibly because the side chains of P3HT are

not interdigitated. However, for both polymers, the incorporation of dopants in the layers of alkyl side chains requires a structural reorganization especially when side chains are interdigitated (see the schematic illustration in figure 3.3.D).

Lattice expansion along the side chains, partial removal of interdigitation as well as tilting of the backbones and side chains are the potential mechanisms by which the structure of the doped phase can adapt to a given concentration of dopants. It is worth to mention that both the alkyl side chain sublattices of P3HT and of C_{12}-PBTTT are particularly loose and offer the possibility to harbor dopant molecules. Indeed, the areas per alkyl stem are 24.5 $Å^2$ for C_{14}-PBTTT and 27 $Å^2$ for P3HT (form I). Both values are substantially higher than the 18.4 $Å^2$ for the classical polymethylene subcell, indicating that the layers of side chains can indeed host small molecules such as F_4TCNQ, $FeCl_4^-$ or $FeCl_2$.[24,25,34,35]

2.3. Nanomorphology of the thin films

Both C_{12}-PBTTT and P3HT show coexistence of crystalline and amorphous domains but their nano-morphologies are substantially different as revealed by bright field and HR-TEM (see figure 3.5).

Firstly, bright field TEM shows that only the P3HT films have a characteristic periodic lamellar morphology whereas no such morphology is observed for rubbed C_{12}-PBTTT. This difference is further visible in the HR-TEM images of figure 3.5 A and C. Highly ordered domains of π-stacked polythiophene backbones periodically separated by layers of alkyl side chains containing the dopants appear in the form of fringed patterns with a 17.6 Å periodicity for doped P3HT (see figure 3.5 A) and 22.5 Å for doped C_{12}-PBTTT (see figure 3.5 C). The ordered domains have very different lengths of planarized chain segments for both polymers: 50-100 nm for C_{12}-PBTTT and 10-15 nm for P3HT.

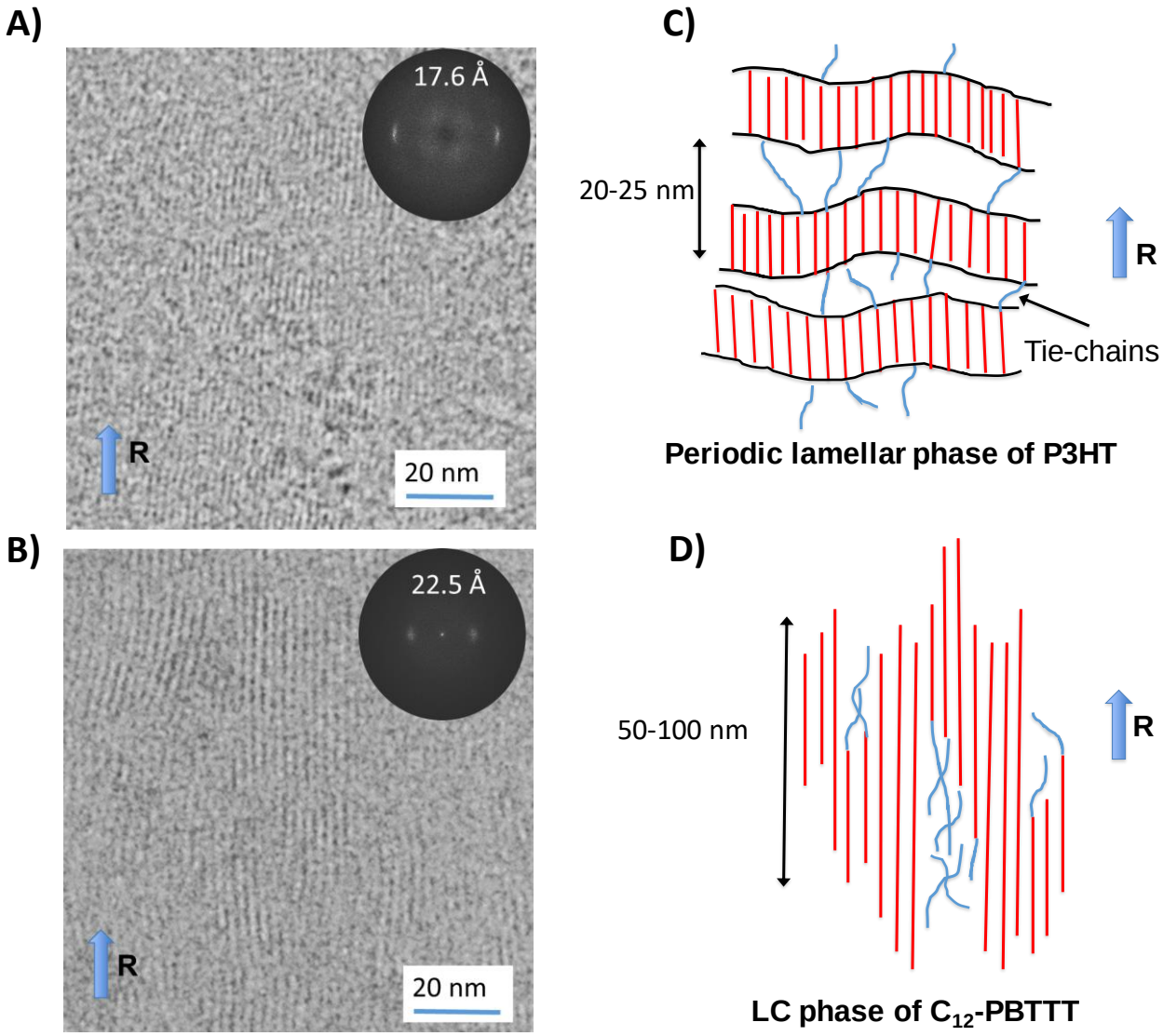

Figure 3.5 *Low dose HRTEM image of $FeCl_3$-doped P3HT A) and C_{12}-PBTTT B) films aligned by high temperature rubbing ([$FeCl_3$] = 4 mM). The insets correspond to the Fast Fourier Transforms. Schematic illustration of the nanomorphology in the C) semi-crystalline lamellar morphology of P3HT and D) LC phase of PBTTT*

These differences in nano-morphologies are related to different persistence lengths of the two polymer chains: 3 nm for P3HT versus 9 nm for C_{12}-PBTTT.[36,37] Accordingly, in strong contrast to the periodic semi-crystalline lamellar structure of P3HT, C_{12}-PBTTT displays rather a liquid-crystal-like morphology with extended planarized chain segments along the chain direction (see illustration in figure 3.5 D&E). As a result, the connectivity between ordered domains is far better along the chain direction in C_{12}-

PBTTT films (see illustration in figure 3.5 E). As seen hereafter, these different nano-morphologies impact the ultimate conductivities of doped oriented films.

2.4. Spectroscopic signatures of doping: Polarized UV-Vis-NIR spectroscopy

TEM has shown that the amount of $FeCl_3$ incorporated in the crystals of C_{12}-PBTTT and P3HT depends on the concentration [$FeCl_3$]. This trend is further supported by polarized UV-vis-NIR spectroscopy that helps visualize the level of chain oxidation versus [$FeCl_3$] (see figure 3.6). Increasing the doping concentration results in a corresponding increase of the polaronic features P1 and P2 and a decrease of the neutral polymer absorption (N). For both polymers, the NIR absorption bands P1 and P2 are polarized parallel to the alignment direction R and the films are strongly birefringent under the polarizing microscope. Most remarkably, the P3HT and PBTTT films doped at 10 mM exhibit a spectrum without significant contribution of the original neutral polymer (1-2%), suggesting an oxidation level of the polymer backbones similar to that of PEDOT-PSS (30-40%).[10] As a result, the films doped with 10 mM $FeCl_3$ are almost optically transparent with a light blue color similar to PEDOT:PSS (excess $FeCl_3$ gives rise to a small band at 374 nm).[38] The presence of the P2 band indicates also that the regime of pure bipolaron formation is not attained for [$FeCl_3$]= 10 mM (for a nondegenerate ground-state polymer, the P2 transition is forbidden for the bipolaron.[39] P1 and P2 are more red-shifted in C_{12}-PBTTT than in P3HT: λ_{max}(P2) = 809 nm for P3HT and 854 nm for C_{12}-PBTTT. Although the position of the P1 peak cannot be observed directly and lies beyond 2500 nm, the slope of the absorbance curve at 2500 nm indicates that the P1 peak is also substantially more red-shifted for C_{12}-PBTTT than for P3HT. Positions of polaronic features are determined by the extent of delocalization and/or crystalline perfection.[40,41] Hence the red-shifted polaron bands in C_{12}-PBTTT suggest a larger polaron delocalization length relatively to P3HT. This is consistent with the larger

extension of aligned and planarized chain segments observed by HR-TEM in C_{12}-PBTTT (see figure 3.5 E).

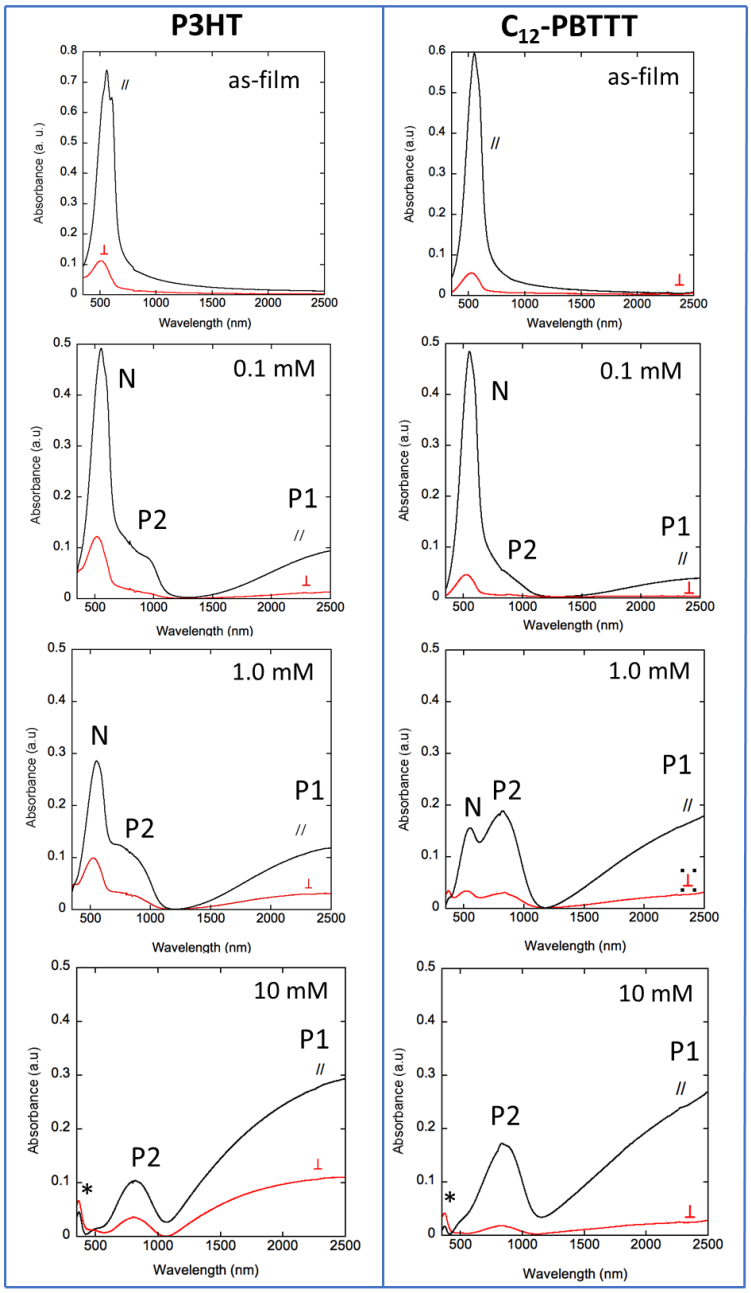

Figure 3.6. *Evolution of the polarized UV-vis-NIR spectrum in oriented P3HT and* C_{12}-PBTTT *thin films prepared by high temperature rubbing and subsequently doped in solution of* $FeCl_3$*/nitromethane of increasing concentration. The light polarization is parallel (//) to the rubbing direction or perpendicular to (⊥). The asterisk highlights the absorption peak of the excess* $FeCl_3$ *present on the film surface.*

Typically, C_{12}-PBTTT films doped with 10 mM $FeCl_3$ have a dichroic ratio of the P2 and P1 band of 10.6, which is very close to 10.8 of undoped C_{12}-PBTTT. These similar values confirm that $FeCl_3$ doping does not alter substantially the orientation of the C_{12}-PBTTT chains. For oriented P3HT films, the situation is different: the dichroic ratios of the P1 and P2 bands decreases with increasing [$FeCl_3$] (see figure 3.7 C). This loss of orientation is possibly related to the loss of both alignment and crystallinity upon intercalation of dopant molecules. This is consistent with the decreased intensity of ED reflections and the loss of vibronic structure in the absorption of the non-doped phase (N).Interestingly, UV-vis spectra for POL $\perp$ R (see figure 3.6) indicate that the amorphous fraction of P3HT and C_{12}-PBTTT is also doped with $FeCl_3$. Indeed, upon doping with increasing [$FeCl_3$], the absorption band of the amorphous phase (at 526 nm in C_{12}-PBTTT and 506 nm in P3HT, (see figure 3.7 A&B) progressively disappears. This result is at variance with the case of F_4TCNQ-doped films for which no evidence for doping of the amorphous domains was seen by polarized UV-vis spectroscopy (see figure 3.7 D&E).[24]

The fact that both crystalline and amorphous phases are doped with $FeCl_3$ explains, at least in part, the higher overall conductivity relatively to F_4TCNQ. [24]

Comparison with F_4TCNQ-doped films indicates that the doping level achieved with $FeCl_3$ is substantially larger. In particular, the remaining proportion of neutral C_{12}-PBTTT and P3HT is much lower (only a few percent) for $FeCl_3$ with respect to F_4TCNQ.[18] Following the work by Miller and coworkers, the high oxidation levels at saturation of C_{12}-PBTTT and P3HT upon doping with $FeCl_3$ could reflect higher dopant miscibility as compared to F_4TCNQ.[29]

Moreover, the spherical shape of the $FeCl_4^-$ anions may also favor closer proximity of the dopant to the polymer backbone as compared to the rod-like F_4TCNQ whose long axis tends to align parallel to the alkyl side chains i.e. in a plane perpendicular to the polymer

backbone.[24,25] As seen hereafter, the higher overall oxidation of P3HT and C_{12}-PBTTT chains achieved upon $FeCl_3$ doping accounts for the improved charge conductivities.

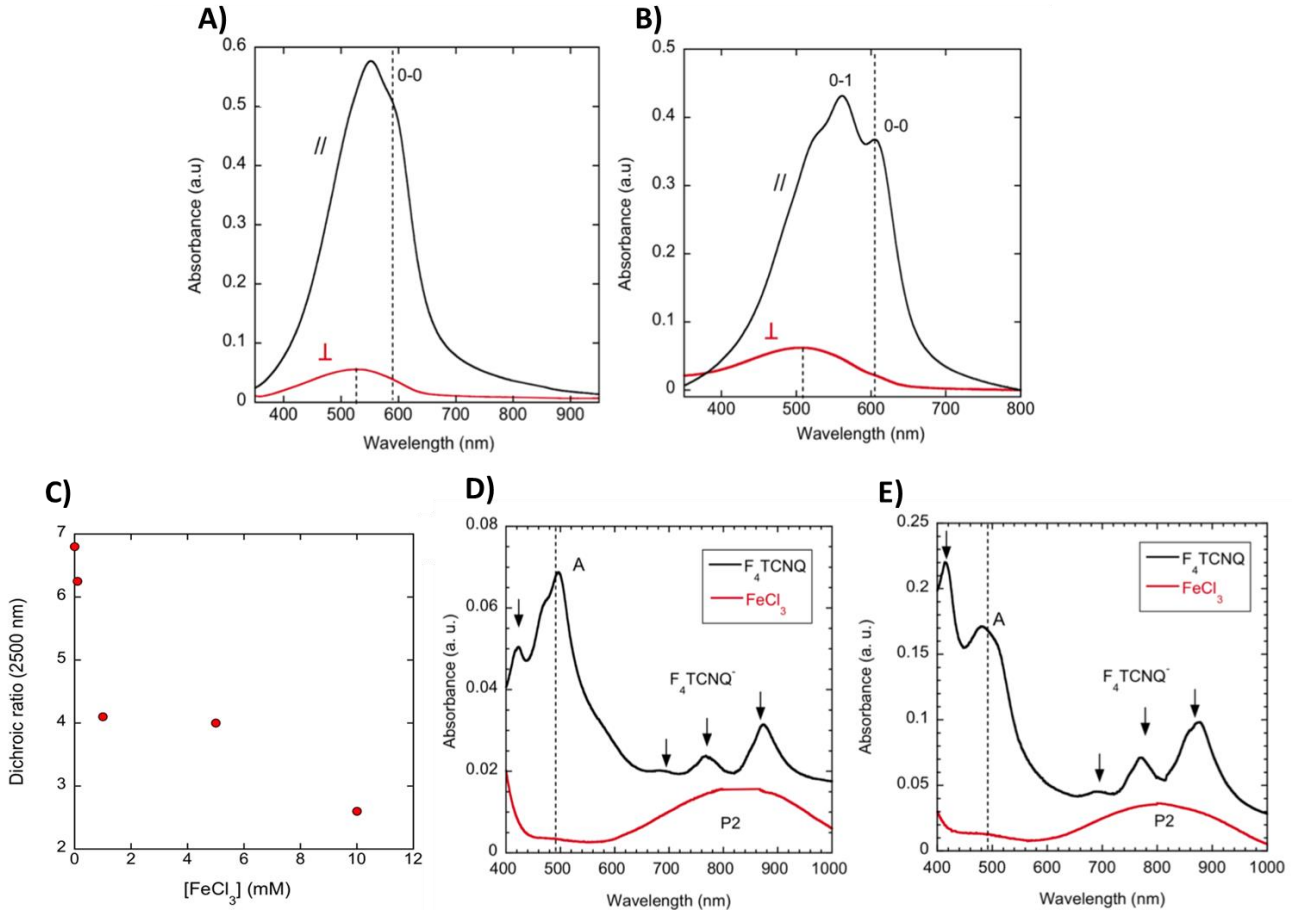

Figure 3.7. *Polarized UV-Vis spectra of rubbed thin films of C_{12}-PBTTT A) and regioregular P3HT (B). C_{12}-PBTTT was rubbed at 125°C and P3HT at 200°C. The absorption spectra recorded for incident light parallel (//) to the rubbing show a vibronic structure and correspond to planarized polymer chains forming π-stacks. The featureless spectra obtained for incident light oriented perpendicular ($\perp$) to the rubbing correspond to the amorphous phase of the polymers. For P3HT, the 0-0 and 0-1 bands are centred at 605 nm and 560 nm whereas the amorphous phase shows a maximum at 506 nm. Likewise, for C_{12}-PBTTT the 0-0 and 0-1 bands are centred at 526 nm and 552 nm whereas the amorphous phase shows a maximum at 526. C) Evolution of the dichroic ratio at 2500 nm of the polaronic P1 band in oriented P3HT films (T_R=180°C) as a function of increasing $FeCl_3$ concentration Comparison of the polarized UV-vis-NIR spectra of oriented C_{12}-PBTTT films D) and P3HT E) after doping with F_4TCNQ and $FeCl_3$ for the incident light polarization perpendicular to the rubbing direction. Polaronic band P2 is well visible in the films doped with $FeCl_3$ whereas in the films doped with F_4TCNQ only the characteristic bands of the F_4TCNQ^- anion are visible (marked with arrows). The absorption of amorphous C_{12}-PBTTT and P3HT is labeled*

A and is well visible in the films after doping with F_4TCNQ but not in the films doped with $FeCl_3$ indicating that the amorphous phase is only doped in the case of $FeCl_3$.

2.5. Anisotropy of charge conductivity.

As demonstrated in the previous section by TEM and UV-vis-NIR spectroscopy, the proportion of oxidized *versus* neutral chains in the oriented P3HT and C_{12}-PBTTT films can be tuned by adjusting [$FeCl_3$] while maintaining the high level of in-plane orientation. This gives a handle to control the charge carrier density in the oriented films and to determine its impact on anisotropic charge transport and TE properties. Therefore, a sequential doping protocol was used to probe the changes in charge conductivity and thermopower on a given oriented film sample: the same oriented film was doped in successive steps with a solution of $FeCl_3$/nitromethane of increasing concentration. This alleviates all issues related to differences in morphology and structure of the rubbed samples that would result in a scattering of the charge conductivity values σ and Seebeck coefficients S. Figure 3.8 shows the evolution of σ and S *versus* $FeCl_3$ concentration for P3HT and C_{12}-PBTTT oriented films that were sequentially doped with $FeCl_3$ solutions of increasing concentration. Table 3.1 collects the highest values of conductivity and power factors for both doped polymers and corresponding values from the literature for iodine-doped PA.

Upon doping, both P3HT and C_{12}-PBTTT show a strong increase of conductivity with a saturation at higher $FeCl_3$ concentration (for both // and $\perp$ directions). In the aligned C_{12}-PBTTT films, the conductivity increases by several orders of magnitude from 150 S/cm at 0.1 mM to 2.2 10^5 S/cm at 5 mM. The highest conductivities of C_{12}-PBTTT surpass the 10^5 S/cm reported for stretch-oriented bulk films of polyacetylene doped with Iodine.[4] However, it is worth to note that it is necessary to realize a progressive doping with increasing dopant concentration to reach such large conductivities. Indeed, C_{12}-PBTTT

films doped directly with a 10 mM solution reach only a 10^4 S/cm conductivity. As a matter of fact, PBTTTs with shorter or longer alkyl side chains showed also very high conductivities (see table 3.2) albeit below those of C_{12}-PBTTT. This specificity of C_{12}-PBTTT was previously noted in the case of F_4TCNQ-doped PBTTTs and reflected a higher doping level for this polymer.[25]

For the highly conducting C_{12}-PBTTT films, one can estimate the charge carrier density based on the structural data indicating that the unit cell contains two $FeCl_4^-$ anions per unit cell, which translates to a maximum of two charge carriers per unit cell i.e. a carrier density of approx. $9 \cdot 10^{20}$ cm^{-3}.[42] This value is larger than the $0.3\text{-}0.95 \cdot 10^{20}$ cm^{-3} reported for FTS-doped PBTTT.[43] However, the present result appears consistent in view of the UV-vis-NIR results indicating full oxidation of the C_{12}-PBTTT backbone contrary to the FTS-doped PBTTT that showed a substantial amount of neutral polymer chains and an oxidation level of only 3.5-11%.[43] As for P3HT, alignment improves substantially the conductivity from 63 S/cm in non-oriented $FeCl_3$-doped P3HT films to 570 S/cm along the rubbing direction in oriented films (for [$FeCl_3$] = 5mM).[38] The anisotropies of charge conductivity are much larger in C_{12}-PBTTT than in P3HT ($\sigma_{//}/\sigma_{\perp}$=70 for C_{12}-PBTTT and 12 for P3HT).

This difference is partly due to different film structures. As shown by TEM, the rubbed C_{12}-PBTTT films have a dominant face-on orientation whereas P3HT has a mixture of edge-on and face-on oriented domains. As a consequence, $\sigma\perp$ is essentially probed along the insulating C_{12} side chains of C_{12}-PBTTT whereas transport along π-stacking and side chains coexist in P3HT films. As an alternative explanation, the reduced anisotropy of the charge conductivity in P3HT could be due to the loss of orientation/crystallinity and/or to the doping of amorphous zones for increasing [$FeCl_3$] as suggested by polarized UV-Vis spectroscopy.

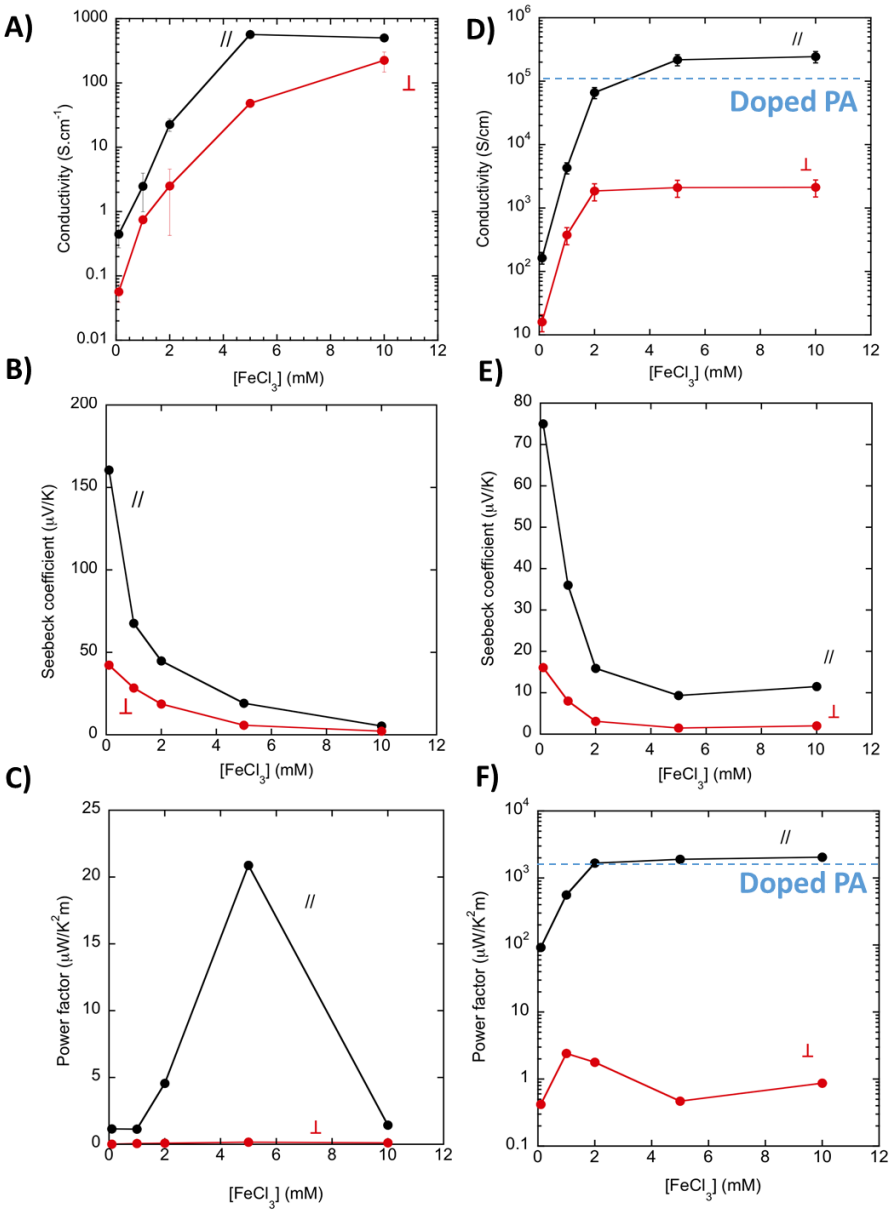

Figure 3.8. *Variation of the charge conductivity σ (A and D), Seebeck coefficient S (B and E) and power factor PF (C and F) as a function of increasing $FeCl_3$ concentration for doped P3HT and C_{12}-PBTTT oriented films. σ, S and PF are measured along the rubbing direction (//) and perpendicular to it (⊥). The lines are guide to the eye. The blue dotted lines in D) and F) show the typical values of conductivity and power factors reached for PA doped with iodine, respectively.*

As a rule, the maximum conductivity of doped P3HT films is always below that of C_{12}-PBTTT. It does not reflect a difference in the degree of in-plane orientation since both polymers have similar high dichroic ratios prior to doping. It is also not due to different

doping levels since the spectroscopic features for 10 mM doped films of P3HT and C_{12}-PBTTT are almost identical.

Table 3.1. *Thermoelectric characteristics of the $FeCl_3$-doped oriented films of C_{12}-PBTTT and P3HT and comparison with stretch-oriented iodine-doped PA.*[3]

Sample	P3HT [$FeCl_3$]=5 mM	C_{12}-PBTTT [$FeCl_3$] =5 mM	I_2-doped PA (ref. 3)
$\sigma_{//}$ (S/cm)	570±100	$(2.2\pm0.5)\cdot10^5$	$6\cdot10^4$
$\sigma_{\perp}$(S/cm)	48±20	2100±300	-
S// (μV/K)	5.4±0.5	9.4±0.5	15
$S_{\perp}$ (μV/K)	2.3±0.5	1.5±0.5	-
Power factor $PF_{//}$ (μW.m^{-1}.K^{-2})	21±6	1944±626	1350

The lower conductivity of doped P3HT must thus reflect intrinsic charge transport limitations related to its semi-crystalline periodic lamellar structure. In doped P3HT films, charges must necessarily channel through the less conductive amorphous zones that harbour chain ends and chain folds, hence, lowering the macroscopic conductivity $\sigma_{//}$. In the liquid crystal-like structure of C_{12}-PBTTT, more effective percolation between ordered domains of highly aligned chains in the rubbing direction (see HRTEM image in figure 3.5 D) results in a larger conductivity $\sigma_{//}$.

Table 3.2. *Maximum conductivity, Seebeck coefficients and power factors obtained for oriented films of various PBTTTs aligned by rubbing (T_R in the range 100-125°C) and doped with $FeCl_3$ as measured in the direction parallel to the rubbing. The details of the film preparation and macromolecular parameters of the PBTTTs are found in chapter 2 and in the experimental section.*

PBTTT side chain length	Conductivity $\sigma_{//}$ (S/cm)	Seebeck Coefficient $S_{//}$ (μV/K)	Power factor $PF_{//}$ ($\mu W/mK^2$)
C8	$1.2\pm0.2\cdot10^4$	9.1±0.5	99±25
C12	$2.2\pm0.5\cdot10^5$	9.4±0.5	1944±626
C14	$1.5\pm0.3\cdot10^4$	14.1±1.0	132±36
C18	$1.7\pm0.4\cdot10^4$	11.9±1.0	241±77

Even in the direction perpendicular to the rubbing, C_{12}-PBTTT films display particularly high conductivities of ≈ 2100 S/cm that are close to those observed in non-oriented FTS-doped C_{14}-PBTTT.[21] This indicates that the conductivity measured in non-oriented PBTTT samples is essentially limited by the charge transport perpendicular to the chains. Achieving such high conductivities in doped C_{12}-PBTTT on a macroscopic scale implies also that charges must be transported quite effectively between the well doped and ordered domains seen in HRTEM. Charge tunnelling between highly conducting domains is the mechanism invoked in a granular metal model of Sheng to account for comparably high conductivities in heavily-doped PA.[44] In strong contrast, in P3HT, the large extension of amorphous interlamellar zones will hamper tunnelling between doped crystalline regions and limit the macroscopic conductivity. This difference in the

electrical conductivity can be also related to a different hopping mechanism in highly conducting PBTTT versus P3HT. Based on temperature-dependent conductivity measurements on FTS doped PBTTT and P3HT, Tanaka et. al proposed that a 2D variable range hopping accounts for transport in PBTTT films while a 1D process is at play in doped P3HT films. [43] The same situation might be observed in the present case for $FeCl_3$ doped films.

2.6. Anisotropy of the Seebeck coefficient.

An enhancement of electrical conductivity along the direction of alignment was reported on most studies on stretch aligned polyacetylenes, polyanilines and polythiophenes.[3,45,46] However, there was no clear trend on the effect of solid-state drawing or stretching on Seebeck coefficient and its anisotropy. For instance, recently stretch aligned thin films of P3HT upon doping with molybdenum tris(dithiolene) showed an anisotropy in electrical conductivity. However, the Seebeck coefficient was not affected by stretching.[47] The situation was different in the case of oriented thin films aligned by high-temperature rubbing. We have seen that the Seebeck coefficients and electrical conductivities were enhanced in the direction of rubbing and they were highly anisotropic.[24,25] Unlike the other studies, the simultaneous enhancement of both electrical conductivity and Seebeck coefficient along the rubbing direction enabled us to obtain improved power factors parallel to the chain direction.

As seen in figure 3.8 B and E, the thermopower variation with dopant concentration is inverse to that of charge conductivity: both Seebeck coefficients $S_{//}$ and $S_{\perp}$ decrease with [$FeCl_3$]. In all samples, the thermopower probed along the chain direction is larger than that measured perpendicular: $S_{//} > S_{\perp}$.[23] The anisotropy factor of the Seebeck coefficient $S_{//}/S_{\perp}$ tends to decrease with increasing $FeCl_3$ concentration for both polymers. The anisotropies are higher for C_{12}-PBTTT (4.6) than for P3HT (2.4). Overall, as observed

previously for F_4TCNQ-doped P3HT, the anisotropy in thermopower is always smaller than that of the charge conductivity.[24,25]

The samples with the highest conductivities have very small thermopowers (see table 3.1). For instance, the rubbed C_{12}-PBTTT sequentially doped with 5 mM $FeCl_3$/nitromethane have $\sigma_{//}$=2.2 10^5 S/cm and $S_{//}$=9.4±0.5 µV/K. Their Seebeck coefficients measured perpendicular to the alignment are even smaller with $S_{\perp}$=1.5 ± 0.5 µV/K. Such low thermopowers are characteristic of metals.[48] For comparison, oriented films of PA doped with iodine have $S_{//}$=15 µV/K.[3,4]

At this point, we focus on the origin of the anisotropy of the thermopower S in oriented doped films of P3HT and C_{12}-PBTTT. The present situation bears similarity with the case of doped oriented PA fibres that show $S_{//}/S_{\perp}>1$.[49][50] Kaiser proposed a heterogeneous model of metallic fibrils separated by electrical barriers to explain this observation.[50] In doped PA, semi-conducting barriers alternate with metallic domains and modulate the thermopower and its anisotropy. The situation is similar for doped oriented P3HT and C_{12}-PBTTT (see figure 3.9). Indeed, HRTEM evidences the semi-crystalline morphology of doped P3HT and C_{12}-PBTTT with a clear coexistence of highly ordered domains and amorphous interlamellar zones. Moreover, it is known that the charge conductivity is higher in crystalline *versus* amorphous domains of doped P3HT (typically a few S/cm are obtained in F_4TCNQ-doped regio-regular P3HT versus 0.01 S/cm in regio-random amorphous P3HT).[22] This difference in charge transport between amorphous and crystalline domains must translate into a corresponding difference of the thermopower S_a and S_χ for amorphous and crystalline domains, respectively, with $S_a > S_\chi$. Accordingly, the semi-crystalline morphology of oriented conducting polymer films can be analyzed by using a heterogeneous material model similar to that proposed for doped PA.

When the temperature gradient ΔT is oriented parallel to the rubbing 9 (see figure 3.9 A), it is distributed over a succession of crystalline and disordered (amorphous) domains connected in series. We consider that the sample consists of a fraction χ of crystalline domains. The crystalline domains are characterized by an average temperature gradient ΔT_χ (along the chain direction) and disordered/amorphous domains by an average temperature gradient ΔT_a. We also assume that the heat current flows along the same path as the charges, so that the temperature gradients across crystalline and amorphous domains are proportional to their thermal resistances ($\Delta T_\chi \propto W_\chi$ and $\Delta T_a \propto W_a$ with W_χ and W_a the thermal resistances of crystalline and amorphous domains, respectively). Hence, the Seebeck coefficient in the rubbing direction $S_{//}$ can be written as: [46]

$$S_{//}=\alpha S_\chi +(1-\alpha)\, Sa \quad (1)$$

Where α is given by:

$$\alpha = \frac{\chi W_\chi}{\chi W_\chi + (1-\chi) W_a} \quad (2)$$

In the case of P3HT, the crystallinity χ is determined by the rubbing temperature and is close to 50% for T_R= 200°C.[26] In semi-crystalline polymers such as polyolefins, the thermal resistance of crystalline lamellae along the chain direction W_χ is small whereas the one perpendicular to the chains is significantly larger and comparable to that of the amorphous phase i.e. $W_\chi << W_a$.[51] This implies $S_{//} \approx S_a$ i.e. the Seebeck coefficient $S_{//}$ is dominated by the contribution from the doped amorphous and less conducting phase.

Let us now consider what happens when the temperature gradient is oriented perpendicular to the chain direction (see figure 3.9 B). In this situation, crystalline and disordered zones are put in parallel along the temperature gradient and charges are

short-circuited through the most conductive domains i.e. along the crystalline domains. As seen in TEM of the rubbed 180°C P3HT sample, the crystalline lamellae make a quite continuous conduction path given their lateral extension perpendicular to the rubbing direction (several hundreds of nm) and the way such lamellae are interconnected. Accordingly, charges will be tunnelled out of the sample within the crystalline domains in the direction perpendicular to the rubbing and this implies that the observed Seebeck coefficient $S_{\perp}$ is dominated by that of the most conductive lamellae and not by the disordered (amorphous) domains. This implies that $S_{\perp} \approx S_a$. As a consequence, the Seebeck coefficient anisotropy becomes $S_{//}/S_{\perp} \approx S_a/S_{\chi} > 1$.

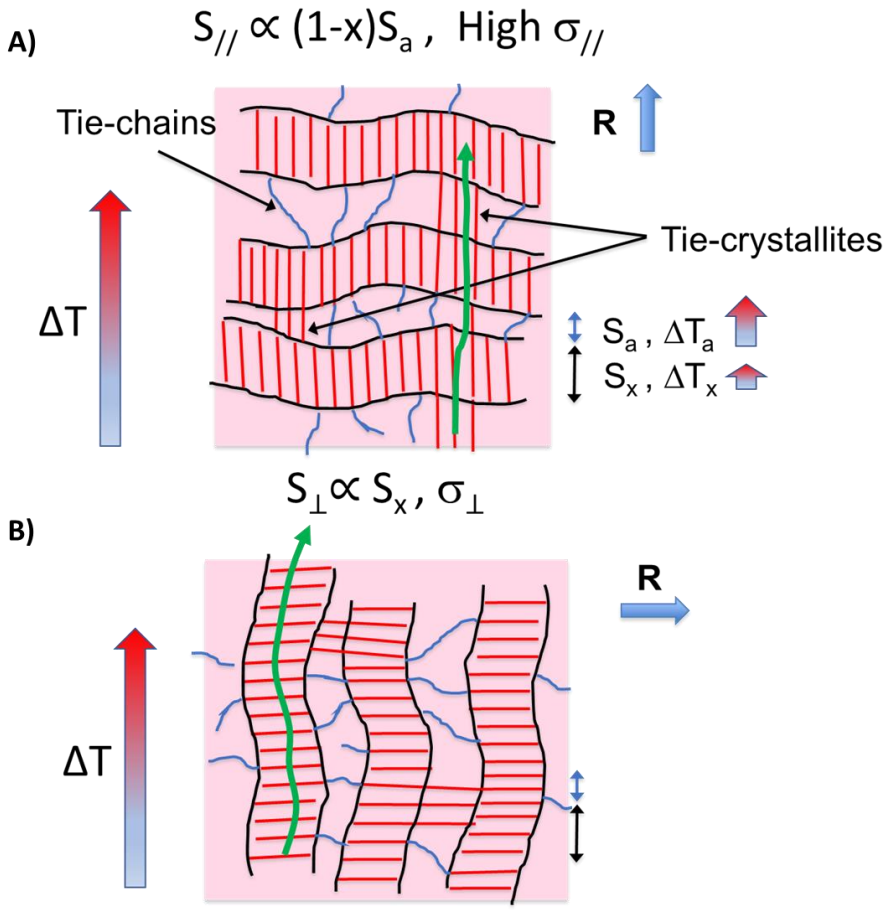

Figure 3.9. *Schematic representation for the observed differences in the Seebeck coefficient of oriented polymer films. A) When the rubbing direction is // to the applied temperature gradient and B) Rubbing direction is perpendicular to the applied temperature gradient.*

The present analysis indicates that a nanostructured morphology in conducting polymers such as doped P3HT or PBTTT that results in a modulation of electronic properties can be beneficial in oriented films since both the thermopower $S_{//}$ and the conductivity $\sigma_{//}$ are increased in the direction of polymer chains. It is important to recall that one major strategy to improve TE properties in inorganic systems is also based on material nano-structuring. Indeed, the objective of nano-structuring inorganic materials such as Bi_2Te_3 is to break the heat transport in the materials through enhanced scattering of phonons at multiple interfaces between domains without breaking charge transport.[52]

The resulting power factors for the most conductive C_{12}-PBTTT films are very high and can reach values close to 1.94 mW·m^{-1}·K^{-2}, a value slightly larger than for I_2-doped PA (1.35 mW·m^{-1}·K^{-2}) (see figure 3.8 C and F). Such power factors are quite large compared to those of non-oriented films of C_{12}-PBTTT doped with F_4TCNQ from the vapor phase (0.1 mW·m^{-1}·K^{-2}). The combination of orientation and higher oxidation of the C_{12}-PBTTT polymer after $FeCl_3$ doping accounts for the remarkable power factors obtained in rubbed thin films. Previous UV-vis studies indicate that a high proportion of neutral polymer chains is present in oriented P3HT and C_{12}-PBTTT films after doping with F_4TCNQ. This implies a high proportion of semi-conducting chain segments and domains that prevents reaching similarly high conductivities as for $FeCl_3$ doping.

2.7. Correlations between thermopower and charge conductivity in oriented conducting polymer films.

Kang and Snyder have recently demonstrated that details of microscopic charge transport can appear through the correlations between S and σ.[53] A general theoretical frame relating to the S=f(σ) scaling law was recently proposed by these authors. They predicted a scaling behavior with an exponent -1/s where s is a function of the charge

transport mechanism. [53] In PEDOT:TOS the S-σ curve is well fit with s=1 pointing at a transport mechanism dominated by acoustic phonon scattering. The exponent -1/3 with s=3 is obtained for a transport mechanism involving scattering of carriers by ionized impurities. From an experimental point of view, Chabinyc and coworkers made a detailed examination of electrical conductivity measurements of polymers such as PBTTTC$_{14}$, P3HT and P2TDC$_{17}$FT4 (poly(2,5-bis(thiophen-2-yl)-(3,7-diheptadecantyltetrathienoacene) by varying the dopant concentration and obtained a striking relationship between the thermopower and electrical conductivity for a wide range of conductivity for these P-doped polymers. Chabinyc et al. showed that S and σ are related via the relation $S \propto \sigma^{-1/4}$.[54,55] As a consequence, the power factor $PF \propto \sigma^{1/2}$(see figure 3.8 A).*This relationship indicates that the thermoelectric performance of a polymer can be enhanced by improving the conductivity*

In our experiments, the set of S,σ data obtained over a large range of conductivities (1.0-10^5 S/cm) helps further probe the S=f(σ) correlations and its anisotropy especially in a regime of high conductivities ($\sigma > 10^3$ S/cm). This methodology alleviates the experimental difficulties associated with charge carrier determinations in doped films e.g. using AC Hall measurements, especially for such aligned films. The S-σ plots for directions parallel and perpendicular to the chains are shown in fig. 3.8.B and C for C$_{12}$-PBTTT and P3HT, respectively. For both polymers, the S = f(σ) plots show different behavior parallel and normal to the chain directions. In the direction parallel to the chains (**R)**, the correlation between $S_{//}$ and $\sigma_{//}$ is well described by a power-law with an exponent -1/4. This is consistent with previous results by Chabinyc and coworkers for F$_4$TCNQ-doped C$_{14}$-PBTTT. [54,55] In the direction perpendicular to **R**, both polymers show a deviation from the power law, especially for high values of the conductivity. The conductivity $\sigma_{\perp}$ is observed to saturate close to 200 S/cm in P3HT and 2000 S/cm in C$_{12}$-

PBTTT. The departure from the scaling law in the case of $S_{\perp}$- $\sigma_{\perp}$ can have different origins. First, it could be related to some intrinsic structural change in the films when the doping concentration becomes important. We observe that the dichroic ratio for the P1 band as well as the intensity of the reflections in the ED pattern of doped P3HT films tend to decrease when [$FeCl_3$] approaches 10 mM. A disordering of the layers of π-stacked backbones may be induced by the introduction of increasing amounts of $FeCl_3$ in the layers of side chains for both P3HT and C_{12}-PBTTT. This disordering may account for a "saturation" of the conductivity along the chain direction for high $FeCl_3$ concentration.

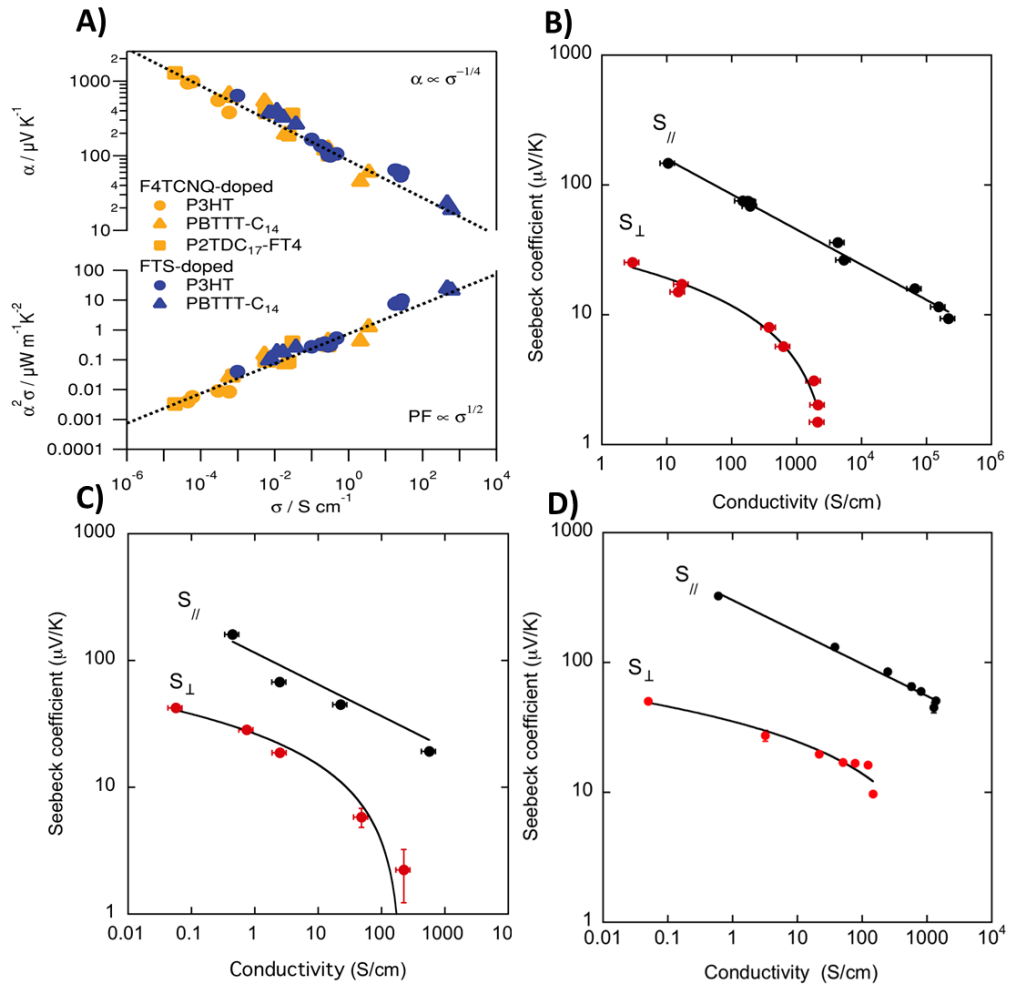

Figure 3.8. *Correlation between thermopower S and charge conductivity. A) F_4TCNQ and FTS doped non-oriented films of PBTTT, P3HT, P_2TDC_{17} -FT_4, which follows the relation $S_{//} \propto \sigma^{-1/4}$. B) Highly oriented thin films of* C_{12}-PBTTT *(T_R=125°C) and C) P3HT (T_R=180°C) doped with $FeCl_3$. // and ⊥ refer to the direction of the measurements*

respectively parallel and perpendicular to the chain direction. D) oriented thin films of C_{12}-PBTTT (T_R=125°C) doped with F_4TCNQ.) The full lines correspond to the results of the fit using a scaling law $S_{//} \propto \sigma^{1/4}$ and $S_{\perp} \propto -ln(\sigma)$. Figure A is reproduced from reference 52.

Alternatively, the departure from the power-law may indicate a different transport mechanism in the direction perpendicular to the polymer chains. As a matter of fact, attempts to fit the $S_{\perp}$-$\sigma_{\perp}$ plot indicate that $S_{\perp}$ scales rather well with ln($\sigma_{\perp}$). A similar dependence was reported by Mateeva et al. for oriented polyaniline films for which the S-σ relation was fitted with the equation:[56]

$$S_i = \frac{-1}{\beta}\left(\frac{k_B}{e}\right) ln\left(\frac{\sigma_i}{\sigma_i^{max}}\right) \quad (3)$$

with k_B the Boltzmann constant, e the charge of the electron and β a dimensionless coefficient. *i* refers to the direction either parallel (//) or perpendicular (⊥) to the chain direction.[56]

When fitted with equation (3), one obtains $\sigma_{\perp}^{max}$=3809 S/cm and β=26.7 for C_{12}-PBTTT and $\sigma_{\perp}^{max}$=211 S/cm and β=17.5 for P3HT. These results clearly indicate different intrinsic limitations in charge transport perpendicular to the chain direction for both polymers: charge transport perpendicular to the chains is larger in C_{12}-PBTTT than in P3HT. Regarding the factor β, previous studies on polyaniline reported β ≈ 9 whereas much higher values are obtained in the present case for $FeCl_3$-doped P3HT and C_{12}-PBTTT. In oriented polyaniline samples, Mateeva et al. observed that equation (3) is verified both parallel and normal to the chain direction (albeit for a reduced domain of conductivities well below that measured in the present case). This is clearly not true for C_{12}-PBTTT and P3HT that both show a power-law dependence along the chain direction and an apparent logarithmic dependence perpendicular to the chains. Altogether, these results indicate that the S-σ correlations in C_{12}-PBTTT are different along the chain

direction and perpendicular to it, supporting different charge transport mechanisms. It is worth to mention that Kroon[57] et. al observed a departure from the $S \propto \sigma^{-1/4}$ law for σ >1S/cm in non-oriented films of a oligo ethylated – polythiophene. We attribute this behavior to a mixing of the transport phenomena parallel and perpendicular to the polymer chains.

Interestingly, the same scaling relations ($S \propto \sigma^{-1/4}$) is observed for F_4TCNQ-doped C_{12}-PBTTT (figure3.8 D), indicating that they are apparently independent of the chemical nature of the dopant. The similarity of the behavior for $FeCl_3$ and F_4TCNQ further supports the fact that the high conductivity in $FeCl_3$-doped films is not related to a contribution from ionic conductivity that should result in a departure from the $S \propto \sigma^{-1/4}$ scaling law. To the best of our knowledge, it is the first time that such a difference between the S-σ correlations is evidenced along and normal to the chain direction. As a matter of fact, different S-σ correlations along and normal to the chain direction would further explain, at least in part, the large spread in experimental data in reference 48 and 49 as the measurements concern isotropic films for which both contributions parallel and normal to the chain direction can combine to different extents.

3. Conclusion

Controlling crystallization and orientation of polymer semiconductors prior to doping gives a unique handle over the charge transport and thermoelectric properties of the obtained conducting polymer films. This strategy is versatile and can be applied to numerous doped polymer semiconductors including n-type polymers[58] or low-bandgap polymers[59,60] that can be oriented by different methods such as blade-coating, high temperature rubbing or epitaxy and subsequently doped using different types of dopants and doping methods. *Central to this approach is the preservation of high order present in the pristine polymer semiconductors upon doping.* This is possible when the

dopants intercalate progressively into the layers of side chains by incremental increase of the dopant concentration in such a way that dopant intercalation preserves orientation and π-stacking of the conjugated polymer backbones. Three conditions are identified to obtain conductivities of 10^5 S/cm:

i) Achieve high in-plane orientation of conjugated polymers with a high persistence length

ii) Ensure regular intercalation of dopant molecules in the polymer structure to form bimolecular polymer-dopant crystals and

iii) Maintain a percolating nano-morphology along the chain direction e.g. via a liquid-crystal-like morphology (semi-crystalline lamellar morphologies are detrimental).

iv) Moreover, using a heterogeneous model approach based on the semi-crystalline structure of the doped and aligned polymer films, we are able to account for the anisotropy of the Seebeck coefficient that is enhanced in the direction of alignment.

Two different charge transport behaviors are evidenced in the directions parallel and normal to the polymer chains: $S_{//} \propto \sigma^{-1/4}$ prevails in the direction parallel and $S_{\perp} \propto \ln(\sigma)$ in the direction normal to the polymer chains. Regarding TE applications, the combination of effective chain alignment and controlled oxidation by sequential doping helps to reach a record power factor of 2 mW·m^{-1}·K^{-2} that could result in high ZT factors provided the thermal conductivity is well contained along the chain direction. Such a result is important as it sets a new upper limit for the ultimate TE power factor of such conducting polymers, but, it will be essential to further address the important issue of thermal conductivity and its correlation to the charge conductivity to obtain TE polymers with outstanding performances.

In the next chapter, we will focus on doped C_{12}-PBTTT films with F_6TCNNQ that is leading to a more stable doped state of the polymer films.

Bibiliography

[1] H. S. A. J. Heeger, A. G. MacDiarmid, *Macromolecules* **2002**, *35*, 1137.

[2] A. J. Heeger, *J. Phys. Chem. B* **2001**, *105*, 8475.

[3] Y. Nogami, H. Kaneko, T. Ishiguro, A. Takahashi, J. Tsukamoto, N. Hosoito, *Solid State Commun.* **1990**, *76*, 583.

[4] J. Tsukamoto, A. Takahashi, K. Kawasaki, *Jpn. J. Appl. Phys.* **1990**, *29*, 125.

[5] Y. W. Park, C. Park, Y. S. Lee, C. O. Yoon, H. Shirakawa, Y. Suezaki and K. Akagi, Sol. Stat. Comm. 1988, 65, 147.

[6] J. Mei, Z. Bao, *Chem. Mater.* **2014**, *26*, 604.

[7] H. Sirringhaus, P. J. Brown, R. H. Friend, M. M. Nielsen, K. Bechgaard, B. M. W. Langeveld-Voss, A. J. H. Spiering, R. A. J. Janssen, E. W. Meijer, P. Herwig, D. M. de Leeuw, *Nature* **1999**, *401*, 685.

[8] S. Holliday, J. E. Donaghey, I. McCulloch, *Chem. Mater.* **2014**, *26*, 647.

[9] H. Zhou, L. Yang, W. You, *Macromolecules* **2012**, *45*, 607.

[10] O. Bubnova, X. Crispin, *Energy Environ. Sci.* **2012**, *5*, 9345.

[11] O. Bubnova, Z. U. Khan, A. Malti, S. Braun, M. Fahlman, M. Berggren, X. Crispin, *Nat. Mater.* **2011**, *10*, 429.

[12] Q. Wei, M. Mukaida, Y. Naitoh, T. Ishida, *Adv. Mater.* **2013**, *25*, 2831.

[13] A. M. Nardes, R. A. J. Janssen, M. Kemerink, *Adv. Funct. Mater.* **2008**, *18*, 865.

[14] M. Brinkmann, J.-C. Wittmann, *Adv. Mater.* **2006**, *18*, 860.

[15] L. Biniek, N. Leclerc, T. Heiser, R. Bechara, M. Brinkmann, *Macromolecules* **2013**,

46, 4014.

[16] M. Brinkmann, *J. Polym. Sci. Part B Polym. Phys.* **2011**, *49*, 1218.

[17] M. Brinkmann, L. Hartmann, L. Biniek, K. Tremel, N. Kayunkid, *Macromol. Rapid Commun.* **2014**, *35*, 9.

[18] M. Rahimi, A. P. Straub, F. Zhang, X. Zhu, M. Elimelech, C. A. Gorski, B. E. Logan, *Energy Environ. Sci.* **2018**, *11*, 276.

[19] E. J. W. Crossland, K. Tremel, F. Fischer, K. Rahimi, G. Reiter, U. Steiner, S. Ludwigs, *Adv. Mater.* **2012**, *24*, 839.

[20] D. M. DeLongchamp, R. J. Kline, E. K. Lin, D. A. Fischer, L. J. Richter, L. A. Lucas, M. Heeney, I. McCulloch, J. E. Northrup, *Adv. Mater.* **2007**, *19*, 833.

[21] C. Y. Kao, B. Lee, L. S. Wielunski, M. Heeney, I. McCulloch, E. Garfunkel, L. C. Feldman, V. Podzorov, *Adv. Funct. Mater.* **2009**, *19*, 1906.

[22] J. Hynynen, D. Kiefer, L. Yu, R. Kroon, R. Munir, A. Amassian, M. Kemerink, C. Müller, *Macromolecules* **2017**, *50*, 8140.

[23] K. Kang, S. Watanabe, K. Broch, A. Sepe, A. Brown, I. Nasrallah, M. Nikolka, Z. Fei, M. Heeney, D. Matsumoto, K. Marumoto, H. Tanaka, S. I. Kuroda, H. Sirringhaus, *Nat. Mater.* **2016**, *15*, 896.

[24] A. Hamidi-sakr, L. Biniek, J.-L. Bantignies, D. Maurin, L. Herrmann, N. Leclerc, P. Lévêque, V. Vijayakumar, N. Zimmermann, M. Brinkmann, *Adv. Funct. Mater.* **2017**, *27*, 1700173.

[25] V. Vijayakumar, E. Zaborova, L. Biniek, H. Zeng, L. Herrmann, A. Carvalho, O. Boyron, N. Leclerc, M. Brinkmann, *ACS Appl. Mater. Interfaces* **2019**, *11*, 4942.

[26] A. Hamidi-Sakr, L. Biniek, S. Fall, M. Brinkmann, *Adv. Funct. Mater.* **2016**, *26*, 408.

[27] H. Kaneko, T. Ishiguro, *Synth. Met.* **1994**, *65*, 141.

[28] Previous studies on $FeCl_3$-doped Polyacetylene (PA), have shown that the doping mechanism results in the formation of $FeCl_4^-$ and $FeCl_2$ species following the reaction Polymer + 2 $FeCl_3 \rightarrow Polymer^+ + FeCl_4^- + FeCl_2$. H. Sakai, Y. Maeda, T. Kobayahi and H. Shirakawa, *Bull. Chem. Soc. Jpn*, **1983**, 56, 1616.

[29] N. C. Miller, E. Cho, R. Gysel, C. Risko, V. Coropceanu, C. E. Miller, S. Sweetnam, A. Sellinger, M. Heeney, I. McCulloch, J.-L. Brédas, M. F. Toney, M. D. McGehee, *Adv. Energy Mater.* **2012**, *2*, 1208.

[30] N. C. Miller, E. Cho, M. J. N. Junk, R. Gysel, C. Risko, D. Kim, S. Sweetnam, C. E. Miller, L. J. Richter, R. J. Kline, M. Heeney, I. McCulloch, A. Amassian, D. Acevedo-Feliz, C. Knox, M. R. Hansen, D. Dudenko, B. F. Chmelka, M. F. Toney, J.-L. Brédas, M. D. McGehee, *Adv. Mater.* **2012**, *24*, 6071.

[31] B.-K. Yang, C.-A. Wang, W.-Y. Zhang, J. Ruan, *J. Polym. Sci. Part B Polym. Phys.* **2017**, *55*, 1448.

[32] K. E. Aasmundtveit, E. J. Samuelsen, L. A. A. Pettersson, O. Inganäs, T. Johansson, R. Feidenhans'l, *Synth. Met.* **1999**, *101*, 561.

[33] E.-G. Kim, J.-L. Brédas, *J. Am. Chem. Soc.* **2008**, *130*, 16880.

[34] A. Hamidi-Sakr, D. Schiefer, S. Covindarassou, L. Biniek, M. Sommer, M. Brinkmann, *Macromolecules* **2016**, *49*, 3452.

[35] E. Cho, C. Risko, D. Kim, R. Gysel, N. Cates Miller, D. W. Breiby, M. D. McGehee, M. F. Toney, R. J. Kline, J.-L. Bredas, *J. Am. Chem. Soc.* **2012**, *134*, 6177.

[36] B. McCulloch, V. Ho, M. Hoarfrost, C. Stanley, C. Do, W. T. Heller, R. A. Segalman,

Macromolecules **2013**, *46*, 1899.

[37] L.-H. Zhao, R.-Q. Png, J.-M. Zhuo, L.-Y. Wong, J.-C. Tang, Y.-S. Su, L.-L. Chua, *Macromolecules* **2011**, *44*, 9692.

[38] J. Yamamoto, Y. Furukawa, *J. Phys. Chem. B* **2015**, *119*, 4788.

[39] J. Hwang, D. B. Tanner, I. Schwendeman, J. R. Reynolds, *Phys. Rev. B* **2003**, *67*, 115205.

[40] R. Ghosh, C. M. Pochas, F. C. Spano, *J. Phys. Chem. C* **2016**, *120*, 11394.

[41] R. Ghosh, A. R. Chew, J. Onorato, V. Pakhnyuk, C. K. Luscombe, A. Salleo, F. C. Spano, *J. Phys. Chem. C* **2018**, *122*, 18048.

[42] H. Li, M. E. DeCoster, R. M. Ireland, J. Song, P. E. Hopkins, H. E. Katz, *J. Am. Chem. Soc.* **2017**, *139*, 11149.

[43] H. Tanaka, M. Hirate, S. Watanabe, S. Kuroda, *Adv. Mater.* **2014**, *26*, 2376.

[44] P. Sheng, *Phys. Rev. B* **1980**, *21*, 2180.

[45] J. Fanous, M. Schweizer, D. Schawaller, M. R. Buchmeiser, *Macromol. Mater. Eng.* **2012**, *297*, 123.

[46] A. Andreatta, Y. Cao, J. C. Chiang, A. J. Heeger, P. Smith, *Synth. Met.* **1988**, *26*, 383.

[47] J. Hynynen, E. Järsvall, R. Kroon, Y. Zhang, S. Barlow, S. R. Marder, M. Kemerink, A. Lund, C. Müller, *ACS Macro Lett.* **2019**, *8*, 70.

[48] J. Blatt, P. A. Schroeder, C. L. Foiles, D. Greig in *Thermopower of Metals*, Plenum Press, New York and London, **1976**, p. 5.

[49] A. B. Kaiser, *Phys. Rev. B* **1989**, *40*, 2806.

[50] W. Pukacki, J. Plocharski, S. Roth, *Synth. Met.* **1994**, *62*, 253.

[51] C. L. Choy, *Polymer* **1977**, *18*, 984.

[52] M. G. Kanatzidis, *Chem. Mater.* **2010**, *22*, 648.

[53] S. D. Kang, G. J. Snyder, *Nat. Mater.* **2016**, *16*, 252.

[54] S. N. Patel, A. M. Glaudell, K. A. Peterson, E. M. Thomas, K. A. O'Hara, E. Lim, M. L. Chabinyc, *Sci. Adv.* **2017**, *3*, e1700434.

[55] A. M. Glaudell, J. E. Cochran, S. N. Patel, M. L. Chabinyc, *Adv. Energy Mater.* **2015**, *5*, 1401072.

[56] N. Mateeva, H. Niculescu, J. Schlenoff, L. R. Testardi, *J. Appl. Phys.* **1998**, *83*, 3111.

[57] R. Kroon, D. Kiefer, D. Stegerer, L. Yu, M. Sommer, C. Müller, *Adv. Mater.* **2017**, *29*, 1700930.

[58] K. Tremel, F. S. U. Fischer, N. Kayunkid, R. Di Pietro, R. Tkachov, A. Kiriy, D. Neher, S. Ludwigs, M. Brinkmann, *Adv. Energy Mater.* **2014**, *4*, 1301659.

[59] Y. Zhong, L. Biniek, N. Leclerc, S. Ferry, M. Brinkmann, *Macromolecules* **2018**, *51*, 4238.

[60] L. Biniek, A. Hamidi-Sakr, L. Grodd, S. Escoubas, Y. J. Dappe, S. Grigorian, M. Schmutz, M. Brinkmann, *Adv. Electron. Mater.* **2018**, *4*, 1700480.

Chapter 4. Influence of dopant size and doping method on the thermoelectric properties of PBTTT films doped with F_6TCNNQ and F_4TCNQ

F_4TCNQ doping of organic semiconductors such as P3HT and PBTTT has been widely documented in the recent literature. This chapter focuses mainly on doping of C_{12}-PBTTT using a new doping agent, namely F_6TCNNQ. Unlike F_4TCNQ, F_6TCNNQ doping of polythiophenes has been marginally studied. This dopant is chosen because of its deeper LUMO energy level of -5.3 eV, versus -5.1 eV for F_4TCNQ that can enhance charge transfer between C_{12}- PBTTT and F_6TCNNQ. Oriented C_{12}-PBTTT thin films are prepared by high temperature rubbing and sequentially doped with F_6TCNNQ using a new doping method, called “incremental concentration doping” (ICD). The ICD method implies that a given sample is doped by dipping it successively in dopant solutions of increasing concentration. ICD of C_{12}-PBTTT using F_6TCNNQ leads to record electrical conductivities of 2430 S/cm and thermoelectric power factors (PF) 530±200 $\mu W m^{-1} K^{-2}$. Moreover, this method leads to a higher electrical conductivity than the conventional doping method (direct doping). This study demonstrates that a progressive intercalation of dopants in PBTTT crystals using the ICD method helps preserve the high level of order initially present in the aligned C_{12}-PBTTT films.

The diffusion coefficients of both F_6TCNNQ and F_4TCNQ anions have been determined using the doping kinetics followed by UV-Vis NIR spectroscopy. A lower diffusion coefficient is observed for F_6TCNNQ anions, demonstrating the size dependence of diffusion coefficients into the polymer matrix. The longer and bulkier the anion, the lower its diffusion coefficient. Polarized UV-Vis-NIR spectroscopy on these doped thin

films showed that F_6TCNNQ^- anions are better oriented in the layers of the alkyl side chains as compared to F_4TCNQ. The estimation of charge carrier mobilities indicates that ICD leads to higher mobilities than DD. The lower degree of ordering of F_4TCNQ^- anions produced lower electrical conductivity than F_6TCNNQ doped C_{12}-PBTTT thin films.

Chapter 4: Influence of dopant size and doping method on the thermoelectric properties of PBTTT films doped with F_6TCNNQ and F_4TCNQ

1. Introduction

Doped polymers are of central interest in plastic electronics not only for their charge transport properties used for instance in polymer injection layers (PEDOT: PSS) but also for their thermoelectric properties as demonstrated by Crispin and coworkers. [1] Doping polymer semi-conductors such as regioregular poly(3-hexylthiophene) or PBTTT with acceptor molecules such as F_4TCNQ is a common strategy to transform semi-conducting films into conducting ones.[2–6] However, to control their TE properties, it is essential to tune the charge carrier density that is determined by the method of doping and the type of dopant for a given polymer. In particular, the power factor PF that determines the effectivity of a doped polymer for TE properties has been shown to scale with conductivity such as $PF \propto \sqrt{\sigma}$. Enhancing TE properties is therefore achieved by improving charge conductivity of conducting polymers. Various groups have therefore focused on the doping method as a handle to reach improved TE performances in doped polymer films.[7–12] Sequential doping, i.e. the doping of a highly crystalline polymer semiconductor films with a dopant solution in an orthogonal solvent is an effective method to enhance the TE properties as compared to doped polymer films prepared from mixed polymer and dopant solution in a common solvent.[9,10,13,14] Vapor phase doping leads to even higher charge conductivities since it seems to preserve order along the chain direction in the doped polymer crystals. As demonstrated in the previous chapters, dopants are usually intercalated in the layers of alkyl side chains of the polymers[15,16]. Therefore, the amount of dopants incorporated in a thin polymer film depends strongly on the length and packing of alkyl side chains as demonstrated in chapter 2 for PBTTT. The final thermoelectric properties of the doped films can further be enhanced if the films are oriented. Both, thermopower and charge conductivity are enhanced in aligned P3HT and PBTTT films along the chain direction, making it possible to improve substantially the TE power factor of the layers.

The choice of the dopant is also of paramount importance. The LUMO level of the acceptor molecules must be well situated with respect to the HOMO of the p-type polymer. The higher electrical conductivity observed in F_4TCNQ doped polythiophenes is mainly due to the favourable energetical offset between the energy levels of the polymer and F_4TCNQ. For instance, in F_4TCNQ-doped P3HT and PBTTT, the HOMO of these polymers is in the range -4.8 eV - 5.2 eV and the LUMO of the dopant is around -5.24 eV. Besides F_4TCNQ, various strong inorganic dopants such as I_2, $FeCl_3$, WO_3 have also been used to dope the conducting polymers. In chapter 3, we have shown that $FeCl_3$-doping of C_{12}-PBTTT leads to very high conductivities above 10^5 S/cm. However, $FeCl_3$ and the other cited dopants are difficult to use because of both their high instability in air and corrosive nature. [14,17,18].

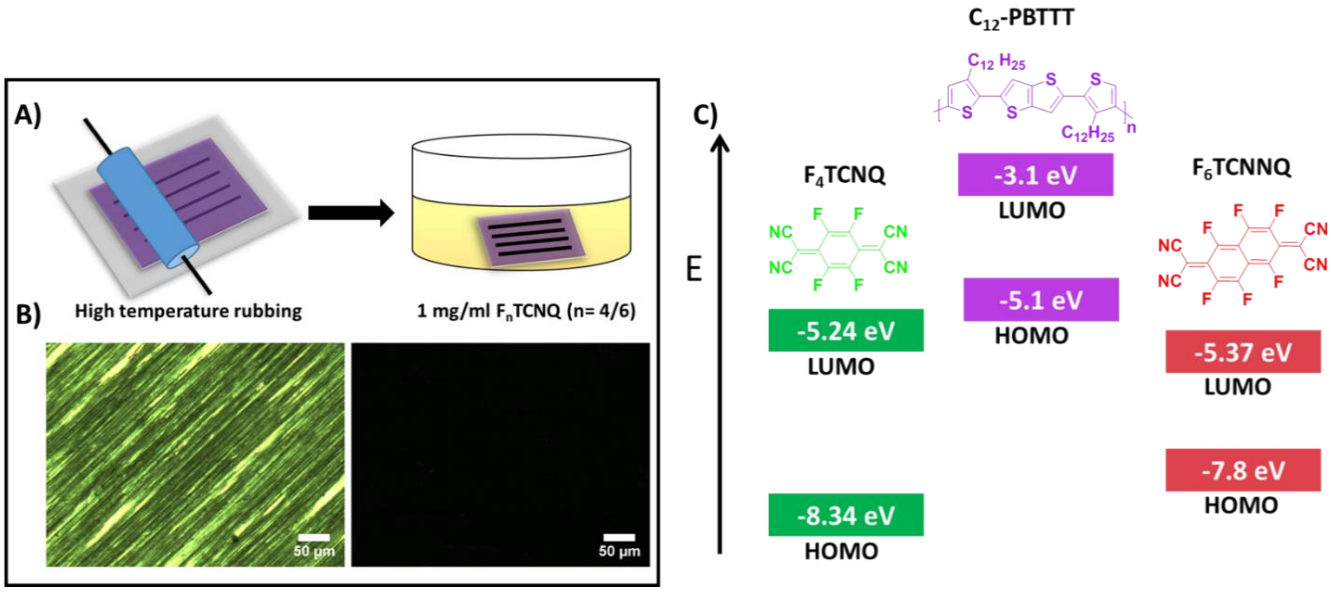

Figure 4.1. *A) Two-step preparation of highly oriented and crystalline C_{12}-PBTTT films. The first step consists of chain alignment and crystallization by high-T rubbing followed by sequential doping in solutions of F_4TCNQ or F_6TCNNQ in acetonitrile. B) Polarized optical microscopic images of F_6TCNNQ doped C_{12}-PBTTT showing high birefringence (T_R =125 ℃ and C_{F4TCNQ}= 1mg/ml) C) Schematic representation of HOMO and LUMO levels F_4TCNQ, F_6TCNNQ and PBTTT.*

It is therefore essential to find alternative dopants to both F_4TCNQ and $FeCl_3$. Instead of using inorganic based doping agents, electron-deficient molecular dopants such as TCNQ and derivatives such as 2-(perfluoronaphthalene-2,6-diylidene)-dimalonitrile (F_6TCNNQ) (see figure 4.1C) were recently introduced for the doping of conducting interlayers in electronic devices[19,20].

Karpov [21] and coworkers first reported the use of F_6TCNNQ to dope effectively P3HT. They reported a high electrical conductivity of ≈ 7 S/cm, which was three times higher than that of F_4TCNQ-doped P3HT. The reason for the higher electrical conductivity was not demonstrated with clarity. They attributed the higher electrical conductivity to a combination of higher charge carrier mobilities and higher doping strength of F_6TCNNQ (-5.37 eV for F_6TCNNQ vs -5.24 eV for F_4TCNQ) leading to a higher charge carrier concentration (see figure 4.1). Moreover, they proposed that similar to F_4TCNQ doping of P3HT, the charge transfer between P3HT and F_6TCNNQ is of integer charge transfer type. [22]

Given the proposed context and state-of-the-art (chapter 1), the present chapter aims at investigating the following important issues:

- To what extent does the doping of C_{12}-PBTTT with F_6TCNNQ differ from that with F_4TCNQ in terms of structure, doping kinetics and resulting TE properties?
- How different is the intercalation of F_4TCNQ and F_6TCNNQ in the layers of alkyl side chains of C_{12}-PBTTT?
- Is there any relationship between the degree of order of the dopant anions in the polymer semiconductor and the resulting electrical conductivities?
- Is there a way to introduce bulky dopants such as F_6TCNNQ in the crystals of C_{12}-PBTTT so as to preserve best the pristine structure of the undoped polymer films?

So far, there is no clear evidence of the effect of F_6TCNNQ doping on the crystal structure of polythiophenes. Moreover, the position and the orientation of the F_6TCNNQ^- anion in doped polythiophenes such as PBTTT and P3HT is not well understood. In this chapter, we investigate the effect of F_6TCNNQ^- and F_4TCNQ-doping on the crystal structure and TE properties of oriented C_{12}-PBTTT. Polarized UV-Vis-NIR spectroscopy and low dose electron diffraction were used to uncover the location and orientation of the dopant anions. We demonstrate that F_6TCNNQ^- anions orient perpendicular to aligned C_{12}-PBTTT chains, as observed for F_4TCNQ^-. The angle-dependent polarized UV-Vis-NIR spectroscopy helped determine the angular distributions of both the dopant anions and polarons in oriented C_{12}-PBTTT and uncover the degree of orientation of dopant anions in the oriented C_{12}-PBTTT films.

It is expected that the dopant size is an important factor that determines the intercalation of the dopant anions into the interdigitated layers of the alkyl side chains of PBTTT. The perpendicular orientation of the dopant anions enabled us to follow their individual diffusion kinetics into the layers of the interdigitated alkyl side chains of C_{12}-PBTTT [16]. A correlation is observed between the dopant size and diffusion coefficient.

Finally, we propose a general method to prepare highly conducting oriented and crystalline C_{12}-PBTTT thin films by a combination of high temperature rubbing followed a modified doping method i.e. incremental concentration doping (ICD). The ICD method implies that a given sample is doped by dipping it successively in dopant solutions of increasing concentration (see figure 4.2). On the other hand, in the conventional doping process (single doping), a film is directly dipped into the solution of at the final concentration of dopant. The changes in the crystal structure of the thin films were followed by low dose electron diffraction for both direct and incremental concentration doping. To the best of our knowledge, this is the first evidence on the impact of two

different doping methods with the same doping agent on the crystal structure and TE properties of PBTTT thin films. Promising thermoelectric performances were observed in oriented C_{12}-PBTTT thin films after incremental concentration doping and record conductivities of 2430±500 S/cm were observed along the chain direction in F_6TCNNQ doped PBTTT thin films.

2. Results and discussion.

2.1 Fabrication of highly oriented conducting PBTTT thin films

It has been shown in the previous chapters that polymers such as PBTTT can be easily oriented by rubbing at high temperature[23]. Highly oriented crystalline polymer films of C_{12}-PBTTT with dichroic ratio≈7 were obtained by rubbing at 125 °C.

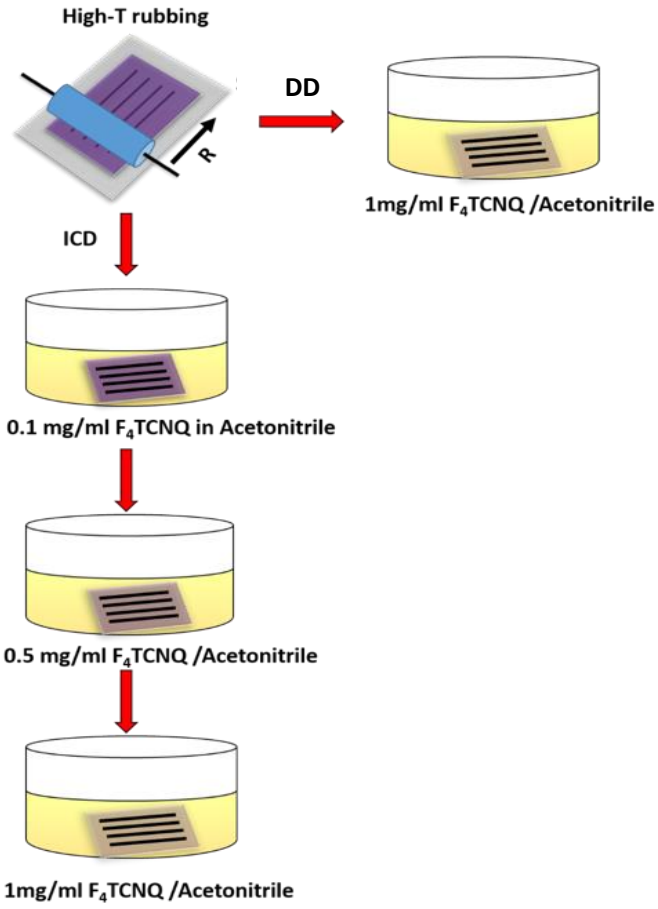

Figure 4.2. *Schematic illustration of incremental concentration doping (ICD) and direct doping.*

The work presented in the previous chapters showed that doping of oriented polythiophene films by sequential doping can lead to very high conductivities. Based on these results, oriented C_{12}-PBTTT thin films were doped sequentially by dipping in solutions of F_4TCNQ and F_6TCNNQ in acetonitrile (see figure 4.1B). The films were subsequently dried with a nitrogen flow. The doped thin films show high levels of orientation, which is evidenced by polarized optical microscopy (see figure 4.1C).

Herein we introduced a new doping procedure, which is called "incremental concentration doping" (ICD). It is a modified doping version of classical sequential doping (see figure 4.2). In ICD, the oriented thin films are doped by dipping a given sample successively in solutions of dopants of increasing concentration.

This is different from the conventional sequential doping (we call it direct doping), that implies that each thin film is dipped a single time in a solution of given concentration (see figure 4.2). In this study, all the thin films are doped by using ICD.

2.2. Polarized UV-Vis-NIR spectroscopy

Polarized UV-vis-NIR spectroscopy is very helpful in determining the amount and orientation of dopant molecules such as F_4TCNQ and F_6TCNNQ in the doped and oriented thin films of C_{12}-PBTTT. Let us first present the spectroscopic signatures of the two dopants. Both F_4TCNQ^- and F_6TCNNQ^- anions display distinct signatures in the form of vibronic structures as seen in figure 4.3. In order to confirm the presence of the F_6TCNNQ^- anions in the thin films of PBTTT, we prepared a solution of pure F_6TCNNQ^- anions by reacting F_6TCNNQ with Ferrocene in DCM, the corresponding UV-Vis-NIR spectrum is shown in figure 4.3, that shows the spectra of both neutral and F_4TCNQ^-. F_6TCNNQ^- anions show characteristic bands at 1143, 976 and 987 nm and there are no corresponding absorption bands in that spectral range for neutral F_6TCNNQ. The latter is characterized by two bands at 481 and 454 nm that do overlap partially with some

bands of the F_6TCNNQ^- anion. As seen in figure 4.3B, the vibronic structure of the F_6TCNNQ^- anions in the doped C_{12}-PBTTT matches quite well that of the anion in solution. There is only a small redshift in the thin films (1157 nm versus 1143 nm in solution).

Having identified the spectral signatures of the F_6TCNNQ^- anion, we can now analyse in more details the polarized UV-vis-NIR spectra of the doped films. The polarized UV-Vis-NIR spectra of both F_6TCNNQ and F_4TCNQ doped C_{12}-PBTTT are highly informative. As expected, the polaronic bands P1 and P2 are polarized along the rubbing direction and their intensities increase with doping concentration and saturate once the concentration reaches 0.5 mg/ml. Even for very low doping concentrations such as 0.01 mg/ml, the P1 and P2 bands were present. Contrary to the polaronic bands, the absorption bands of the neutral polymer (N) decreased with increasing dopant concentration. As expected, a higher reduction in the absorption of neutral polymer in F_6TCNNQ doped C_{12}-PBTTT indicates higher oxidation of polymer chains. This observation further confirms that the deeper LUMO level of F_6TCNNQ (-5.37 eV) compared to -5.24 eV in F_4TCNQ is more favourable for charge transfer.

The polarized UV-Vis-NIR spectra along the perpendicular direction are different from the spectra along the parallel direction. The highly polarized spectra along the perpendicular direction provide fruitful information regarding the location and orientation of the dopant anions in the C_{12}-PBTTT crystals. As observed in our previous works[15,16] and previous chapter 2, both F_4TCNQ^- and F_6TCNNQ^- anion bands are polarized perpendicular to the rubbing direction. For the films doped with F_6TCNNQ, the anion bands are similar to those observed for the anions in dichloromethane (DCM) (see figure 4.3).

For both F_4TCNQ and F_6TCNNQ dopants, the intensity of the anion bands increased with doping concentration and saturated for C= 0.5-1.0 mg/ml. The polaron bands P1 and P2

show a similar saturation for POL//R. Interestingly, no absorption from the polarons is seen for POL ⊥R.

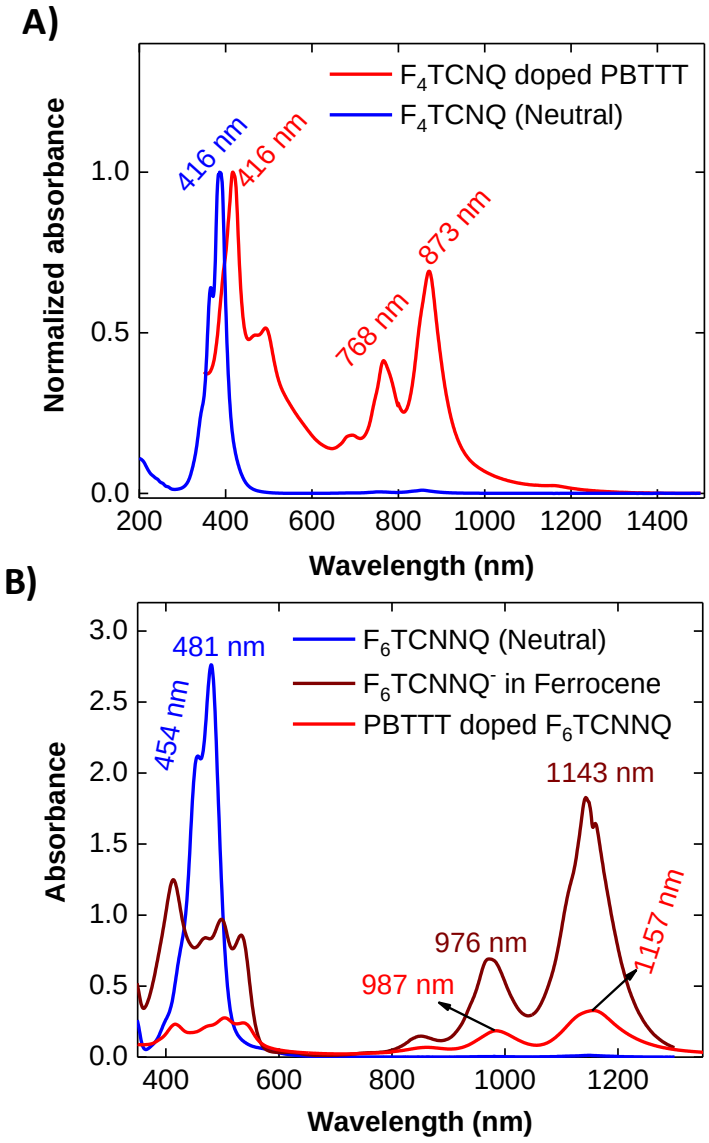

Figure 4.3. *A) Absorption bands of F_4TCNQ^- anions in doped PBTTT thin films and absorption of neutral F_4TCNQ in solution. B) Absorption in solution of neutral F_6TCNNQ (blue)andF_6TCNNQ^- anion (brown) after treating with Ferrocene. The absorption of F_6TCNNQ^- anion in thin films is shown in red.*

The polarization of the F_6TCNNQ^- bands for POL⊥R indicates that the long axis of the F_6TCNNQ molecule is oriented in a plane perpendicular to C_{12}-PBTTT chains, as for F_4TCNQ (see figure 4.4 C). This demonstrates that, similar to the F_4TCNQ^- anion,

F_6TCNNQ^- anions are oriented perpendicular to the aligned PBTTT backbones in the layers of the interdigitated side chains.

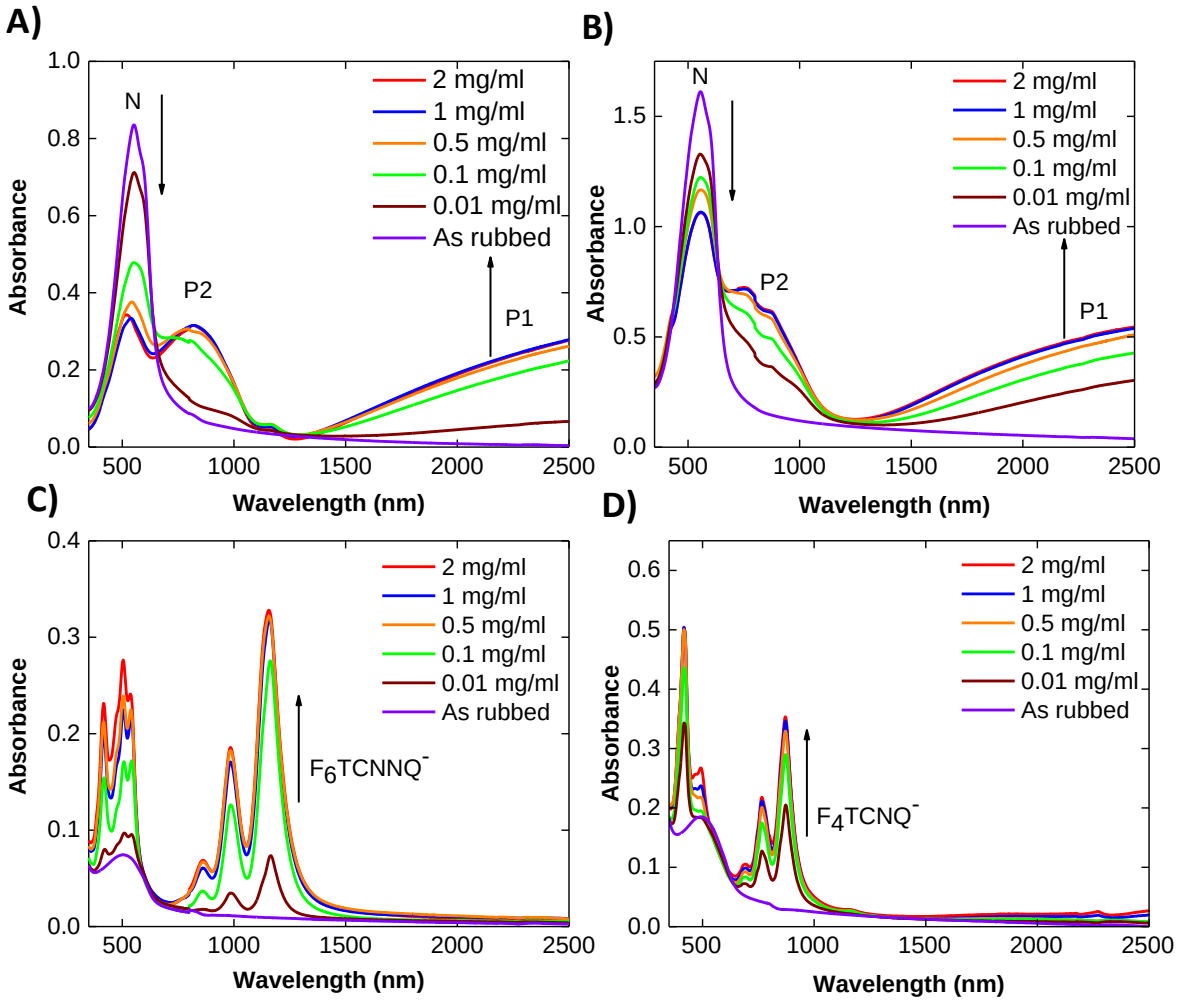

Figure 4.4. *Concentration dependent doping of C_{12}-PBTTT with F_4TCNQ and F_6TCNNQ in acetonitrile. A) and B) represent the evolution of the UV-Vis-NIR spectra for POL//R as a function of doping concentration for F_6TCNNQ^- and F_4TCNQ-doped C_{12}-PBTTT, respectively. C) and D) show the evolution of the F_6TCNNQ^- and F_4TCNQ^- bands as a function of increasing doping concentration for POL ⊥R. P1 and P2 correspond to polaronic bands of doped C_{12}-PBTTT and the neutral polymer absorption is labelled as N.*

2.3. Angular distribution of dopant anions and polarons

To further understand the degree of order and distribution of the dopant anions and polarons in the oriented C_{12}-PBTTT, angle-dependent polarized UV-Vis-NIR spectroscopy was used. Oriented C_{12}-PBTTT thin films were prepared and doped by dipping in 1 mg/ml

of the corresponding dopant solutions. Then the angle-dependent UV-Vis-NIR spectroscopy was recorded by changing the polarization angle of the incident light with respect to the direction of rubbing from 0° to 90° with an interval of 15° for both F_4TCNQ and F_6TCNNQ doped PBTTT thin films (see figure 4.5C and 4.5D).

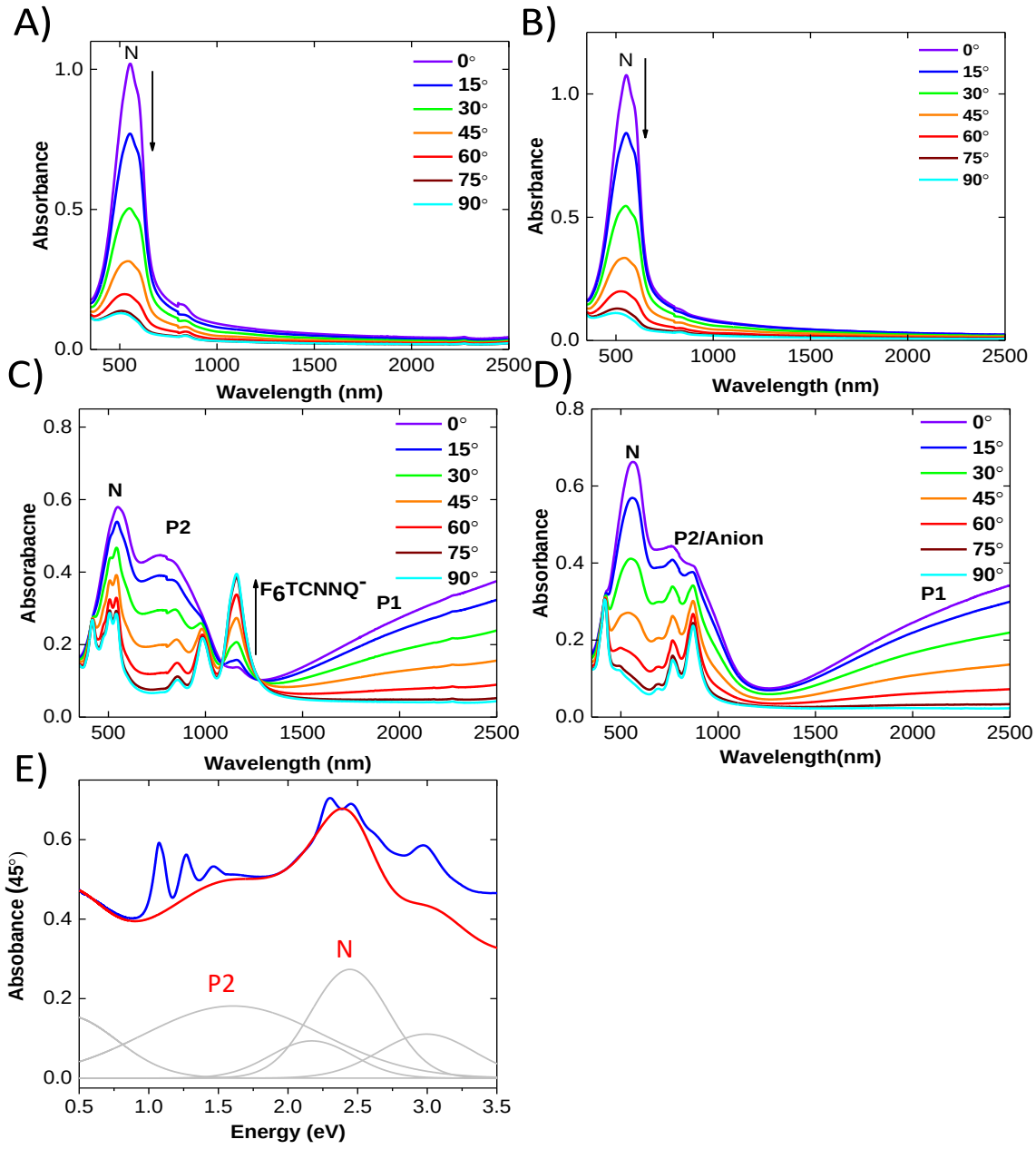

Figure 4.5. A) and B) represents *UV–Vis–NIR absorption spectra of oriented C_{12}-PBTTT (before doping) plotted for different angles (every 15°) between the direction of polarization and the rubbing direction. C) and D) Polarized UV–Vis–NIR absorption spectra of F_6TCNNQ doped PBTTT and F_4TCNQ doped PBTTT plotted for*

different angles (every 15°) between the direction of polarization and the direction of rubbing of the film. At 0°, the incident light is parallel to the direction of rubbing (POL // R) whereas at 90° it is perpendicular to the rubbing direction (POL ⊥ R). E) Example of deconvolution of the UV-Vis-NIR spectra for C_{12}-PBTTT thin films doped with F_6TCNNQ when the incident polarization angle is 45°. The spectra on top (blue) result from the overlap of the anionic contribution at 1158 nm, with the polaronic (P2) and N components. The spectra in red contain the sum of all components beneath the anion bands. The actual absorbance of the anion is obtained by subtraction of the red baseline from the initial spectra.

The angular distribution studies on oriented polymers before and after doping helps to determine the in-plane orientation of the aligned polymer chains, polarons and the dopant anions. Therefore, the angle-dependent UV-Vis-NIR spectroscopy on oriented polymer films provides a better understanding of the degree of orientation of both F_4TCNQ^- and F_6TCNNQ^- in the layers of the alkyl side chains of PBTTT.

For an incident polarization of 0°(POL // R), a very small contribution of both dopant anions F_4TCNQ^- and F_6TCNNQ^- bands is observed. For increasing polarization angle, their intensities increase whereas the contributions from the polarons (P1 and P2) decreased. Both F_4TCNQ^- and F_6TCNNQ^- anions showed their maximum absorption when the incident light is polarized perpendicular to the rubbing direction (90°) while the polaronic bands have a maximum at 0°. The plot of the intensities of absorbance of the neutral polymer, polarons and the dopant anions as a function of incident polarization angle help determine the in-plane angular distribution of the polarons and anions in oriented C_{12}-PBTTT. The overlap of the anionic bands (873 nm for F_4TCNQ and 1158 nm for F_6TCNNQ) with the broad polaronic contribution made it difficult to evaluate the true absorbance of the anions. Hence, it was necessary to deconvolute the as-obtained spectra in order to extract the actual absorbance of the anion by subtracting the contribution from the polaron P2 (see figure 4.5E). The angular dependence of the

F_4TCNQ^- and F_6TCNNQ^- absorption after the subtraction of the P2 contribution is represented in figure 4.6 C and D, respectively.

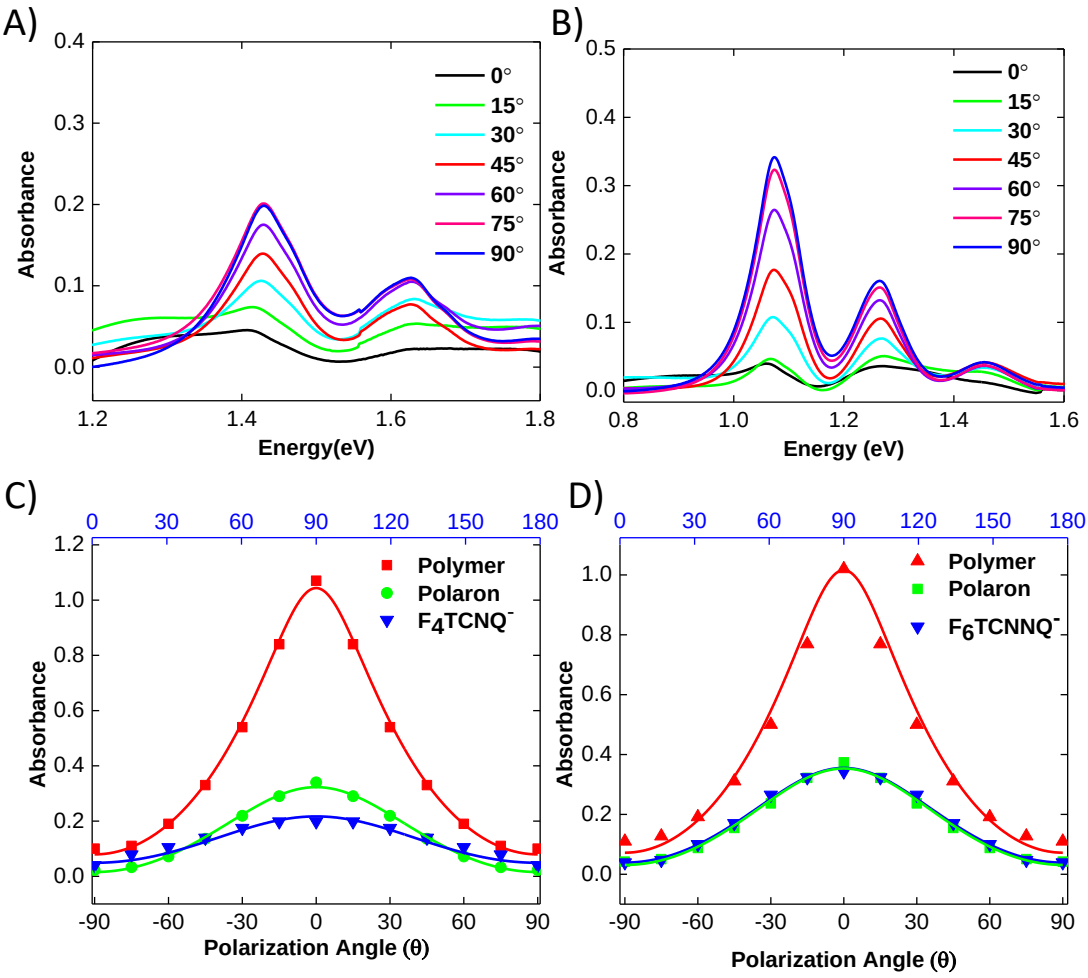

Figure 4.6. *Absorbance of the dopant anions after subtracting the background absorbance of the polaronic contribution P2 for A) F_4TCNQ^- and B) for F_6TCNNQ^-. C) Angular distribution of absorption bands of pristine C_{12}-PBTTT before doping, the F_4TCNQ^- anion (λ= 873nm) and the P1 band (λ= 2500 nm). D) Angular distribution of the absorption bands of oriented pristine C_{12}-PBTTT before doping, the F_6TCNNQ^- anion (λ= 1158 nm) and the polaronic P1 band (λ= 2500 nm).*

The figures 4.6C and D depict the angular distributions of the absorption for the polarons, F_4TCNQ^- and F_6TCNNQ^- anions in oriented C_{12}-PBTTT. The resulting curves are fitted using the equation.[24]

$$A(\lambda,\theta) = A_0 - \log\left[1 - \frac{\beta}{\beta+1}(1 + 3cos2\theta)\right] \quad (1)$$

Where,

$$\beta = \frac{1}{3}\tanh(\Delta A \frac{ln10}{2}) \quad (2)$$

Here A_0 is the unpolarised offset absorption contribution related to the non-aligned fraction of C_{12}-PBTTT and $\Delta A = A_{max} - A_{min}$, Amax (0°, //) and A_{min} (90°, ⊥) for P1 and A_{max} (90°, ⊥) and A_{min} (0°, //) for both F_4TCNQ^- and F_6TCNNQ^-.

The very small value of the absorption offset (A_0 = 0.07) before doping indicates that most of the chains are aligned and there is almost no contribution from a non-oriented fraction of C_{12}-PBTTT. The absorption offsets for both polarons and anions are also very small (≈ 0.05), which further confirms that the high degree of alignment of C_{12}-PBTTT is maintained after doping. The same observation was also obtained by Untilova[(ref)] and coworkers for the angular distribution measurements of F_4TCNQ-doped P3HT films. In addition to this, the maximum of the angular distributions of both F_4TCNQ^- and F_6TCNNQ^- anions are clearly centred at 90°. This implies that the long axis of the dopants is indeed oriented around a plane orthogonal to the average polymer chain direction and not tilted. A clearer idea about the degree of orientation of both polarons and anions in the oriented C_{12}-PBTTT matrix was obtained from the comparison of the dichroic ratio (DR) and 3D order parameters (OP), for the polaron, the anion and the pristine polymer.

Those values are collected in table 4.1. The 3D order parameter is calculated from the dichroic ratio using equation (3):

$$OP = \frac{DR-1}{DR+2} \quad (3)$$

$$DR = \frac{Abs//}{Abs\perp} \quad (4)$$

Where Abs// is the absorption parallel to the rubbing and Abs⊥ is the absorption perpendicular to the rubbing direction. DR is the dichroic ratio.

Table 4.1. Characteristics of angular distribution curves of F_4TCNQ and F_6TCNNQ doped PBTTT C_{12}

Dopant+Polymer	F_4TCNQ doped PBTTT C_{12}			F_6TCNNQ doped PBTTT C_{12}		
	As rubbed PBTTT	F_4TCNQ^-	Polaron (P1)	As rubbed PBTTT	F_6TCNNQ^-	Polaron (P1)
Half-width at half maxima	±28.5°	±47°	±38°	±28.9°	±38°	±41°
Dichroic ratio (D_R)	10.7	4.95	15	9.3	8.8	9.3
Order parameter (S)	0.7	0.5	0.7	0.7	0.7	0.73

In the case of F_4TCNQ doping, the calculated order parameters (OP) was 0.7 for the oriented C_{12}-PBTTT and it was equal to 0.7 for the polarons. The similar values of the order parameter for both polarons and the oriented PBTTT chains indicates that doping does not alter the alignment of the chains. Surprisingly, the order parameter calculated for the F_4TCNQ^- anions (0.56) is substantially lower as compared to that of the polarons (0.7). Similar trends were obtained by Untilova and coworkers regarding the angular distribution of F_4TCNQ in oriented P3HT films(ref). It suggests that the F_4TCNQ dopants are not strictly located in a plane orthogonal to the polymer chains, but are distributed around this average orientation.

The case of F_6TCNNQ doping is different. In this case, the polymer chains, polarons and the dopant F_6TCNNQ^- anions showed similar OP ≈0.7. This result supports the idea that, unlike F_4TCNQ^- anions, the long axis of F_6TCNNQ^- lies essentially in a plane that is perpendicular to the oriented C_{12}-PBTTT chains with little angular spread around this average plane. In other words, the orientation of the F_6TCNNQ dopants is defined in a better way with respect to the polythiophene chains as compared to F_4TCNQ. The better

orientation of the F_6TCNNQ^- molecules in the layers of alkyl side chains of C_{12}-PBTTT might be due to stronger Coulombic interactions between the F_6TCNNQ^- anion and the polaronic charges on the polymer backbone possibly because of shorter inter-charge distances. Indeed, the longer molecular axis of the F_6TCNNQ^- anion compared to F_4TCNQ^- (1.47 nm versus 1.1 nm) may bring the negatively charged F_6TCNNQ^- anions in closer proximity to the polaron. This is true since the lattice expansion experienced for both F_4TCNQ and F_6TCNNQ are of comparable magnitude (see below). However, such an effect should result in a blue-shift of the polaronic bands in F_6TCNNQ-doped films and it may also result in a stronger localization of the polaronic charges, which could be detrimental for charge transport properties. A precise comprehension of this effect would require simulations of the position and orientation of F_6TCNNQ when intercalated into the side chain layers of C_{12}-PBTTT. In the following section, we will evaluate the impact of dopant geometry on the diffusion coefficient into the C_{12}-PBTTT layers.

2.4. Doping kinetics

As seen in chapter 2, the fact that the spectra for POL $\perp$ R are dominated by the absorption of the dopant anions helped determine the precise diffusion coefficients of F_4TCNQ^- and F_6TCNNQ^- anions into the layers of the alkyl side chains of the thin films. As shown in chapter 2[15,16], polarized UV- Vis-NIR spectroscopy can be used to follow the time dependence of the absorbance of both F_4TCNQ^- (875 nm) and F_6TCNNQ^- (1158 nm) anions (see figure 4.7) versus doping time. To measure the kinetics of dopant diffusion into the C_{12}-PBTTT thin films, the oriented films were dipped in 1 mg/ml solution of dopant in acetonitrile for various time intervals.

The contact time of the oriented polymer with the dopant solution is increased and the corresponding UV-Vis-NIR spectra along both perpendicular and parallel directions are

recorded (see figure 4.7A-D). The signals of the dopant anions are visible even for short contact time of 5s and their intensity increases and saturate with doping time.

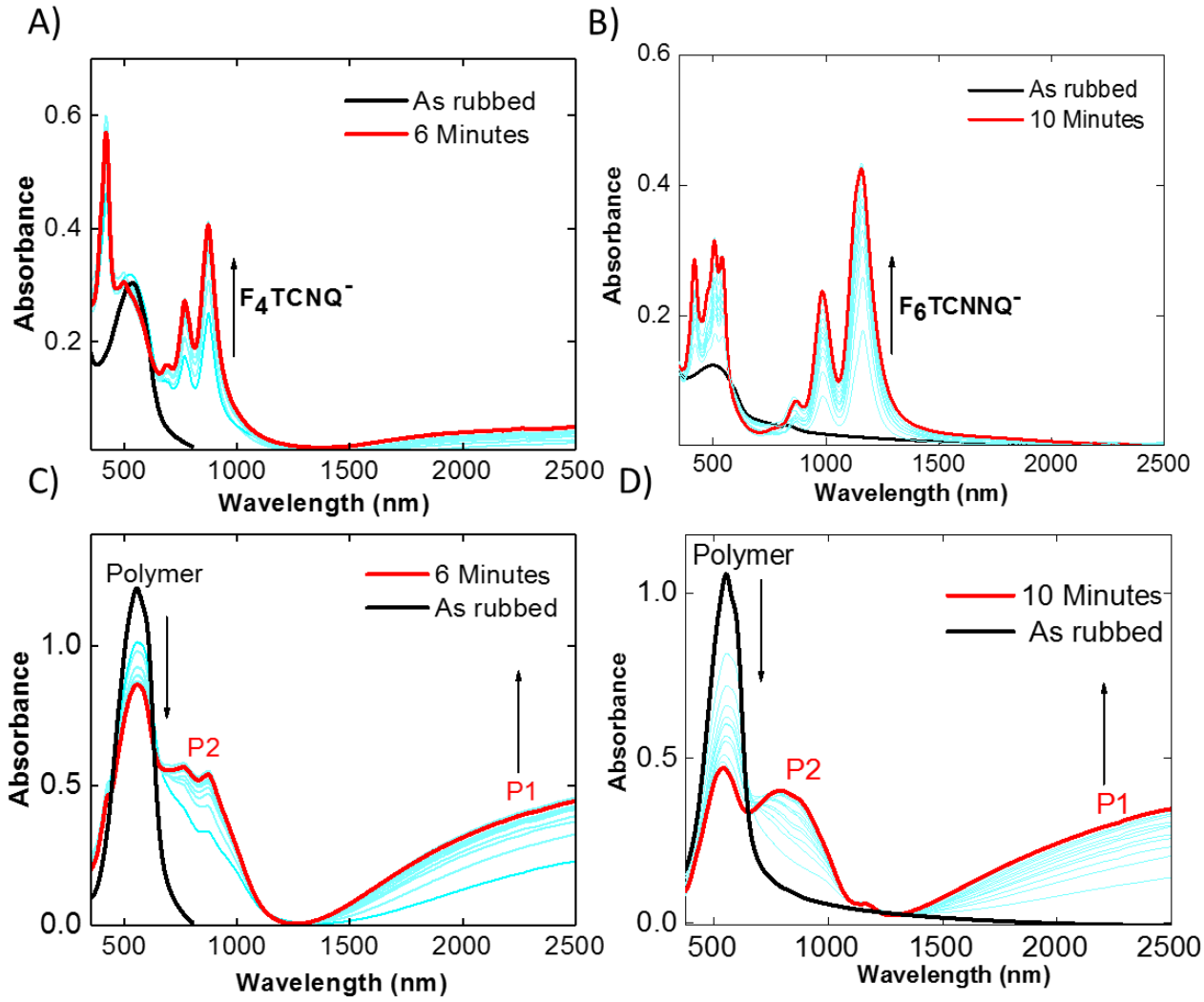

Figure 4.7. *Doping kinetics of C_{12}-PBTTT thin films doped with 1 mg/ml F_4TCNQ and F_6TCNNQ. A) and B) represent the time dependence of the absorption for both F_4TCNQ^- and F_6TCNNQ^- anions along the perpendicular directions. C) and D) Evolution of the polaronic bands P1 and P2 in F_4TCNQ and F_6TCNNQ doped PBTTT C_{12}, respectively.*

For short doping times, the absorption of both dopant anions scales like $\sqrt{t}$. This is an indication for a diffusion-limited doping mechanism. The saturation observed for longer doping times is due to the finite film thickness: the whole film is doped after 6-10 min (see Figure 4.7.A). Each polymer/dopant system is characterized by a typical doping time

τ. However, this time constant increases with film thickness as previously observed in PBTTT polymers doped with F_4TCNQ (see chapter 2).[16] The plot of normalized intensity of anions vs $t^{1/2}/l$ helped determine the diffusion coefficients of F_4TCNQ^- and F_6TCNNQ^- and this representation is independent of the polymer film thickness. The following phenomenological equation was used to fit the absorbance of the anion as a function of the doping time:

$$A_x(t) = A_0\left(1 - \exp\left(-\frac{\sqrt{D}}{l}(t)^{\frac{1}{2}}\right)\right) \qquad (5)$$

Where A is the absorption at wavelength λ of the anion (λ = 873 nm for F_4TCNQ^- and 1158 for F_6TCNNQ^-). A_0 is the absorbance of the anion at saturation, l is the film thickness and D is the diffusion coefficient of F_4TCNQ^- or F_6TCNNQ^- in the matrix of C_{12}-PBTTT.

The larger F_6TCNNQ^- anion shows a lower 2×10^{-12} cm^2/s diffusion coefficient with respect to 9×10^{-12} cm^2/s for F_4TCNQ^- (see figure 4.8A). Both diffusion coefficients were close to the diffusion coefficients of iodine into the P3HT films reported by Maliakal (2.5×10^{-11} cm^2/s) [25]. This result points at the impact of the size of the dopant anions on the diffusion into the highly interdigitated side chain layers.[26] It suggests that the smaller anions such as F_4TCNQ^- can diffuse and intercalate into the alkyl side chains faster than the longer and bulkier anions of F_6TCNNQ^-. However, as seen hereafter, the amount of dopants at saturation in the layers of C_{12}-PBTTT is not related to their diffusion kinetics.

The spectra measured along the parallel direction are also really instructive. The polaronic absorption bands in the doped PBTTT namely P1 and P2 are polarized along the // direction for both F_4TCNQ and F_6TCNNQ doped films as observed previously by Hamid-Sakr et.al[15]. Similar to the anion spectra along the perpendicular direction, the absorption of the polarons can be seen already after 5s and continues to increase and

to saturate with doping time. The spectra along the parallel direction are similar for both dopants.

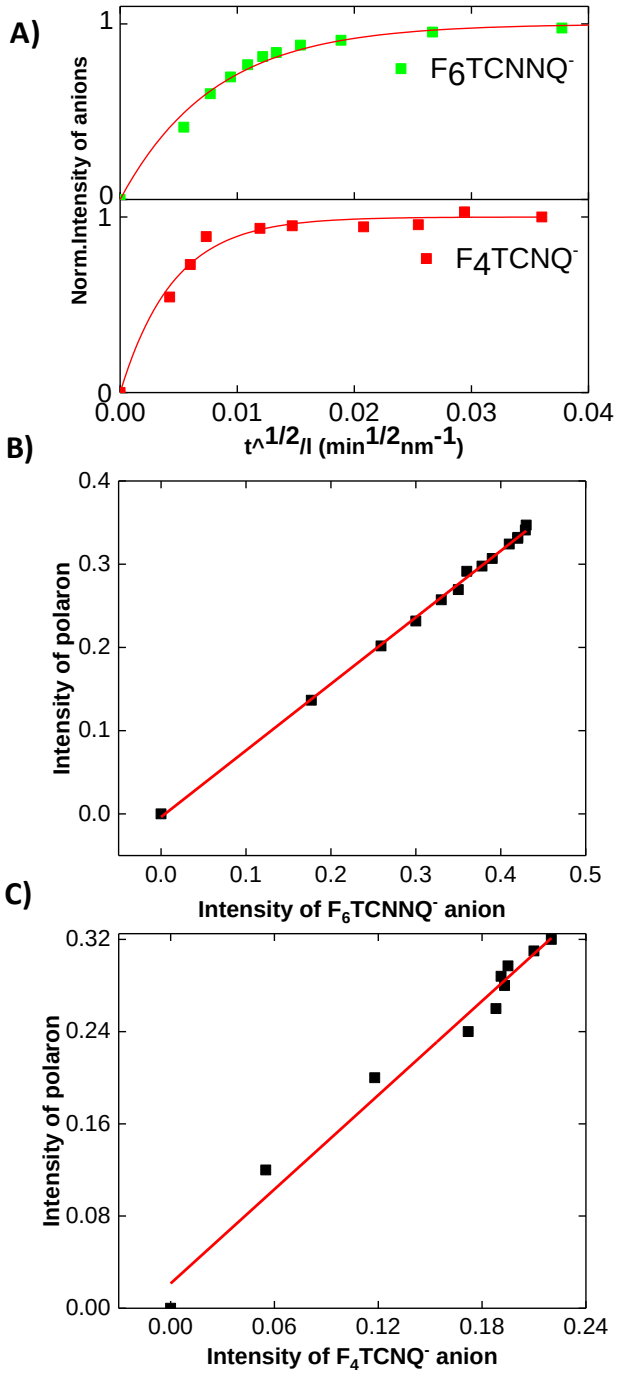

Figure 4.8. *A) Plot of normalized absorptions of both F_6TCNNQ (λ=1158 nm) and F_4TCNQ (λ=1158 nm) vs $t^{1/2}/l$ to determine the diffusion coefficients. B)-C) Plot of absorbance of the dopant anions vs that of the polarons (2500 nm). The linear fit supports integer charge transfer between C_{12}-PBTTT and both F_4TCNQ and F_6TCNNQ.*

As expected, the F_6TCNNQ doped C_{12}-PBTTT showed a higher degree of polymer chain oxidation than F_4TCNQ doped PBTTT since the remaining contribution of neutral polymer N is lower for this dopant (see figure 4.4.A&B). The higher degree of chain oxidation in F_6TCNNQ doped C_{12}-PBTTT indicates a higher degree of charge transfer between the polymer and dopant anion.

Moreover, the integer charge transfer between polymer and dopant is verified from the linear dependence between the absorbance of the polarons and the anions of F_4TCNQ^- and F_6TCNNQ^- (see figure 4.8B&C). A perfectly linear relationship between the intensity of absorbance of the anions and polarons observed for both dopants supports the integer charge transfer in oriented PBTTT for both F_4TCNQ^- and F_6TCNNQ^-. The relation between F_6TCNNQ^- and polaron absorbance is remarkably linear due to the reduced error in absorbance measurement for the 1158 nm band that does not overlap with the PBTTT polaron bands.

3. Influence of the method of sequential doping on the charge conductivity.

The electrical conductivity of the oriented C_{12}-PBTTT film has been measured as a function of dopant concentration. Two different procedures were used to dope the oriented films i.e. incremental concentration doping (ICD) and direct doping. In ICD, each sample is doped by dipping it successively in the solutions of dopants of increasing concentration up to a given concentration while in the direct doping procedure, each sample is dipped a single time in a solution of a given concentration. Typically for ICD, we consider the doping in successive solutions of 0.01, 0.1, 0.5, 1, 2 and 5 mg/ml.

As observed previously [14–16,27], the doping of all oriented thin films produced higher electrical conductivity along the rubbing direction than perpendicular to it. The conductivity in the direction perpendicular to the rubbing at saturation is close to that

of non-oriented thin films (for F_6TCNNQ and F_4TCNQ doped C_{12}-PBTTT we measure 65±4 S/cm and 120±94 S/cm, respectively). More interestingly, the incremental doping on the same device results in higher electrical conductivities as compared to single doping. Incremental addition of F_4TCNQ to PBTTT (5 mg/ml) produces a remarkably high electrical conductivity of ≈ 1380±700 along the rubbing direction. Surprisingly, the directly doped sample at the same concentration showed a conductivity of ≈ 920±60 S/cm on average. ICD produced 1.5 times higher electrical conductivity than direct doping in the case of F_4TCNQ doping.

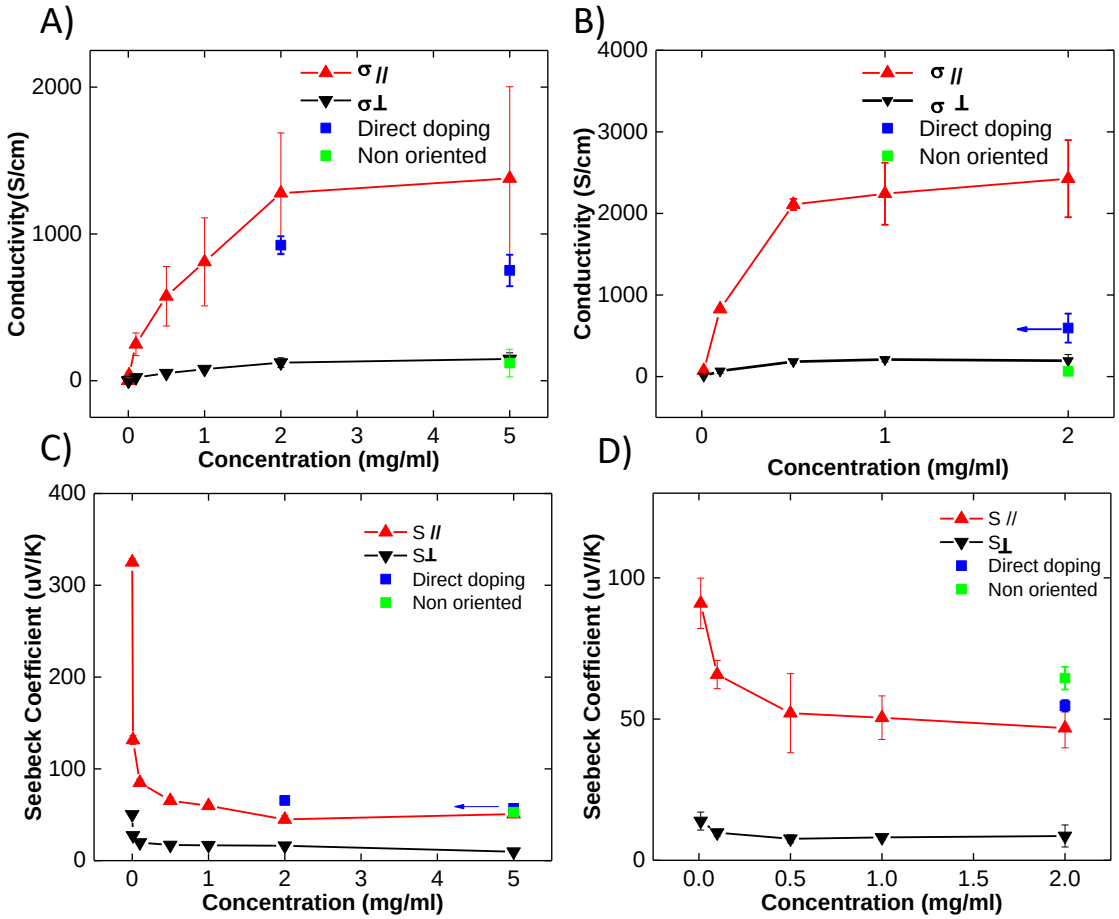

Figure 4.8. *Evolution of the charge conductivity (A and B) and of the Seebeck coefficient (C and D) as a function of increasing doping concentration of F_4TCNQ and F_6TCNNQ in oriented films of C_{12} -PBTTT, respectively. The curves correspond to the sample doped by incremental increase of doping concentration (ICD). Both S and σ are measured parallel (red) and perpendicular (black) to the rubbing directions. For comparison, we also show the*

values of samples obtained for direct doping at high doping concentration (2 and 5 mg/ml for F_4TCNQ and 5 mg/ml for F_6TCNNQ). The conductivity of non-oriented samples were also measured at maximum doping concentration.

The same trend is observed for F_6TCNNQ. ICD of oriented C_{12}-PBTTT (2 mg/ml) results in record values of electrical conductivities of ≈ 2430±500 S/cm *versus* 600±200 S/cm for direct doping. The electrical conductivities measured perpendicular to the rubbing direction are similar to those observed for the non-oriented films of C_{12}-PBTTT (65±4 S/cm and 120±94 S/cm for F_6TCNNQ and F_4TCNQ, respectively). This further confirms that the poor electrical conductivity in non-oriented samples is limited by the poor transport perpendicular to the polymer chains.

To better understand the reason for such an effect, we performed a test experiment that rules out the possible role of the solvent (ACN) on the film structure in the case of ICD. Indeed, it might be that the improved conductivity observed in ICD samples is related to some structural reorganization in the films upon multiple dips in ACN that could be beneficial for the charge transport properties. Therefore, an oriented C_{12}-PBTTT thin film was dipped 4 times in pure ACN before single doping (2 mg/ml of F_6TCNNQ in acetonitrile) (4ACN+DD). The two samples were compared using UV-Vis NIR spectra and electrical conductivity measurements.

As seen in figure 4.9, the polarized UV-Vis-NIR of both ICD and 4ACN+DD films show the same intensities of polaronic bands P1 and P2 and almost similar contribution from the neutral polymer. This implies that there is no clear difference in the doping level between a sample experiencing ICD or 4ACN+DD. The observed electrical conductivities of 4ACN+DD and DD films were ≈ 970+200 S/cm, and 600±200 S/cm, respectively. On the other hand, ICD produced samples with a conductivity of 2430 S/cm, which is 3-4 times higher than for the DD method. Since polarized UV-Vis-NIR spectroscopy shows

that both ICD and single doping (ICD and 4ACN+DD) lead to similar charge polaron concentrations, then the observed higher electrical conductivities for ICD films must be more related to a difference in the charge carrier mobility.

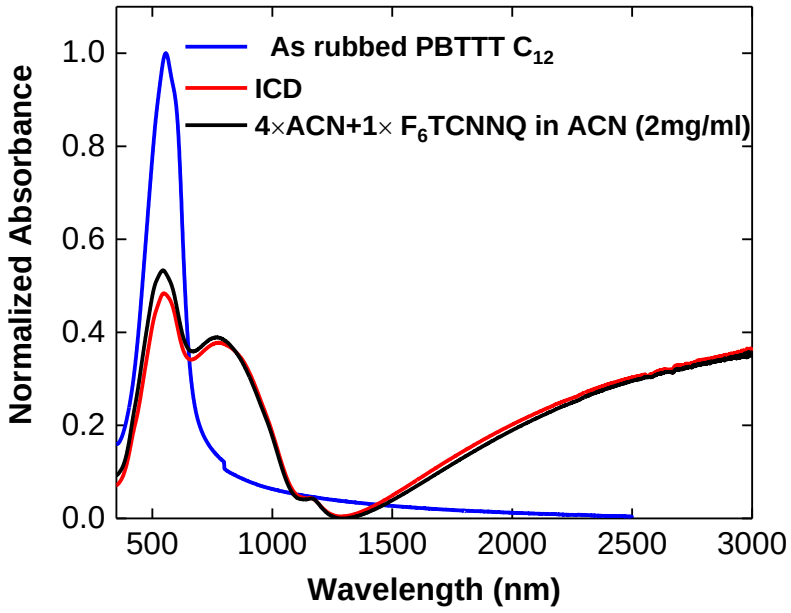

Figure 4.9. *Polarized UV-Vis-NIR spectra of doped PBTTT thin films doped by ICD and dipping in acetonitrile. In the ICD, the thin film is dipped in increasing doping concentration of 0.01, 0.1, 0.5, 1 and 2 mg/ml F_6TCNNQ in ACN. To exclude the effect of solvent, another thin film dipped 4 times in ACN and then directly doped by dipping in 2mg/ml F_6TCNNQ in ACN*

For both dopants, slow and progressive intercalation of dopants leads to a higher electrical conductivity in oriented C_{12}-PBTTT. This underlines the importance to preserve the crystallinity and initial orientation of the original semiconducting polymer films. Clearly, the way the molecular dopants are introduced into the polymer matrix is also an important parameter that influences the TE performances. As observed in previous investigations, the maximum electrical conductivity from a conducting polymer can be reached only if the molecular dopant is introduced without affecting the initial structure of the thin film. Incremental solution doping bears some similarity with vapour phase doping in the sense that the dopants can be incorporated in the polymer matrix in a

progressive and non-destructive manner[28]. Interestingly, the oriented C_{12}-PBTTT films doped by ICD show a much higher electrical conductivity than non-oriented vapour-doped films of PBTTT (670 S/cm) and P3HT (12.7 S/cm) as observed by Patel and Hynynen respectively. [28,29]

The observed high electrical conductivity in the F_4TCNQ and F_6TCNQ doped PBTTT thin film can be attributed to various reasons. First of all, high degree of in-plane chain alignment in the oriented PBTTT must be one important factor that can contribute to the observed high electrical conductivity in incrementally doped C_{12} PBTTT thin films. For instance, Chabinyc and coworkers proposed that the electrical conductivity in conjugated polymers such as PBTTT and P3HT mainly depends on the processing methods and the conductivity scales with the length scale of oriented backbones.[28] This was evidenced by soft –X-ray scattering measurements on vapor doped thin films of PBTTT. They showed that, higher orientation along the polymer backbone followed by doping from the vapor phase without affecting the initial thin film microstructure can produce high electrical conductivity of 670 S/cm and a PF of 120 $\mu Wm^{-1}K^{-2}$ in PBTTT thin films doped with F_4TCNQ. In our case, rubbed C_{12} PBTTT shows a high degree of chain orientation along the direction of rubbing. The electron diffraction measurements on oriented PBTTT show strong reflections (see figure 4.12 and 4.13) along the direction of the rubbing (mainly 003 and 004 represents the chain direction) and confirms the high degree of chain orientation in our samples. This high degree of chain alignment followed by incremental doping can lead to an apparent higher electrical conductivities and charge carrier mobilities (see table 4.2 for the calculated mobilities) similar to vapor doped PBTTT thin films.

The higher electrical conductivity observed in F_6TCNNQ doped C_{12} PBTTT can have different origins. The angular distribution measurements on the doped thin films

indicate that F_6TCNNQ^- anions are better oriented in the layers of the alkyl side-chains of PBTTT with an order parameter of 0.7. In strong contrast, the dopant F_4TCNQ^- anions are less ordered in the layers of the side chains. Hence a high degree of chain alignment and better ordering of the dopant F_6TCNNQ can produce higher charge carrier mobilities using ICD. This high mobility could be the reason for higher electrical conductivity incrementally doped F_6TCNNQ/ C_{12}-PBTTT (see table 4.2 for the calculated mobilities).

4. Influence of doping method on Seebeck coefficients and correlations with charge conductivity.

Seebeck coefficients were also anisotropic and higher Seebeck coefficients were measured along the rubbing direction for both F_4TCNQ and F_6TCNNQ doped C_{12}-PBTTT. The values of the Seebeck coefficients were little affected by the doping method. For instance, ICD with F_4TCNQ (5 mg/ml) leads to $S_{//}$= 50.7±4 µV/K while for DD $S_{//}$= 57±3 µV/K (see figure 4.8 C and D). This difference is consistent with the higher conductivity seen for ICD *versus* DD. Similarly, ICD with F_6TCNNQ (2 mg/ml) leads to $S_{//}$=47±7 µV/K versus 64.5±3 µV/K for DD at the same concentration. It is worth to mention that the Seebeck coefficients of non-oriented samples were similar to the values measured along the chain direction (52.6±3 µV/K for F_4TCNQ and 64.5±4 µV/K F_6TCNNQ), indicating that alignment is not detrimental for the Seebeck coefficient while it is highly beneficial to enhance charge conductivity.

As expected, the increase of electrical conductivity in oriented C_{12}-PBTTT thin films enhances the power factors along the chain direction. Incremental concentration doping (ICD) of C_{12}-PBTTT films with F_4TCNQ and F_6TCNNQ produced very high-power factors of 355±200 $\mu Wm^{-1}K^{-2}$ and 530±200 $\mu Wm^{-1}K^{-2}$, respectively. The PF obtained for $FeCl_3$ doped C_{12}-PBTTT is 1.9 $\mu W \cdot m^{-1} \cdot K^{-2}$ (see chapter 3) 3 times higher than F_6TCNNQ doped PBTTTT. As expected, ICD provided higher power factors than DD for both F_4TCNQ and F_6TCNNQ.

The poor electrical conductivities of the non-oriented C_{12}-PBTTT thin film lead to a PF that is lower by more than one order of magnitude compared to the aligned films: only 33 $\mu W \cdot m^{-1} \cdot K^{-2}$ for F_4TCNQ and 27±3 $\mu W \cdot m^{-1} \cdot K^{-2}$ for F_6TCNNQ. The dependence of PF with doping concentration (figure 4.10) shows the same characteristic increase and saturation for concentrations in the range 2-5 mg/ml for both dopants.

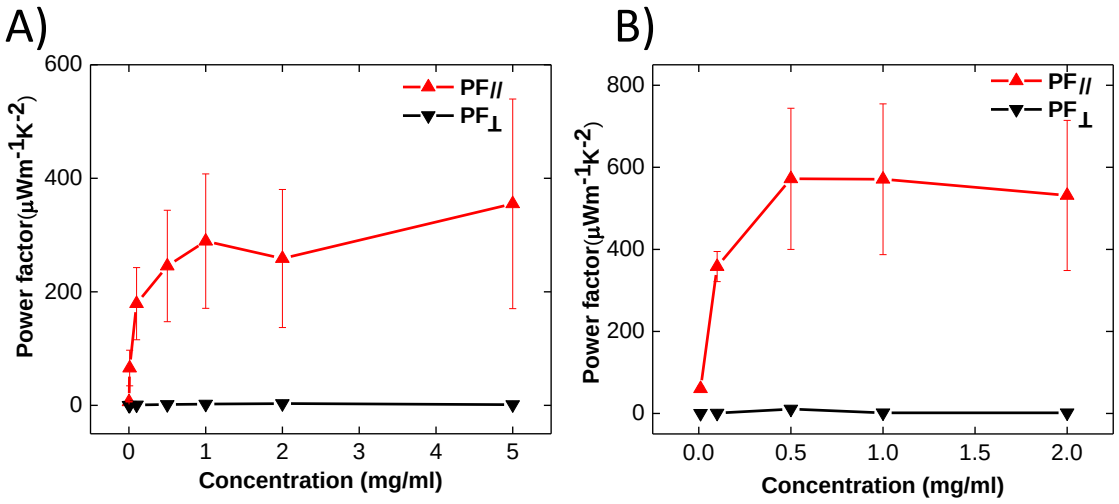

Figure 4.10. *Evolution of the power factor as a function of increasing doping concentration of A) F_4TCNQ and B) F_6TCNNQ doped films of C_{12}-PBTTT. Films were oriented by high temperature rubbing at 125°C and doped by incremental increase of doping concentration.*

The ICD method is particularly useful to probe S-σ correlations because a single sample of well-defined initial structure and orientation is progressively doped at higher dopant concentration, which alleviates all issues related to sample-to-sample statistics due to structural variations. In the previous chapter 3, we have demonstrated that the S-σ correlation is well described as proposed by Chabinyc[4] and coworkers by the relation $S_{//} \propto \sigma_{//}^{-1/4}$ for F_4TCNQ and $FeCl_3$ dopants in the direction parallel to the polymer chains. In oriented samples, we have observed a different correlation in the direction perpendicular to the backbone, namely $S_{\perp} \propto -\ln(\sigma_{\perp})$. The open question relative to these correlations is whether or not they depend on the chemical nature of the dopant. This

is why we collected all S,σ data for films doped by ICD with the dopants F_4TCNQ, F_6TCNNQ and $FeCl_3$ on the same plot (see figure 4.11). The correlations were plotted for both parallel and perpendicular orientations with respect to the chain direction.

Table 4.2. *Summary of maximum electrical conductivities, Seebeck coefficient and power factors observed upon incremental and single doping methods.DD: direct doping. ICD: Incremental Concentration Doping. TE properties obtained for vapor doped F_4TCNQ/ PBTTT thin film are also included from reference 8.*

Dopant	Doping method	σ (S/cm)	S (μV/K)	PF $\mu Wm^{-1}K^{-2}$
F_6TCNNQ	ICD	2430±500	47±7	530±200
	DD	600±200	64.5±3	247±74
	4ACN+DD	970±200	55±1	293±63
F_4TCNQ	ICD	1380±700	50.7±4	355±200
	DD	920±60	57±3	300±20
F_4TCNQ	Vapor Phase[8]	670	42	120

It is remarkable to see that all the data points align on the same master curves over 5 decades of charge conductivity, regardless of the dopant and for both directions parallel and perpendicular to the C_{12}-PBTTT chains. ***This demonstrates that the S-σ correlation in C_{12}-PBTTT is not dependent on the chemical nature of the dopant but mainly on the structure, packing and electronic structure of the oxidized polymer.*** Accordingly, this correlation is characteristic of the charge transport mechanism of the polymer C_{12}-PBTTT that is only marginally affected by the type of dopant. The only notable difference related to the dopants is the limit in conductivity that is reached for each dopant. This

limit correlates with the maximum doping/oxidation levels reached for each dopant that follows the sequence $F_4TCNQ<F_6TCNNQ<FeCl_3$.

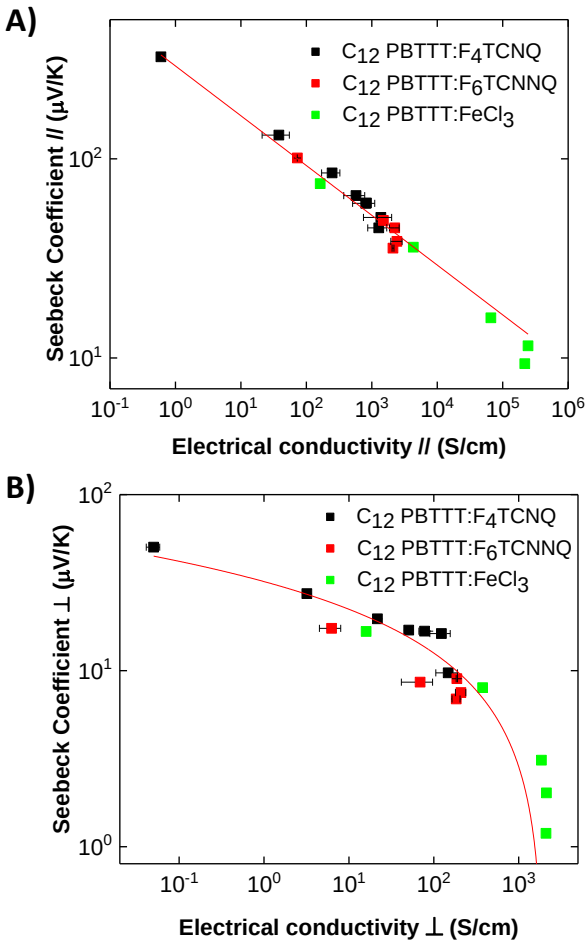

Figure 4.11. *Correlation between Seebeck coefficient S and electrical conductivity σ in highly oriented thin films of C_{12}-PBTTT (T_R=125°C) doped with F_4TCNQ (black squares), F_6TCNNQ (red squares) and $FeCl_3$ (green squares). The full lines correspond to the results of the fit using the scaling laws $S_{//} \propto \sigma_{//}^{-1/4}$ and $S_{\perp} \propto -\ln(\sigma_{\perp})$.*

5. Impact of doping methods on the crystal structure

As seen in the previous chapters, doping results in the intercalation of dopant molecules in the layers of alkyl side chains. The extension of lattice expansion is correlated with the initial length of side chains: the shorter the side chains, the larger the lattice expansion

along the alkyl side chains. Hereafter, we want to investigate the impact of dopant size on the lattice of C_{12}-PBTTT upon doping.[8,10,15,30]

Similarly, to the previous chapter, we followed the structural changes in both F_4TCNQ and F_6TCNNQ doped C_{12}-PBTTT thin films by low dose electron diffraction. Given the different TE properties evidenced for samples doped using the ICD or DD method, we also investigate to what extent the two doping methods affect the structure of the C_{12}-PBTTT films.

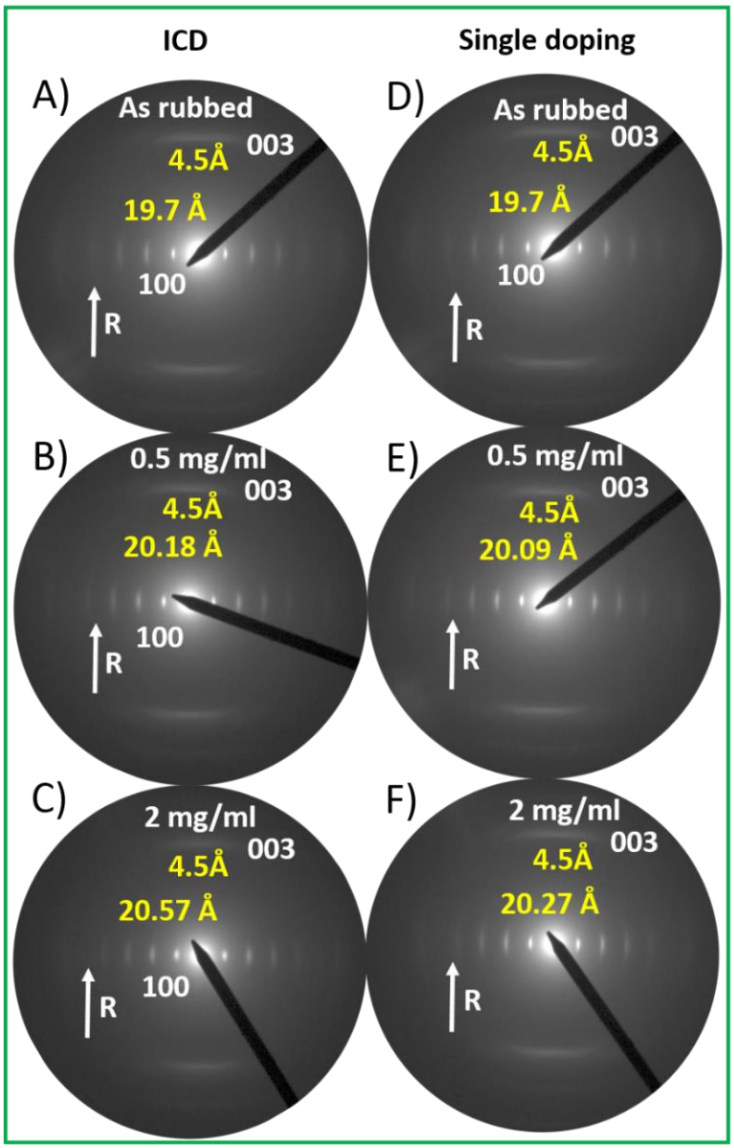

Figure 4.12. *Evolution of the electron diffraction patterns in doped C_{12}-PBTTT upon incremental concentration doping (A-C) and with single doping with F_4TCNQ (D-F). R represents the rubbing direction.*

For TEM investigations, the oriented C_{12}-PBTTT thin films prepared on NaPSS by high temperature rubbing were carbon-coated and the films were recovered on copper TEM grids by floating on water.

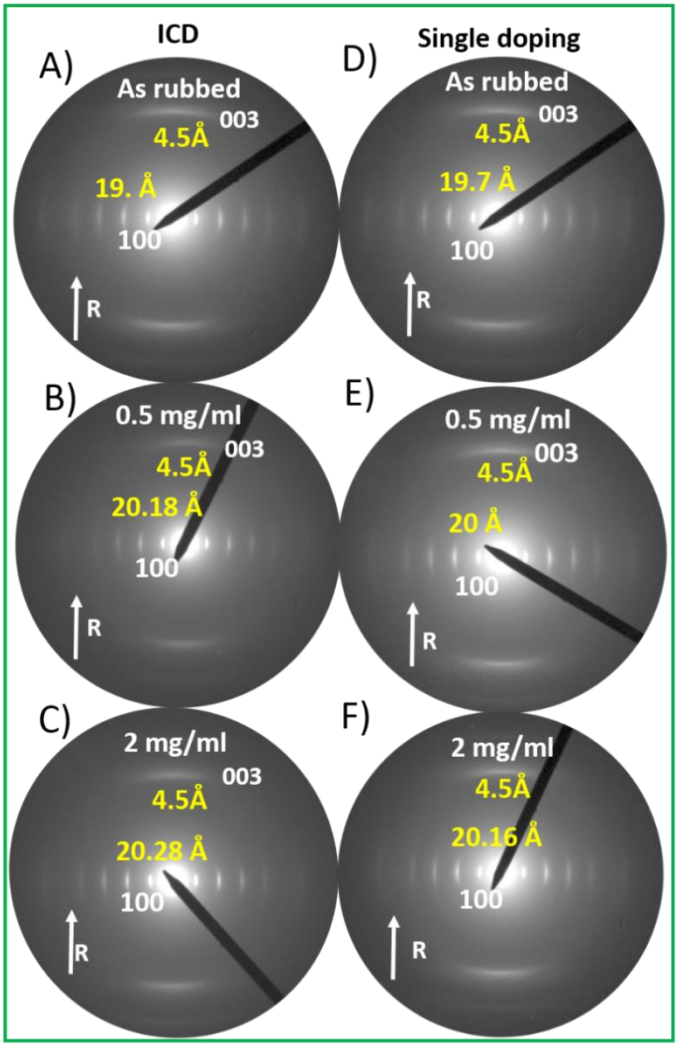

Figure 4.13. *Evolution of the electron diffraction patterns of F_6TCNNQ doped C_{12}-PBTTT (A-C) sequential addition (D-F) single doping as a function of dopant concentration represent the rubbing direction*

The TEM grids were doped by ICD using dopant solutions (F_4TCNQ or F_6TCNNQ) in acetonitrile in the glove box. The dopant solution was allowed to stay on the TEM grid for 20-30 s and the excess solution was removed by blotting. The structural variation in the doped thin films was followed by electron diffraction using a transmission electron microscope. In the direct doping method, carbon-coated TEM grids were doped directly

at a given concentration of dopants. In the case of ICD, the grids were doped by dipping in solutions of increasing concentration up to the desired concentration.

This study report one of the first investigations on how the crystal structure of C_{12}-PBTTT is affected by different doping procedures using the same dopant. As shown hereafter, interesting results are obtained by the two different doping procedures.

The thin films of C_{12}-PBTTT prepared by high temperature rubbing show a sequence of h00 (h=1,2,3,4) reflections along the equatorial direction. The 003 reflection along the rubbing direction represents the periodicity along the backbone direction. The thin films were mainly in face-on orientation as indicated by the absence of the equatorial diffraction peak corresponding to the π- stacking (d_{020}) (see figure 4.12 and 4.13).

Figure 4.14 depicts the unit cell parameter variation as a function of dopant concentration for both ICD and DD methods. In both cases, doping induces an expansion along the side chain direction of the C_{12}-PBTTT unit cell. The ICD thin films show a larger interlayer spacing variation up to 20.57 Å *versus* 20.27 Å for DD films. Also, a slight broadening of the diffraction peaks along the equatorial direction is observed for ICD samples (see figure 4.13C) suggesting some disordering in the lamellar packing upon doping. For F_6TCNNQ, the same trends are observed as for F_4TCNQ: the final lattice expansion at saturation is larger for ICD than for DD (d_{100} spacing of 20.28 Å vs 20.16 Å for ICD and DD, respectively). Surprisingly, ICD with the longer and bulkier F_6TCNNQ produced a lower d_{100} spacing of 20.28Å than for F_4TCNQ-doped films. Incidentally, the lattice expansion for both F_4TCNQ and F_6TCNNQ is significantly reduced with respect to $FeCl_3$ (d_{100} =23.7 Å). Accordingly, the lattice expansion in C_{12}-PBTTT is not correlated to the dimensions of the dopants: F_4TCNQ has a long axis of 12 Å versus 14.4 Å for F_6TCNNQ. UV-Vis-NIR spectroscopy has shown that the doping level for ICD at saturation are 14% and 20% (dopant per thiophene cycle), respectively. Hence, the lower lattice

expansion for F_6TCNNQ is not associated with a lower doping level. The study of the doping kinetics indicates solely that the diffusion coefficient of F_6TCNNQ into the structure of C_{12}-PBTTT is slightly lower as compared to F_4TCNQ. Accordingly, it seems that steric hindrance cannot be considered as the reason for a lower lattice expansion with F_6TCNNQ.

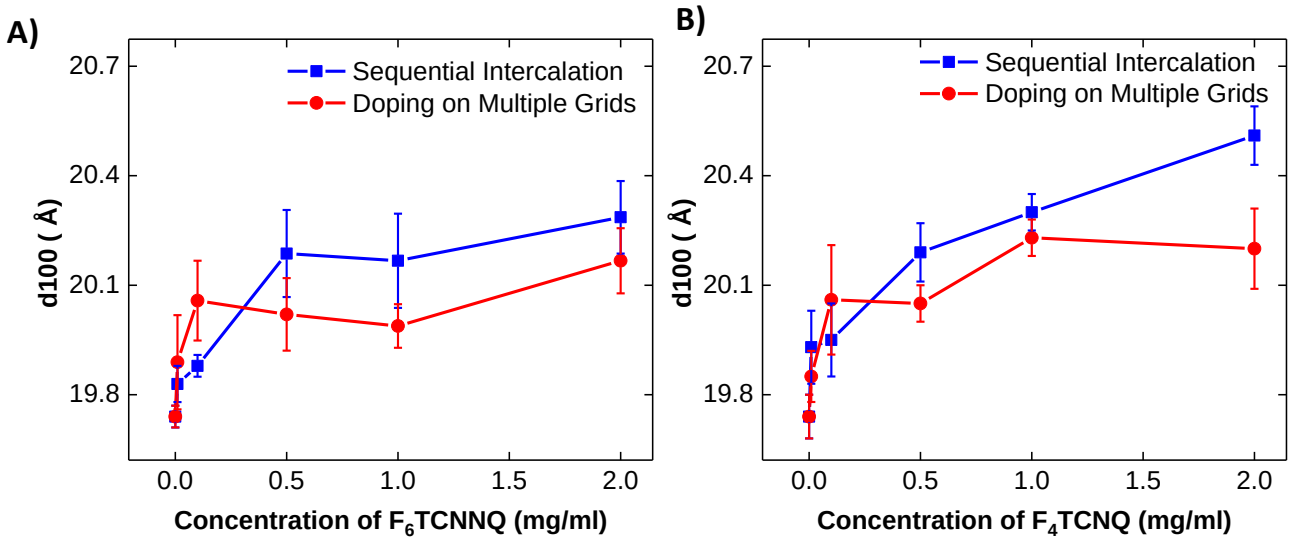

Figure 4.14. *Evolution of d_{100} spacing of the sequentially and directly doped C_{12}-PBTTT. A) Variation of d_{100} spacing of sequentially and singly doped F_6TCNNQ/C_{12}-PBTTT. A) Variation of d_{100} spacing of sequentially and singly doped F_4TCNQ/C_{12}-PBTTT*

A careful analysis of the lattice expansion for ICD and DD from figure 4.14 indicates that the doping method influences the intercalation of the dopants as a function of doping concentration. For both dopants, the lattice expansion is faster at low concentrations for DD as compared to ICD. The situation changes beyond 0.5 mg/ml. The lattice expansion becomes larger for ICD than DD. As a consequence, DD leads to a rather fast saturation in lattice expansion contrary to ICD for which saturation is not even observed at 2 mg/ml for F_6TCNNQ. These observations demonstrate that ICD seems to allow for a more progressive and efficient dopant intercalation as compared to DD.

6. Estimation of doping level and mobilities

Of importance for charge transport properties are the charge carrier density and the charge mobility that determine the resulting charge conductivity. The exact determination of charge carrier density is difficult and would require to use specific tools such as the Hall effect.[31] A rough estimation of the carrier density can be obtained from the measurement of absorbance of the polaron or of the anion since we have shown that integer charge transfer is involved in the doping process of C_{12}-PBTTT with F_4TCNQ and F_6TCNNQ. However, doing so, one assumes that each anion generates one polaronic charge that can contribute to charge transport. To extract charge mobilities, the major assumption is that all polaronic charges seen by UV-Vis-NIR spectroscopy contribute to the charge transport process. This may not be true in absolute value as demonstrated by Pingel and Neher who showed that only 5% of charges generated by doping correspond to free charge carriers by doping P3HT with F_4TCNQ.[22]

To determine the anion concentration in the films, we determined the molar extinction coefficient of F_6TCNNQ^- anion in solution (in DCM). We find $\varepsilon_{F6TCNNQ}$-= 53300 $L{\cdot}Mol^{-1}{\cdot}cm^{-1}$ at 1153 nm. From the absorbance and the film thickness, one can extract a density of anions, hence of polarons, of 8.1×10^{20} cm^{-3}. The polaron density calculated for the F_4TCNQ doped C_{12} PBTTT is $\approx 5.7\times10^{20}$ cm^{-3}. Based on AC Hall effect measurements, Scholes and coworkers also reported similar charge carrier densities in non-oriented P3HT films doped from F_4TCNQ[31]. This implies that the determined polaron densities using the extinction coefficients of the anions are reasonable.

A second approach implies to know the extinction coefficient of the polarons (ε_{P2}). Here, we propose two approaches. First, we make use of the extinction coefficient determined by Charge Modulated Spectroscopy (CMS). We use the Beer-Lambert law as proposed

by Tanaka[32] and coworkers for FTS-doped PBTTT thin films. According to Beer- Lambert law,

$$A_{Pol} = \varepsilon_{P2} n t \qquad (5)$$

Where A_{POL} is the absorbance of the PBTTT polarons at 1.67 eV, ε_{P2} is the effective absorption cross-section of the polaron, t is the film thickness and n is the polaron density. CMS yields the absorption coefficients of C_{12}-PBTTT polarons $\sigma_{pol} = 6\times10^{-16}$ cm^2 [33,34]. Only the contribution to the absorption of the free charge carriers involved in charge transport is determined using CMS whereas in conventional UV-Vis-NIR spectroscopy the absorption stems from both trapped and mobile polarons. By considering a film thickness of (40 nm F_6TCNNQ doped (ICD) C_{12}-PBTTT and 80 nm for F_4TCNNQ doped (ICD) C_{12}-PBTTT) and the relation $\varepsilon_{P2}=(\log e)\,\sigma_{pol,}$ the polaron density is in the range 2.83 - 3×10^{20} cm^{-3} for F_6TCNNQ doped C_{12} PBTTT (2mg/ml) and 3.2×10^{20} cm^{-3} . Since the DD film shows the same polaronic absorption as the ICD film (see figure 4.9), a similar polaron density of 3.3×10^{20} cm^{-3} is obtained.

Finally, we can also use a different value for ε_{P1} using the results obtained by polarized UV-Vis-NIR for the $FeCl_3$-doped C_{12}-PBTTT. In chapter 3, we have observed that C_{12}-PBTTT is fully oxidized after doping with 10 mM $FeCl_3$. The corresponding spectrum (see Figure 3.6 in chapter 3) shows no neutral form of the neutral polymer and only P1 and P2 absorption bands. Therefore, knowing the stoichiometry of the doped films (from EDX), we can show that a unit cell contains two $FeCl_4^-$ charges i.e. 2 polarons for 8 thiophene cycles. Knowing the absorption at 2500 nm and the film thickness, we extract $\varepsilon_{P2}=9.6\times10^{-17}$ cm^2. This value is significantly different from the previous one obtained by CMS. The difference is related to the fact that our calibration with the $FeCl_3$-doped films takes into account the UV-Vis-NIR absorption that stems from both mobile and trapped polarons. Using this value of ε_{P1}, we extract a charge carrier density of $6.2\cdot10^{20}$ cm^{-3} for

F_6TCNNQ doped C_{12}-PBTTT (ICD) thin films and ≈ $6.7 \cdot 10^{20}$ cm^{-3} for F_4TCNQ (ICD) doped C_{12}-PBTTT. As expected, the carrier density extracted from the polaron absorption using ε_{P2} is lower than the value obtained using ε_{P1}, since ε_{P1} corresponds to free and trapped charge carriers.

Table 4.3. *Calculated charge carrier densities as obtained from the UV-Vis-NIR absorption signal of the polaron and dopant anion.*

	Density of charge carriers (cm^{-3})		Mobility (cm^2/V. s)			
	F_6TCNNQ/C_{12} PBTTT	F_4TCNQ/C_{12} PBTTT	F_6TCNNQ/C_{12} PBTTT		F_4TCNQ/C_{12} PBTTT	
			ICD	single	ICD	single
Polaron density based on ε_{P1} (our calibration with $FeCl_3$)	6.2×10^{20}	6.7×10^{20}	24	6	13	8.5
Polaron density based on $\varepsilon_{F6TCNNQ}$	8.1×10^{20}	5.7×10^{20}	18.8	4.6	15.3	10
Polaron density based on ε_{P2} (Tanaka et.al)	2.8 to 3×10^{20}	3.2×10^{20}	53.6	13.25	26	17.4

As a matter of facts, the polaron densities extracted from ε_{P1} and $\varepsilon_{F6TCNNQ}$ are fairly similar, which is consistent with integer charge transfer and suggests that the extinction coefficients determined in solution for F_6TCNNQ are consistent.

An estimate of the charge carrier mobility was calculated for both incremental and singly doped thin films using the charge carrier densities extracted based on the ε_{P1} and $\varepsilon_{F6TCNNQ}$ and charge modulated spectroscopy (based on reference 32). The values are summarized in table 4.3. The average mobilities calculated for ICD with F_6TCNNQ and

F_4TCNQ are higher than for DD films. i.e., $\mu_{ICD} > \mu_{DD}$. As an example, the average mobility calculated for ICD is ≈ 32 cm^2/V. s and ≈8 cm^2/V. s for DD with F_6TCNNQ. Average mobilities of 27 cm^2/V. s and 11.9 cm^2/V. s are obtained for F_4TCNQ with ICD and DD respectively. Since both ICD and single doped thin films gave the same intensities of the P1 band, it is assumed that both doping methods lead to same polaron density (see figure 4.9). It is worth to mention that a lower charge carrier density corresponding to a few percent of the density extracted from UV-Vis-NIR data, as suggested by Pingel and Neher for rr-P3HT, would result in even larger charge mobilities. [22]

Such values of charge mobilities are 1-2 orders of magnitude larger than those measured in OFETs of C_{14}-PBTTT with oriented chains. Lee et al. observed mobilities of up to 0.4 $cm^2/V\cdot s$ in oriented thin films. [35] Xue and coworkers also reported high mobilities of 1.67 $cm^2/V\cdot s$ in stretch aligned films of C_{14}-PBTTT.[36] More recently, Scholes and coworkers also reported similar mobilities of 0.12 cm^2/V.s in non-oriented thin films of P3HT, sequentially doped with F_4TCNQ from a charge carrier concentration of 4.9×10^{20} cm^{-3}. [31] The difference between charge mobilities extracted from OFET and from highly doped system has multiple origins. First, the carrier density is much smaller than in our doped films. Second, the transport of charges is 3D in doped films whereas it is more 2D in OFETS. The estimated mobilities in our films are >10 cm^2/V.s, which is assumed to be a limit to observe band-like transport.[37]

There are several reasons why mobilities can be so high in our doped films. First, doping induces a stiffening and planarization of the polymer backbone whose structure becomes more quinoidal. At low doping concentration, the counterions tend to trap and localize the polarons and bipolarons because the Coulomb potential of the counterions extends quite far in the polymer (due to a low dielectric constant). Because of this, counterions act as traps for polarons and charge mobility is reduced. When the doping

level increases, one observes a progressive overlap between the electric fields produced by the counterions, which results in a reduced hopping barrier and the charge carrier mobility tends to increase.[38][39] When the Coulomb traps fully overlap, then they form a band that tends to boost the charge carrier mobility. This is most likely why the charge mobilities can be so high in C_{12}-PBTTT doped with F_6TCNNQ or $FeCl_3$. Second, we may also consider that doping influences the polymer microstructure in thin films. As shown in a recent work by Untilova et al., doping can promote some ordering in the smectic-like phase of rr-P3HT (ref). Doping allows polythiophene backbones to reorganize towards a more ordered state upon intercalation of F_4TCNQ dopants in the layers of alkyl side chains. We may suggest a similar phenomenon to occur in the present case in the more disordered parts of the PBTTT films. This would be similar to the observation by Chabynic and coworkers of doping-induced order in the amorphous phase of ra-P3HT. To conclude, we propose that ICD can produce such high mobility samples because i) the progressive intercalation of dopants preserves the pristine orientation order of PBTTTT, ii) dopants are introduced in a regular manner in the lattice of C_{12}-PBTTT.

7.Conclusion

High temperature rubbing is a simple and versatile method, which can be applied to a wide variety of polymers. Similar to our previous works, we have applied high temperature rubbing to C_{12}-PBTTT films and doped them with F_6TCNNQ and F_4TCNQ to produce highly conducting thin films. A combination of Polarized UV-Vis-NIR spectroscopy and electron diffraction measurements demonstrates that, similar to F_4TCNQ^- anions, F_6TCNNQ^- anions are also oriented perpendicular to the polymer backbone and prefer to reside in the alkyl side chains of C_{12}-PBTTT crystals. [15,16] Moreover, we show that F_6TCNNQ^- anion are better oriented and lie in a plane strictly perpendicular to the C_{12}-PBTTT backbone whereas F_4TCNQ^- anions are more distributed

around this direction. Similarly, to rr-P3HT, doping C_{12}-PBTTT with F_6TCNNQ and F_4TCNQ produces an expansion of the unit cell along the d_{100} and a compression along the π stacking direction but the extent of lattice expansion along the alkyl side chain is not correlated to the long axis dimension of the dopant. The kinetics of doping was followed by UV-Vis-NIR spectroscopy and confirms that the longer and bulkier F_6TCNNQ^- anion has a lower diffusion coefficient (2×10^{-12} cm^2/s) than F_4TCNQ^- anions (9×10^{-12} cm^2/s).

In addition to this, we introduce a new doping method called incremental concentration doping (ICD). Incremental concentration doping leads to higher electrical conductivities and higher power factors in oriented C_{12}-PBTTT than direct doping. ICD produced 4 times higher electrical conductivities (2430±500 S/cm) than direct doping (600±500 S/cm) and produced a record power factor of 530±200 $\mu Wm^{-1}K^{-2}$. Also, similar to our previous results, non-oriented PBTTT sample limited electrical conductivities of 120±90 S/cm and 65±4 S/cm. A combination of alignment and incremental concentration doping produced 37 times higher electrical conductivities in F_4TCNQ doped C_{12}-PBTTT and 11 times higher electrical conductivities for F_4TCNQ-doped films. It is shown that ICD and DD result in similar doping levels using UV-Vis-NIR spectroscopy. Therefore, the observed difference in charge conductivity is ascribed to the preservation of pristine order and higher mobilities observed in ICD doped C_{12} PBTTT. The enhanced electrical conductivities observed in F_6TCNNQ doped C_{12}-PBTTT is further pointing that the degree of ordering of the dopant anion is an important factor that determines the electrical conductivity in semiconducting polymers. Higher electrical conductivities are always observed in the oriented C_{12}-PBTTT films when the dopants are introduced in a progressive manner in the films by ICD. This result demonstrates how important the doping process is in determining the resulting TE properties of the polymer thin films. From that perspective, ICD is more similar to vapor phase doping whereby the dopants enter the polymer films

progressively during evaporation. Our recent results on electrical conductivities on other semiconducting polymers further demonstrate that ICD is a versatile method that can be applied to different semi-crystalline polymers for better thermoelectric performance.

Bibliography

[1] O. Bubnova, Z. U. Khan, A. Malti, S. Braun, M. Fahlman, M. Berggren, X. Crispin, *Nat. Mater.* **2011**, *10*, 429.

[2] E. F. Aziz, A. Vollmer, S. Eisebitt, W. Eberhardt, P. Pingel, D. Neher, N. Koch, *Adv. Mater.* **2007**, *19*, 3257.

[3] K.-H. Yim, G. L. Whiting, C. E. Murphy, J. J. M. Halls, J. H. Burroughes, R. H. Friend, J.-S. Kim, *Adv. Mater.* **2008**, *20*, 3319.

[4] A. M. Glaudell, J. E. Cochran, S. N. Patel, M. L. Chabinyc, *Adv. Energy Mater.* **2015**, *5*, 1401072.

[5] D. Kiefer, L. Yu, E. Fransson, A. Gómez, D. Primetzhofer, A. Amassian, M. Campoy-Quiles, C. Müller, *Adv. Sci.* **2017**, *4*, 1600203.

[6] D. T. Duong, C. Wang, E. Antono, M. F. Toney, A. Salleo, *Org. Electron. physics, Mater. Appl.* **2013**, *14*, 1330.

[7] C. Y. Kao, B. Lee, L. S. Wielunski, M. Heeney, I. McCulloch, E. Garfunkel, L. C. Feldman, V. Podzorov, *Adv. Funct. Mater.* **2009**, *19*, 1906.

[8] S. N. Patel, A. M. Glaudell, K. A. Peterson, E. M. Thomas, K. A. O'Hara, E. E. Lim, M. L. Chabinyc, K. O'Hara, E. E. Lim, M. L. Chabinyc, B. Oschmann, J. Lawrence, M. W. Schulze, J. M. Ren, A. Anastasaki, Y. Luo, M. D. Nothling, C. W. Pester, K. T. Delaney, L. A. Connal, A. J. McGrath, P. G. Clark, C. M. Bates, C. J. Hawker, *Sci. Adv.* **2017**, *3*, e1700434.

[9] D. T. Scholes, S. A. Hawks, P. Y. Yee, H. Wu, J. R. Lindemuth, S. H. Tolbert, B. J. Schwartz, *J. Phys. Chem. Lett.* **2015**, *6*, 4786.

[10] D. T. Scholes, P. Y. Yee, J. R. Lindemuth, H. Kang, J. Onorato, R. Ghosh, C. K.

Luscombe, F. C. Spano, S. H. Tolbert, B. J. Schwartz, *Adv. Funct. Mater.* **2017**, *27*, 0.

[11] J. E. Cochran, M. J. N. Junk, A. M. Glaudell, P. L. Miller, J. S. Cowart, M. F. Toney, C. J. Hawker, B. F. Chmelka, M. L. Chabinyc, *Macromolecules* **2014**, *47*, 6836.

[12] J. Hynynen, D. Kiefer, C. Muller, *Rsc Adv.* **2018**, *8*, 1593.

[13] I. E. Jacobs, E. W. Aasen, J. L. Oliveira, T. N. Fonseca, J. D. Roehling, J. Li, G. Zhang, M. P. Augustine, M. Mascal, A. J. Moulé, *J. Mater. Chem. C* **2016**, *4*, 3454.

[14] V. Vijayakumar, Y. Zhong, V. Untilova, M. Bahri, L. Herrmann, L. Biniek, N. Leclerc, M. Brinkmann, *Adv. Energy Mater.* **2019**, *9*, 1900266.

[15] A. Hamidi-sakr, L. Biniek, J.-L. Bantignies, D. Maurin, L. Herrmann, N. Leclerc, P. Lévêque, V. Vijayakumar, N. Zimmermann, M. Brinkmann, *Adv. Funct. Mater.* **2017**, *27*, 1700173.

[16] V. Vijayakumar, E. Zaborova, L. Biniek, H. Zeng, L. Herrmann, A. Carvalho, O. Boyron, N. Leclerc, M. Brinkmann, *ACS Appl. Mater. Interfaces* **2019**, *11*, 4942.

[17] D. B. Romero, M. Schaer, L. Zuppiroli, B. Cesar, B. François, *Appl. Phys. Lett.* **1995**, *67*, 1659.

[18] F. Huang, A. G. MacDiarmid, B. R. Hsieh, *Appl. Phys. Lett.* **1997**, *71*, 2415.

[19] C. Weichsel, L. Burtone, S. Reineke, S. I. Hintschich, M. C. Gather, K. Leo, B. Lüssem, *Phys. Rev. B* **2012**, *86*, 75204.

[20] P. K. Koech, A. B. Padmaperuma, L. Wang, J. S. Swensen, E. Polikarpov, J. T. Darsell, J. E. Rainbolt, D. J. Gaspar, *Chem. Mater.* **2010**, *22*, 3926.

[21] Y. Karpov, T. Erdmann, M. Stamm, U. Lappan, O. Guskova, M. Malanin, I. Raguzin,

T. Beryozkina, V. Bakulev, F. Günther, S. Gemming, G. Seifert, M. Hambsch, S. Mannsfeld, B. Voit, A. Kiriy, *Macromolecules* **2017**, *50*, 914.

[22] P. Pingel, D. Neher, *Phys. Rev. B* **2013**, *87*, 115209.

[23] L. Biniek, N. Leclerc, T. Heiser, R. Bechara, M. Brinkmann, *Macromolecules* **2013**, *46*, 4014.

[24] R. Sata, H. Suzuki, N. Ueno, Y. Morisawa, M. Hatanaka, T. Wakabayashia, *Chinese J. Chem. Phys.* **2019**, *32*, 175.

[25] A. J. Maliakal, *ACS Appl. Mater. Interfaces* **2013**, *5*, 8300.

[26] E. Cho, C. Risko, D. Kim, R. Gysel, N. Cates Miller, D. W. Breiby, M. D. McGehee, M. F. Toney, R. J. Kline, J.-L. Bredas, *J. Am. Chem. Soc.* **2012**, *134*, 6177.

[27] Y. M. Gross, D. Trefz, C. Dingler, D. Bauer, V. Vijayakumar, V. Untilova, L. Biniek, M. Brinkmann, S. Ludwigs, *Chem. Mater.* **2019**, *31*, 3542.

[28] S. N. Patel, A. M. Glaudell, K. A. Peterson, E. M. Thomas, K. A. O'Hara, E. Lim, M. L. Chabinyc, *Sci. Adv.* **2017**, *3*, e1700434.

[29] J. Hynynen, D. Kiefer, L. Yu, R. Kroon, R. Munir, A. Amassian, M. Kemerink, C. Müller, *Macromolecules* **2017**, *50*, 8140.

[30] P. Y. Yee, D. T. Scholes, B. J. Schwartz, S. H. Tolbert, *J. Phys. Chem. Lett.* **2019**, acs. jpclett.9b02070.

[31] D. T. Scholes, P. Y. Yee, J. R. Lindemuth, H. Kang, J. Onorato, R. Ghosh, C. K. Luscombe, F. C. Spano, S. H. Tolbert, B. J. Schwartz, *Adv. Funct. Mater.* **2017**, *27*, 1702654.

[32] H. Tanaka, M. Hirate, S. Watanabe, S. I. Kuroda, *Adv. Mater.* **2014**, *26*, 2376.

[33] M. C. Gwinner, R. Di Pietro, Y. Vaynzof, K. J. Greenberg, P. K. H. Ho, R. H. Friend, H. Sirringhaus, *Adv. Funct. Mater.* **2011**, *21*, 1432.

[34] N. Zhao, Y.-Y. Noh, J.-F. Chang, M. Heeney, I. McCulloch, H. Sirringhaus, *Adv. Mater.* **2009**, *21*, 3759.

[35] M. J. Lee, D. Gupta, N. Zhao, M. Heeney, I. McCulloch, H. Sirringhaus, *Adv. Funct. Mater.* **2011**, *21*, 932.

[36] X. Xue, G. Chandler, X. Zhang, R. J. Kline, Z. Fei, M. Heeney, P. J. Diemer, O. D. Jurchescu, B. T. O'Connor, *ACS Appl. Mater. Interfaces* **2015**, *7*, 26726.

[37] H. Bässler, A. Köhler, in (Ed.: R.M. Metzger), Springer Berlin Heidelberg, Berlin, Heidelberg, **2011**, pp. 1–65.

[38] Y. Lu, J. Y. Wang, J. Pei, *Chem. Mater.* **2019**, *31*, 6412.

[39] O. Bubnova, X. Crispin, *Energy Environ. Sci.* **2012**, *5*, 9345.

Conclusions and perspectives

Conclusions and perspectives

The aim of my thesis was to investigate the effect of polymer orientation on thermoelectric properties of doped polythiophenes such as PBTTT and P3HT. We have used a simple and elegant method for aligning polymer semiconductors, which is known as high temperature rubbing. High temperature rubbing is a versatile method, used for aligning different classes of organic semiconductors.[1–3] This method produces highly anisotropic crystalline polymer films as evidenced by polarized UV-Vis-NIR spectroscopy and electron diffraction. Sequential doping of these oriented thin films using suitable doping agents such as F_4TCNQ, F_6TCNNQ and $FeCl_3$ produced highly conducting polymer films.[4–6]. The structural, spectroscopic and thermoelectric characterization of these doped thin films shows a high degree of anisotropy of TE properties.

chapter 2 mainly discusses the relationship between the length of the alkyl side chain of PBTTT families and their thermoelectric properties. In addition to this, we have clearly demonstrated the relationship between the side chain length of PBTTT and the diffusion coefficients of the F_4TCNQ^- anions into the alkyl side chain layers. The perpendicular orientation of the F_4TCNQ^-anion in the alkyl side chains of PBTTT enabled us to follow the doping kinetics. The idea was simple and to the best of our knowledge, it was the first time, the diffusion of the dopant molecule was determined by using such a simple experimental method (polarized UV-Vis-NIR spectroscopy). We have seen that there is an optimum side chain length, (C_{12}-PBTTT) which allows easy diffusion of dopants into the alkyl side chain layers. This lead to higher electrical conductivity.

The electrical conductivities and Seebeck coefficients of these oriented thin films are highly anisotropic and enhanced along the rubbing direction. The enhancement of the electrical conductivities along the rubbing direction was observed for all PBTTTs. It leads to high PFs along the rubbing direction. Thin films of C_{12}-PBTTT show very high electrical

conductivities of 193 S/cm along the rubbing direction and power factors of approximately 100 $\mu W \cdot m^{-2} \cdot K^{-1}$. This study demonstrates the importance of side-chain engineering, which can be used as a tool to enhance the TE properties. Most importantly, we demonstrated that a combination of polymer orientation and sequential doping can be used to improve the thermoelectric properties of semiconducting polymers.

Some of the recent research work on organic thermoelectrics proposed that future efforts to improve the thermoelectric properties of semiconducting polymers must be focused on improving electrical conductivity (σ).[7] This can eventually lead to very high power factors according to the relation $PF \propto \sigma^{1/2}$ as proposed by Glaudell[7] and coworkers. The third chapter demonstrates the use of strong Lewis acid-based doping agents such as $FeCl_3$ on oriented polymers such as C_{12}-PBTTT and P3HT. Sequential doping of liquid crystalline polymers such as C_{12}-PBTTT using $FeCl_3$ leads to record electrical conductivities of 2×10^5 S/cm and power factors of $\approx$ 2 $mWm^{-1}K^{-2}$ along the chain direction. The measured electrical conductivities were higher than for I_2 doped polyacetylene. [8–10] This higher electrical conductivity was obtained by using incremental concentration doping method i.e., each sample is doped by dipping it successively in the solutions of dopants of increasing concentration.

To the best of our knowledge, incremental concentration doping of semiconducting polymers has not been reported yet. The observed high electrical conductivity is mainly related to the regular intercalation of dopant molecules into the polymer structure. Most importantly, we have seen that the relationships between the Seebeck coefficients and electrical conductivitiy along the direction // and $\perp$ to the chains are different. Along the parallel direction, the Seebeck coefficient and the electrical conductivity follow the power-law $S_{//} \propto \sigma_{//}^{-1/4}$. Along the perpendicular direction, $S_{\perp} \propto \ln\sigma_{\perp}$, which is a fingerprint

for different charge transport mechanisms. A more detailed investigation is necessary to further understand the underlying charge transport mechanism.

In the last chapter we investigated the following issues:

i) How does the doping of C_{12}-PBTTT with F_6TCNNQ differ from that with F_4TCNQ in terms of structure, doping kinetics and resulting TE properties?

ii) How different are the intercalation of F_4TCNQ and F_6TCNNQ in the layers of alkyl side chains of C_{12}-PBTTT?

iii) Is there any difference in electrical conductivity in thin films doped by different doping methods such as incremental concentration doping and direct doping, which was previously observed in the case of $FeCl_3$ doped samples.

Similar to our previous results, the diffusion kinetics on oriented PBTTT thin films demonstrated the size dependence of the dopant anions and their diffusion coefficients. As expected, longer and bulkier F_6TCNNQ^- anions showed slightly slower diffusion coefficients than F_4TCNQ^-. Moreover, angle-dependent polarized UV-Vis-NIR spectroscopy suggested that longer and bulkier F_6TCNNQ^- anions are better oriented in the layers of alkyl side chains of C_{12}-PBTTT.

Most importantly, we observed that incremental concentration doping of C_{12}- PBTTT thin films always produced higher conductivity than singly doped films, irrespective of the doping agent. The mobility calculation based on the extinction coefficients of the dopant anions and polarons suggested that the higher electrical conductivity in ICD might be related to the enhanced mobility of charge carriers due to the progressive intercalation of the dopant into the alkyl side chain layers. The higher electrical conductivity observed in incrementally doped C_{12}-PBTTT thin films using F_6TCNNQ^- is

attributed to a better ordering of F_6TCNNQ^- anions in the side chain layers of the polymer.

In summary, the final outcome of the thesis is the following.

1) We proposed a simple method based on polarized UV-Vis-NIR spectroscopy to *follow the diffusion of dopant anions* such as F_4TCNQ^- and F_6TCNNQ^- in the oriented polymer matrix of various PBTTTs.

2) We were able to show that, polymer orientation through high temperature rubbing leads to highly conducting polymer thin films with enhanced electrical conductivities along the direction of rubbing. Moreover, these anisotropic thin films enabled *us to see a difference in the S vs σ relation along and perpendicular to the chain direction.* This is of high importance since such an observation is not accessible from non-oriented semiconductor thin films. This is due to the fact that the measured electrical conductivity and Seebeck coefficient in non-oriented films is a mixture of contributions along c, b and a axes. Hence it is impossible to characterize the transport mechanism in one direction of the polymer crystal. It is worth to mention that, other polymer orientation techniques such as stretching and tensile drawing do not show a clear trend and anisotropy in the Seebeck coefficients but only showed a clear enhancement of electrical conductivity along the direction of applied stress.[9,11,12][13] In our case, $S_{//}$ is always larger than $S_{\perp}$.

3) We proposed a simple method to characterize the orientation of dopant molecules such as F_6TCNNQ and F_4TCNQ in the layers of the alkyl side chains using angle-dependent polarized UV –Vis-NIR spectroscopy.

4) We introduced a new doping method called *incremental concentration doping (ICD).* Incremental concentration doping leads to higher electrical conductivities and higher power factors in oriented C_{12}-PBTTT than direct doping.

The ongoing project on incremental doping on other polymers further confirms that ICD is versatile and can be applied to a large palette of polymer semiconductors and dopants to enhance the TE properties. We believe that some of the results and publications from this thesis might be of high interest for the experimental and theoretical physicist to investigate further the underlying physical processes associated with TE properties. Also, the fundamental understandings and the results obtained from this thesis might be a small but important contribution to the field of plastic electronics.

However, there is always room for future developments. There is no doubt that the future of TE research on p-doped polymers must be based on enhancing electrical conductivity by introducing high crystallinity and long-range order along the polymer backbone. Preliminary results by electron diffraction measurements suggest that the introduction of ethylene glycol and ether-based side chains on PBTTT enhanced the order along the chain direction. Incremental concentration doping of these polymers by F_6TCNNQ can lead to electrical conductivities $> 2\times10^4$ S/cm. This further confirms that long-range order along the polymer backbone and suitable doping methods such us ICD can provide enhanced TE properties. Side chain engineering can be combined to the methods of doping and orientation proposed in this thesis to further boost TE properties.

The measurement of ultimate thermal conductivity is also an important parameter, which can affect the ZT value of a TE material. Hence, it is important to measure the thermal conductivity of these oriented polymers. Our preliminary results on thermal conductivity measurements on oriented P3HT suggest that the rubbing process does not substantially increase the in-plane thermal conductivity and still results in an enhancement by a factor of 25 of the ZT value compared to non-oriented films. A thermoelectric device is an alternative array of p and n-type organic materials. Oriented TE devices would be possible only after extending the high temperature rubbing method

to n-type polymers. Gross and coworkers demonstrated that n-type polymers such as P(NDI2OD-T2) can also align using high temperature rubbing.[14] Vapor doping of oriented P(NDI2OD-T2) with tetrakis(dimethylamino)ethylene (TDAE) leads to a higher electrical conductivity of 8.3×10^{-3} S/cm along the chain direction, which was 6 times higher than the direction perpendicular to the chains direction. This demonstrates the versatility of the high-T-rubbing method, that can be also applied to n-type polymers.

Combining alignment with side-chain engineering of polymers, dopant engineering and doping methods might be an interesting strategy forward to make oriented TE devices with enhanced electrical conductivities.

Bibliography

[1] A. Hamidi-Sakr, L. Biniek, S. Fall, M. Brinkmann, *Adv. Funct. Mater.* **2016**, *26*, 408.

[2] L. Biniek, N. Leclerc, T. Heiser, R. Bechara, M. Brinkmann, *Macromolecules* **2013**, *46*, 4014.

[3] L. Biniek, S. Pouget, D. Djurado, E. Gonthier, K. Tremel, N. Kayunkid, E. Zaborova, N. Crespo-Monteiro, O. Boyron, N. Leclerc, S. Ludwigs, M. Brinkmann, *Macromolecules* **2014**, *47*, 3871.

[4] V. Vijayakumar, Y. Zhong, V. Untilova, M. Bahri, L. Herrmann, L. Biniek, N. Leclerc, M. Brinkmann, *Adv. Energy Mater.* **2019**, *9*, 1900266.

[5] A. Hamidi-sakr, L. Biniek, J.-L. Bantignies, D. Maurin, L. Herrmann, N. Leclerc, P. Lévêque, V. Vijayakumar, N. Zimmermann, M. Brinkmann, *Adv. Funct. Mater.* **2017**, *27*, 1700173.

[6] V. Vijayakumar, E. Zaborova, L. Biniek, H. Zeng, L. Herrmann, A. Carvalho, O. Boyron, N. Leclerc, M. Brinkmann, *ACS Appl. Mater. Interfaces* **2019**, *11*, 4942.

[7] A. M. Glaudell, J. E. Cochran, S. N. Patel, M. L. Chabinyc, *Adv. Energy Mater.* **2015**, *5*, 1401072.

[8] A. J. Heeger, *J. Phys. Chem. B* **2001**, *105*, 8475.

[9] Y. Nogami, H. Kaneko, T. Ishiguro, A. Takahashi, J. Tsukamoto, N. Hosoito, *Solid State Commun.* **1990**, *76*, 583.

[10] J. Tsukamoto, A. Takahashi, K. Kawasaki, *Jpn. J. Appl. Phys.* **1990**, *29*, 125.

[11] J. Fanous, M. Schweizer, D. Schawaller, M. R. Buchmeiser, *Macromol. Mater. Eng.* **2012**, *297*, 123.

[12] A. Andreatta, Y. Cao, J. C. Chiang, A. J. Heeger, P. Smith, *Synth. Met.* **1988**, *26*, 383.

[13] J. Hynynen, E. Järsvall, R. Kroon, Y. Zhang, S. Barlow, S. R. Marder, M. Kemerink, A. Lund, C. Müller, *ACS Macro Lett.* **2019**, *8*, 70.

[14] Y. M. Gross, D. Trefz, C. Dingler, D. Bauer, V. Vijayakumar, V. Untilova, L. Biniek, M. Brinkmann, S. Ludwigs, *Chem. Mater.* **2019**, *31*, 3542.

Experimental details

Experimental Details

1. Polymer synthesis and characterization

C_8-PBTTT, C_{12}-PBTTT, C_{14}-PBTTT, and C_{18}-PBTTT were synthesized by N. Leclerc and E. Zaborova following the detailed procedure according to the references.[1–5] P3HT was purchased from Merck. 2,3,5,5-tetrafluoro(tetracyanoquinodimethane) (F_4TCNQ) was purchased from TCI and solvents such as anhydrous acetonitrile, anhydrous nitromethane, Sodium polystyrenesulfonate (NaPSS), anhydrous $FeCl_3$ and were obtained from Aldrich. The F_6TCNNQ dopant has been synthesized[6] by P.Durand according to the reference (6). All the chemicals were used as received. The macromolecular parameters are collected in Table 1.

Table 1. *Macromolecular parameters of the semiconducting polymers used in this study. (Gel permeation chromatography was performed in hot tri-chlorobenzene versus PS standard)*

Polymer	M_n (g/mol)	M_w (g/mol)	PDI
PBTTT C_8	13000	24000	1.84
PBTTT C_{12}	26000	45000	1.73
PBTTT C_{14}	17000	51000	1.64
PBTTT C_{18}	31000	51000	3
P3HT	24200	43600	1.8

1.1 General procedure for the synthesis of polymers

Poly(2,5-bis(3-alkylthiophen-2-yl)thieno[3,2-b]thiophene):

A Schlenk tube was charged with a stirrer bar, 5,5’-dibromo-4,4’-dialkylbithiophene (0.537 mmol), 2,5-bis(trimethylstannyl)-thieno[3,2-b]thiophene (250 mg, 0.537 mmol),

tris(dibenzylideneacetone)dipalladium (0) (10 mg, 2 mol %), tri(*o*-tolyl)phosphine (13 mg, 8 mol %) and toluene (1.8 ml). The reaction mixture was purged with argon and was heated at 115°C during 24 h. Then 2-(trimethylstannyl)thiophene was added and the reaction mixture was heated again at 115°C during 4 h. Then 2-bromothiophene was added and the reaction mixture was heated at 115°C for additional 4 h. After cooling to 50°C, the reaction mixture was precipitated into a mixture of methanol (100 ml) and concentrated hydrochloric acid (7 ml) and stirred for 4 h at 20°C. The precipitate was filtered and extracted (via Soxhlet) with methanol, acetone, chloroform and chlorobenzene. The solution of sodium diethyldithiocarbamate trihydrate in water was added to the last two fractions and the mixtures were heated at 50°C during 3 h.

The organic layer was separated, dried on sodium sulphate, filtered and partially concentrated under reduced pressure. The resulting solution was precipitated in methanol. The polymer was collected by filtration and dried under vacuum to afford the product.

Poly(2,5-bis(3-octylthiophen-2-yl)thieno[3,2-b]thiophene) (C_8):

SEC (TCB) Mn (29,600 g/mol), Mw (54,000 g/mol). λ max 538 nm (solid film, $CHCl_3$ fraction), λ max 550 nm (solid film, C_6H_5Cl fraction). ^{1}H NMR (400 MHz, $C_2D_2Cl_4$, 85°C) δ 7.38 (s, 2H), 7.15 (s, 2H), 2.90 (br t, 4H), 1.89-1.73 (m, 4H), 1.58-1.32 (m, 20H), 1.04-0.93 (br t, 6H)

Poly(2,5-bis(3-dodecylthiophen-2-yl)thieno[3,2-b]thiophene) (C_{12}):

SEC (TCB) Mn (29,600 g/mol), Mw (54,000 g/mol). λ max 544 nm (solid film, $CHCl_3$ fraction), λ max 553 nm (solid film, C_6H_5Cl fraction). ^{1}H NMR (400 MHz, $C_2D_2Cl_4$, 85°C) δ 7.38 (s, 2H), 7.15 (s, 2H), 2.90 (br t, 4H), 1.88-1.76 (m, 4H), 1.58-1.32 (m, 36H), 1.03-0.93 (br t, 6H).

Poly(2,5-bis(3-tetradecylthiophen-2-yl)thieno[3,2-b]thiophene) (C_{14}):

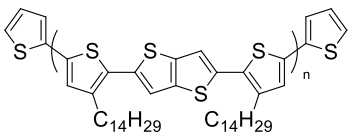

GPC (TCB) Mn (29,600 g/mol), Mw (54,000 g/mol). λ max 546 nm (solid film, $CHCl_3$ fraction), λ max 554 nm (solid film, C_6H_5Cl fraction). ^{1}H NMR (400 MHz, $C_2D_2Cl_4$, 85°C) δ 7.38 (s, 2H), 7.15 (s, 2H), 2.89 (br t, 4H), 1.88-1.73 (m, 4H), 1.58-1.29 (m, 44H), 0.84-1.03 (br t, 6H).

Poly(2,5-bis(3-octadecylthiophen-2-yl)thieno[3,2-b]thiophene) (C_{18}):

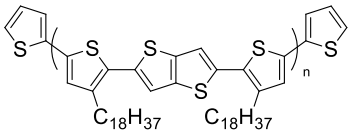

GPC (TCB) Mn (29,600 g/mol), Mw (54,000 g/mol). λ max 542 nm (solid film, $CHCl_3$ fraction), λ max 548 nm (solid film, C_6H_5Cl fraction). ^{1}H NMR (400 MHz, $C_2D_2Cl_4$, 85°C) δ 7.37 (s, 2H), 7.13 (s, 2H), 2.89 (br s, 4H), 1.81 (br s, 4H), 1.58-1.25 (m, 60H), 1.03-0.92 (br t, 6H).

2. preparation of conducting polymer films

2.1 Preparation of glass slides

The glass slides for the thin film preparation are cleaned by sonicating in different solvents such as acetone, isopropanol, helmanex (diluted to 10% in Milli-Q water) for approximately 15 minutes. These glass slides are transferred to Milli-Q water and sonicated for 15 minutes to remove excess helmanex solution and kept in isopropanol. The isopropanol is dried under nitrogen flush before doctor blading the films.

2.2 Thin film preparation, orientation by high-temperature rubbing.

Thin films of PBTTT were prepared by doctor blading from a hot solution of 10 mg/ml PBTTT in ortho-dichlorobenzene (o-DCB) on a glass substrate at 160°C. Films are then aligned using a homemade rubbing machine.

The rubbing machine was originally developed in the Sycommor group (L. Herrmann, P. Allgayer, J.-C. Wittmann and M. Brinkmann) for the preparation of alignment layers and further improved for the orientation of polymer semiconductors used in OFET (L. Biniek et al.).[7,8]

The rubbing machine is composed of a metallic cylinder (diameter 4 cm) covered by a microfiber tissue (see figure 1). The cylinder can be rotated at a speed of approximately 300 RPM during the rubbing process. The cylinder is applied with a 2-3 bar pressure on the thin film. Most importantly, the temperature of the film during rubbing can be controlled. Calibration of the temperature was performed to account for the difference between the set temperature and actual temperature on the surface of the glass substrate.

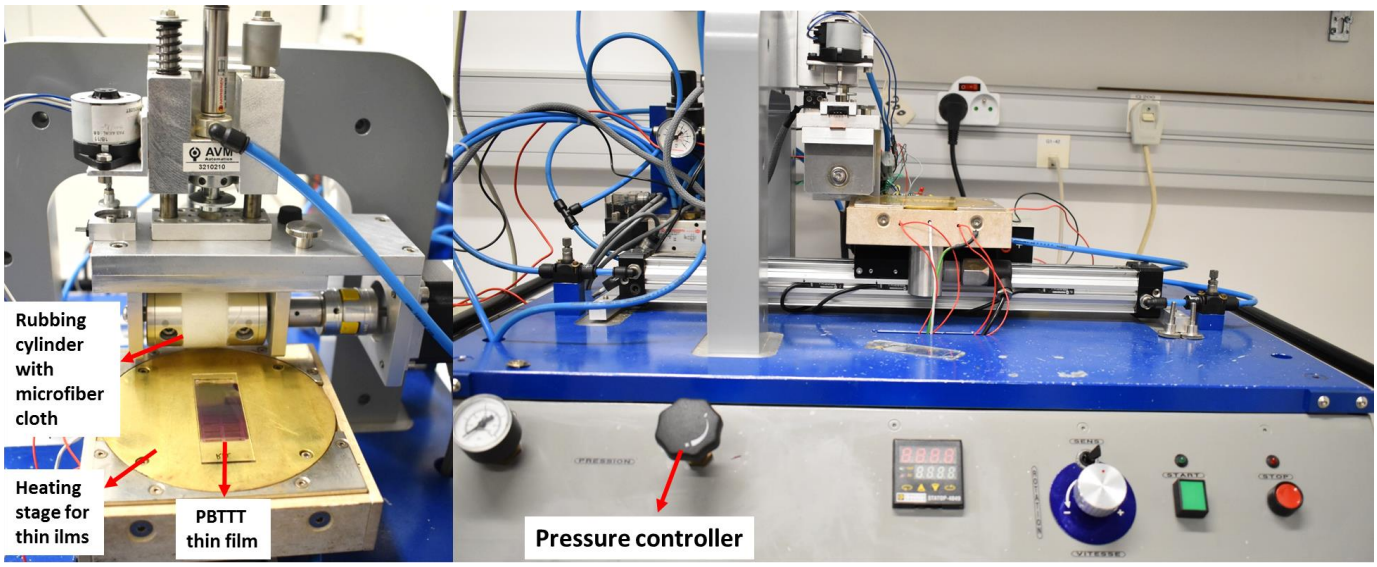

Figure 1. *A) Front view of rubbing machine B) side view of the rubbing machine.*

The films were rubbed at different rubbing temperatures (T_R) depending on the polymer (125°C for C_8 PBTTT, C_{12} PBTTT, C_{18} PBTTT, and 100°C for C_{14} PBTTT). The films of P3HT were rubbed at 180 °C to achieve a high degree of orientation as proposed by Hamidi-Sakr and coworkers[9,10]. The rubbing was done inside a glove box under nitrogen atmosphere to avoid oxidation of the polymer. To determine the film thickness after rubbing, the films were melt-annealed at 300 °C in nitrogen in a Linkam hot stage (HS-95 controller and LTS420 stage) to randomize the in-plane chain direction and the thickness was extracted from the UV-vis absorbance.

2.3 Doping methods

A) F_4TCNQ doping of polythiophenes

A 1 mg/ml solution of F_4TCNQ was prepared by dissolving F_4TCNQ in anhydrous acetonitrile in a glass vial. Doped PBTTT films were prepared by dipping the polymer films in the dopant solution for different time intervals (for doping kinetics).Films were dried using nitrogen to remove the excess F_4TCNQ solution.

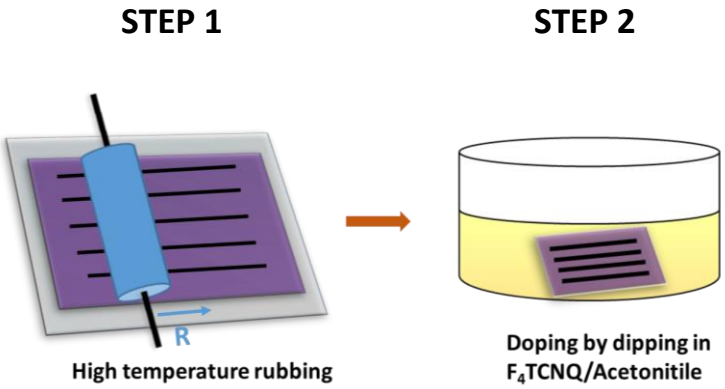

Figure 2. *Schematic illustration of the orientation of PBTTT thin films by high-temperature rubbing and doping.*

B) $FeCl_3$ doping of polythiophenes

All doping experiments were carried out in a glove box (Jacomex) with P_{O2}< 3 ppm and P_{H2O}<1 ppm. 10 mM $FeCl_3$ solutions were prepared by dissolving 8 mg of $FeCl_3$ in 5 ml anhydrous nitromethane in a glass vial and subsequent dilution yielded the solutions with concentrations in the range 0.1 - 5 mM. Doping was done by dipping the oriented polymer film in the dopant solution for 30 s to 1 min until no color change was any more visible. Ageing of the $FeCl_3$-doped films is observed when the samples are placed in ambient (dark). Therefore, all electrical characterizations were performed in a glovebox whereas UV-Vis-NIR measurements were performed within 1-2 min after the transfer of the sample to the spectrometer in ambient to avoid substantial dedoping.

C) Incremental concentration doping (ICD) and direct doping (DD) of polythiophenes using F_6TCNNQ and F_4TCNQ.

Two different procedures were used to dope the oriented PBTTT i.e., incremental doping (ICD) and direct doping (DD). In ICD each sample is doped by dipping it successively in the solutions of dopants of increasing concentration. The excess F_6TCNNQ or F_4TCNQ crystals on the backside of the glass slides were cleaned using small amounts of acetone before measuring the polarized UV-Vis-NIR spectra. In the DD procedure, each sample is dipped a single time in a solution of a given concentration. All doping experiments, electrical conductivity measurements and Seebeck coefficients measurements were carried out in a glove box with P_{O2}< 1 ppm and P_{H2O}<1 ppm to avoid dedoping. The polarized UV-Vis-NIR measurements were done within 2 to 3 minutes after doping to avoid dedoping.

3. Sample preparation for TEM

A) F_4TCNQ doped PBTTT

Samples for transmission electron microscopy were prepared by spin coating (3000 rpm) a thin layer of NaPSS (10 mg/ml aq) on a precleaned glass substrate and this substrate was used for the preparation of oriented polymer film as described above. Doping was done by dipping the oriented polymer film in the dopant solution for the different time intervals. Thew were subsequently removed from the glass substrate by floating on distilled water and recovered on TEM copper grids. The films were coated with a thin amorphous carbon layer using an auto 306 Edwards evaporator.

TEM was performed in the bright field and diffraction modes using a CM12 Philips microscope equipped with an MVIII (Soft Imaging System) Charge Coupled Device camera. Beam exposure was set to a minimum using the low dose system to avoid de-

doping under the electron beam that is observed when the same zone is exposed for a prolonged period of time.

B) $FeCl_3$ doped P3HT and C_{12} PBTTT

The preparation of the samples for TEM analysis involved three steps:

i) Floating the oriented polymer films (P3HT or PBTTT) on distilled water and recover them on TEM copper grids

ii) Coat the films with a thin amorphous carbon layer

iii) Dope the TEM grids directly in the glove box by dropping 20 µl of $FeCl_3$/nitromethane solution on the grid. After 30s, the grids were blotted with a piece of absorbing paper to remove the excess of dopant solution.

To avoid sample ageing upon transfer in ambient atmosphere, the TEM grids were mounted on the TEM sample holder inside the glove box and the holder was then transferred to the TEM in an air-tight container. The samples were only swiftly exposed to air (1-2s) just before introducing the sample holder into the TEM.

C) Incremental concentration doping using F_6TCNNQ and F_4TCNQ

In order to verify the impact of the doping method, i.e. incremental concentration doping and single doping low dose electron diffraction were performed on doped PBTTT thin films. For TEM investigations, the oriented PBTTT thin films prepared on NaPSS by high-temperature rubbing were carbon-coated and recovered on copper TEM grids. The TEM grids were doped by incremental concentration doping using dopant solutions (F_4TCNQ or F_6TCNNQ) in acetonitrile in the glove box. The dopant solution was allowed to stay on the TEM grid for 20 to 30 s and the excess solution was removed by blotting. In the direct doping method, carbon-coated TEM grids were doped directly at a given concentration of dopants.

4. Scanning electron microscopy

Scanning electron microscopy done by A. Carvalho. The experements were performed at 1kV with a HITACHI SU8010 FEG-SEM on as-prepared films (no coating) to verify the uniformity of the rubbed layers.

5. Scanning transmission electron microscopy- dispersive X-ray spectroscopy (STEM-EDX)

STEM-EDX experiments were performed using a Cs-corrected JEOL JEM-2100F microscope operated at 100 keV to avoid dedoping of the films under the beam. energy dispersive X-Ray spectroscopy (EDX) mapping was performed using a JEOL Silicon Drift Detector (DrySD60GV: sensor size 60 mm^2) with a solid angle of approximately 0.5 rad". The EDX measurements were done at IPCMS by M. Bahri and O. Ersen.

6. Cyclic voltammetry

Cyclic voltammetric measurements were done by N. Leclerc at ICPESS. Oxidation potentials were determined by voltammetry with a conventional 3-electrode system using a voltammetric analyser equipped with a platinum microdisk (2 mm^2) working electrode and a platinum wire counter electrode. The reference electrode is constituted of a non-aqueous silver electrode including the following electrolyte solution: 0.01 M silver nitrate + 0.1 M Tetrabutylammonium perchlorate in Acetonitrile. Potentials were calibrated versus the saturated calomel electrode (SCE), using the ferrocene/ferrocenium (*Fc/Fc*$^+$) couple as an internal reference and a conventional scan rate of 100 mV/s. Recrystallized tetrabutylammonium hexafluorophosphate (Bu_4NPF_6) was used as the supporting electrolyte (0.1 M) in distilled and anhydrous acetonitrile (ACN). All potentials are referred to the SCE electrode that was calibrated at 0.41 V vs Fc/Fc^+ system. Following the work of Jenekhe *et al.* [11], we estimated the ionization potential (IP) or highest occupied molecular orbital (HOMO) from the redox data. The

HOMO levels were calculated from the following equations, using the oxidation and reduction onset potentials: HOMO (eV) = −[E_{onset}ox (vs SCE) + 4.4], based on an SCE energy level of 4.4 eV relative to the vacuum.

7. Polarized UV-Vis-NIR spectroscopy

The orientation of the polymer films was probed by UV-Vis-NIR absorption (350-2500 nm) using a Cary 5000 spectrometer with polarized incident light and spectral resolution of 1 nm. The UV-Vis-NIR spectra of the doped polymer film were measured along the parallel and perpendicular to the direction of rubbing. The orientation of the film with respect to the polarization of the incident light is controlled by a goniometer. The parallel configuration is the position where the $\mathbf{c}_{PBTTT}$ axis is parallel to the light polarization. For each sample, a spectrum in the parallel and perpendicular configuration were measured as a function of doping time. Angle dependent polarized UV-Vis-NIR spectroscopic measurements were performed by rotating the angle of light polarization for different polarization angle from 0° to 90°for with an interval of 15°.

8. Differential Scanning Calorimetry

DSC measurements were performed on a DSC Q2000 from TA Instruments under nitrogen atmosphere using a sample mass in the range 1.5-2.5 mg. The samples were heated to 250°C with a heating rate of 10°C.min^{-1}, then cooled to 20°C at 5°C/min.

9. Electrical conductivity and thermopower measurements

Rather than evaporating gold contacts on top of the oriented and doped films, we prepared all oriented films on NaPSS/glass substrate and recovered the films by floating them on distilled water and transferred them on the pre-patterned devices. Doing so, we avoided the problem of film dedoping when submitting the films to a secondary vacuum during evaporation. All devices were fabricated on glass substrates, cleaned by

ultrasonication in acetone, ethanol, hellmanex, deionized water, and isopropanol. The device fabrication was done by N. Zimmermann at ICUBE.

The cleaned substrates were dried under nitrogen prior to use. Gold electrical contacts (40 nm thick) in a four-point probe geometry (1 mm spacing between electrodes, 5 mm length) were deposited via controlled thermal evaporation through a shadow mask, at an average rate of 4-6 Å/s. The first layer of Chromium (2.5 nm thick) was deposited prior to the gold to promote a good adhesion on the glass substrates (evaporation rate 0.5-1 Å/s). The contact geometry used for the electrical conductivity and thermopower measurements is shown in figure 3 and 4.

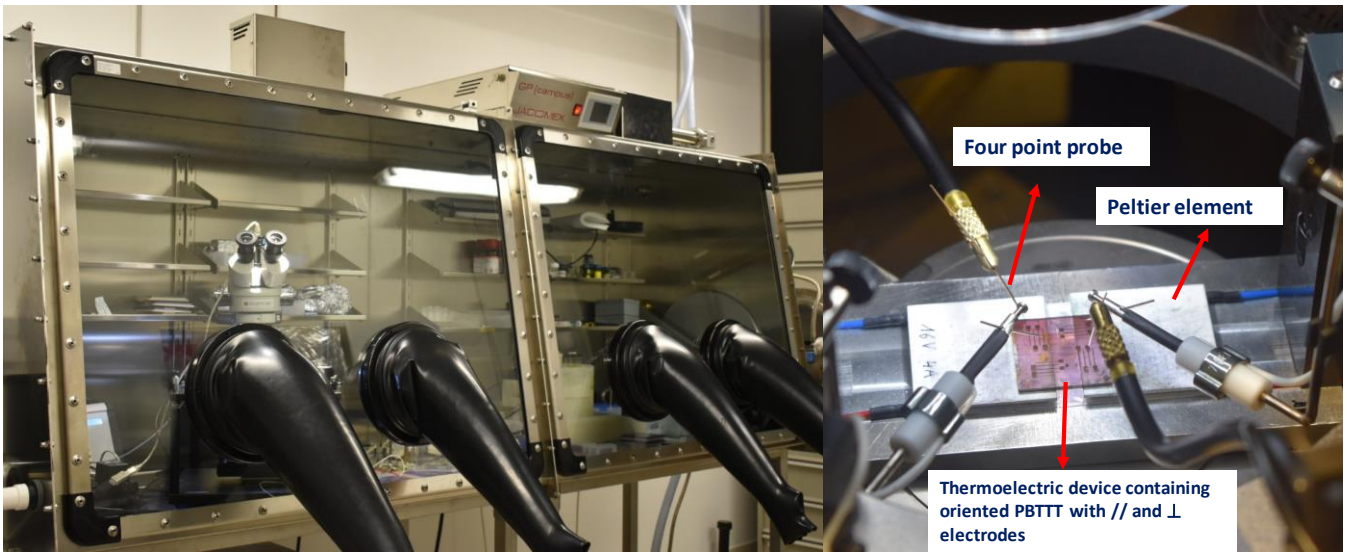

Figure 3. *Photographic images of the glove box, electrical conductivity and Seebeck coefficient measurement setup.*

On the same substrate, two devices are oriented along the rubbing direction) and two others in the perpendicular direction, which allows us to determine the charge transport and thermoelectric anisotropy on the same substrate (see figure 4 and 5). Four-point-probe measurements of electrical conductivity were performed using a Keithley 4200-SCS and a lab assistant semi probe station in a Jacomex glovebox under N_2 atmosphere. To derive the resistivity ρ from the sheet resistance R measured on the device geometry

given in figure 3, we have first determined the geometrical correction factor C such that $\rho = C\ R\ t$ where t is the film thickness.

To that aim, we have used a classical four-point probe system on a non-oriented doped P3HT film to obtain a reference value of the resistivity given by $\rho = 4.53Rt$. Using this value of the resistivity we determined the geometrical correction factor for our four-line electrode geometry by measuring the sheet resistance on the same sample and obtained C=1.81 i.e. $\rho=1.81Rt$. The average conductivity value for a given doping condition and polymer was taken as the average of four devices.

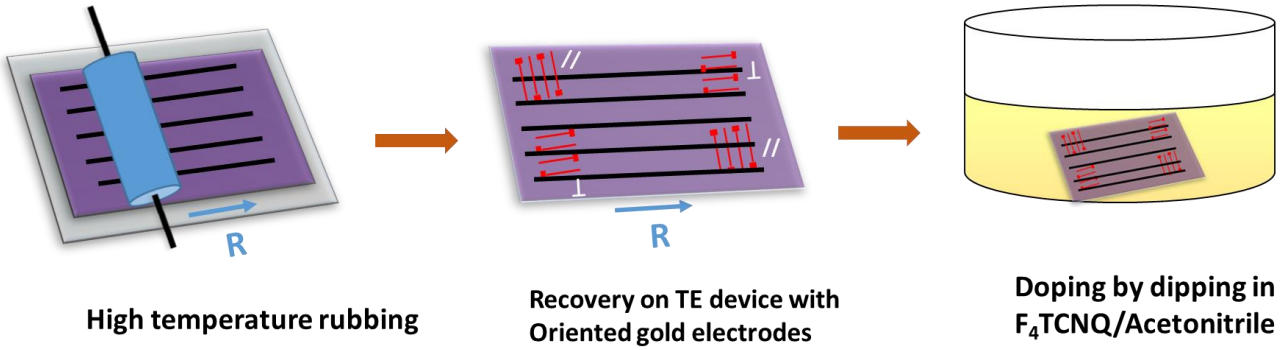

Figure 4. *Schematic representation of high temperature rubbing and recovery of oriented thin films on patterned devices with oriented electrodes // and ⊥ to the rubbing direction. The TE device is dipped in the corresponding dopant solution for successful doping.*

Thermopower measurements were conducted on the same devices in a glove box. The thermopower was measured via the differential temperature method: a temperature gradient is established across the sample either along the rubbing direction or perpendicular to it.

The measurements were performed by using a homemade setup made of one heating and one cooling Peltier cells (3 mm gap) (see figure 5) providing a controllable temperature difference ΔT.[9] Temperatures of the cold and warm sides were measured in a non-contact mode using two IR sensors avoiding thus thermal contact issues. The

Seebeck tension was measured using a Keithley 2634B source meter and a semiprobe lab assistant probe station in ambient conditions. The Seebeck coefficient is calculated from the slope of V_{therm} versus temperature difference ΔT for ΔT varying in a range ±10K around T=23±2°C.

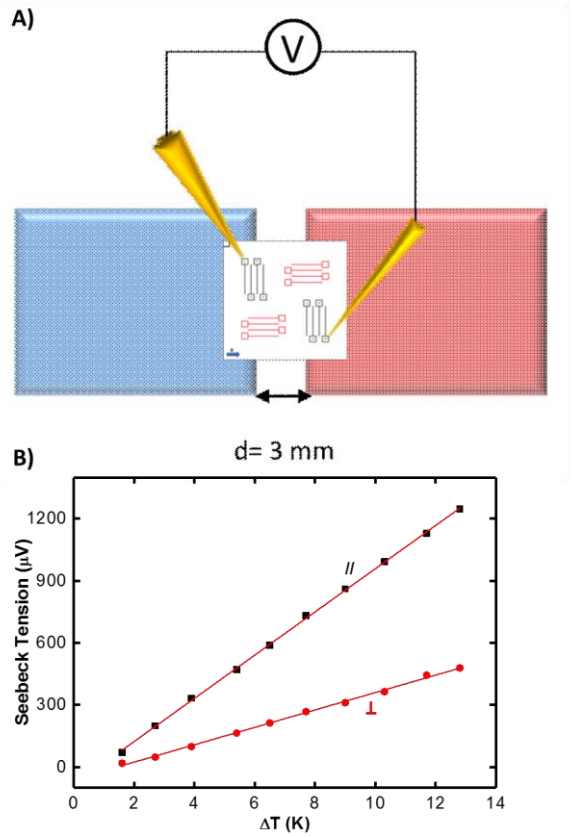

Figure 5. *Schematic illustration of the experimental setup used for measuring the Seebeck coefficient of oriented PBTTT thin films along the direction parallel and perpendicular to the rubbing direction. The two curves represent the Seebeck coefficients measured along the parallel (black) and perpendicular (red) directions. Figure 4A is reproduced from reference 9.*

Bibliography

[1] L. S. Fuller, B. Iddon, K. A. Smith, *J. Chem. Soc. Perkin Trans. 1* **1997**, 3465.

[2] H. D. R. Calado, T. Matencio, C. L. Donnici, L. A. Cury, J. Rieumont, J.-M. Pernaut, *Synth. Met.* **2008**, *158*, 1037.

[3] N. Leclerc, A. Michaud, K. Sirois, J.-F. Morin, M. Leclerc, *Adv. Funct. Mater.* **2006**, *16*, 1694.

[4] M. Zagórska, B. Krische, *Polymer.* **1990**, *31*, 1379.

[5] X. Guo, R. P. Ortiz, Y. Zheng, M.-G. Kim, S. Zhang, Y. Hu, G. Lu, A. Facchetti, T. J. Marks, *J. Am. Chem. Soc.* **2011**, *133*, 13685.

[6] P. K. Koech, A. B. Padmaperuma, L. Wang, J. S. Swensen, E. Polikarpov, J. T. Darsell, J. E. Rainbolt, D. J. Gaspar, *Chem. Mater.* **2010**, *22*, 3926.

[7] C. Vergnat, S. Uttiya, S. Pratontep, T. Kerdcharoen, J.-F. Legrand, M. Brinkmann, *Synth. Met.* **2011**, *161*, 251.

[8] M. Brinkmann, S. Pratontep, C. Chaumont, J.-C. Wittmann, *Macromolecules* **2007**, *40*, 9420.

[9] A. Hamidi-sakr, L. Biniek, J.-L. Bantignies, D. Maurin, L. Herrmann, N. Leclerc, P. Lévêque, V. Vijayakumar, N. Zimmermann, M. Brinkmann, *Adv. Funct. Mater.* **2017**, *27*, 1700173.

[10] A. Hamidi-Sakr, L. Biniek, S. Fall, M. Brinkmann, *Adv. Funct. Mater.* **2016**, *26*, 408.

[11] A. P. Kulkarni, C. J. Tonzola, A. Babel, S. A. Jenekhe, *Chem. Mater.* **2004**, *16*, 4556.

Résumé de la thèse

Vishnu Vijayakumar

Films minces de polythiophènes orientés et conducteurs pour applications en thermoélectricité.

Directeur de la thèse : Martin Brinkmann

Résumé de la thèse

Cette thèse traite de la fabrication de films minces orientés de polymères conducteurs pour applications en thermoélectricité. Plus, précisément, nous nous sommes penchés sur une série de polythiophènes, les PBTTTs dopés séquentiellement avec différents dopants (F_4TCNQ, F_6TCNNQ et $FeCl_3$). Il s'agissait de comprendre comment contrôler et améliorer les propriétés TE de cette famille de polythiophène en tirant parti de leur alignement par une technique de brossage mécanique à haute température. La thèse est organisée autour de quatre chapitres et une conclusion.

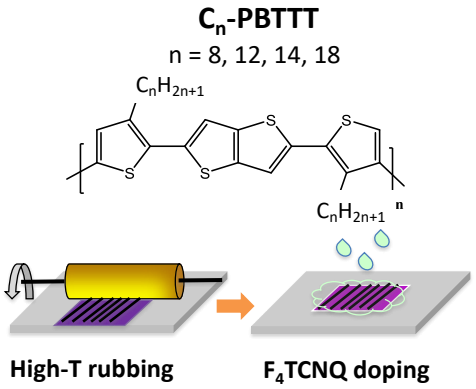

Figure 1. *Structure chimique des PBTTTs étudiés et illustration du procédé de fabrication des couches minces par brossage mécanique et dopage séquentiel avec F_4TCNQ/ACN.*

Le premier chapitre concerne une étude bibliographique de l'état-de-l'art sur les polymères conducteurs utilisés récemment pour leur propriétés thermo-électriques. Nous y abordons différentes notions fondamentales : i) la structure électronique des polymères conjugués, ii) la structure et la morphologie des polymères conjugués, iii) les mécanismes de dopage et propriétés électroniques associées, iii) les structures des polymères dopés et vi) les bases de la physique de l'effet thermoélectrique dans les polymères conducteurs. Le second chapitre rapporte une première série de résultats sur l'effet de la longueur des chaînes alkyls de PBTTT sur l'efficacité du dopage séquentiel par le dopant F_4TCNQ. Nous avons travaillé sur la famille des PBTTTs connus pour leur

mobilité de charge élevées à l'état non-dopé. Des PBTTTs portant des chaînes alkyls de C_8 jusqu'à C_{18} ont été étudiés (cf Figure 1).

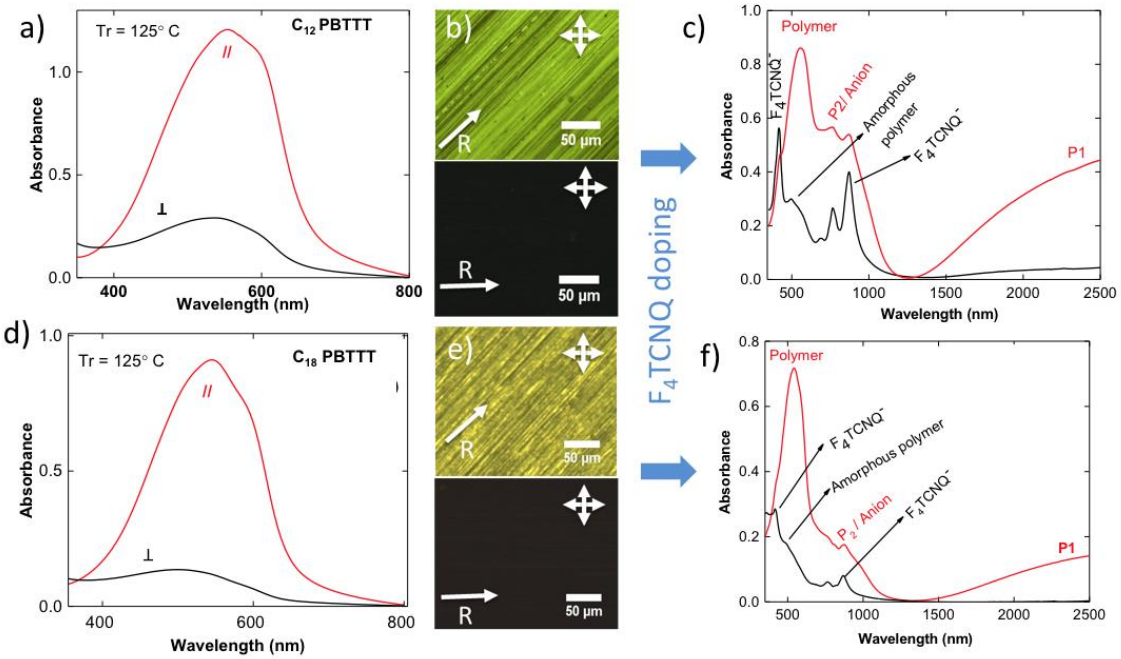

Figure 2. *Exemple d'alignement induit par brossage à haute température (T_R=125°C) pour des films de C_{12}-PBTTT et de C_{18}-PBTTT. (a) et (d) spectres UV-vis polarisés avant dopage et (c) et (f) après dopage avec F_4TCNQ/ACN (1mg/ml) (// et ⊥ désignent l'orientation de la polarisation de la lumière par rapport à la direction de brossage). (b) and (e) Images sous microscope optique polarisé montrant la forte biréfringence des films après brossage et dopage.*

Dans un premier temps, nous avons déterminé les conditions permettant d'aligner ces polymères en utilisant la méthode de brossage mécanique à haute température et ensuite de les transformer en couches conductrices par dopage séquentiel en solution de F_4TCNQ/ACN. Comme pour le P3HT, nous avons montré que le dopage préserve l'alignement des couches brossées quel que soit les chaînes alkyls du PBTTT (figure 2). La spectroscopie UV-Vis-NIR polarisée montre des signatures caractéristiques des polarons (bandes P1, P2) et du polymère neutre (N) pour POL//R et des bandes typiques des anions du F_4TCNQ pour POL perpendiculaire à R (R : direction de brossage des couches minces) (cf Figure 2). Dans tous les cas, les bandes de l'anion F_4TCNQ sont

orientées perpendiculairement aux chaînes du polymère, ce qui démontre l'intercalation des dopants dans les couches de chaînes alkyls des PBTTTs, quel que soit la longueur des chaînes alkyls.

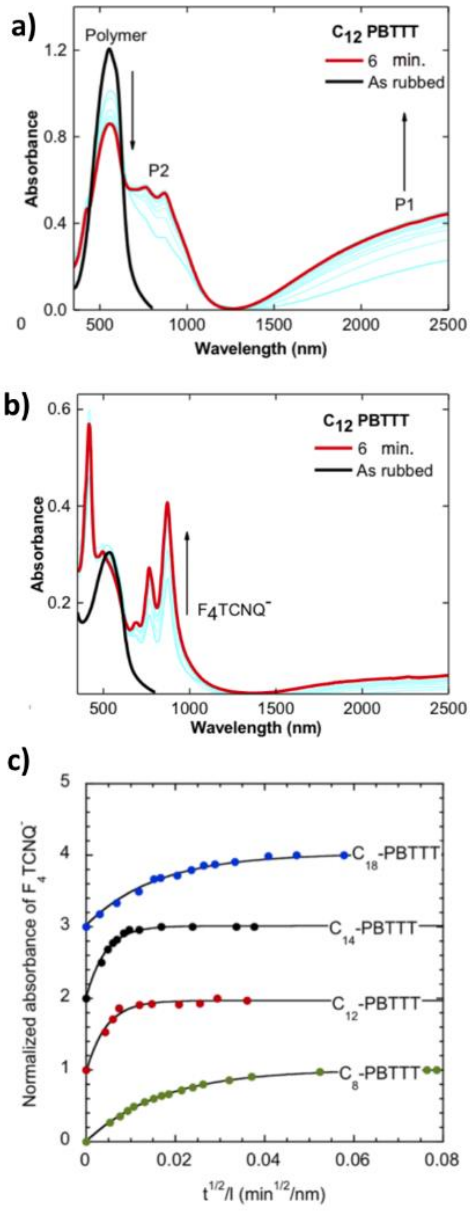

Figure 3. *a) et b) Cinétique de dopage de films minces de C_{12}-PBTTT suivie par spectroscopie polarisée UV-vis-NIR avec la polarisation POL //R et POL perpendiculaire à R, respectivement. C) Cinétiques de dopage de films orientés de PBTTTs portant des chaînes alkyls de longueurs différentes (C_8 à C_{18}) en solution de F_4TCNQ/ACN (1 mg/ml) obtenues à partir de l'absorbance de F_4TCNQ^- à 875 nm.*

Afin de maîtriser le dopage des films, nous avons étudié les cinétiques de dopage en solution de F_4TCNQ dans l'acétonitrile (ACN). Ainsi, nous avons pu montrer que la longueur des chaînes alkyls contrôle à la fois i) le taux de dopage final (teneur en F_4TCNQ) et ii) la vitesse du dopage.

Ainsi, on a montré que le dopage se faisait le mieux (taux de dopage élevé) et plus rapidement pour des PBTTTs ayant des chaînes alkyls en C_{12} et C_{14}. En revanche, les PBTTTs ayant des chaînes très longues en C_{18} ou très courtes en C_8 présentent des taux de dopage plus faibles et des cinétiques lentes. Dans le cas des chaînes en C_{18}, ceci a été attribué au caractère cristallisé des chaînes en C_{18}, ce qui se voit en effet dans les diagrammes de DSC de ce polymère (pics de fusion/cristallisation très nets). En revanche, pour le C_8-PBTTT, nous proposons que le caractère trop désordonné des chaînes alkyls ne permet pas la bonne diffusion et intercalation des dopants dans les couches de chaînes alkyls en C_8.

Une analyse quantitative de la cinétique de dopage a été réalisée en traçant l'absorbance de l'anion $F_4TCNQ^{-\cdot}$ $A_{875}(t)$ (à 875nm) en fonction du temps de dopage t (Figure 3). Afin de s'affranchir des problèmes de temps de diffusion différents pour des épaisseurs de films différentes, nous avons tracé les cinétiques en fonction de $t^{1/2}/l$ avec l, l'épaisseur des films. Les polymères ayant des chaînes alkyls différentes montrent des cinétiques de dopage différentes. Un ajustement des données a été réalisé à l'aide de l'équation phénoménologique suivante:

$$A_{875}(t) = A_0\left(1 - \exp\left(-\frac{\sqrt{D}}{l}(t)^{1/2}\right)\right) \quad (1)$$

Où A_0 est l'absorbance finale à saturation et D est le coefficient de diffusion caractéristique du F_4TCNQ et l est l'épaisseur des films.

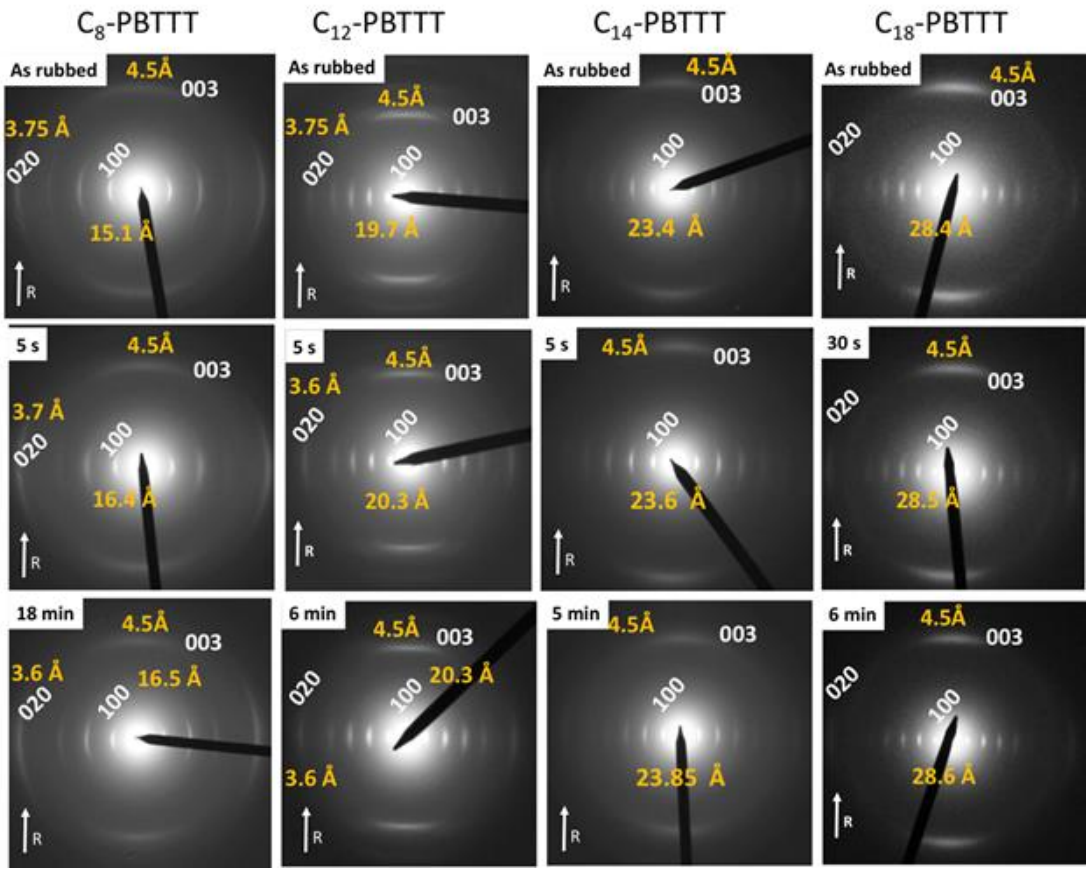

Figure 4. *Evolution des clichés de diffraction électronique de films minces de différents PBTTTs orientés par brossage (T_R=125°C) et dopés avec F_4TCNQ pour différents temps de dopage. Les distances réticulaires correspondant à la périodicité lamellaire (le long des chaînes alkyls) d_{100} et selon le π-stacking d_{020} sont notées en bleu. La flèche R indique la direction de brossage des films minces.*

Comme le montre la figure 3, les points expérimentaux des cinétiques de dopage des PBTTTs avec F_4TCNQ sont bien ajustés à l'aide de l'équation (1). Pour les temps courts, les cinétiques suivent une loi en $\sqrt{t}$ suggérant un mécanisme limité par la diffusion des dopants dans les films minces. En effet, cette situation peut être analysée comme la diffusion à partir d'un réservoir de concentration constante de F_4TCNQ en solution via la surface du film vers l'intérieur du film mince. L'équation (1) permet ainsi d'extraire les temps de diffusion caractéristique des dopants dans les films polymères τ et, connaissant leur épaisseur, d'obtenir des constantes de diffusion D. En représentant les cinétiques en fonction de la variable $\sqrt{t}/l$, on peut directement remonter aux

coefficients de diffusion D et on obtient une représentation des courbes de cinétiques indépendante de l'épaisseur des films (les temps de diffusion caractéristique dans les couches t sont fonction de l'épaisseur des films).

Ayant déterminé les conditions de dopage optimale et les cinétiques correspondantes, nous avons étudié l'évolution de la structure des films orientés de PBTTTs par diffraction électronique. Comme le montre les clichés de diffraction de la figure 4, Le dopage préserve globalement l'alignement et la structure des films orientés. Toutefois, nous observons pour tous les PBTTTs une modification des paramètres de maille. La figure 4 montre ainsi que les mailles présentent une expansion dans la direction des chaînes alkyls et une contraction selon la direction du π-stacking.

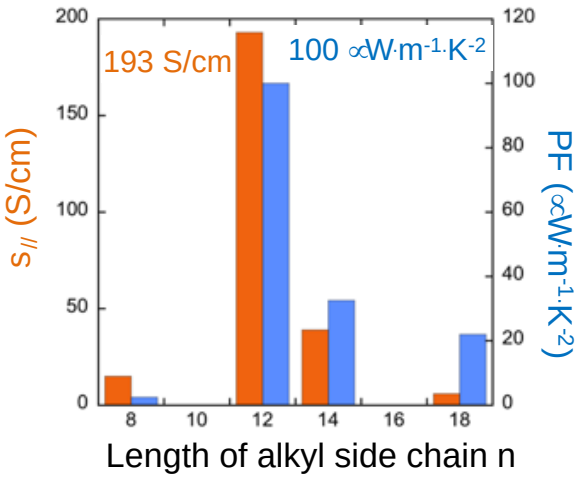

Figure 5. *Variation de la conductivité mesurée dans le sens du brossage et du facteur de puissance PF en fonction de la longueur des chaînes alkyls d'une famille de PBTTT.*

Nous avons ensuite mesuré les propriétés de conductivité des PBTTTs ainsi que leur propriété thermoélectrique. Comme le montre la figure 5, il existe bel et bien un optimum pour les propriétés TE en termes de longueur de chaînes alkyls. Ainsi les films de C_{12}-PBTTT permettent d'atteindre des conductivités électrique de 193 S/cm et des facteurs de puissance de 100 $\mu W \cdot m^{-1} \cdot K^{-2}$. Il s'agit là des valeurs les plus élevées obtenues

pour ce polymère. Les valeurs de σ et PF sont bien en retrait par rapport à ces deux valeurs pour tous les autres PBTTTs étudiés. ***Notre étude montre clairement l'existence d'une corrélation entre le taux de dopage, la longueur des chaînes alkyls et les propriétés TE obtenues.***

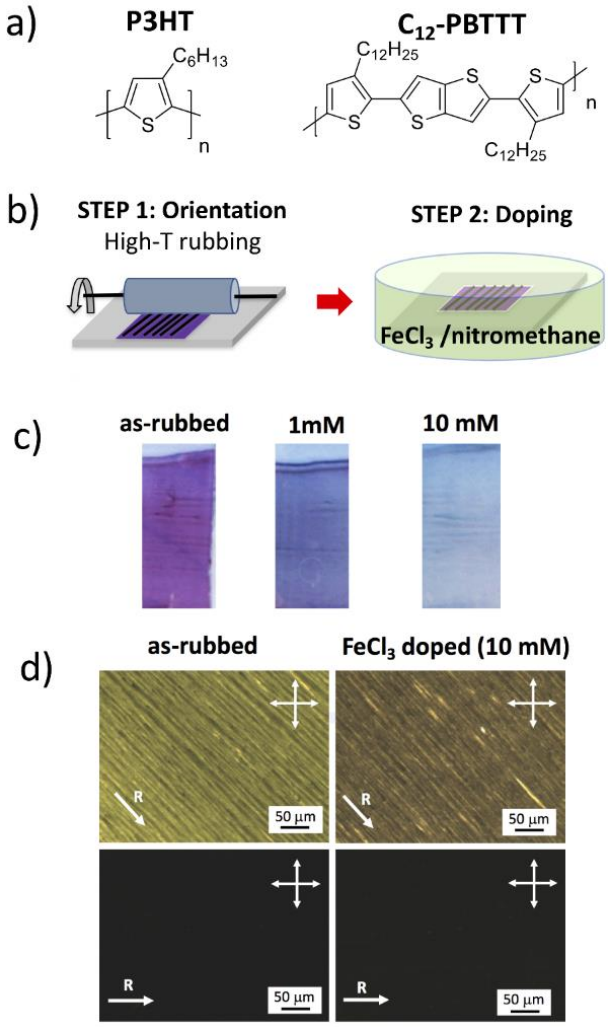

Figure 6. *a) Structures chimique du P3HT et du PBTTT étudiés. b) Méthode de préparation des couches orientées conductrices par brossage à haute température et dopage en solution de $FeCl_3$/nitrométhane. c) Evolution de la couleur des couches minces en fonction du dopage à 1mM et 10mM. d) Comparaison des biréfringences des films brossés de C_{12}-PBTTT avant et après dopage avec $FeCl_3$.*

Le chapitre 3 se focalise sur le dopage des films de C_{12}-PBTTT (poly(2,5-bis(3-dodecyl-2-thienyl)thieno[3,2-*b*]thiophene)) par $FeCl_3$ et compare les propriétés TE obtenues avec

celles du P3HT (poly(3-hexylthiophene régio-régulier)). Le choix du dopant $FeCl_3$ a été dicté par son pouvoir d'oxydation supérieur au F_4TCNQ. La comparaison des deux systèmes à base de P3HT et PBTTT (Figure 6.a) est pertinente car P3HT présente une structure semi-cristalline avec alternance périodique de zones cristallines et amorphes alors que le PBTTT présente plutôt une structure liquide-cristalline (cf Figure 7).

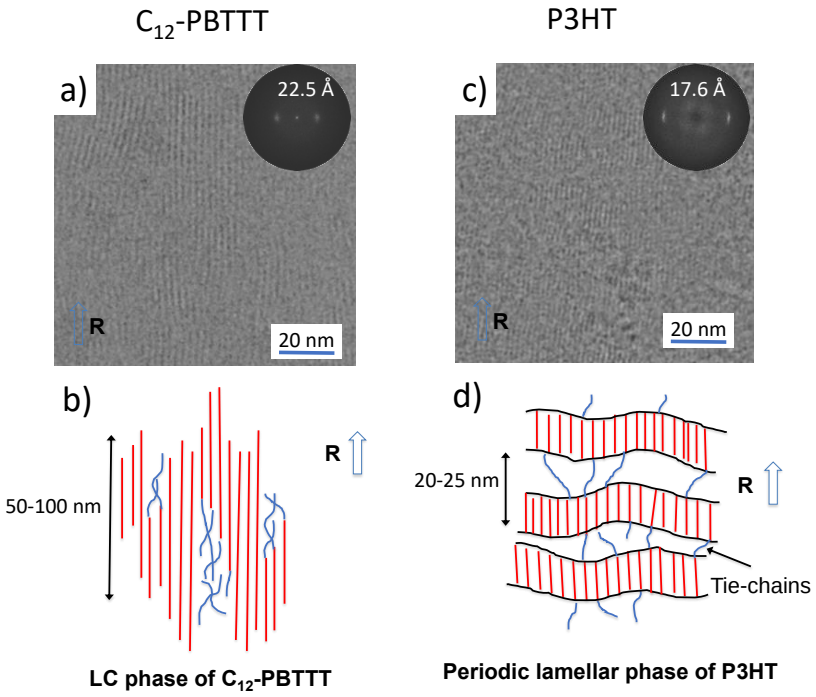

Figure 7. *Comparaison des structures liquide cristalline et semi-cristalline du C_{12}-PBTTT et du P3HT, respectivement. a) et c) images obtenues en mode low dose et haute résolution des films minces alignés et dopés de C_{12}-PBTTT. b) et d) illustration des structures liquide cristalline et semi-cristalline du C_{12}-PBTTT et du P3HT, respectivement.*

Dans le contexte des polymères conducteurs, nous nous sommes intéressés aux questions suivantes : Est-il possible d'atteindre des conductivités de 10^5 S/cm pour des films orientés de P3HT ou de C_{12}-PBTTT et quels sont les facteurs limitant la conductivité des charges ? Pour répondre à ces questions, nous avons étudié la possibilité d'atteindre des degrés d'oxidation élevés dans des couches orientées de P3HT et de C_{12}-PBTTT. Le chapitre 3 traite successivement: i) des modifications structurale et spectroscopique

induites par le dopage avec $FeCl_3$ sur des couches alignées de P3HT et C_{12}-PBTTT, ii) de l'évolution de la conductivité et des propriétés thermoélectriques avec le taux de dopage et iii) des corrélations entre coefficient Seebeck S et la conductivité des charges σ dans des films orientés de P3HT et C_{12}-PBTTT.

De la même manière que pour le dopage des couches minces de C_{12}-PBTTT avec F_4TCNQ, le dopage avec $FeCl_3$ permet de maintenir l'orientation des chaînes de C_{12}-PBTTT et de P3HT aprsè dopage en solution $FeCl_3$/nitrométhane (cf images POM de la figure 6). Tout au plus peut-on noter une perte d'orientation pour P3HT pour des concentrations élevées de $FeCl_3$ (> 5 mM). La diffraction électronique montre aussi que l'ordre est globalement préservé lors du dopage des couches avec $FeCl_3$ (cf Figure 8). Comme le montre la figure 8, le dopage modifie les paramètres de maille du C_{12}-PBTTT et du P3HT, mais, selon des proportions différentes. Dans les deux cas, la maille se dilate selon la direction des chaînes alkyls (100) et se contracte dans la direction du □-stacking (020). Ceci démontre que le $FeCl_3$ pénètre dans les cristaux de C_{12}-PBTTT et de P3HT et que les paramètres de maille varient en fonction de la quantité de dopant incorporé. Dans les deux cas, on atteint une concentration de dopant maximale qui se traduit par une saturation des paramètres de maille pour [$FeCl_3$] approchant 10 mM. d_{100} augmente de 19.7 Å (pristine) à 23.6 Å (10 mM) dans le C_{12}-PBTTT et de 16.4 Å (pristine) à 18.1 Å (10 mM) pour P3HT.

Très symptomatique est l'évolution du volume de la maille ΔV pour les deux polymères. En faisant l'hypothèse de mailles orthorhombique et de deux chaînes par maille pour les deux polymères, on trouve ΔV=20-30 $Å^3$ pour P3HT *et* ΔV=230-250 $Å^3$ pour C_{12}-PBTTT. L'intercalation de petites molécules telles $PC_{71}BM$ dans la structure du PBTTT est bien documentée dans la littérature. [29-31] Ainsi, $PC_{71}BM$ forme des intercalates avec C_{14}-PBTTT. Il en est de même dans les systèmes dopés C_{12}-PBTTT/ $FeCl_3$. La variation ΔV pour C_{12}-PBTTT est parfaitement compatible avec une intercalation de 2 $FeCl_2$ et 2 $FeCl_4^-$ dans

la maille du C_{12}-PBTTT. Ceci implique une steochiométrie Fe/S=2 qui est semblable à celle observée pour la phase fortement dopée du PEDOT : Tos. Des mesures par EDX-STEM ont permis de confirmer cette steochiométrie. Les spectres EDX permettent de déterminer le rapport Fe/S= 1.9±0.2 pour C12-PBTTT contre 2.5±0.2 pour P3HT.

Ces résultats structuraux ont été confirmés par spectroscopie optique UV-vis-NIR polarisée qui permet en particulier de visualiser le degré d'oxydation des chaînes polymère en fonction de [$FeCl_3$]. L'augmentation du taux de dopage résulte en une augmentation de l'intensité des bandes polaroniques P1 et P2 et une baisse de l'absorbance du polymère neutre (N) (cf Figure 9). Comme attendu, les bandes polaroniques sont polarisées dans le sens du brossage i.e. des chaînes polymère. De manière très caractéristique, pour 10 mM, les spectres sont dominés par les bandes polaroniques avec une contribution mineure du polymère non dopé (N) (inférieure à 1-2 %).

On obtient des spectres semblables à ceux du PEDOT-PSS, suggérant des degrés d'oxidation de la chaîne de l'ordre de 30-40 %.[10] En conséquence, les films sont quasi-transparents optiquement avec une faible coloration bleutée. La position des bandes polaroniques du C_{12}-PBTTT et du P3HT indique une plus grande délocalisation des polarons pour C_{12}-PBTTT, en accord avec l'observation structurale par HR-TEM montrant une persistance d'orientation plus forte pour ce polymère (cf Figure 7).

Comme montré par spectroscopie UV-vis-NIR, la proportion de chaînes de C_{12}-PBTTT et P3HT oxydée peut être ajustée par la concentration de dopant [$FeCl_3$]. Ceci donne la possibilité de contrôler la densité de porteurs de charge dans les films orientés et de déterminer son impact sur l'anisotropie de transport de charge et de propriétés TE. Ainsi, un film orienté de chaque polymère a été dopé à l'aide de solutions de

concentration croissante de $FeCl_3$ et pour chaque concentration, nous avons mesuré la conductivité et le coefficient de Seebeck.

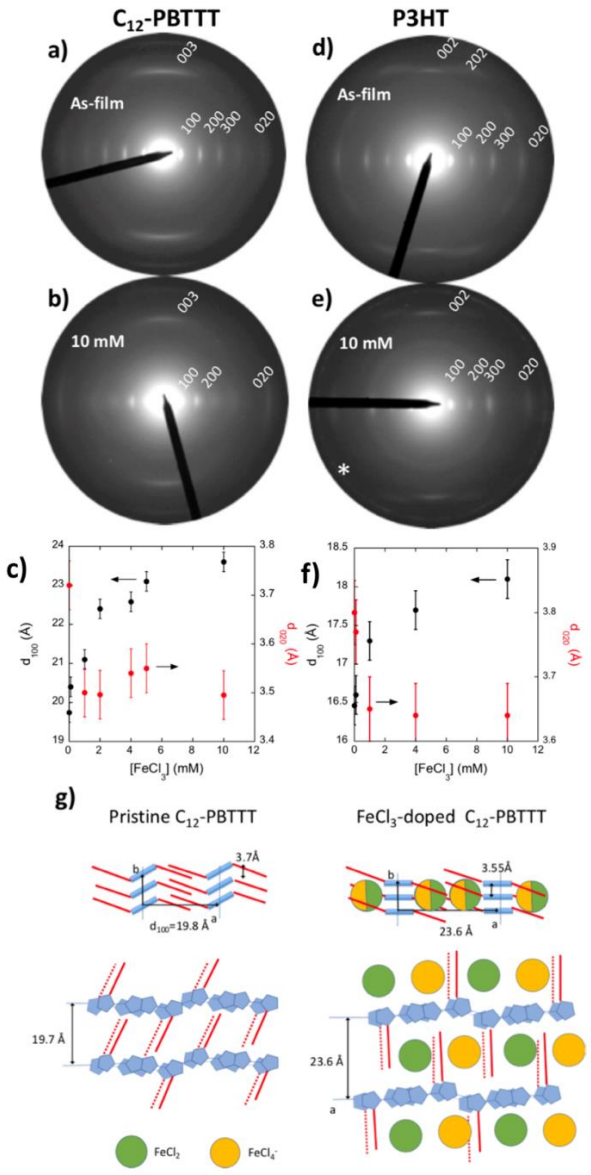

Figure 8. *Evolution de la structure dans les films minces alignés de P3HT et C_{12}-PBTTT lors du dopage par $FeCl_3$ en solution dans le nitrométhane d'après des mesures en diffraction électronique. Clichés de diffraction électronique de C_{12}-PBTTT avant (a) et après (b) dopage avec 10 mM $FeCl_3$. c) Périodicité lamellaire d_{100} et de π-stacking en fonction de la concentration de $FeCl_3$ dans le nitrométhane pour C_{12}-PBTTT. Clichés de diffraction électronique du P3HT avant (d) et après (e) dopage avec 10 mM $FeCl_3$. Dans la figure (e), l'asterisk désigne un anneau de Scherrer lié à l'excès de $FeCl_3$ en surface des films dopés de P3HT. f) Périodicité lamellaire d_{100} et de π-stacking en fonction de la concentration de $FeCl_3$ dans le nitrométhane pour des films de P3HT. (g) Illustration*

du changement structural induit par dopage avec $FeCl_3$ du C_{12}-PBTTT ([$FeCl_3$] =10 mM) donnant lieu à la formation d'un cristal bimoléculaire.

La Figure 5 montre l'évolution de σ et S en fonction de [$FeCl_3$] pour des films de P3HT et C_{12}-PBTTT. Table 1 collects the highest values of conductivity and power factors for both doped polymers and corresponding values from the literature for iodine-doped PA. La conductivité des films de P3HT et C_{12}-PBTTT augmente très fortement avec la concentration de $FeCl_3$ dans les deux directions parallèle et perpendiculaire au brossage. Dans le cas de C_{12}-PBTTT, la conductivité augmente de plusieurs ordres de grandeur entre 150 S/cm à 0.1 mM et 2.2 10^5 S/cm à 5 mM. Cette dernière valeur est de l'ordre de grandeur de la conductivité du polyacétylène orienté dopé à l'iode.

Concernant le P3HT, l'orientation donne lieu à une augmentation substantielle de la conductivité qui passe de 63 S/cm dans les films on-orienté à 570 S/cm dans la direction du brossage pour les films orientés (pour [$FeCl_3$] =5mM). L'anisotropie des conductivités reste supérieure dans le cas du C_{12}-PBTTT par rapport au P3HT ($\sigma_{//}/\sigma_{\perp}$=70 pour C_{12}-PBTTT contre 12 pour P3HT). Cette différence est partiellement liée à la différence des structures deux films de P3HT et C_{12}-PBTTT. Les films de C_{12}-PBTTT sont en orientation face-on alors que ceux de P3HT montrent un mélange face-on et edge-on. Par conséquent, $\sigma_{\perp}$ est mesuré essentiellement le long des chaînes C_{12} isolantes du C_{12}-PBTTT alors que les charges sont transportées le long du π-stacking et des chaînes alkyls dans les films de P3HT. D'autre part, on note que les films de P3HT perdent partiellement leur orientation dans le plan lors du dopage à forte concentration (cf figure 9).

La conductivité des films de P3HT est toujours largement inférieure à celle du C_{12}-PBTTT. Cette différence n'est pas liée à une différence de densité de porteurs de charge à en juger par la spectroscopie UV-Vis-NIR, à une différence d'alignement des films. La faible conductivité observée pour P3HT est attribuée à la structure semi-cristalline de ce polymère. Dans le P3HT, les charges doivent passer par des zones désordonnées

amorphes (cf Figure 7). En revanche, la structure liquide-cristalline du C_{12}-PBTTT, donne lieu à une meilleure percolation entre domaines ordonnés, ce qui permet d'atteindre des conductivités très élevées (cf images HRTEM de la Figure 7). Il faut noter que, même dans la direction perpendiculaire aux chaînes de PBTTT, le transport reste très important (conductivités de ~ 2100 S/cm proches de celles rapportées pour des films de C_{14}-PBTTT dopé avec des fluoro-trichlorosilanes).

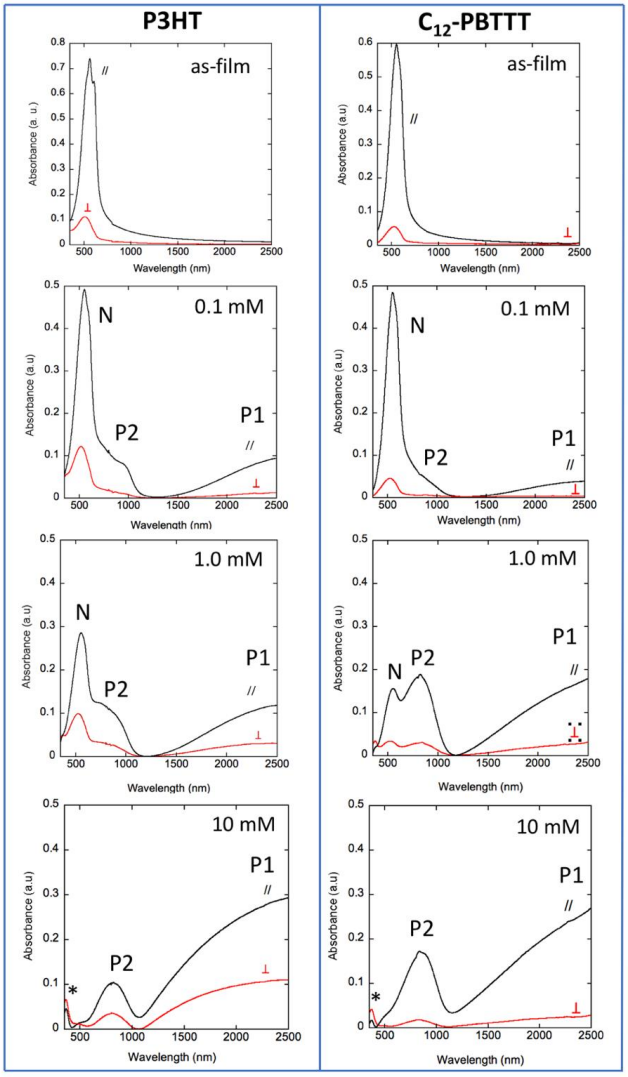

Figure 9. *Evolution du spectre UV-vis-NIR polarisé pour des films orientés de P3HT et* C_{12}-PBTTT *alignés par brossage à haute température et dopés en solution de* $FeCl_3$*/nitrométhane de concentration croissante. La polarisation de la lumière est soit parallèle (//), soit perpendiculaire (⊥) à la direction de brossage R.*

Des conductivités aussi élevées de l'ordre de 10^5 S/cm peuvent être expliquée en évoquant le modèle de métaux granulaires de Sheng utilisé pour le polyacétylène fortement dopé. Dans ce modèle, le transport à travers les zones très désordonnées se fait via l'effet tunnel. Dans le cas du P3HT, on a une morphologie lamellaire et des zones inter-lamellaire amorphes étendues qui empêchent l'effet tunnel entre les zones cristallines bien conductrices.

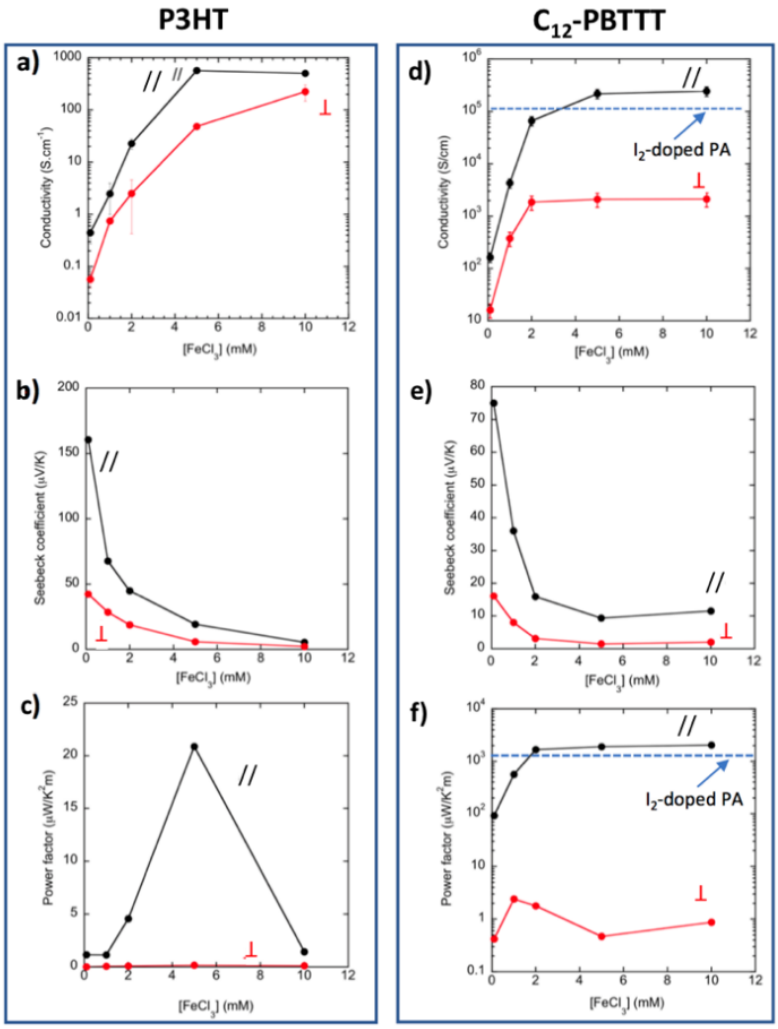

Figure 10. *Variation de la conductivité de charge σ (a et d), du coefficient Seebeck S (b et e) et du facteur de puissance PF (c et f) en fonction de la concentration de $FeCl_3$ pour des films orientés et de dopés de P3HT et C_{12}-PBTTT. σ, S et PF sont mesurés parallèlement (//) et perpendiculairement à la direction de brossage ($\perp$). Les lignes en continu sont des guides pour les yeux. Les lignes pointillées en bleu dans les figures d) et e) montrent les valeurs typiques observées pour le polyacétylène dopé à l'iode.*

L'obtention de films très orientés et conducteur de P3HT et de C_{12}-PBTTT après dopage avec $FeCl_3$, nous a permis d'étudier les corrélations entre conductivité et coefficient Seebeck, en particulier dans un domaine de conductivité très étendu et c'est là une première pour des polymères conducteurs orientés. Comme l'illustre la figure 11, on montre que dans la direction parallèle au brossage, $S_{//} \propto \sigma_{//}^{-1/4}$ pour les deux polymères. En revanche, dans la direction perpendiculaire au brossage, on observe une loi différente telle que $S_{\perp} \propto \ln(\sigma_{\perp})$. Ceci démontre l'existence de deux mécanismes de transports de charges différents dans ces deux directions parallèles et perpendiculaires aux chaînes des deux polymères.

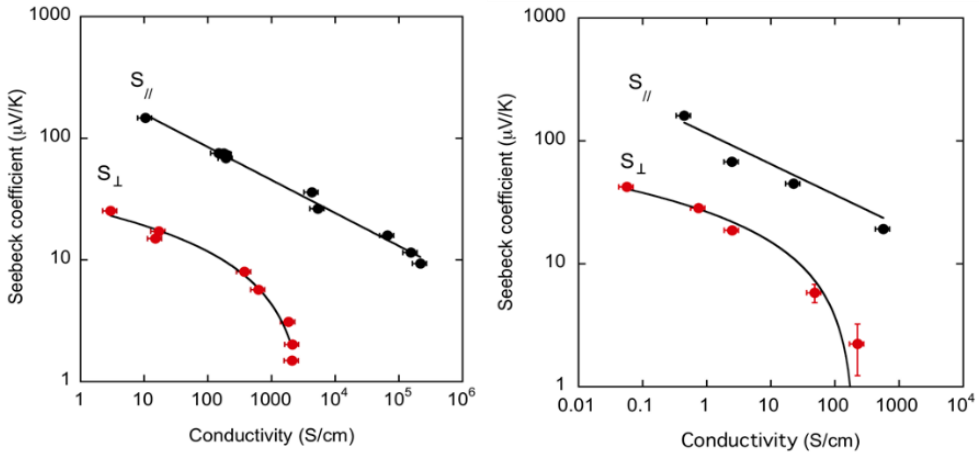

Figure 11. *Correlation entre le coefficient Seebeck S et la conductivité σ dans les films très orientés de a)* C_{12}-PBTTT *(T_R=125°C) et b) P3HT (T_R=180°C) dopé avec $FeCl_3$. Les indices // et $\perp$ font référence à la direction de mesure du transport de charge par rapport à la direction de brossage. Les courbes continues font correspondent à l'ajustement des points expérimentaux à l'aide des lois d'échelle $S_{//} \propto \sigma^{-1/4}$ et $S_{\perp} \propto -\ln(\sigma)$.*

Le dernier chapitre vise à comprendre l'effet de la taille et de la géométrie du dopant sur les propriétés TE des couches minces dopées de C_{12}-PBTTT et sur la structure des couches. On a déterminé la distribution d'orientation précise des dopants dans les couches de chaînes alkyls par spectroscopie UV-vis-NIR polarisée. Nous avons aussi évalué comment la méthode de dopage influence les propriétés TE obtenues. En particulier, on a considéré deux modes de dopages : i) par augmentation progressive de

la concentration de dopage (dopage APC) et ii) par dopage directe (dopage D) à une concentration donnée.

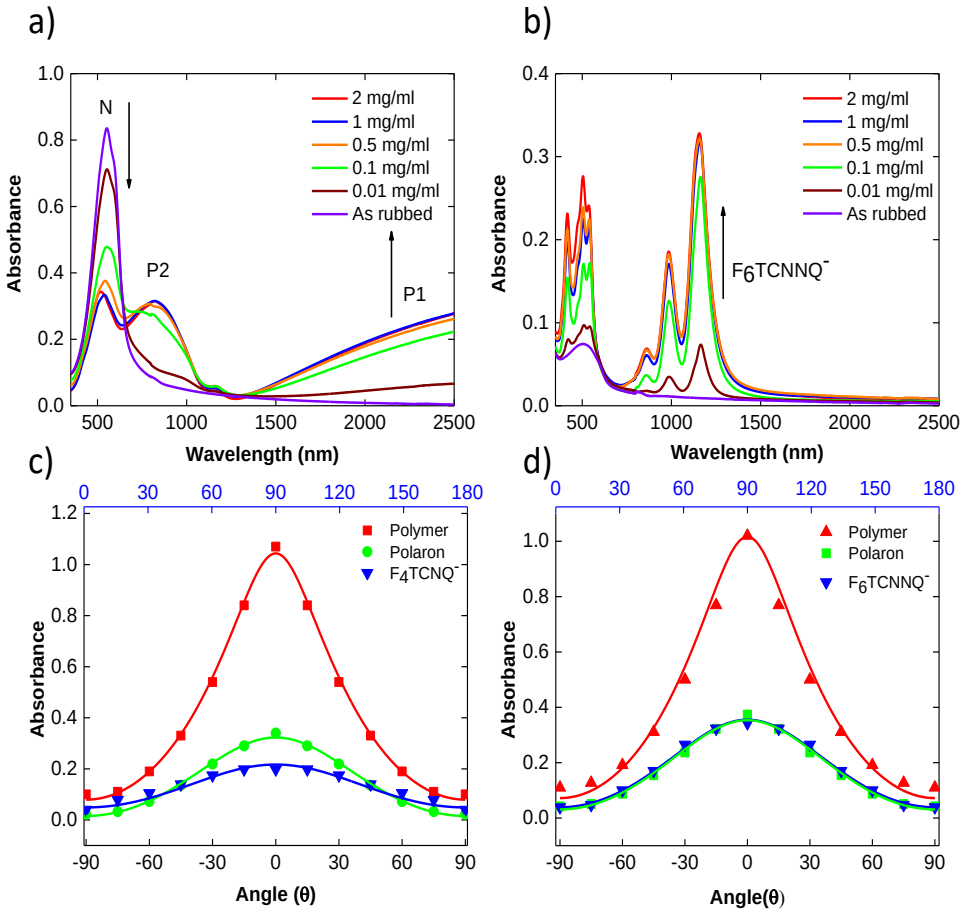

Figure 12. *Spectres UV-Vis-NIR de films orientés de C_{12}-PBTTT dopé avec F_6TCNNQ en fonction de la concentration de dopant dans l'acétonitrile. a) spectres mesurés dans la direction du brossage (//) et b) dans la direction perpendiculaire au brossage (⊥). c) et d) intensités des bandes caractéristiques des anions F_4TCNQ et F_6TCNNQ des chaînes de C_{12}-PBTTT (avant dopage) et du polaron (P1) en fonction de l'angle de polarisation.*

Le dopant retenu est le F_6TCNNQ qui est un dérivé proche du F_4TCNQ avec un cœur aromatique plus étendu du type naphthalène et portant 6 atomes de fluor, ce qui a pour conséquence de rabaisser le niveau LUMO du dopant à -5.37 eV (contre -5.2 eV pour F_4TCNQ). Le F_6TCNNQ permet d'atteindre des conductivités de l'ordre de 7 S/cm dans les films non orientés de P3HT. Nous avons montré par spectroscopie UV-vis-NIR polarisée que les dopants F_4TCNQ et F_6TCNNQ sont localisés dans les couches de chaînes

alkyls et ont leur grand axe orienté dans un plan perpendiculaire aux chaînes de C_{12}-PBTTT. La distribution d'orientation des dopants autour du plan perpendiculaire au chaînes de polythiophène dans les couches alkyls a été déterminée à partir de la dépendance angulaire des bandes d'absorption des deux anions et en la comparant à celle des chaînes polythiophènes (Figure 12). L'analyse a permis de mesurer précisément les paramètres d'ordre traduisant l'orientation des anions, du polaron et des chaînes du polymère dans les films avant dopage (tableau 1).

Tableau 1. *Caractéristiques issues de l'analyse de la distribution angulaire des films minces de C_{12}-PBTTT dopés avec F_4TCNQ et F_6TCNNQ.*

Dopant+Polymer	F_4TCNQ doped PBTTT C_{12}			F_6TCNNQ doped PBTTT C_{12}		
	As rubbed PBTTT	F_4TCNQ^-	Polaron (P1)	As rubbed PBTTT	F_6TCNNQ^-	Polaron (P1)
Half-width at half maxima	±28.5°	±47°	±38°	±28.9°	±38°	±41°
Dichroic ratio (D_R)	10.7	4.95	15	9.3	8.8	9.3
Order parameter (S)	0.7	0.5	0.7	0.7	0.7	0.73

L'orientation des dopants de type F_6TCNNQ est plus proche du plan orthogonal aux chaînes de PBTTT que pour F_4TCNQ dont l'orientation moyenne s'écarte davantage de cette direction. L'impact de l'intercalation sur la structure a aussi été déterminée par diffraction électronique et on a ainsi pu déterminer l'influence de l'intercalation sur les paramètres de maille de C_{12}-PBTTT. Malgré une taille plus grande, la maille du C_{12}-PBTTT ne présente pas une augmentation de volume supérieure. En étudiant par UV-vis-NIR la cinétique de diffusion de F_4TCNQ et F_6TCNQ dans les couches orientées de C_{12}-PBTTT, nous avons montré que les coefficients de diffusion du F_4TCNQ est supérieur à celui du F_6TCNNQ (2.5×10^{-12} cm^2/s contre $9\cdot10^{-12}$ cm^2/s pour F_4TCNQ). Ceci traduit la dimension

plus grande du F_6TCNNQ qui limite sa diffusion dans les couches de chaînes alkyls du C_{12}-PBTTT.

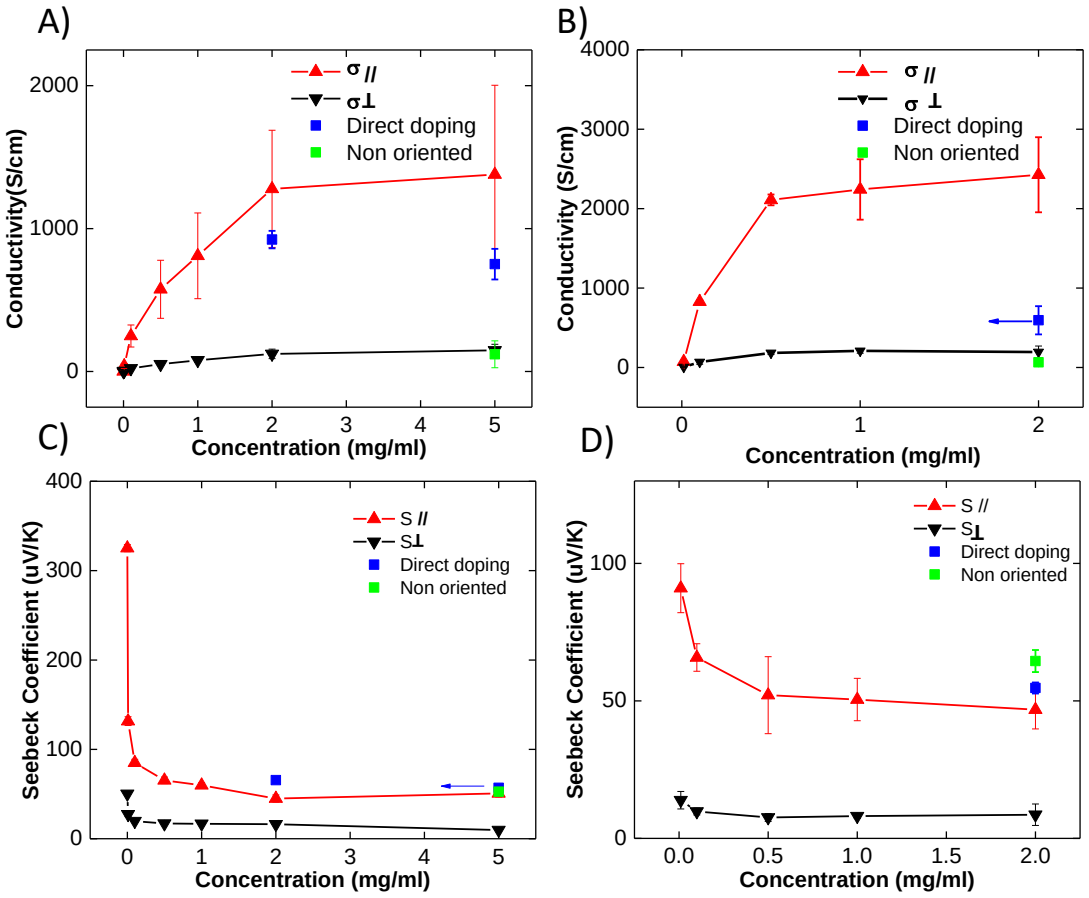

Figure 13. *Evolution de la conductivité de charge (A et B) et du coefficient Seebeck (C et D) en fonction de la concentration de dopant F_4TCNQ et F_6TCNNQ dans les films orientés de C12-PBTTT, respectivement. S et σ sont mesurés parallèlement and perpendiculairement à la direction de brossage. Pour comparaison, nous montrons aussi les valeurs des échantillons dopés de manière directe à forte concentration (2 et 5 mg/ml pour F_4TCNQ et 5 mg/ml pour F_6TCNNQ). On indique aussi la conductivité des échantillons non orientés pour comparaison.*

Dans la seconde partie de ce chapitre, nous avons évalué l'impact de deux méthodes de dopage (dopage APC et D) sur les propriétés de conductivité et TE des films minces de C_{12}-PBTTT dopés avec F_6TCNNQ. Ainsi on a montré que l'augmentation progressive de la concentration de dopage par trempage successif dans des solutions de dopant de concentration croissante permet d'atteindre des conductivités de charge

significativement plus élevées que par dopage directe. Ainsi, par APC on atteint 2430 S/cm et un facteur de puissance de 583 ±180 $uWm^{-1}K^{-2}$ contre 600±200 S/cm pour des films ayant subi un dopage direct avec F_6TCNNQ. La valeur obtenue par dopage APC est une valeur record pour des polythiophènes dopés avec ce dopant. Il s'agit de la première étude démontrant l'importance du protocole de dopage sur les conductivités observées

En conclusion, cette thèse a démontré les effets bénéfiques de l'alignement des polymères de type polythiophène sur les propriétés de conductivité de charge et thermoélectriques après dopage. Différents paramètres tels la longueur des chaînes alkyls, la nature chimique et la géométrie du dopant ainsi que le protocole de dopage ont des impacts très forts sur les propriétés TE observées. De manière remarquable, on a pu obtenir des valeurs de conductivité et de facteur de puissance record dans le domaine TE organique grâce à la maîtrise de l'alignement des couches minces. Cette approche est très générale et pourra être transposée à une large palette de nouveaux polymères y compris de type n.

Université de Strasbourg
Excellence University

Vishnu VIJAYAKUMAR

École doctorale
Physique, chimie-physique
ED 182
Université de Strasbourg

Highly oriented conducting polythiophene films for thermoelectric applications

Résumé

Cette thèse concerne la fabrication de matériaux thermoélectriques (TE) à base de films minces orientés de polythiophènes (PBTTT). Le brossage à haute température produit des films minces de cristallinité et d'orientation contrôlées. Différentes méthodes de dopage avec des dopants tels F_4TCNQ, F_6TCNNQ et $FeCl_3$ ont permis de fabriquer des films polymère conducteurs orientés aux propriétés TE anisotropes. Une combinaison de spectroscopie UV-vis-NIR polarisée et de MET donne accès à l'orientation et à la quantité de dopants intercalés dans les cristaux polymère. Le coefficient de diffusion du dopant est corrélé à la longueur des chaînes alkyls des polymères : les PBTTTs ayant des chaînes alkyls en C_{12} présentent les meilleurs propriétés TE en raison d'une diffusion rapide et efficace des dopants dans le polymère. Finalement, nous avons étudié l'effet du type de dopant (son électronégativité, sa taille) sur les propriétés TE des films. Le dopage de films orientés de C_{12}-PBTTT avec $FeCl_3$ permet d'atteindre des valeurs records de conductivité de $2\cdot 10^5$ S/cm et des facteurs de puissance de l'ordre de 1 mW/mK^2.

Summary

The aim of this thesis is to develop new polymeric thermoelectric (TE) materials based on oriented polythiophene (PBTTT) films. High-temperature rubbing produces oriented films of controlled orientation and crystallinity. Various doping methods with suitable dopants (F_4TCNQ, F_6TCNNQ and $FeCl_3$) produced enhanced TE properties along the rubbing direction. A combination of polarized UV-Vis-NIR spectroscopy and TEM uncovered the amount and orientation of dopants intercalated in the crystals of PBTTT. The diffusion coefficient of dopants is correlated to the length of alkyl side chains: PBTTT with C_{12} side chains shows the best TE properties because of a fast and effective diffusion of dopants in the polymer films. Finally, we evaluated the impact of dopant (geometry, electronegativity) on the TE properties. Doping oriented PBTTT with $FeCl_3$ helped reach record electrical conductivity of 2×10^5 S/cm and TE power factors of 1 mW/mK^2.

Keywords: Conducting polymers, Structure, Thermoelectricity, Transmission electron microscopy